Continuous Time State-space Model Identification with Application to Magnetic Bearing Systems

Rosmiwati Mohd Mokhtar

(Doctor of Philosophy)

2008

RMIT

Continuous Time State-space Model Identification with Application to Magnetic Bearing Systems

A thesis submitted in fulfillment of the requirements for the degree of

Doctor of Philosophy

Rosmiwati Mohd Mokhtar

Bachelor of Engineering with Honours (Electrical & Electronic Engineering)

Master of Science (Electrical & Electronic Engineering)

School of Electrical and Computer Engineering

Science, Engineering and Technology Portfolio

RMIT University

March 2008

Declaration

I certify that except where due acknowledgement has been made, the work is that of the author alone; the work has not been submitted previously, in whole or in part, to qualify for any other academic award; the content of the thesis is the result of work which has been carried out since the official commencement date of the approved research program; and, any editorial work, paid or unpaid, carried out by a third party is acknowledged.

Rosmiwati Mohd Mokhtar

March 14^{th}, 2008

Acknowledgements

First of all I would like to express my sincere appreciation and gratitude to my supervisor, Prof. Liuping Wang for her overwhelming supervision, advice, encouragement and support throughout my candidature at RMIT University. It has been a great experience and privilege to work with her and to benefit from her rich knowledge. Her determination and enthusiasm will always inspire me in the future. Thanks and appreciations are also extended to my co-supervisor, Dr. Thurai Vinay and my former co-supervisor Dr. Lijiang Qin for their help and support.

Special acknowledgment also goes to the Ministry of Higher Education, Malaysia, Universiti Sains Malaysia and School of Electrical & Computer Engineering (SECE), RMIT University for the financial support during my research years. Not to forget, to all SECE academic, administrative and technical staff for their assistance and cooperation in providing such a wonderful research environment at RMIT University.

I would like to sincerely thank my colleagues Dr. Seedahmed Sharif Mahmoud, Dr. Esref Turker, Dr. James Nealand, Dr. Simon Mutzenich, Dr. Nguyen-Vu Truong, Tim Barry, Sheeraz Memon, Ishtiaque Ahmed and Abdurezagh Salem Elmezughi for their tremendous guidance and support during this work. Appreciations and thanks also to Dr. Zuraini Dahari, Nadeen Abbas, Zuratul Ain Abd Hamid, Rashidah Arsat, Dayang Nur Fatimah Awang Iskandarzulkarnain and Fadhilah Ibrahim for being such a wonderful friend indeed. Not to forget, all the residence of Malaysia Hall, Melbourne 2007-2008.

The support, faith and endless love of my family - my parents, Mohd Mokhtar Hassan and Saadiah Musa, my husband, Norarham Yusof and son, Arham Hakimi have been essential for this achievement to become reality.

Contents

Abstract

This thesis presents the identification of continuous time linear multi-variable systems using state-space models. A data-driven approach in realization by the subspace methods is carried out in developing the models. In this thesis, the approach by subspace methods is considered for both open-loop and closed-loop continuous time system identification. The Laguerre filter network, the instrumental variables and the frequency sampling filters are adopted in the framework of subspace model identification. More specifically, the Laguerre filters play a role in avoiding problems with differentiation in the Laplace operator, which leads to a simple algebraic relation. It also has the ability to cope with noise at high frequency region due to its orthogonality functions. The instrumental variables help to eliminate the process and measurement noise that may occur in the systems. The frequency sampling filters are used to compress the raw data, eliminate measurement noise so to obtain a set of clean and unbiased step response data. The combination of these techniques allows for the estimation of high quality models, in which, it leads to successful performance of the continuous time system identification overall. The application based on a magnetic bearing system apparatus is used to demonstrate the efficacy of the proposed techniques.

List of Figures

List of Tables

List of Symbols

x_L, x_R	Left-side and right-side bearing on $x-$axis plane
y_L, y_R	Left-side and right-side bearing on $y-$axis plane
$u(t)$	System input in continuous time
$y(t)$	System output in continuous time
$x(t)$	System states in continuous time
U, Y, X	Column vectors of input, output and states
$h(t)$	Process output disturbance
$v(t)$	Measurement output disturbance
$\xi(t)$	Measurement input disturbance
H, V, F	Column vectors of noise disturbances
$r(t)$	Reference signal
$u_c(t)$	Output signal from controller
l	Number of input
m	Number of output
n	Model order
N	Number of data
A, B, C, D	State space system matrices
A_w, B_w, C_w, D_w	State space system matrices with $w-$operator
A_m, B_m, C_m, D_m	Actual state space system matrices
$G(s), \hat{G}(s)$	System transfer function and estimated transfer function
$y(t), \hat{y}(t)$	Measured output and estimated output
I	Identity matrix
ω	Sampling frequency
Δt	Sampling time

w	Laguerre operator
ℓ	Laguerre filter
$L(s)$	Laguerre filter network
p	Design parameter for Laguerre filter
i	Number of term for observability and Toeplitz matrix
$\mathcal{O}_i$	Observability matrix
Γ_i	Toeplitz matrix
$G^f_{i,N}$	Filtered transfer function matrices
$\Omega^f_{i,N}$	Filtered impulse response matrices
$U^f_{i,N}, Y^f_{i,N}$	Filtered input and filtered output matrices
$H^f_{i,N}, V^f_{i,N}, F^f_{i,N}$	Filtered noise disturbance
$\Pi^{\perp}$	Projection matrix
P	Instrumental variable matrix
$P^f_{i,N}$	Filtered instrumental variable matrices
$\Upsilon^{\dagger}$	Moore-Penrose pseudo inverse
$\top$	Transpose
Ψ_i	Noise observability matrix
$\mathrm{eig}(A)$	Eigenvalues of A
$\mathrm{var}(y)$	Variance of variable y
A^{-1}	Pseudo inverse of the matrix A
$\mathbf{Re}\ z$	Real part of the complex number z
$\mathbf{Im}\ z$	Imaginary part of the complex number z
$U^f_{0,i,N}, Y^f_{0,i,N}$	Past input and past output
$U^f_{i,j,N}, Y^f_{i,j,N}$	Future input and future output
$\Phi^f_{0,i,N}$	Past Laguerre filter
θ	Parameter vector matrix
$\varphi(t)$	Regressor matrix
J	Performance index
W	Orthogonal matrix for orthogonal decomposition algorithm
$\hat{g}$	Auxiliary parameter vector for orthogonal decomposition algorithm

$\hat{g}_m$	Step response estimates
$\bar{G}(z)$	FSF transfer function
S	Matrix obtained from SVD
$P_m(s)$	Plant transfer function
$C_m(s)$	Controller transfer function
$T_{yr}(s)$	Transfer function from r to y
$T_{ur}(s)$	Transfer function from r to u

Abbreviations and Acronyms

ARMA	Auto Regressive Moving Average
ARMAX	Auto Regressive Moving Average with External Input
ARX	Auto Regressive with External Input
BJ	Box & Jenkins
CCA	Canonical Correlation Analysis
CVA	Canonical Variate Analysis
DSP	Digital Signal Processor
EIV	Error In Variable
FEM	Finite Element Method
FFT	Fast Fourier Transform
FIR	Finite Impulse Response
FR	Future Reference
FSF	Frequency Sampling Filter
GRBS	Generalized Random Binary Signal
IDFT	Inverse Discrete Fourier Transform
IV	Instrumental Variable
LMS	Least Mean Square
LQ	Linear Quadratic
MB	Magnetic Bearing
MIMO	Multi Input Multi Output
MOESP	Multi-variable Output Error State Space

MBPC	Model-based Predictive Control
MPC	Model Predictive Control
MSE	Mean Square Error
N4SID	State Space Subspace System Identification
NAN	Not A Number
NN	Neural Network
OE	Output Error
PD	Proportional Derivative
PEM	Prediction Error Method
PI	Proportional Integral
PID	Proportional Integral Derivative
PMF	Poisson Moment Function
PRESS	Predicted Residual Sum of Squares
RMSE	Root Mean Square Error
RQ	Recursive Quadratic
SISO	Single Input Single Output
SMI	Subspace Model Identification
SNR	Signal to Noise Ratio
SVD	Singular Value Decomposition
SVF	State Variable Filter
VAF	Variance Accounted For
VAR	Variance

Chapter 1

Introduction

1.1 Motivation

Merging towards modernization and rapid development era, the high technology of systems and machine tools are very highly in demand. The need for exploration either for novel technology or perhaps improvising the existence is always desired. Thus, this research will focus on another perspective of system identification in which it involves the subspace methods in identifying continuous time state-space models. Towards the end, the realization of the developed model will be evaluated to identify a magnetic bearing systems.

The motivation of this thesis upstand behind these reasons:

1. Even though the discrete time models can be used to describe such systems, however, in certain practical applications the use of continuous time models is preferable. When investigating the underlying of physical systems, such as time constants, elasticity, mass, etc., these parameters are directly interpreted by continuous time models whereas the discrete time models do not. For instance, the second order continuous time transfer function is given as

$$G(s) = \frac{1}{ms^2 + bs + k}$$

where the parameter m, b and k represent the mass, elasticity and friction accordingly.

On the other hand, the discrete time model of the same process is given as

$$G(z) = \frac{b_0 z + b_1}{a_0 z^2 + a_1 z + a_2}$$

where the parameters do not have any physical meanings. Moreover, additional parameters are introduced in the numerator part due to the effect of sampling and hold mechanisms. Thus, in the areas where analysis of the physical system is in need, such as in biophysics or rotor-dynamics, the continuous time models, which contain the interpretation of the physical parameters are desirable.

The continuous time systems also allow for measurement of non-equidistant sampled data. In the application areas like medicine, transport and traffic systems, the process measurement is not under human control. Since the discrete time models are relying on constant sampling period, therefore the identification of these particular systems is difficult in the framework of uniformly sampling environment. The continuous time models, however, represent the systems at every time instance. Thus, the equidistantly spaced of sampled data is unnecessary. The measurements are only based on points on the continuous line.

In addition, the continuous time models also make the identification of stiff systems more reliable. A stiff system contains both slow and fast dynamics. The areas of chemical engineering, nonlinear mechanics, biochemistry and life science are sources of stiff systems. For these particular systems, identifying slow dynamics requires a large amount of data and leads to long calculation times. With continuous time models, the data can be justified and analysed separately, allowing also for sampling rate and measurement time adjustment. This will significantly reduce the amount of data and the computation time needed for identification.

2. The subspace methods have proven to successfully identify a state space model especially for an open-loop systems. However its consistency and successful rate in identifying a closed-loop systems still open for a challenge. Even though, there are some successful approaches reported in the literature, yet the contributions especially in developing a continuous time model with noisy environment can be counted.

3. Even though the magnetic bearing apparatus has existed for a long time already, there are a lot of issues governing the systems that need to be explored. The bearing stiffness issues, rotor dynamics which lead to rotor unbalance and high frequency oscillations, control system performance and many more, are demanding in terms of stability and robustness

improvements. Thus, obtaining a good model that represents the system will lead to next step of obtaining a good control towards the systems.

4. Combining together the continuous time system using subspace methods and implementing it to magnetic bearing system will provide such an interesting, significant and novel research perspective for each of the area.

1.2 Literature Review

In conjunction with the application towards magnetic bearing systems, this thesis has focussed on several subjects. In broad terms the subjects are: system identification, state-space models, subspace methods and continuous time identification. The following literature review reflects the work completed in recent years in each of these respective areas.

1.2.1 System Identification

System identification is considered as a well known technique for developing mathematical models based on plant input and output data sequences. There are comprehensive literature in the field of system identification which can be referred for instance in the books by Sinha & Kuszta [144], Soderstrom & Stoica [150], Schoukens & Pintelon [137], Johansson [79], Van den Bosch & Van der Klauw [34], Astrom & Wittenmark [13], Ljung [99], and Pintelon & Schoukens [128]. This procedure has been successfully studied in many different areas, such as control system engineering, civil, chemical and environmental engineering, economics, biology and many more. In control engineering for example, system identification provides a useful means to obtain mathematical models for optimization and controller design [54, 101, 180]. In general, the system identification procedures are shown in sequence as follows [13, 99].

1. Experiment design - Preparing the experiment or process plant in terms of what signals to measure, choice of sampling time and choice of excitation signals.
2. Data acquisition - Recording the input and output data from the experiment or process plant.
3. Model selection - Specifying type of models that is required for observation.

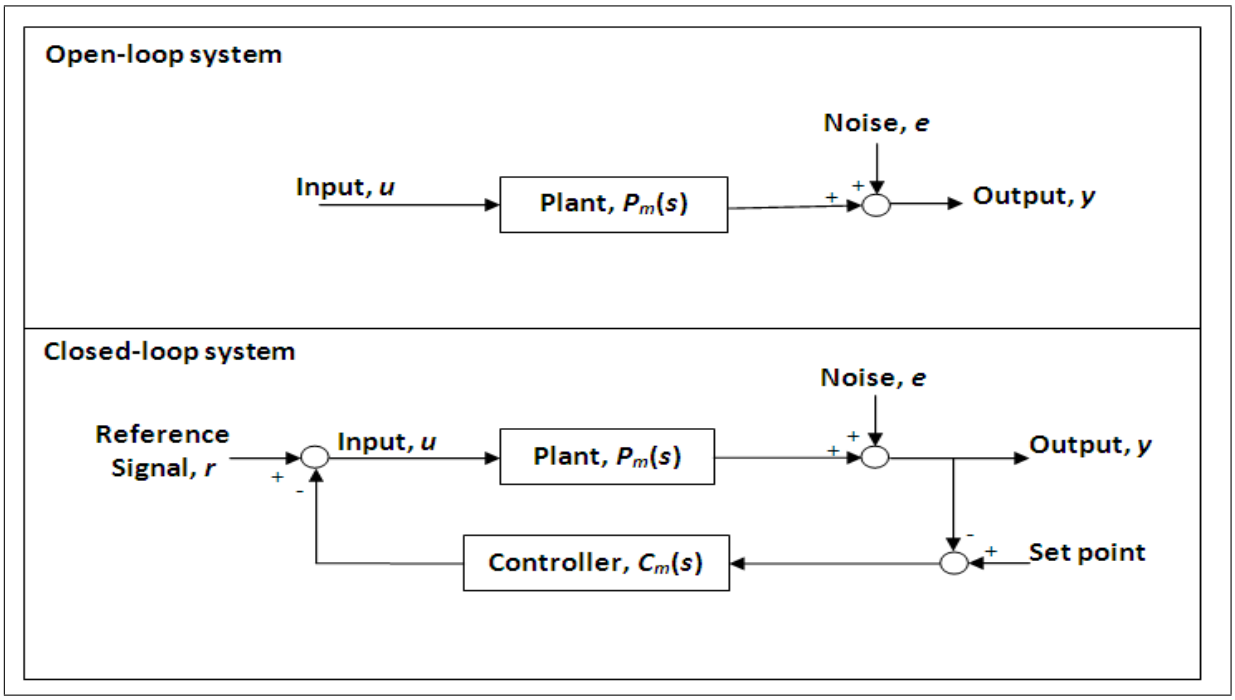

Figure 1.1: Open-loop and closed-loop systems

4. Model estimation - Determining the best model criteria in minimizing the cost function.

5. Model validation - Evaluating the performance capability of the model in describing the systems.

Within the above procedures, there are two types of identification experiment: the open-loop experiment and the closed-loop experiment. Figure (1.1) shows the block diagram that represent both systems. The open-loop identification considers the direct identification from output to input signal. On the other hand, the closed-loop identification results when the identification experiment is performed in closed-loop, in which, the output is fed back to the input using certain feedback mechanism. This setup is unavoidable if the plant must be controlled for safety reason, maintaining high quality production and/or if the open-loop will make the system unstable. The open-loop identification is quite straightforward. However, that does not hold for closed-loop identification.

The area of closed-loop identification can be classified into three groups [44, 84, 99].

1. Direct approach - Ignoring the existence of the feedback loop, the open-loop identification methods are directly applied to the measurable input and output data for identifying the

plant, $P_m(s)$.

2. Indirect approach - Suppose that the reference input, r is available and the controller transfer function, $C_m(s)$ is known. First step involves identification of transfer function, $T_{yr}(s)$ from r to the output y. Second step computes the plant transfer function by using the formula

$$P_m(s) = \frac{T_{yr}(s)}{1 - C_m(s)T_{yr}(s)} \tag{1.1}$$

3. Joint input-output approach - Suppose that the reference input, r is available. First step involves identification of transfer function, $T_{ur}(s)$ and $T_{yr}(s)$ from r to the joint input-output (u, y). Second step computes the plant transfer function using the algebraic relation

$$P_m(s) = \frac{T_{yr}(s)}{T_{ur}(s)} \tag{1.2}$$

The direct approach usually provides with biased estimates unless the noise effect is not so significant and can be neglected. However this situation is not always true in practical applications. Therefore, to compensate the difficulty associated with the bias, modified methods like two stage least squares methods and the projection method are developed [45,138,181,182]. The basic idea is to identify the sensitivity function of the closed-loop system by using autoregressive moving average (ARMA) or finite impulse response (FIR) models, in which the estimate $\hat{u}$ of the input u is generated removing the noise effects. Then, the estimated input $\hat{u}$ and the output y are employed to identify the plant transfer function using a standard open-loop identification technique [84].

The indirect approach requires the information about the controller transfer function is known. Examples of this approach can be referred in [35, 166, 177]. The advantage of the joint input-output approach is that the knowledge of the controller is not required. However, the major drawback is that the identified model has an order equal to the sum of the plant and controller order. Therefore, the model reduction step is required in the procedure. Example of this joint approach can be referred in [84, 170].

System identification can be also classified into online identification and off-line identification. The online identification (also known as recursive identification or real-time identification) deals with problems of building mathematical models at the same time as data is being collected. The identification is said to be online identification if it based on the following criteria [144].

1. It does not require a special input.
2. No batch recorded data or safekeeping data is required.
3. The recursive algorithms, adaptive algorithms or sequential parameter estimation methods are used. In this situation, the identification process is started without the need of large amount of input data. The estimation process can be done with only few initial data and the parameter optimization process is updated continuously for every enter of new data.
4. The total measurement for model optimization is calculated at each sampling period.
5. The identification process is run in short time.

On the other hand, the identification is an off-line procedure if it is based on the following criteria [144].

1. By using appropriate algorithms, the most significant input can be used to develop the model.
2. Large amount of input and output data are recorded and kept for later modelling.
3. During the model estimation process, the data is processed in a block sample and according to the justified cost function.
4. Varieties of formulation procedures can be done as the measurement time is not a constraint.
5. The identification process usually takes longer time.

Next, after the system and identification are configured, the suitable candidate of model to represent the system is desired. The model must provide a good prediction over the dynamical properties of a given system under various operating conditions. Models that describe the systems may be in various forms. The two most popular realization approaches for developing a model in system identification are prediction error optimization approach developed by Astrom, Bohlin and Eykoff (refer to [11, 12, 21, 39]), and the state-space realization approach developed by Ho and Kalman [62]. The interest of this thesis goes to the state-space realization approach.

1.2.2 State-space Model

In the state-space realization approach, the relationship between the input, noise, and output signals is written as a system of first-order differential or difference equations using an auxiliary state vector $x(t)$. Since its first introduction in the 60's by Ho and Kalman [62], and later in 1978 with improved algorithm proposed by Kung [91], this method has opened a clearer approach in system identification perspective. Even though the approach by these three researchers had only allowed for the determination of a state-space model from impulse responses, but it did provide with clearer information about the system order (according to *Singular Value Decomposition*, SVD), therefore less tuning parameters were necessary and multi-variable models can be represented in a straightforward manner.

The use of a state-space model to describe the dynamical systems is getting more popular as the insights into physical mechanisms of the system become more transparent. In addition, the state-space mathematical modelling involves vectors and matrices in a unique geometrical framework. It offers the key advantages on providing low parameter sensitivity with respect to perturbations for high order systems. It also shows its ability to present multi-input and multi-output systems with minimal state dimensions.

In this thesis, the state-space model formulation is chosen to complement with the subspace methods in which the subspace-based state-space modelling techniques will be utilized. The books by Van Overschee & De Moor [165], Ljung [99] and Katayama [84]; and the thesis by McKelvey [106], Haverkamp [57], Shi [142] and Barry [14] provide excellent overview in this particular area.

1.2.3 Subspace Methods

Subspace methods in a formulation of state-space models have given such a promising achievement in modelling and identification of multi-variable systems. In addition, subspace identification algorithms also do not require an explicit parametrization. The only parameter needed for user specification is the system order, in which it can be explicitly determined by inspection of a singular value spectrum. The subspace identification algorithm also requires no nonlinear parametric optimization and no iterative procedures, thus abolishes the problems of local minima

and model convergence.

The common and popular approaches in the *Subspace Model Identification* (SMI) family are the CVA (*Canonical Variate Analysis*) method introduced by Larimore [92, 93], the MOESP (*Multi-variable Output Error State Space*) algorithm introduced by Verhaegen and Dewilde [172, 173] and the N4SID (*State Space Subspace System Identification*) algorithm introduced by Van Overschee & De Moor [167, 168]. The CVA [92, 93] method perform a *Canonical Correlation Analysis* (CCA) on two data sets: A matrix of past input/output data and a matrix of future output data. Based on the properties of a Markov process and the maximum likelihood function, the dominant canonical variate of those two data sets are considered the approximates of the state variables. The system matrices are estimated by fitting the estimated states to the state-space model by least squares regression [142]. This method works with the assumption that the process inputs are not auto-correlated.

The MOESP algorithm [172, 173] employs the *Quadratic Recursive* (QR) decomposition to factorize the joint input and output data matrices into a triangular coefficient matrix R and an orthonormal signal matrix Q. The working matrix is estimated using the SVD, the matrices A and C are obtained from the extended observability matrix, and the matrices B and D are solved by least squares regression. On the other hand, the N4SID algorithm [167, 168] performs a projection of future outputs/inputs onto the past data. Then, the SVD is performed to the projection results to determine the model order and estimate the state variables. The system matrices are solved from least squares regression. This algorithm works with the assumption that noises that appear in the systems are zero mean, random Gaussian distributions and are independent of process inputs. The inputs are persistently exciting and the number of data points is sufficiently large.

These realization methods have sparkled the development of many other SMI algorithms (for examples in [32, 109, 174, 175]). Subspace methods have also shown promising performance in some applications such as modelling of flexible structure [55, 109], flexible aircraft [33], aircraft dynamics [58], power transformer [6], antenna array system [95], chemical industry (distillation column) [40] and semiconductor exposure apparatus [86].

In addition to its numerical simplicity and requiring of no iterative procedures, the subspace method is also convenient for optimal estimation and control. However, without special treatment, the subspace method usually gives bias when implemented on a system that works under closed-loop operation. This is due to the correlation between the input and the output noise in closed-loop system in which it can't be solved with only ordinary subspace methods [44, 84, 99]. However, with special treatment, now the subspace methods are also able to identify the closed loop system. The idea of implementing the subspace methods for identification of a closed-loop system has been studied in early 90s (see for examples in [30, 85, 100, 166, 170]). In some cases, the assumption that the input is not correlated with the output noise is always made or if any, it will be in at least in one sample delay.

Recent paper by Qin has given a good overview on subspace identification for open-loop and closed-loop systems [132]. Improvising the subspace method to be applicable with consistent estimates over closed-loop systems has shown some promising achievement (See recent examples in [29, 84, 96, 132, 133]). In state-space model identification however, most of the subspace approaches usually proposed in discrete time model. Only few reported on dealing with continuous time model [58, 80, 81, 126, 164]. The main difficulty in handling continuous time models is probably due to the presence of the derivative operator associated with the input and output signals [163].

1.2.4 Continuous Time System Identification

In general, the continuous time identification falls into two distinguish categories: The indirect approach and direct approach [162, 163]. The indirect approach basically view the situation at two points: First by using a non-parametric model like impulse response, step response or frequency response function [52,134,186]. Second step is to estimate continuous time parameters from the estimated discrete time model. This approach is possible as the continuous time Laplace operator s and the discrete time z operator is in relation as $s = \ln(z)/\Delta$, where Δ is the sampling period of the discrete time model. However this conversion may yields into complex arithmetics especially when the system is unstable. Furthermore, problems are also encountered in the choice of the sampling time Δ. A slow sampling time leads to loss of information, while a fast sampling time tends to cluster the poles of the discrete time model near $z = 1$. This results in numerical ill-conditioning [145]. Nevertheless, the use of frequency sampling filters approach has

shown promising achievement in overcoming the problems with slow dynamics and fast sampling rate (see some of the examples in [48, 49, 179–182]). The benefits from this approach will be one of the subject that will be researched in this thesis.

In contrast, the direct approach often approximates the derivative operator that is associated with input and output signal using a filter. The *State Variable Filter* (SVF) methods are one of the examples [183]. In a paper by Johannson and his colleagues, a filter of $f(s) = \frac{p}{s+p}$ is used [82]. However, this process of filtering results in a strong attenuation of signals above the cutoff frequency of $f(s)$ [57]. In avoiding those problems, the Laguerre filter is introduced [31, 57, 59]. The advantage of using the Laguerre filter avoids problem with differentiation in Laplace operator, leads to simple algebraic and is its ability to cope with process and measurement noise in an effective way due to its orthogonality functions. The research that will be carried out in this thesis will also use the benefits of Laguerre filter. Other than using filter approach, there are also reported direct approach using *Poisson Moment Function* (PMF) as can be referred in [15, 16, 47], using the $\delta-$operator model as can be referred in [66, 147] and using the random distribution approach as in [126].

Along the lines of subspace model identification, this research will perform an investigation over state-space model identification of near continuous time systems. A causal model is developed as to preserve its stability and offer suitability for online implementation of continuous time system identification. The scope will include research being performed from open-loop identification to closed-loop identification using the subspace methods. In addition, this research will involve both time domain data and frequency domain data. In all those, a verification over single input single output systems and multi-variable systems are carried out. To build a concrete platform, there are three important tools that contribute in developing the model: The Laguerre filters, frequency sampling filters and the instrumental variables.

1.3 Research Contributions

This thesis will provide novel and significant contributions listed as follows.

- The significant development of continuous time state-space models using subspace methods with application to multi-variable magnetic bearing systems.

- A novel approach in identification of multi-variable magnetic bearing systems by using subspace methods with adoption of Laguerre filters and instrumental variables for continuous time model.
- A novel approach in identification of continuous time systems by using future horizon for instrumental variables.
- A novel approach in identification of continuous time model in closed-loop operation using Laguerre filters and instrumental variables.
- The development of a novel continuous time model identification by combining the usage of frequency sampling filters, subspace methods and Laguerre filters.
- Significant contributions on design analysis via frequency response and step response observations.
- Significant contributions on design analysis for optimal instrumental variable and tuning parameters.
- Significant contributions on identification analysis over single-input-single-output and multi-input-multi-output systems with and without disturbances.

1.4 Publications and Presentations Arising from this Research

Journal Publications

Rosmiwati Mohd-Mokhtar and Liuping Wang, Continuous Time System Identification using Subspace Methods, *ANZIAM J.* Vol. 47, pp. 712-732, 2007.

Conference Publications

R. Mohd-Mokhtar, L. Wang, L. Qin and T. Barry, Continuous Time System Identification of Magnetic Bearing Systems using Frequency Response Data, *5th. Asian Control Conf.*, Melbourne, Australia, pp. 2066-2072, 2004.

Rosmiwati Mohd-Mokhtar and Liuping Wang, System Identification of MIMO Magnetic Bearing via Continuous Time and Frequency Response Data, *In Proc. of IEEE Int. Conf. on Mechatronics*, Taipei, Taiwan, pp. 191-196, 2005.

Rosmiwati Mohd-Mokhtar and Liuping Wang, Continuous Time State Space Model Identification using Closed-loop data, *2nd. Asia Int. Conf. on Modelling & Simulation*, Kuala Lumpur, Malaysia, pp. 812-817, 2008.

Rosmiwati Mohd-Mokhtar and Liuping Wang, 2-stage Approach for Continuous Time Identification using Step Response Estimates, *IEEE Int. Conf. on Systems, Man & Cybernetics*, Singapore, 2008. Published.

Rosmiwati Mohd-Mokhtar and Liuping Wang, Continuous Time System Identification using Subspace Methods, *7th. Annual EMAC Conf.*, Melbourne, Australia, 2005.

Rosmiwati Mohd-Mokhtar and Liuping Wang, A Review on Identification and Control Methodologies for Magnetic Bearing Systems, *Int. Conf. on Robotics, Vision, Information and Signal Processing*, Penang, Malaysia, pp. 232-236, 2005.

1.5 Thesis Outline

The remainder of this thesis composed of six chapters and briefly outline as follows.

Chapter 2 overviews the magnetic bearing systems, which discusses hardware and software configuration in a laboratory apparatus. The investigation is specifically for the test stand magnetic bearing system available at Royal Melbourne Institute of Technology University.

Chapter 3 discusses the procedures for building a state space model to identify the continuous time systems. A subspace method is used to develop the continuous time models with the aid of Laguerre filter and the instrumental variable. The instrumental variable component involves both of input and output components in which its purpose is to cope with process and measurement noise. The innovation of constructing filtered data matrices using differential equations provides better computation and easily maintainable parametrization. In addition, the use of causal Laguerre filters and instrumental variables has improved the quality of the model

in the presence of process and measurement noise. This causality condition also guarantees the filter stability. The performance of the proposed model is evaluated by identifying two systems: the simulated noise-free systems and the simulated noise-added systems. The identification procedure runs for both SISO and MIMO systems.

In Chapter 4 the thesis explores a subspace method that is used in identifying a state space model for a system operating in closed-loop. As a continuous time closed-loop identification is one of the prime subject, the Laguerre filter network is also used in the identification procedure. The regression matrix is based on past horizon. To maintain the stability and causality of the filter, the extended future horizon is used as instrumental variables and the matrix configurations are manipulated in such a way to satisfy the closed-loop conditions. There are two approaches that will be discussed in this chapter. First approach is based on *Error in Variable* (EIV) system identification and second approach is based on Gaussian reference signal method. This configuration will give consistent estimates for the deterministic part of the state space model.

Next in Chapter 5 the indirect identification procedure is proposed. The 2-stage identification procedure is performed. The first step is the identification of the system step response from the experimental data using the *Frequency Sampling Filter* (FSF) approach. This first stage is also referred as data compression stage in which the raw data will be analysed, the noise will be eliminated and the data is finally compressed into an empirical model of the analysed data. The second step is the identification of a continuous time state space model using subspace methods from the identified step response. The subspace identification algorithm used to identify the impulse response data now is used to identify the step response data. The key ingredients behind the FSF model is justified and the used of *Predicted REsidual Sums of Square* (PRESS) statistic and the orthogonal decomposition algorithm is also demonstrated. This approach provides with "clean" data and unbiased estimation towards closed-loop identification. Next, the open-loop identification using subspace methods leads to improved performance and better sensitivity and stability condition.

Chapter 6 discusses on continuous time state space model identification using subspace approach with respect to frequency response data. The strategy of implementing the subspace methods with additional $w-$operator has improved system performance and stability, as well as provided with better conditioning in regards with all the data matrices employed in the identification algorithm. In addition, the instrumental variables are also adopted to the algorithm with the

goal to cope with measurement noise. The performance capability of the proposed identification algorithm is justified with identifying model from sets of simulated noise-added data and a set of real data from MB systems. As for the MB data, the raw input and output data are first analysed using the FSF approach to obtain the frequency response estimates. This procedure will avoid the biased measurement with respect to direct frequency response obtained using FFT. The identification results show promising achievements for system identification overall.

Chapter 7 is a concluding chapter. The Chapter contains some remarks emphasizing the achieved goal, narrowing down the difficulties and suggesting the future research are stated in this chapter.

Chapter 2

Magnetic Bearing Systems

2.1 Introduction

Magnetic bearing (MB) is an essential tool in modern life as it consumes no mechanical contact and no lubrication, while providing high speed, high accuracy and high dynamic performance in numerous applications. It also guarantees low rotating loss and low maintenance cost as well as a longer life time. This technology rapidly grows and has been widely used in many applications such as semiconductor manufacturing equipment, chemical, oil and gas plantation, cryogenic equipment, machine tools and many more. In spite of all the advantages and useful contributions towards advanced and high-tech machinery and equipment, magnetic bearing however, is a mechanism with a high complexity therefore, to gain understanding of magnetic bearing systems demands knowledge on mechanical, electrical, electronics and control throughout.

As a kick start for identification and control in which the focus will be partially on magnetic bearing system application, it is better to have a brief overview about the magnetic bearing system configurations, requirements and related problems. Part of this Chapter is taken from author's review paper on identification and control for magnetic bearing systems [114]. This chapter will also discuss on magnetic bearing hardware and software configuration. This investigation specifically emphasizes the test stand magnetic bearing system available at Royal Melbourne Institute of Technology University. However, it can be applied to other magnetic bearing systems in general.

This chapter is organized as follows. In Section 2.3, the issues concerning magnetic bearing dynamics, stabilities and uncertainties are justified. Problems such as synchronous disturbance, eddy current effect, rotor unbalance, losses and many more may influence the performance of magnetic bearing system operation. Section 2.4 discusses on developing mathematical model and controller design of the magnetic bearing system. The magnetic bearing trade-off is also addressed in which it attracts attention towards the importance of researching into system identification and control of the magnetic bearing system. Section 2.5 gives some concluding remarks.

2.2 Investigation on Test Stand Magnetic Bearing Apparatus

Magnetic bearing system specification and configuration can be better studied and researched by installing the similar working apparatus in the laboratory. One in many examples is the development of test stand magnetic bearing apparatus. In general, there are four distinctive components that involved in the magnetic bearing system operation; the bearings which consist of the rotor and the electromagnetic actuator, position sensor, power amplifier and controller (see Figure 2.1). Its principle lies on the fact that the electromagnet (stator) will attract the ferrous material (rotor) of magnetic bearing. By using a stationary electromagnet and rotating ferrous material, a shaft is levitated in a magnetic field while maintaining accurate position of the shaft under varying loads.

Overall, MB system incorporates three distinct technologies: Bearings and sensors, control system and control algorithm. Bearings and sensors are electromechanical hardware in which the supporting forces are applied and input signals are collected from the installed machine. The control system provides the power and control electronics for signal conditioning, calculating of correcting forces and sends the resultant commands to the power amplifiers for each axis of control. On the other hand, control algorithms are software programs used in processing of the input signals after conditioning, and calculating the command signals before sending action to the power amplifiers [1]. Details on each of the component involved will be discussed in the following section.

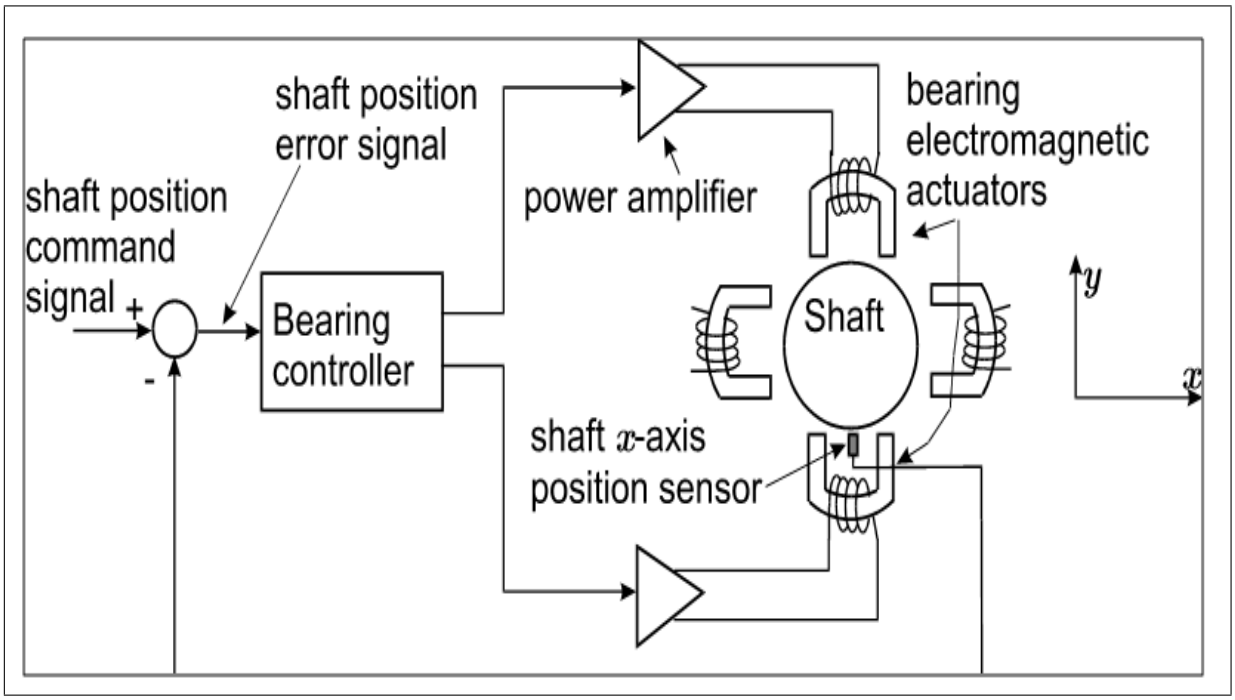

Figure 2.1: Magnetic bearing system

2.2.1 Two-sided Bearings

The two bearing actuators are employed to support a shaft on which a disk is fixed at the middle point and two journals are fixed at the end of the shaft [Refer to Figure 2.2]. In some technical applications, this prototype is more reliable as compared to single-sided bearings. By adding another identical magnet, it exerts forces in the opposite direction of each other. This configuration makes the bearing as gravity independent as well as improves the bearing dynamics since forces on the rotor can be exerted in both directions of each axis. Furthermore, the geometry condition of the rotor such as surface quality and the homogeneity of the material must be properly identified as a bad surface will results in noise disturbances, and geometry errors may cause disturbances on the rotational frequency [140].

The system has four coil currents which need to be manipulated, and four shaft displacement which need to be measured and controlled. During the rotating mode, all four parameters are involved and the model is gyroscopically coupled at a given running speed. Thus, it leads to 4×4 transfer function matrix and is dependent upon the running speed of the rotor. On the other hand, during the levitating only mode (assuming zero shaft speed), the dynamics in the $x - z$ plane and $y - z$ plane are assumed to be decoupled and identical. Since no cross coupling

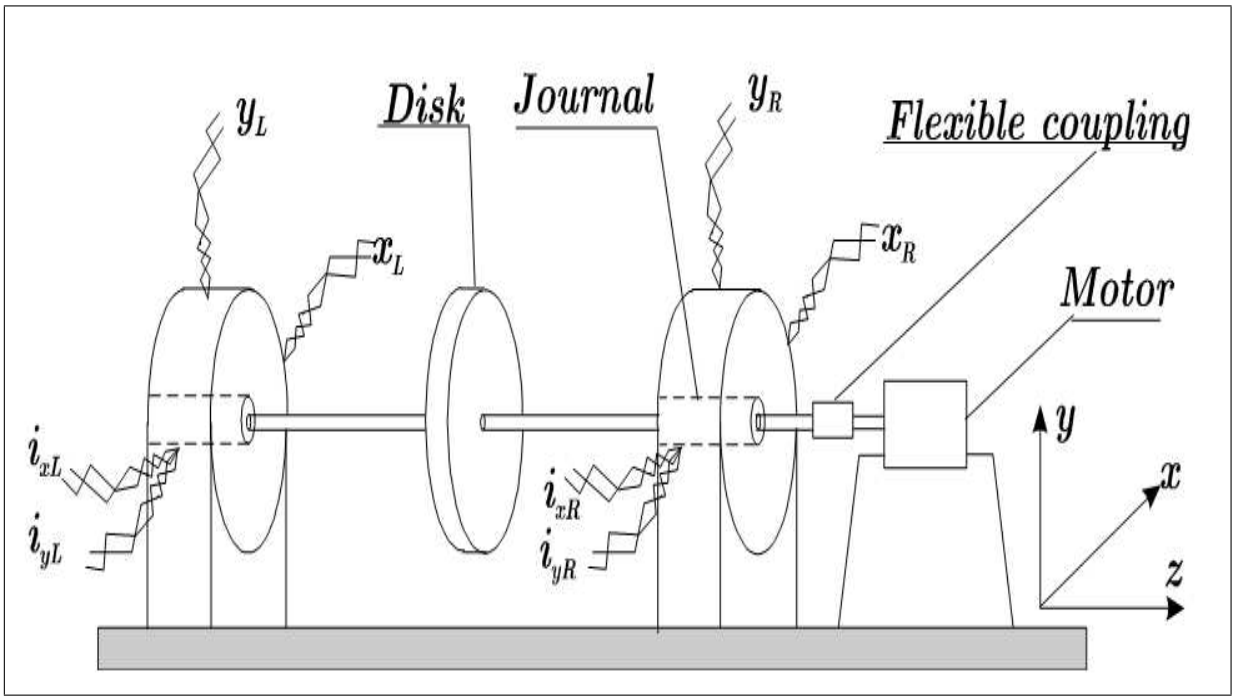

Figure 2.2: Schematic drawing for test-stand magnetic bearing apparatus

effects present, it leads in two separate dynamics systems which can be modelled as a 2×2 transfer function matrix.

2.2.2 Displacement Sensors

The efficiency of a magnetic bearing is very much dependent on the efficiency of the displacement sensors used. They measure the translational displacements of the rotor relative to the magnetic bearing stator, convert them into electrical voltage signal and pass the signal to the bearing control system component. Normally, the sensors are calibrated so that when the shaft is in the desired position, the sensors produce a null voltage. When the shaft is moved above this desired position, a positive voltage is produced and when it is moved below, a negative voltage results ($x-$axis). Same configuration involves as the shaft moves to the left or right direction ($y-$axis). Depending on the application of the magnetic bearing, different types of displacement sensors are used, for examples inductive displacement sensors, eddy-current sensors, capacitive displacement sensors, magnetic displacement sensors and optical displacement sensors [140]. For the test-stand that is available at RMIT University, it is equipped with the inductive displacement sensors.

2.2.3 Controllers

From the displacement sensors, the controllers receive the voltage signals, process the information and send current request to the amplifiers. First, the voltage signal is passed through the anti-aliasing filters to eliminate high frequency noise from the signal. This noise can cause the signal to inaccurately represent the position of the shaft. In addition, as the controller periodically samples the signal, some of the high-frequency information can "fold over" into false low frequency information, thus aliasing the information received by the controller.

Decades ago, the magnetic bearing controller design is based on analog control where hardwires and circuits are the working domain for controlling the MB systems. Their tolerance towards system changes is limited, and modifications or changes are difficult and expensive to make. The analog controllers have less flexibility in terms of manipulating, monitoring, diagnosing and treating the system easily. The introduction of digital controller into magnetic bearing system has really advanced the magnetic bearing control system [7, 20]. With digital processor that equipped with Analog to Digital (A-D) and Digital to Analog (D-A) converters, more advanced control algorithms and/or various additional control actions can be implemented as the system operation can now be monitored and diagnosed through software version and all the communications between human and apparatus are performed via the attached host computer.

Therefore, with the introduction of digital control, after the high frequency content is removed, the position signal is sampled by the A-D converter. This converts the voltage signal to a form that can be processed by the digital signal processor. The digital information is then passed through a digital filter and the output proportional to the amount of current required to correct the position error in the shaft is produced. The requested current is again compared, filtered and sampled through D-A converter before is sent to the amplifiers.

The development of the controllers for the magnetic bearing apparatus available at RMIT has been started off with analogue controller. At the early stage, the prototype of analog *Proportional Derivative* (P-D) control was used. After the introduction of digital control, the *Digital Signal Processor* (DSP) controller is used. This DSP controller was based on a fixed-point TMS320C25 produced by Texas Instrument Company [130]. However, the drawback of using this controller was that the difficulty of implementing the high order control algorithms. This was due to the

limitation on precision measure for the fixed-point DSP. Later, the fixed-point DSP has been replaced with TMS320C6701 floating point DSP [161]. This new controller configuration has suppressed the drawback that occurred before and thus, has allowed the implementation of more advanced control algorithms.

2.2.4 Power Amplifiers

From the controllers, the power amplifiers convert the control signals to control currents. Each bearing axis has a pair of amplifiers to provide current to the bearing coils and provide an attractive force to correct the position of the rotor along that particular axis [1]. There are two types of power amplifiers: analog amplifiers and switching amplifiers (also known as pulse width modulated amplifiers). The analog amplifiers have simple structure and are usually used for sensitive applications as well as applications that require moderate power. For the high power system requirement, the analog amplifiers will have limitation as high losses will influence very much the magnetic bearing system operation. Therefore, in applications with power above approximately 0.6kVA, switching amplifiers are exclusively used [140]. Apart from low losses in comparison with analog power amplifiers, the switching amplifiers also have its drawback as switching may cause electromagnetic disturbances due to oscillations in the current. However, the shorter the switching period, T, the weaker the oscillations in the current [140]. As for the magnetic bearing apparatus available in the laboratory, the analog power amplifiers are used.

2.3 Arising Issues in Magnetic Bearing System Operation

Apart from general information on how the magnetic bearing system is operated, one might wonder as well what kind of issues that may arise during the operation. With all the advantages of magnetic bearing as compared to conventional one, no doubt there are still technical issues that occur in magnetic bearing system operation and therefore have opened opportunity in researching, enhancing and upgrading its system performance. In this section, the issues are divided into two categories: the characteristic issues and the dynamics issues.

2.3.1 Characteristic Issues

The characteristic issues visualized on material behaviour and properties of the suspended (rotating) weight over the operating range (speed, acceleration, dynamic forces). The knowledge regarding these issues are highly desired especially during the magnetic bearing prototype design. There are few other features related to characteristic issues such as bearing load, size, temperature, carrying force and speed limit (circumferential and rotational), but four that will be discussed are iron losses, precision, damping and stiffness.

Iron Losses

Iron loss (or core loss) is a form of energy loss (mostly released as heat) due to a variety of mechanisms related to the fluctuating of magnetic field, such as hysteresis and eddy-currents. The hysteresis loss occurs in the ferromagnetic bearing bushes of the rotor. This loss depends on the structural shape, rotor speed, the material used for the bearing bushes, and the distribution of flux density, B, over the circumference of the bushes [140]. The hysteresis losses are somehow unavoidable, but a proper chosen material proportional to the speed requirement of the operating devices may help to reduce the losses. The eddy-currents are generated when the flux density within the iron core change. A compact core will generate large eddy-currents. To reduce the eddy-current losses, the iron core is usually divided into insulated or laminated sheets, or in particles (sinter cores).

Precision

Precision in magnetic bearing system operation means how precise can the position of the rotor axis be guaranteed. Whether rotating or not, the magnetic bearing levitate an object over the feedback control based on the position measurement from the displacement sensor. Precision control relies on the quality of a sensor signal and the displacement sensors are very sensitive to the surface quality. Therefore, for high precision, additional algorithms to detect and compensate the unnecessary signal contents induced by the geometric errors of the rotor are required [139].

Damping and Stiffness

Damping and stiffness are two important characteristics require for the magnetic bearing system and are determined by the controller. Without damping, the magnetic bearing systems will oscillate and become unstable. The required damping can be introduced using derivative control. The derivative component causes the gain to rise with frequency and causes the phase to rise to 90 degrees phase lead. This phase lead is associated with damping. On the other hand, the required stiffness can be introduced using integrative control. However the bearing stiffness is frequency dependent. Within the control frequency range, the stiffness is still held. Above the cut-off frequency of the controller, stiffness drops significantly before rising quadratically at higher frequencies due to inertia of the rotor [1, 140].

2.3.2 Rotor Dynamics

Rotor dynamics are another challenging issue that need a serious attention while dealing with magnetic bearing system apparatus. Two main contributors are the gyroscopic effects and rotor imbalance. The gyroscopic effect can be described as a dynamical changes to the system due to rotation while rotor imbalance is a dynamical changes to the system due to rotation over certain speed and frequency. Here, two important terms involved: moment of inertia and critical speed. In the field of rotor dynamics, moment of inertia (also called rotational inertia) refers to the fact that a rotating rigid body maintains its state of uniform rotational motion. Its angular momentum is unchanged, unless an external torque is applied [4]. However, due to inertia properties of the rotor, the bearing stiffness will drop significantly just after the cut-off frequency before rising quadratically at higher frequencies [140]. On the other hand, the critical speed is the theoretical angular velocity which excites the natural frequency of a screw or gear [2]. As the critical speed approaches the objects's natural frequency, its shaft begins to resonate which leads to excessive systemic vibration.

The rotor dynamic instability which responses to rotor imbalance will initiate synchronous vibration phenomena, whirling phenomena, transient disturbance and many more [169]. In practical, the rotor imbalance is never zero. It acts as a disturbance input on the rotor.

2.4 Control Engineering Perspective

In general, magnetic bearing is a mechatronic by-product that requires knowledge from mechanical, electrical, electronics, computer and control. As to control engineer's perspective, it may come to an agreement that the field of interest will possibly on modelling the systems and attempts to improve, upgrade and enhance the control system and control algorithm. Therefore, this section will elaborate on literature view over developing a model and implementation of control algorithms.

2.4.1 Building Mathematical Models

In block diagram, the magnetic bearing plant system can be illustrated as in Figure (2.3), where $r(t)$, $u(t)$, $u_c(t)$, $y(t)$, $v(t)$ and $h(t)$ are the reference input signal, input signal, output signal from controller, output signal, measurement noise and process noise respectively. The set point is the fixed command signal that will make correction (if any) with respect to the difference coming from the output system (displacement sensor). Obviously seen that the magnetic bearing system is a closed-loop system and the feedback mechanism is a must for the system to be in stable operation. With respect to magnetic bearing system realization, the strong motivation for modelling and identification lies behind two reasons. First, it gives clearer prediction over magnetic bearing dynamic properties under various operating conditions. Second, a precise parametric model of magnetic bearing plant is required for controller design [46]. The class of models can be classified into two categories: analytical models and empirical models. The analytical model or also known as physical modelling can be obtained for example by performing finite element analysis of the rotor, modal analysis of the rotor or static force measurement of the bearings. However this procedure has a few drawbacks as effects like eddy currents, hysteresis, and sensor/amplifier dynamics can not be assessed easily. The related measurements also can not be carried out with the assembled machine.

On the other hand, the empirical model is the model that obtained based on study and analysis of the input and output data collected from the system. This is also known as system identification. As compared to physical modelling, system identification gives more flexible approaches into the insights of the systems. A common model representation is a direct transfer function

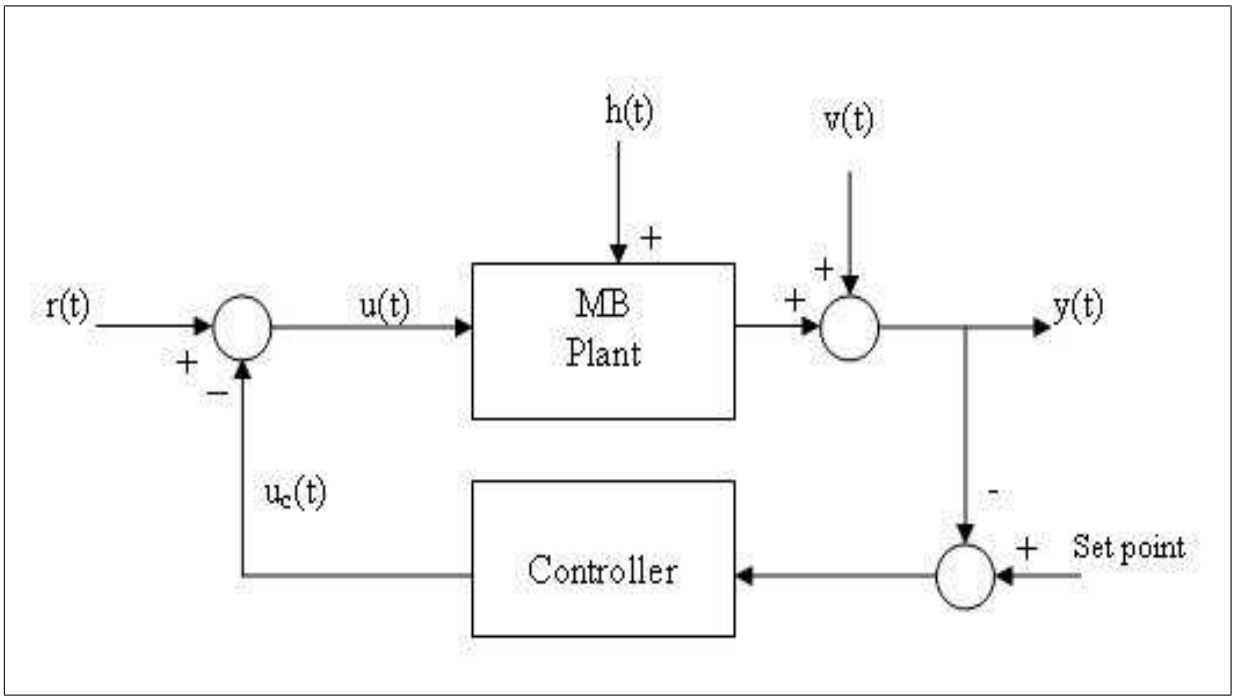

Figure 2.3: Magnetic bearing model

model which can be seen for example in [5,141]. Another quite popular mathematical model that can describe the magnetic bearing system in the form of matrix representation is a state-space model. Consider a continuous time model of a magnetic bearing system, which can be described by the following sets of equations.

$$\dot{x}(t) = Ax(t) + Bu(t) + h(t) \tag{2.1}$$

$$y(t) = Cx(t) + Du(t) + v(t) \tag{2.2}$$

$$u(t) = r(t) - u_c(t) \tag{2.3}$$

where $x(t) \in R^n$ is the state-vector, $u(t) \in R^m$ is the measured input signals and $y(t) \in R^l$ is the measured output signals. The signals $h(t) \in R^n$ and $v(t) \in R^l$ represent the process and measurement noise respectively. $A \in R^{n\times n}$, $B \in R^{n\times m}$, $C \in R^{l\times n}$ and $D \in R^{l\times m}$ are the system matrices. $\dot{x}$ means the time derivative of x. The identification of magnetic bearing system using this model formulation can be referred in [101,119,151,154]. Besides these two models, there are also reported formulations using neural network in the form of *Auto Regressive Moving Average* (ARMA) model as referred in [50] and Hamiltonian model as in [135].

With the same motivation and goal aiming as mentioned before, there are many approaches and methods that have been developed for the purpose of modelling and system identification.

For instance, the use of *Finite Element Method* (FEM) as in [9,22,36,75,185,190,191], *State Space Subspace System Identification* (4SID) method as in [151], extended influence coefficient method as in [88], eigenvalues move method as in [61], harmonic balance and curve fitting method as in [26, 27], fringing range method as in [131], adaptive forced balancing method as in [37], output inter-sampling scheme as in [154], *Multi-variable Output Error State Space* (MOESP) with *Instrumental Variable* (IV) method as in [115, 116, 119], semi-analytic calculation as in [110], modified least mean square (LMS) algorithm as in [89], using the linear wavelet parametrization as in [157], Genetic Algorithm as in [23,25], *Neural Network* (NN) model as in [50, 76] and fuzzy model as in [63, 65, 187].

For this thesis, the author is studied on subspace methods. This topic becomes subject of interest as the subspace identification algorithm requires no nonlinear parametric optimization and no iterative procedures, which makes them convenient for optimal estimation and control. Working together within state-space formulation, it offers the key advantages on providing low parameter sensitivity with respect to perturbations for high order systems. It also shows its ability to present multi-input and multi-output systems with minimal state dimensions.

2.4.2 Control System Design

As mentioned in previous section, rotor imbalance, rotor vibration, precision levitation, synchronous disturbance, stiffness and damping are related to dynamics, stabilities and uncertainties issues that always arise in magnetic bearing system especially when it has to be operated in high speed and high frequency range. Those issues are very much relied on control system and control algorithm. The magnetic bearing system is open loop unstable, therefore the feedback is compulsory in guaranteeing its stability, and the control algorithm which can be regarded as the "brain" and "heart" of overall MB functionality, plays an important role.

Proportional Derivative (P-D) control is the most common control method that is employed to magnetic bearing system. Here, the proportional feedback works as mechanical stiffness and the differential feedback coefficient as mechanical damping. The decentralized PD controllers are sufficient enough to make the rotor levitated at zero spinning speed [130]. However, PD controllers always have a steady state offset from the set point. This is due to the fact that the PD controllers only deliver a non-zero output if there is a position error. If the shaft is at

the requested set point the output of the controller would be zero because the error would be zero [1]. To overcome the problem, the *Integrator*, I, is added and PID controllers are introduced to the MB systems [74, 136].

Either PD or PID controllers, their performances on rotor stability can be acknowledged only when the system operates at low frequency range and is subjected to the bearing sensor, which is located in the middle of the bearing (collocated). As frequency increases, the transfer function gain will go to infinity. For the non-collocated bearing sensor, the shaft will start to oscillate because the sensor fails to see the correct motion of the bearing at high frequency. To solve the problem, higher ordered controller is necessary. Additional poles and zeros and notch filter are also placed in the control system in order to improve the control loop stability [46, 60].

To date, there are many control methods that have been proposed, for example H^{∞} control [43, 56, 105, 123, 153], $\mu-$ synthesis control [41, 42, 72, 122, 125], sliding mode control [28, 73, 155, 156, 158], Q-parameterization control [83, 94, 111–113], adaptive control [19, 98, 159, 184, 189], fuzzy control [8, 64, 71, 87, 143], neural network control [38, 77, 78, 124, 194] and many more. Some of these methods have shown good performances in addressing problems like rotor imbalance, gyroscopic effect, disturbances rejections, noises and plant uncertainties as compared to PID controller. However, while trying to solve the control problems, other issues such as, suffering from high order controller (e.g. in H^{∞} control), mismatch between reference model and true system, excessive gains etc. may arise.

Model predictive control (MPC) or *model-based predictive control* (MBPC) is another interesting topic in advanced control technique that has a significant and widespread impact on industrial process control [103, 176]. The idea of implementing the MPC has added another new methodology to a real application of MB plant system [67]. The research on this control method has drawn significant interest as MPC has shown ability to handle multi-variable control problems naturally, to operate closer to hard and soft constraints, and to take account of actuator limitations. These will facilitate advances on designing magnetic bearing control system with improved stability, robustness, reliability while addressing all the limitations and implementation issues that may occur in conventional control method.

2.4.3 Magnetic Bearing Systems Trade-off

No doubt, when the requirement for magnetic bearing to be operated in high speed and high frequency range as well as to cope with plant "elastic system", the need for high performance and robust model and control design is highly desired. Nevertheless, there are tradeoffs on control theory that one has to consider. For high performance, very high accuracy of the model is needed, while for high robustness, only low stiffness can be realized [140]. Searching for optimal balancing between the tradeoff is really crucial in magnetic bearing control design. Thus, this area is still open for research and exploration, and identification and control system design for magnetic bearing system become subject of interest.

2.5 Summary

This chapter has given on overview of magnetic bearing system apparatus. All the components involved with its functionality are briefly described. The issue that arises during magnetic bearing system operation is also discussed. The importance of research in identification and control of magnetic bearing system are addressed together with the literature review towards existing methods on identification and control of magnetic bearing systems. With the current standing technology of magnetic bearing system, the limitations still occur and advanced prototype according to market demand are highly desired. It has opened chances and room of improvement to researcher to deeply explore this challenging technology.

Chapter 3

Continuous Time Identification using Subspace Methods

3.1 Introduction

This chapter discusses on building a state-space model to identify the continuous time systems via time-domain approach. A subspace method is used to develop the identification model with the aid of Laguerre filter and the instrumental variable. This approach is partially influenced by the ideas of Yang [188] in conjunction with the work by Van Overschee and De Moor [164], and work by Haverkamp *et al.* [59], in which the subspace method with the aid of Laguerre filters and instrumental variable is used to identify a frequency response data. In Yang [188], the Laguerre filter is used to filter the data matrices and the instrumental variable matrix is constructed based on the higher order of the Laguerre filters. In other similar work reported by Haverkamp *et al.* [57, 58], the subspace method with the aid of the bilinear transformation of $w = \frac{s-p}{s+p}$ which also leads to the usage of Laguerre filters and instrumental variable is used in time domain system identification.

In this chapter, the role of Laguerre filters and the instrumental variables is studied. The use of Laguerre filter has overcome the problem with derivative operator that is associated with the input and output signals in continuous time system identification. The innovation of constructing filtered data matrices using differential equations provides better computation and

easily maintainable parametrization. In addition, the use of the instrumental variables have improved the quality of the model in the presence of process and measurement noise. The causality condition also guarantees the filter stability.

The content for this chapter is partially taken from a published paper by the author as can be referred in [116] with an addition where the identification is also performed to the multi-variable systems. The content of this chapter goes as follows. In Section 3.2 the approach using the bilinear transformation is discussed. This transformation will lead to the introduction of Laguerre filter. The role of this filter generates the sequence of filtered input and output signals. The subspace method for continuous time system identification developed in a state space model formulation will be discussed in Section 3.3. The framework of subspace state-space identification algorithm is also outlined in this section. Up to this point, the subspace method is successful in identifying the noise-free system. However, the estimation is biased when the noise is added to the system. This has led to the introduction of the instrumental variables, which will be discussed in Section 3.4. Also in this section, the experimental identification results are shown to illustrate the performance of the subspace method on identifying the noise-added continuous time systems for single input single output and multi-variable data systems. In addition, the capability of the proposed model is also evaluated by comparing the performance with other linear parametric models available in MATLAB system identification toolbox. Section 3.5 provides with some implementation issues that relate to developing accurate model and searching for optimal condition as to guarantee a successful system identification. Finally, Section 3.6 concludes the chapter.

3.2 Bilinear Transformation of State-space Models

In mathematical formulation, the continuous time system is given by the following state-space model equations

$$\dot{x}(t) = Ax(t) + Bu(t) \tag{3.1}$$

$$y(t) = Cx(t) + Du(t) \tag{3.2}$$

Here, $x(t) \in R^n$ is the state-vector, $u(t) \in R^m$ is the measured input signals and $y(t) \in R^l$ is the measured output signals. The $\dot{x}$ means the time derivative of x. The $x(t) \in R^n$, $u(t) \in R^m$

and $y(t) \in R^l$ are the model vectors. $A \in R^{n\times n}$, $B \in R^{n\times m}$, $C \in R^{l\times n}$ and $D \in R^{l\times m}$ are the system matrices. Their definitions and roles are as follow [165].

- $A \in R^{n\times n}$ is called the (dynamical) system matrix. It describes the dynamics of the system (as completely characterized by its eigenvalues).
- $B \in R^{n\times m}$ is the input matrix which represents the linear transformation by which the deterministic inputs influence the next state.
- $C \in R^{l\times n}$ is the output matrix which describes how the internal state is transferred to the outside world in the measurements of $y(t)$.
- $D \in R^{l\times m}$ is called the direct feed-through term. In continuous time systems this term is most often 0.

In the Laplace domain, these equations become

$$sX(s) = AX(s) + BU(s) \tag{3.3}$$

$$Y(s) = CX(s) + DU(s) \tag{3.4}$$

where

$$X(s) = \int_0^\infty x(t)e^{-st}dt$$
$$U(s) = \int_0^\infty u(t)e^{-st}dt$$
$$Y(s) = \int_0^\infty y(t)e^{-st}dt$$

As seen in Equations (3.1-3.2), the state-space model involves derivatives of the state variables. Thus, implementing this model like the discrete time counterpart will result in numerically unstable solutions. For instance, the time domain solution involves the differential operator as

$$\dot{x}(t) = \frac{x(t+\Delta t) - x(t)}{\Delta t}$$

in which this will amplify the noise, especially in higher frequencies. Therefore, in the literature of continuous time system identification, filters are used in the identification procedure (see for examples in [31, 59, 82, 183]).

The common approach to the estimation function model is to use a state variable filter which applies to the input and output data. The advantage of this approach is that the continuous

time parameters are found directly. However, it requires high order discrete time filters for the approximation of the differentiation operator. Scaling is often needed to prevent numerical problems with the filtered signals [57]. In addition, the use of discrete approximation somehow may amplify the noise in higher frequency regions, therefore certain mechanism need to be applied in order to achieve reliable estimation.

In the context of subspace continuous time system identification, a bilinear operator is used to replace the differentiation represented by the Laplace operator, s. In Johansson *et al.*, a filter of $f(s) = \frac{p}{s+p}$ is used [82]. However, as the model order increased, this process of filtering results in a strong attenuation of signals above the cutoff frequency of $f(s)$ [57]. Figure (3.1) illustrates the problem. On the other hand, the use of bilinear operator in the form of $w = \frac{s-p}{s+p}$ will also lead to the filtering of the input and output data. The system can be identified based on a state-space model in the w-operator. The obtained model can be transformed back to the common continuous time state-space model using simple algebraic relations.

The $w-$operator is actually playing a role as an all-pass filter. At any frequency range, this filter neither amplifies nor attenuates the signals. Figure (3.2) illustrates this condition. Since the frequency content of the signals remains unchanged, the additional scaling of the filtered signals is unnecessary. However, the condition of all-pass filter will not eliminate the high frequency noise. Thus, problem with high frequency noise still remains. Interestingly, the use of bilinear operator w leads to the use of Laguerre filters. The bode plot of frequency response based on Lagurre filter is shown in Figure (3.3). The use of Laguerre filter avoids problem with differentiation in Laplace operator, leads to simple algebraic relation and shows ability to cope with process and measurement noise in an effective way due to its orthogonality functions. This will be shown in more details in the following section.

3.2.1 $w-$operator and Laguerre Filter

The $w-$operator works in correlation between first order all-pass filter and Laguerre filter. This relation can be exploited in the identification of continuous time systems. The i-th continuous time Laguerre filter is given by

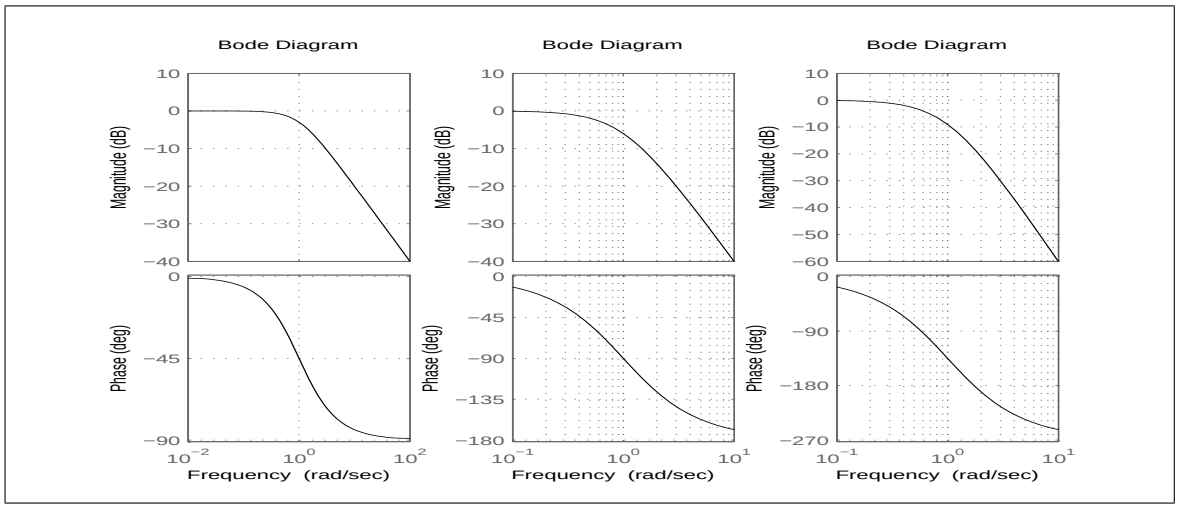

Figure 3.1: Bode diagram of 1st- 3rd order Johansson filters [82]

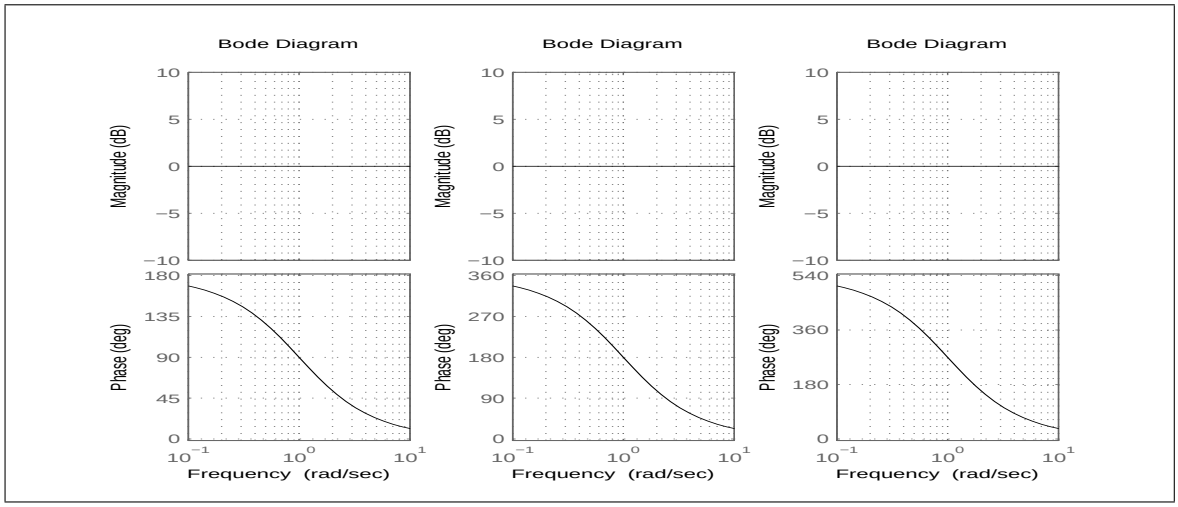

Figure 3.2: Bode diagram of 1st- 3rd order all-pass filters

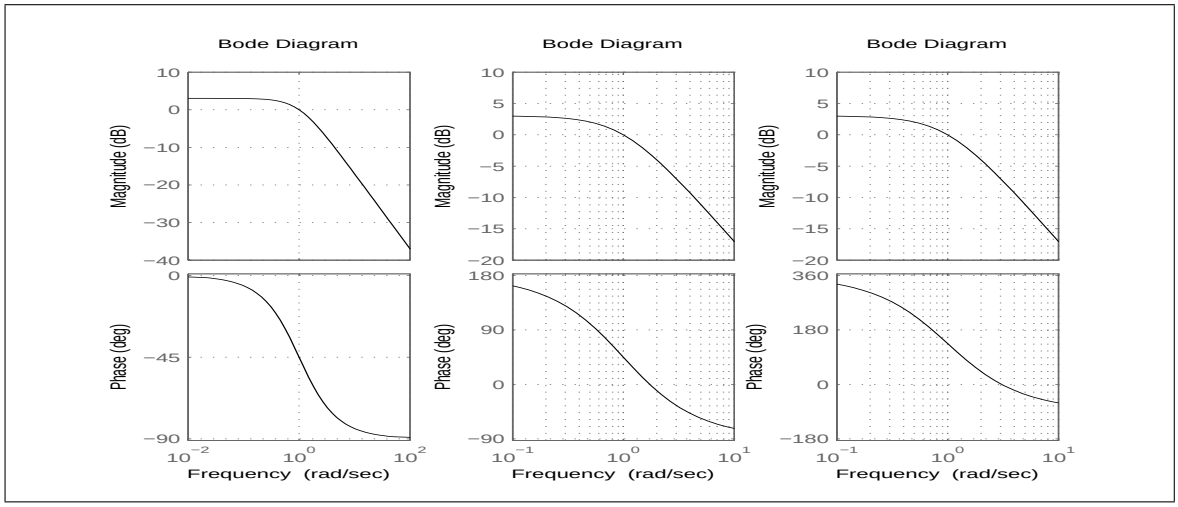

Figure 3.3: Bode diagram of 1st- 3rd order Laguerre filters

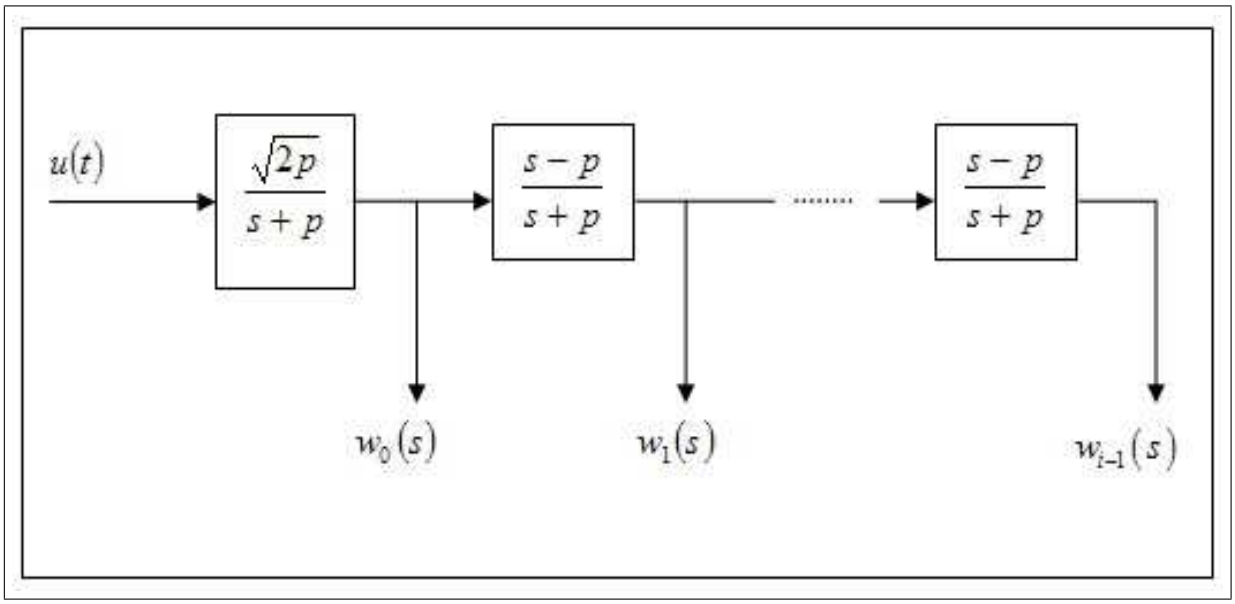

Figure 3.4: Laguerre filter network

$$L_\sigma(s) = \sqrt{2p}\frac{(s-p)^\sigma}{(s+p)^{\sigma+1}}, \qquad (\sigma = 0, 1, \ldots, i-1) \tag{3.5}$$

where $p > 0$ is the scaling factor to ensure that the filters are stable.

The structure of this filter bank is shown in Figure (3.4). The w-operator that corresponds to the all-pass filter has the form

$$w(s) = \frac{s-p}{s+p}, \quad s = p\frac{1+w}{1-w} \quad p > 0 \tag{3.6}$$

where

$$\begin{aligned} w &= \frac{s-p}{s+p} \\ w(s+p) &= s-p \\ ws+wp &= s-p \\ ws-s &= -p-wp \\ -s(1-w) &= -p(1+w) \\ s &= p\frac{1+w}{1-w} \end{aligned}$$

The notation of Laguerre filter in the form of $w-$operator is given by

$$L_\sigma(s) = w_0(s)w_\sigma(s), \qquad (\sigma = 1, \ldots, i-1) \tag{3.7}$$

where

$$w_0 = \frac{\sqrt{2p}}{s+p} \tag{3.8}$$

3.2.2 State-space Model Description

With $w-$operator been described as in Equation (3.6), now, substitute s with $p\frac{1+w}{1-w}$ in the state equation of (3.3) gives

$$\begin{aligned}
p\frac{1+w}{1-w}X(s) &= AX(s) + BU(s) \\
p(1+w)X(s) &= A(1-w)X(s) + B(1-w)U(s) \\
pX(s) + pwX(s) &= AX(s) - AwX(s) + B(1-w)U(s) \\
pwX(s) + AwX(s) &= AX(s) - pX(s) + B(1-w)U(s) \\
w(A+pI_n)X(s) &= (A-pI_n)X(s) + B(1-w)U(s) \\
wX(s) &= (A+pI_n)^{-1}(A-pI_n)X(s) + (A+pI_n)^{-1}B(1-w)U(s)
\end{aligned}$$

Solving for $1-w$,

$$\begin{aligned}
1-w &= 1 - \left(\frac{s-p}{s+p}\right) \\
&= \frac{s+p-s+p}{s+p} \\
&= \frac{2p}{s+p}
\end{aligned} \tag{3.9}$$

Substitute Equation (3.8) into Equation (3.9) gives

$$\begin{aligned}
1-w &= \frac{2p}{s+p} \\
&= \frac{2p}{\frac{\sqrt{2p}}{w_0}} \\
&= \sqrt{2p}w_0
\end{aligned}$$

Therefore now the state equation becomes

$$\begin{aligned}
wX(s) &= (A+pI_n)^{-1}(A-pI_n)X(s) + \sqrt{2p}(A+pI_n)^{-1}Bw_0U(s) \\
wX(s) &= A_wX(s) + B_ww_0U(s)
\end{aligned}$$

Thus, the A_w and B_w are obtained as

$$\begin{aligned}
A_w &= (A+pI_n)^{-1}(A-pI_n) \\
B_w &= \sqrt{2p}(A+pI_n)^{-1}B
\end{aligned}$$

Then, solve the output of state equation (3.4) as

$$\begin{aligned}
(1-w)Y(s) &= C(1-w)X(s) + D(1-w)U(s) \\
&= CX(s) - CwX(s) + D(1-w)U(s) \\
&= CX(s) - C[A_wX(s) + B_ww_0U(s)] + D(1-w)U(s) \\
&= CX(s) - CA_wX(s) - CB_ww_0U(s) + D(1-w)U(s) \\
\sqrt{2p}w_0Y(s) &= CX(s) - CA_wX(s) - CB_ww_0U(s) + \sqrt{2p}Dw_0U(s) \\
&= (C - CA_w)X(s) + (\sqrt{2p}D - CB_w)w_0U(s) \\
w_0Y(s) &= \frac{1}{\sqrt{2p}}(C - CA_w)X(s) + \frac{1}{\sqrt{2p}}(\sqrt{2p}D - CB_w)w_0U(s) \\
&= C_wX(s) + D_ww_0U(s)
\end{aligned}$$

which results in

$$\begin{aligned}
C_w &= \frac{1}{\sqrt{2p}}(C - CA_w) \\
&= \frac{1}{\sqrt{2p}}(C - C(A + pI_n)^{-1}(A - pI_n)) \\
&= \frac{1}{\sqrt{2p}}(C(A + pI_n)^{-1}(A + pI_n) - C(A + pI_n)^{-1}(A - pI_n)) \\
&= \frac{1}{\sqrt{2p}}(2pC(A + pI_n)^{-1}) \\
&= \sqrt{2p}C(A + pI_n)^{-1}
\end{aligned}$$

and,

$$\begin{aligned}
D_w &= \frac{1}{\sqrt{2p}}(\sqrt{2p}D - CB_w) \\
&= \frac{1}{\sqrt{2p}}(\sqrt{2p}D - C\sqrt{2p}(A + pI_n)^{-1}B) \\
&= D - C(A + pI_n)^{-1}B
\end{aligned}$$

Therefore, the model description in Equations (3.3-3.4) can be transformed into

$$wX(s) = A_wX(s) + B_ww_0U(s) \tag{3.10}$$

$$w_0Y(s) = C_wX(s) + D_ww_0U(s) \tag{3.11}$$

with

$$\begin{aligned}
A_w &= (A + pI_n)^{-1}(A - pI_n) \\
B_w &= \sqrt{2p}(A + pI_n)^{-1}B \\
C_w &= \sqrt{2p}C(A + pI_n)^{-1} \\
D_w &= D - C(A + pI_n)^{-1}B
\end{aligned} \tag{3.12}$$

Explicitly,

$$wX(s) = \frac{s-p}{s+p}X(s)$$
$$w_0Y(s) = \frac{\sqrt{2p}}{s+p}Y(s)$$
$$w_0U(s) = \frac{\sqrt{2p}}{s+p}U(s)$$

Note that the input signal and output signal are filtered by the first order filter. Thus, the state-space model equations can be rewritten as

$$[wx](t) = A_w x(t) + B_w[w_0 u](t) \tag{3.13}$$
$$[w_0 y](t) = C_w x(t) + D_w[w_0 u](t) \tag{3.14}$$

The transformation from A_w matrix to A matrix is given as

$$\begin{aligned} A_w &= (A + pI_n)^{-1}(A - pI_n) \\ (A + pI_n)A_w &= A - pI_n \\ AA_w + pA_w &= A - pI_n \\ pA_w + pI_n &= A - AA_w \\ p(I_n + A_w) &= A(I_n - A_w) \\ A &= p(I_n - A_w)^{-1}(I_n + A_w) \end{aligned}$$

B_w is transformed as

$$\begin{aligned} B_w &= \sqrt{2p}(A + pI_n)^{-1}B \\ \frac{1}{\sqrt{2p}}(A + pI_n)B_w &= B \\ B &= \frac{1}{\sqrt{2p}}[p(I_n - A_w)^{-1}(I_n + A_w) + pI_n]B_w \\ &= \frac{1}{\sqrt{2p}}[p(I_n - A_w)^{-1}(I_n + A_w) + p(I_n - A_w)^{-1}(I_n - A_w)]B_w \\ &= \frac{1}{\sqrt{2p}}[p(I_n - A_w)^{-1}[I_n + A_w + I_n - A_w]B_w] \\ &= \frac{1}{\sqrt{2p}}[2p(I_n - A_w)^{-1}B_w] \\ &= \sqrt{2p}(I_n - A_w)^{-1}B_w \end{aligned}$$

C_w is transformed as

$$\begin{aligned}
C_w &= \sqrt{2p}C(A+pI_n)^{-1} \\
C_w(A+pI_n) &= \sqrt{2p}C \\
\sqrt{2p}C &= C_w[p(I_n-A_w)^{-1}(I_n+A_w)+pI_n] \\
\sqrt{2p}C &= C_w[p(I_n-A_w)^{-1}(I_n+A_w)+p(I_n-A_w)^{-1}(I_n-A_w)] \\
\sqrt{2p}C &= C_w p(I_n-A_w)^{-1}[I_n+A_w+I_n-A_w] \\
\sqrt{2p}C &= 2pC_w(I_n-A_w)^{-1} \\
C &= \sqrt{2p}C_w(I_n-A_w)^{-1}
\end{aligned}$$

and D_w is transformed as

$$\begin{aligned}
D_w &= D - C(A+pI_n)^{-1}B \\
D &= D_w + C(A+pI_n)^{-1}B \\
&= D_w + \sqrt{2p}C_w(I_n-A_w)^{-1}[p(I_n-A_w)^{-1}(I_n+A_w)+pI_n]^{-1}\sqrt{2p}(I_n-A_w)^{-1}B_w \\
&= D_w + 2pC_w(I_n-A_w)^{-1}[p(I_n-A_w)^{-1}(I_n+A_w)+p(I_n-A_w)^{-1}(I_n-A_w)]^{-1} \\
&\times (I_n-A_w)^{-1}B_w \\
&= D_w + 2pC_w(I_n-A_w)^{-1}[p(I_n-A_w)^{-1}(I_n+A_w+I_n-A_w)]^{-1}(I_n-A_w)^{-1}B_w \\
&= D_w + 2pC_w(I_n-A_w)^{-1}[2p(I_n-A_w)^{-1}]^{-1}(I_n-A_w)^{-1}B_w \\
&= D_w + 2pC_w(I_n-A_w)^{-1}\frac{(I_n-A_w)}{2p}(I_n-A_w)^{-1}B_w \\
&= D_w + C_w(I_n-A_w)^{-1}B_w
\end{aligned}$$

In summary,

$$\begin{aligned}
A &= p(I_n-A_w)^{-1}(I_n+A_w) \\
B &= \sqrt{2p}(I_n-A_w)^{-1}B_w \\
C &= \sqrt{2p}C_w(I_n-A_w)^{-1} \\
D &= D_w + C_w(I_n-A_w)^{-1}B_w
\end{aligned} \tag{3.15}$$

3.2.3 Constructing Data Matrices

Based on the model description given in Equations (3.13-3.14), data equations are constructed as

$$\begin{aligned}
w_0 y(t) &= C_w x(t) + D_w w_0 u(t) \\
w_0 w y(t) &= C_w w x(t) + D_w w_0 w u(t) \\
&= C_w [A_w x(t) + B_w w_0 u(t)] + D_w w_0 w u(t) \\
&= C_w A_w x(t) + C_w B_w w_0 u(t) + D_w w_0 w u(t) \\
w_0 w^2 y(t) &= C_w A_w w x(t) + C_w B_w w_0 w u(t) + D_w w_0 w^2 u(t) \\
&= C_w A_w [A_w x(t) + B_w w_0 u(t)] + C_w B_w w_0 w u(t) + D_w w_0 w^2 u(t) \\
&= C_w A_w^2 x(t) + C_w A_w B_w w_0 u(t) + C_w B_w w_0 w u(t) + D_w w_0 w^2 u(t)
\end{aligned}$$

By repetitively multiplying with w, the data equations are rearranged as follows.

$$\begin{bmatrix} [w_0 y](t) \\ [w_1 y](t) \\ \vdots \\ [w_{i-1} y](t) \end{bmatrix} = \begin{bmatrix} C_w \\ C_w A_w \\ \vdots \\ C_w A_w^{i-1} \end{bmatrix} x(t) + \begin{bmatrix} D_w & 0 & \cdots & 0 \\ C_w B_w & D_w & \ddots & \vdots \\ \vdots & \ddots & \ddots & 0 \\ C_w A_w^{i-2} B_w & \cdots & C_w B_w & D_w \end{bmatrix} \begin{bmatrix} [w_0 u](t) \\ [w_1 u](t) \\ \vdots \\ [w_{i-1} u](t) \end{bmatrix} \tag{3.16}$$

Introduce the following notations

$$\mathcal{O}_j = \begin{bmatrix} C_w \\ C_w A_w \\ \vdots \\ C_w A_w^{j-1} \end{bmatrix}; \qquad \Gamma_j = \begin{bmatrix} D_w & 0 & \cdots & 0 \\ C_w B_w & D_w & \ddots & \vdots \\ \vdots & \ddots & \ddots & 0 \\ C_w A_w^{j-2} B_w & \cdots & C_w B_w & D_w \end{bmatrix}$$

where $\mathcal{O}_j$ is the extended observability matrix and Γ_j is the Toeplitz matrix. Now to make the problem more general, define the output as $Y_{i,j}^f(t)$ and the input as $U_{i,j}^f(t)$ give

$$Y_{i,j}^f(t) = \begin{bmatrix} [w_i y](t) \\ [w_{i+1} y](t) \\ \vdots \\ [w_{i+j-1} y](t) \end{bmatrix}; \qquad U_{i,j}^f(t) = \begin{bmatrix} [w_i u](t) \\ [w_{i+1} u](t) \\ \vdots \\ [w_{i+j-1} u](t) \end{bmatrix}$$

With these notations, the continuous time data equation can be rewritten in a compact form as follows

$$Y^f_{i,j}(t) = \mathcal{O}_j \hat{X}(t) + \Gamma_j U^f_{i,j}(t) \tag{3.17}$$

Using the sampled data at sampling times $t_1, t_2, \ldots, t_N$, the block of Hankel matrices are obtained as

$$Y^f_{i,j,N} = \begin{bmatrix} [w_i y](t_1) & [w_i y](t_2) & \ldots & [w_i y](t_N) \\ [w_{i+1} y](t_1) & [w_{i+1} y](t_2) & \ldots & [w_{i+1} y](t_N) \\ \vdots & \vdots & \vdots & \vdots \\ [w_{i+j-1} y](t_1) & [w_{i+j-1} y](t_2) & \ldots & [w_{i+j-1} y](t_N) \end{bmatrix} \tag{3.18}$$

$$U^f_{i,j,N} = \begin{bmatrix} [w_i u](t_1) & [w_i u](t_2) & \ldots & [w_i u](t_N) \\ [w_{i+1} u](t_1) & [w_{i+1} u](t_2) & \ldots & [w_{i+1} u](t_N) \\ \vdots & \vdots & \vdots & \vdots \\ [w_{i+j-1} u](t_1) & [w_{i+j-1} u](t_2) & \ldots & [w_{i+j-1} u](t_N) \end{bmatrix} \tag{3.19}$$

$$X_{i,N} = \begin{bmatrix} x(t_1) & x(t_2) & \ldots & x(t_N) \end{bmatrix} \tag{3.20}$$

With these matrices, the sampled data equation becomes

$$Y^f_{i,j,N}(t) = \mathcal{O}_j \hat{X}_{i,N}(t) + \Gamma_j U^f_{i,j,N}(t) \tag{3.21}$$

3.2.4 Constructing Filtered Data Matrices

Now that the data matrices are obtained, next issue is how to generate the filtered data matrices. With $w_i(t)$ denotes the time domain representation of the Laguerre filters, therefore $[w_i y](t)$ and $[w_i u](t)$ denotes the convolution of $y(t)$ and $u(t)$ with $w_i(t)$ in which are represented as

$$[w_i y](t) = \int_0^t w_i(t-\tau) y(\tau) d\tau$$
$$[w_i u](t) = \int_0^t w_i(t-\tau) u(\tau) d\tau$$

There are few ways that could be implemented in order to generate the Laguerre functions (see for details in [180]). Here, the numerical solution of the differential equations is used. Refer

back to Figure (3.4), the zero-th order Laguerre filter is described in differential equations as

$$\begin{aligned} W_0(s) &= \frac{\sqrt{2p}}{s+p} \\ (s+p)W_0(s) &= \sqrt{2p} \\ sW_0(s) + pW_0(s) &= \sqrt{2p} \\ \mathcal{L}^{-1}[sW_0(s) + pW_0(s)] &= \mathcal{L}^{-1}[\sqrt{2p}] \\ \dot{w}_0(t) + pw_0(t) &= \sqrt{2p} \\ \dot{w}_0(t) &= -pw_0(t) + \sqrt{2p} \end{aligned}$$

The first order Laguerre filter can be described as

$$\begin{aligned} \frac{W_1(s)}{W_0(s)} &= \frac{s-p}{s+p} \\ (s+p)W_1(s) &= (s-p)W_0(s) \\ sW_1(s) + pW_1(s) &= sW_0(s) - pW_0(s) \\ \mathcal{L}^{-1}[sW_1(s) + pW_1(s)] &= \mathcal{L}^{-1}[sW_0(s) - pW_0(s)] \\ \dot{w}_1(t) + pw_1(t) &= \dot{w}_0(t) - pw_0(t) \\ \dot{w}_1(t) &= -pw_1(t) + \dot{w}_0(t) - pw_0(t) \\ &= -pw_1(t) - pw_0(t) + \sqrt{2p} - pw_0(t) \\ &= -pw_1(t) - 2pw_0(t) + \sqrt{2p} \end{aligned}$$

By continuing generate the sequence for the $i-$th order, the equations are arranged in the following form:

$$\begin{bmatrix} \dot{w}_0(t) \\ \dot{w}_1(t) \\ \vdots \\ \dot{w}_{i-1}(t) \end{bmatrix} = \begin{bmatrix} -p & 0 & \dots & 0 \\ -2p & -p & \dots & 0 \\ \vdots & \ddots & \ddots & \vdots \\ -2p & \dots & -2p & -p \end{bmatrix} \begin{bmatrix} w_0(t) \\ w_1(t) \\ \vdots \\ w_{i-1}(t) \end{bmatrix} \tag{3.22}$$

with the initial conditions

$$\begin{bmatrix} w_0(0) \\ w_1(0) \\ \vdots \\ w_{i-1}(0) \end{bmatrix} = \sqrt{2p} \begin{bmatrix} 1 \\ 1 \\ \vdots \\ 1 \end{bmatrix} \tag{3.23}$$

Hence, a set of continuous time Laguerre functions can be found numerically by iteratively solving the following difference equations

$$\begin{bmatrix} w_0(t_{a+1}) \\ w_1(t_{a+1}) \\ \vdots \\ w_{i-1}(t_{a+1}) \end{bmatrix} \approx \begin{bmatrix} -p & 0 & \dots & 0 \\ -2p & -p & \dots & 0 \\ \vdots & \ddots & \ddots & \vdots \\ -2p & \dots & -2p & -p \end{bmatrix} \begin{bmatrix} w_0(t_a) \\ w_1(t_a) \\ \vdots \\ w_{i-1}(t_a) \end{bmatrix} \Delta t + \begin{bmatrix} w_0(t_a) \\ w_1(t_a) \\ \vdots \\ w_{i-1}(t_a) \end{bmatrix} \tag{3.24}$$

with

$$\begin{bmatrix} w_0(t_0) \\ w_1(t_0) \\ \vdots \\ w_{i-1}(t_0) \end{bmatrix} = \sqrt{2p} \begin{bmatrix} 1 \\ 1 \\ \vdots \\ 1 \end{bmatrix} \tag{3.25}$$

and $\Delta t = t_{a+1} - t_a$ being the integration step size (sampling rate).

As to generate the filtered input, and instead of performing a convolution, the data matrices can be developed via implementation of the solution of the differential equations

$$\begin{bmatrix} \dot{u}_{w_0}(t) \\ \dot{u}_{w_1}(t) \\ \vdots \\ \dot{u}_{w_{i-1}}(t) \end{bmatrix} = \begin{bmatrix} -p & 0 & \dots & 0 \\ -2p & -p & \dots & 0 \\ \vdots & \ddots & \ddots & \vdots \\ -2p & \dots & -2p & -p \end{bmatrix} \begin{bmatrix} u_{w_0}(t) \\ u_{w_1}(t) \\ \vdots \\ u_{w_{i-1}}(t) \end{bmatrix} + \sqrt{2p} \begin{bmatrix} 1 \\ 1 \\ \vdots \\ 1 \end{bmatrix} u(t) \tag{3.26}$$

Therefore, a set of filtered input can be generated numerically by iteratively solving the difference equations

$$\begin{aligned} \begin{bmatrix} u_0^f(t_{a+1}) \\ u_1^f(t_{a+1}) \\ \vdots \\ u_{i-1}^f(t_{a+1}) \end{bmatrix} \approx & \begin{bmatrix} u_0^f(t_a) \\ u_1^f(t_a) \\ \vdots \\ u_{i-1}^f(t_a) \end{bmatrix} + \begin{bmatrix} -p & 0 & \dots & 0 \\ -2p & -p & \dots & 0 \\ \vdots & \ddots & \ddots & \vdots \\ -2p & \dots & -2p & -p \end{bmatrix} \begin{bmatrix} u_0^f(t_a) \\ u_1^f(t_a) \\ \vdots \\ u_{i-1}^f(t_a) \end{bmatrix} \Delta t \\ & + \sqrt{2p} \begin{bmatrix} 1 \\ 1 \\ \vdots \\ 1 \end{bmatrix} u(t_a) \Delta t \end{aligned} \tag{3.27}$$

with zero initial condition of $u_i^f(t)$. The filtered output is also constructed in a similar way and is expressed as

$$\begin{bmatrix} y_0^f(t_{a+1}) \\ y_1^f(t_{a+1}) \\ \vdots \\ y_{i-1}^f(t_{a+1}) \end{bmatrix} \approx \begin{bmatrix} y_0^f(t_a) \\ y_1^f(t_a) \\ \vdots \\ y_{i-1}^f(t_a) \end{bmatrix} + \begin{bmatrix} -p & 0 & \dots & 0 \\ -2p & -p & \dots & 0 \\ \vdots & \ddots & \ddots & \vdots \\ -2p & \dots & -2p & -p \end{bmatrix} \begin{bmatrix} y_0^f(t_a) \\ y_1^f(t_a) \\ \vdots \\ y_{i-1}^f(t_a) \end{bmatrix} \Delta t$$
$$+ \sqrt{2p} \begin{bmatrix} 1 \\ 1 \\ \vdots \\ 1 \end{bmatrix} y(t_a)\Delta t \tag{3.28}$$

with zero initial condition of $y_i^f(t)$.

3.3 Subspace Methods for Estimating State-space Models

Consider now a problem to estimate the system matrices A, B, C and D in the state-space model. With the assumption that the state-space representation is a minimal realization, the input and output relationship expressed in Equations (3.1-3.2) can also be described by

$$\hat{x}(t+1) = T^{-1}AT\hat{x}(t) + T^{-1}Bu(t) \tag{3.29}$$
$$y(t) = CT\hat{t} + Du(t) \tag{3.30}$$

where $T \in R^n$ is any invertible matrix that correspond as $\hat{x} = T^{-1}x(t)$. To simplify the notation, define $\hat{A}$ as matrix A accurate to within similarity transform. Thus,

$$\hat{x}(t+1) = \hat{A}\hat{x}(t) + \hat{B}u(t) \tag{3.31}$$
$$y(t) = \hat{C}\hat{x}(t) + \hat{D}u(t) \tag{3.32}$$

The identification algorithm is developed based on the following information:

- The extended observability matrix can be estimated based on the availability of input signal $u(t)$ and output signal $y(t)$.

- The $\hat{A}$ and $\hat{C}$ matrices can be determined from the extended observability matrix

$$\mathcal{O}_j = \begin{bmatrix} C_w \\ C_w A_w \\ \vdots \\ C_w A_w^{j-1} \end{bmatrix}$$

- With the knowledge of $\hat{A}$ and $\hat{C}$, the matrices $\hat{B}$ and $\hat{D}$ can be estimated using a least squares solution from

$$\hat{y}(\ t \ \Big|\ B, D\ ) = \hat{C}(qI_n - \hat{A})^{-1}\hat{B}u(t) + \hat{D}u(t)$$

3.3.1 Estimating Extended Observability Matrix

Refer back to the Equation (3.21)

$$Y^f_{i,j,N}(t) = \mathcal{O}_j \hat{X}_{i,N}(t) + \Gamma_j U^f_{i,j,N}(t)$$

The next step is to isolate the $\mathcal{O}_j$ term using known data structures. Thus, the second term on the right-hand side need to be eliminated. Before doing so, the data equation notation is simplified for easier recognition and is defined as

$$\mathbf{Y} = \mathcal{O}_j \mathbf{X} + \Gamma_j \mathbf{U} \tag{3.33}$$

This second term on the right-hand side can be removed by introducing a projection on the null space of $\mathbf{U}$ which is defined as

$$\Pi^{\perp}_{\mathbf{U}^\top} = I - \mathbf{U}^\top(\mathbf{U}\mathbf{U}^\top)^{-1}\mathbf{U} \tag{3.34}$$

where I is the identity matrix. If $\mathbf{U}\mathbf{U}^\top$ is singular, then the Moore-Penrose pseudo-inverse of $\mathbf{U}^\top$ (denotes as $(\mathbf{U}^\top)^\dagger$) can be taken. Mathematically, it is equivalent to

$$\Upsilon^\dagger = (\Upsilon^\top\Upsilon)^{-1}\Upsilon^\top$$

The pseudo-inverse is computed recursively using singular value decomposition (SVD) describes as [53]

$$\Upsilon = USV^\top$$
$$\Upsilon^\dagger = VS^\dagger U^\top$$

Therefore equation (3.34) can be written as

$$\Pi_{\mathbf{U}^\top}^{\perp} = I - \mathbf{U}^\top(\mathbf{U}^\top)^\dagger$$

Multiply this projection on $\mathbf{U}$ gives

$$\begin{aligned}\mathbf{U}\Pi_{\mathbf{U}^\top}^{\perp} &= \mathbf{U} - (\mathbf{U}\mathbf{U}^\top(\mathbf{U}\mathbf{U}^\top)^{-1})\mathbf{U} \\ &= \mathbf{U} - I\mathbf{U} \\ &= 0\end{aligned}$$

Thus, by multiplying Equation (3.34) to both side of Equation (3.33), the term Γ_j will be removed as $\mathbf{U}\Pi_{\mathbf{U}^\top}^{\perp} = 0$. Therefore, the data equation reduces to

$$\mathbf{Y}\Pi_{\mathbf{U}^\top}^{\perp} = \mathcal{O}_j\mathbf{X}\Pi_{\mathbf{U}^\top}^{\perp} \tag{3.35}$$

Since $\mathbf{X}$ is unknown, an approximation of $\mathcal{O}_j$ must be determined. There are few ways on how to estimate the $\mathcal{O}_j$ matrix. Suppose that Equation (3.35) has $n \times n^*$ dimension, an estimate of $\mathcal{O}_j$ can be made using a singular value decomposition (SVD). Thus,

$$\mathbf{Y}\Pi_{\mathbf{U}^\top}^{\perp} = USV^\top = U\begin{bmatrix} s_1 & 0 & \dots & 0 \\ 0 & s_2 & \dots & 0 \\ \vdots & \vdots & \ddots & \vdots \\ 0 & 0 & \dots & s_{n^*} \\ 0 & 0 & \dots & 0 \\ \vdots & \vdots & \ddots & \vdots \\ 0 & 0 & \dots & 0 \end{bmatrix} V^\top$$

where U and V are orthogonal matrices of dimension $n \times n$ and $n^* \times n^*$ respectively such that $UU^\top = I$ and $VV^\top = I$. S is a $n \times n^*$ matrix with the singular values located along the diagonal and zeros elsewhere. Define the following matrices using MATLAB notation

$$U_1 = U(:, 1 : n^*) \tag{3.36}$$

$$S_1 = S(1 : n^*, :) \tag{3.37}$$

$$V_1^\top = V(:, 1 : n^*) \tag{3.38}$$

Therefore, without loss of information, the $\mathbf{Y}\Pi_{\mathbf{U}^\top}^{\perp}$ can be reconstructed from

$$\mathbf{Y}\Pi_{\mathbf{U}^\top}^{\perp} = U_1 S_1 V_1^\top$$

For some invertible matrix T of rank n^*,

$$\mathbf{Y}\Pi^{\perp}_{\mathbf{U}^\top} = \mathcal{O}_j T$$

Therefore, the following equalities is obtained as

$$\begin{aligned} \hat{\mathcal{O}}_j &\equiv U_1 \Lambda \\ \hat{T} &\equiv \Lambda_{-1} V_1^\top \end{aligned} \tag{3.39}$$

where Λ could be S_1, $S_1^{\frac{1}{2}}$ or I, and

$$\Lambda_{-1} = \begin{cases} I & \text{if} \quad \Lambda = S_1 \\ S_1^{\frac{1}{2}} & \text{if} \quad \Lambda = S_1^{\frac{1}{2}} \\ S_1 & \text{if} \quad \Lambda = I \end{cases}$$

The extended observability matrix $\mathcal{O}_j$ can be also estimated by performing the linear quadratic (LQ) factorization and SVD to the working matrices. In this thesis, the recursive quadratic (RQ) factorization using the modified Gram-Schmidt algorithm is used.

Let $L_i(s)$ be a bank of causal Laguerre filters ($p > 0$). Let $u(t)$ and $y(t)$ be the input and output plant data described in Equation (3.1) and Equation (3.2). Let $U^f_{0,i,N}$ and $Y^f_{0,i,N}$ be constructed from $u(t)$ and $y(t)$, according to Equation (3.18) and Equation (3.19).

Consider the RQ factorization

$$\begin{bmatrix} U^f_{0,i,N} \\ Y^f_{0,i,N} \end{bmatrix} = \begin{bmatrix} R_{11} & 0 \\ R_{21} & R_{22} \end{bmatrix} \begin{bmatrix} Q_1 \\ Q_2 \end{bmatrix}^\top \tag{3.40}$$

Then the following holds

$$R_{22} = \mathcal{O}_i \hat{X}_{0,N} Q_2^\top$$

Proof:

From the first row of RQ factorization

$$U^f_{0,i,N} = R_{11} Q_1^\top$$

From the second row,

$$\begin{aligned} Y^f_{0,i,N} &= R_{21}Q_1^\top + R_{22}Q_2^\top \\ Y^f_{0,i,N}Q_2^\top &= R_{21}Q_1Q_2^\top + R_{22}Q_2Q_2^\top \\ &= R_{22} \end{aligned}$$

as $Q_1Q_2^\top = 0$ *and* $Q_2Q_2^\top = I$. *From the data Equation* (3.21)

$$\begin{aligned} Y^f_{0,i,N}Q_2^\top &= \mathcal{O}_i\hat{X}_{0,N}Q_2^\top + \Gamma_i U^f_{0,i,N}Q_2^\top \\ &= \mathcal{O}_i\hat{X}_{0,N}Q_2^\top + \Gamma_i R_{11}Q_1Q_2^\top \\ &= \mathcal{O}_i\hat{X}_{0,N}Q_2^\top \end{aligned}$$

This completes the proof.

Now, perform the SVD to the working matrix R_{22}

$$R_{22} = \begin{bmatrix} U_n & U_0 \end{bmatrix} \begin{bmatrix} S_n & 0 \\ 0 & S_0 \end{bmatrix} \begin{bmatrix} V_n^\top \\ V_0^\top \end{bmatrix}$$

For $n-$th model order, the observability matrix is obtained based on

$$\hat{\mathcal{O}} = U_n(1:i, 1:n)$$

3.3.2 Estimating A and C Matrix

The next step now is to extract the state-space matrices A_w and C_w from the extended observability matrix $\mathcal{O}_j$, and transform it back to get the $\hat{A}$ and $\hat{C}$ matrices. The issue on estimating the $\hat{A}$ and $\hat{C}$ matrix for the state space model is not difficult and many possible solutions have been discussed in literature [84, 99, 102, 165]. First, recall back the continuous time subspace identification where the estimated extended observability matrix for the system is defined as

$$\hat{\mathcal{O}}_j = \begin{bmatrix} C_w \\ C_wA_w \\ C_wA_w^2 \\ \vdots \\ C_wA_w^{j-1} \end{bmatrix}$$

The value of C_w can be directly extracted from the first row of $\hat{\mathcal{O}}_j$. To compute the A_w, the shift property can be implemented by manipulating

$$\bar{\mathcal{O}}_j = \begin{bmatrix} C_w A_w \\ C_w A_w^2 \\ C_w A_w^3 \\ \vdots \\ C_w A_w^{j-1} \end{bmatrix}$$

In which

$$A_w = (\hat{\mathcal{O}}_j)^{\dagger} \bar{\mathcal{O}}_j$$

where $(\cdot)^{\dagger}$ denotes the Moore-Penrose pseudo-inverse [102].

On the other hand, this information can be obtained over the following notation

$$\begin{aligned} A_w &= (J_1 U_n)^{\dagger} J_2 U_n \\ C_w &= J_3 U_n \\ J_1 &= \begin{bmatrix} I_{(i-1)l} & 0_{(i-1)l \times l} \end{bmatrix} \\ J_2 &= \begin{bmatrix} 0_{(i-1)l \times l} & I_{(i-1)l} \end{bmatrix} \\ J_3 &= \begin{bmatrix} I_{l \times l} & 0_{l \times (i-1)l} \end{bmatrix} \\ \Upsilon^{\dagger} &= (\Upsilon^{\top} \Upsilon)^{-1} \Upsilon^{\top} \end{aligned}$$

where U_n is the first n-th column of U after performing the SVD [108, 109]. Next, the $\hat{A}$ and $\hat{C}$ can be obtained using the relations:

$$\begin{aligned} \hat{A} &= p(I_n + A_w)(I_n - A_w)^{-1} \\ \hat{C} &= \sqrt{2p} C_w (I_n - A_w)^{-1} \end{aligned}$$

3.3.3 Estimating B and D Matrix

If $\hat{A}$ and $\hat{C}$ are known, solving the linear least squares problem is the answer in order to estimate $\hat{B}$ and $\hat{D}$ using the following predictor [99]

$$\hat{y}(\ t \ \Big|\ B, D\ ) = \hat{C}(qI_n - \hat{A})^{-1} \hat{B} u(t) + \hat{D} u(t)$$

where

$$\begin{bmatrix} y(t_1) \\ y(t_2) \\ \vdots \\ y(t_N) \end{bmatrix} = \begin{bmatrix} \hat{C}(qI_n - \hat{A})^{-1}u(t_1) & I_l u(t_1) \\ \hat{C}(qI_n - \hat{A})^{-1}u(t_2) & I_l u(t_2) \\ \vdots & \vdots \\ \hat{C}(qI_n - \hat{A})^{-1}u(t_N) & I_l u(t_N) \end{bmatrix} \begin{bmatrix} \hat{B} \\ \hat{D} \end{bmatrix}$$

Define,

$$\varphi(t) = \begin{bmatrix} \hat{C}(qI_n - \hat{A})^{-1}u(t_1) & I_l u(t_1) \\ \hat{C}(qI_n - \hat{A})^{-1}u(t_2) & I_l u(t_2) \\ \vdots & \vdots \\ \hat{C}(qI_n - \hat{A})^{-1}u(t_N) & I_l u(t_N) \end{bmatrix}$$

Therefore,

$$\hat{y}(t) = \varphi(t)\theta$$

$$\hat{y}(t) = \varphi(t) \begin{bmatrix} \mathrm{Vec}(B) \\ \mathrm{Vec}(D) \end{bmatrix}$$

And,

$$\theta = (\varphi(t)^\top \varphi(t))^{-1} \varphi(t)^\top \hat{y}(t)$$

3.3.4 Identification Procedure

In summary, the subspace system identification is presented as follows. Given N data samples of a system with m inputs and l outputs,

1. Construct the filtered data matrices of $U^f_{0,i,N}$ and $Y^f_{0,i,N}$ according to Equation (3.18) and Equation (3.19).

2. Perform the RQ decomposition

$$\begin{bmatrix} U^f_{0,i,N} \\ Y^f_{0,i,N} \end{bmatrix} = \begin{bmatrix} R_{11} & 0 \\ R_{21} & R_{22} \end{bmatrix} \begin{bmatrix} Q_1 \\ Q_2 \end{bmatrix}$$

3. Perform the singular value decomposition to the working matrix R_{22}:

$$R_{22} = USV^\top$$

4. Determine the model order n from the singular value in S.

5. Determine the system matrices (A_w, C_w).

   $A_w = (J_1 U_n)^{\dagger} J_2 U_n$

   $C_w = J_3 U_n$

   $J_1 = \begin{bmatrix} I_{(i-1)l} & 0_{(i-1)l \times l} \end{bmatrix}$

   $J_2 = \begin{bmatrix} 0_{(i-1)l \times l} & I_{(i-1)l} \end{bmatrix}$

   $J_3 = \begin{bmatrix} I_{l \times l} & 0_{l \times (i-1)l} \end{bmatrix}$

   $\Upsilon^{\dagger} = (\Upsilon^{\top}\Upsilon)^{-1}\Upsilon^{\top}$

   The $\hat{A}$ and $\hat{C}$ can be obtained using the relations:

$$\begin{aligned} \hat{A} &= p(I_n + A_w)(I_n - A_w)^{-1} \\ \hat{C} &= \sqrt{2p} C_w (I_n - A_w)^{-1} \end{aligned}$$

6. Solve least squares problem from model structure:

$$y(\ t \ \Big|\ B, D\ ) = \hat{C}(qI_n - \hat{A})^{-1}\hat{B}u(t) + \hat{D}u(t)$$

7. Reconstruct B and D from $\begin{bmatrix} \hat{B} \\ \hat{D} \end{bmatrix}$

8. Generate the estimated output, $\hat{y}(t)$.

3.3.5 Simulation Results

Consider the sixth order plant model example presented in [164, 188]. The state space model is developed based on the following set up.

$$A_m = \begin{bmatrix} 0 & 1 & 0 & 0 & 0 & 0 \\ -1 & -0.2 & 0 & 0 & 0 & 0 \\ 0 & 0 & 0 & 1 & 0 & 0 \\ 0 & 0 & -25 & -0.5 & 0 & 0 \\ 0 & 0 & 0 & 0 & 0 & 1 \\ 0 & 0 & 0 & 0 & -9 & -0.12 \end{bmatrix}; \quad B_m = \begin{bmatrix} 0 \\ 1 \\ 0 \\ 1 \\ 0 \\ 1 \end{bmatrix}; \quad C_m = \begin{bmatrix} 1 \\ 0 \\ 1 \\ 0 \\ 1 \\ 0 \end{bmatrix}^{\top}; \quad D_m = [0];$$

The system and model specification can be referred in Table 3.1. The input signal, $u(t)$ is generated using a *Generalized Random Binary Signal* (GRBS) sequences. The plot of input and output data can be seen as in Figure (3.5). This data set is further divided into estimation data set and validation data set. The performance of the estimated model is assessed based on

Table 3.1: System and model configuration - SISO noise-free system

Symbol	Description	Value
G_m	System response	$[A_m, B_m, C_m, D_m]$
p	Laguerre parameter	1
i	Expanding observability matrix	10
n	Model order	6
Δt	Sampling time	0.001
N	Number of sampled data	4000
N_{est}	Estimation data	2000
N_{val}	Validation data	2000
V	Noise disturbance	NA

the fit between the measured output (grey) and the estimated (black) output. The results are illustrated in Figure (3.6). The Bode plot of the estimated frequency response (dashed line) is compared with the measured frequency response (solid line). The result is illustrated in Figure (3.7). From this figure, it shows that the subspace method can identify the noise-free system successfully. The estimated of (A, B, C, D) system matrices are given as

$$\hat{A} = \begin{bmatrix} -0.7390 & 5.9937 & 1.7313 & -1.2829 & -0.3322 & 0.7731 \\ -4.2122 & 0.1328 & -0.0621 & 3.2247 & 0.6086 & -1.2844 \\ 0.0024 & 0.1063 & -0.0732 & 4.8284 & 0.5739 & -1.2186 \\ 0.0014 & 0.0003 & -1.8391 & 0.0293 & -0.1229 & 0.4250 \\ 0.0000 & 0.0000 & -0.0001 & -0.0203 & -0.0284 & 1.0745 \\ 0.0000 & 0.0000 & -0.0000 & 0.0000 & -0.9311 & -0.1765 \end{bmatrix};$$

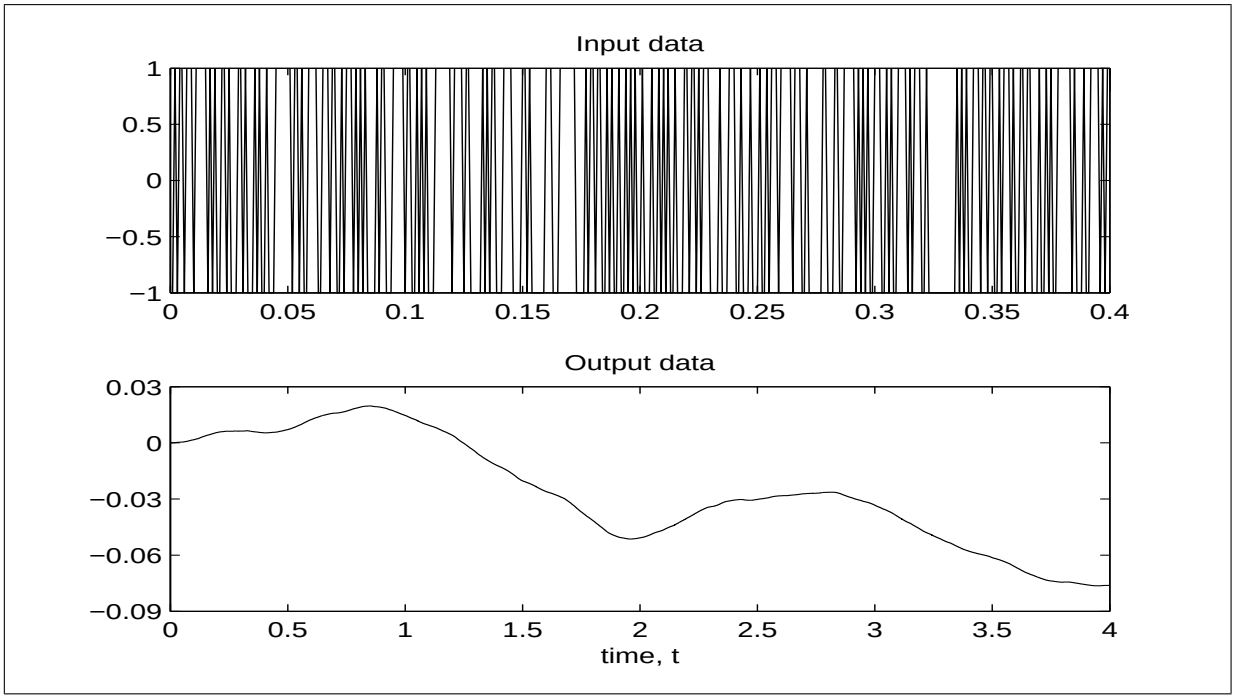

Figure 3.5: Plot of input & output - SISO noise-free system. (*Note*: The input data is re-scaled to only display 400 data points)

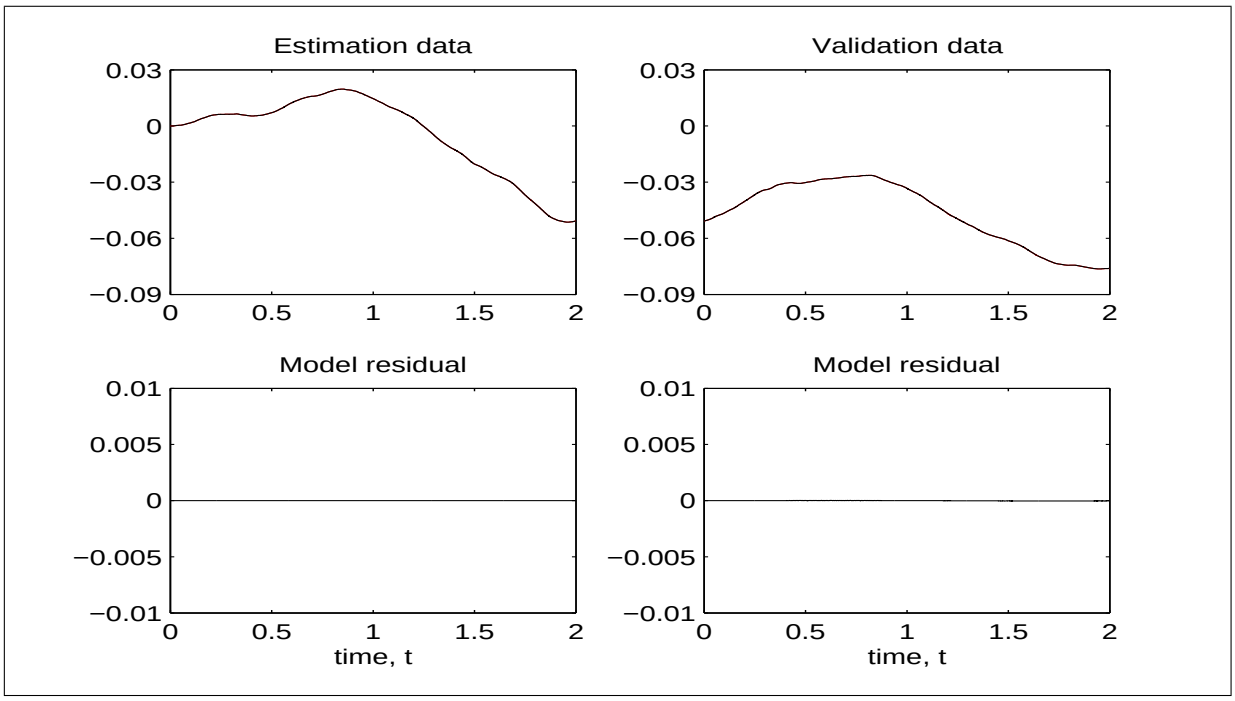

Figure 3.6: Superimposed of output data - SISO noise-free system. True system (dashed grey) & estimated model (solid black)

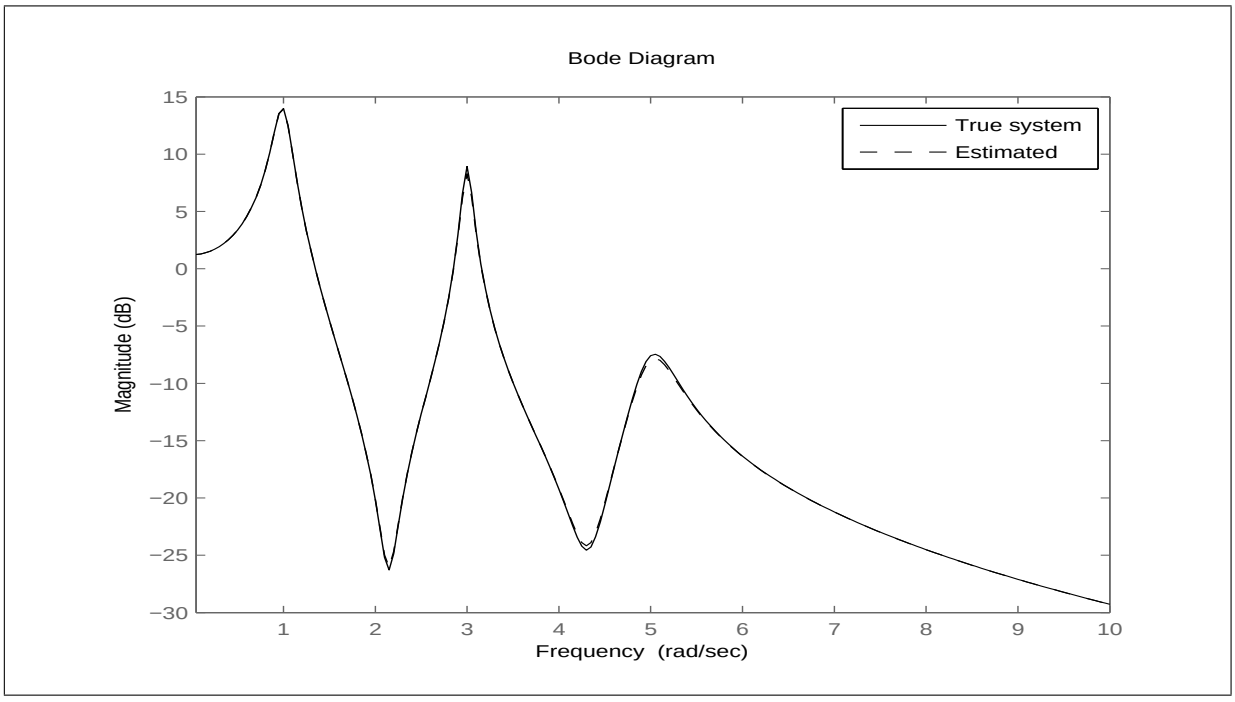

Figure 3.7: Superimposed of frequency response - SISO noise-free system

$$\hat{B} = \begin{bmatrix} 0.0449 \\ -0.0957 \\ 0.3490 \\ -0.8788 \\ 3.9007 \\ -0.4493 \end{bmatrix}; \qquad \hat{C} = \begin{bmatrix} 0.0335 \\ -1.5944 \\ -1.4136 \\ -1.0530 \\ -0.1265 \\ 0.2095 \end{bmatrix}^{\top}; \qquad \hat{D} = [0];$$

The transfer function of the system and the one generated from the estimated model is represented as

$$G_m(s) = \frac{3s^4 + 1.64s^3 + 70.184s^2 + 14.92s + 259}{s^6 + 0.82s^5 + 35.184s^4 + 14.932s^3 + 260.56s^2 + 52.5s + 225}$$
$$\hat{G}(s) = \frac{2.9983s^4 + 1.6784s^3 + 70.1526s^2 + 15.3497s + 258.8453}{s^6 + 0.8549s^5 + 35.1921s^4 + 15.4484s^3 + 260.5844s^2 + 53.1531s + 224.9071}$$

and the eigenvalues of A_m and $\hat{A}$ are:

$$\text{eig}(A_m) = [-0.1000 \pm 0.9950j; -0.2500 \pm 4.9937j; -0.0600 \pm 2.9994j]$$
$$\text{eig}(\hat{A}) = [-0.1005 \pm 0.9948j; -0.2624 \pm 4.9925j; -0.0645 \pm 2.9992j]$$

As seen, eigenvalues of $\hat{A}$ are very similar to eigenvalues of A_m.

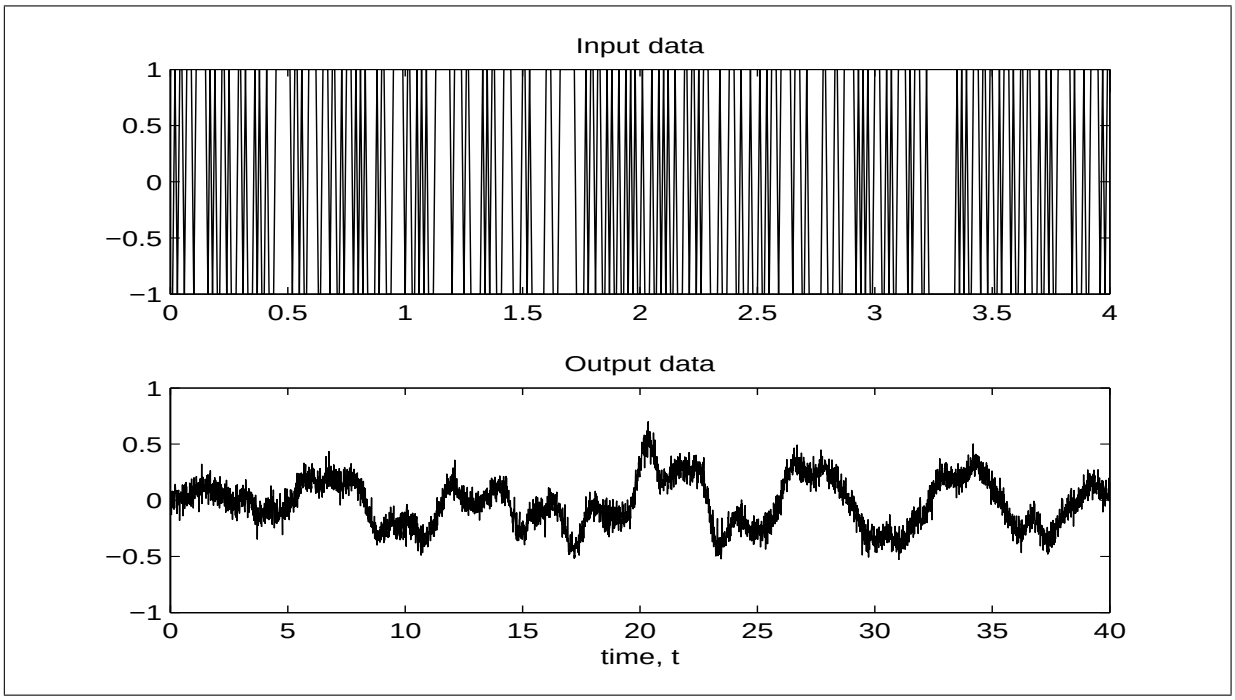

Figure 3.8: Plot of input & output - SISO noise-added system. (*Note*: The input data is re-scaled to only display 500 data points)

Now consider that the system is disturbed by the zero mean, white Gaussian process noise, $h(t)$ and zero mean, white Gaussian measurement noise, $v(t)$. The state-space model describes the system as

$$\dot{x}(t) = Ax(t) + Bu(t) + h(t) \tag{3.41}$$

$$y(t) = Cx(t) + Du(t) + v(t) \tag{3.42}$$

At the same sampling time of $\Delta t = 0.001s$, the model is unable to identify the system at all even for a very low noise disturbance. Thus, the sampling time is slower to $\Delta t = 0.01s$. For instance, the process noise, $h(t)$ and the measurement noise, $v(t)$ of about 20dB SNR is generated based on the following notation

$$h(t) = v(t) = 0.07 \times e(t);$$

where $e(t)$ are unit variance, zero-mean, white Gaussian noise. The "seed" value to generate the process noise, $h(t)$ is set to 1, whereas the "seed" value to generate the measurement noise, $v(t)$ is set to 2. Therefore, at sampling time $\Delta t = 0.01s$, about $N = 4000$ data is measured. The plot of the input and output is displayed in Figure (3.8). The data is further divided into two set, the estimation data, $N_{est} = 2000$ and the validation data, $N_{val} = 2000$. For this system identification, the Laguerre parameter, p is set equal to 6, the parameter to expand

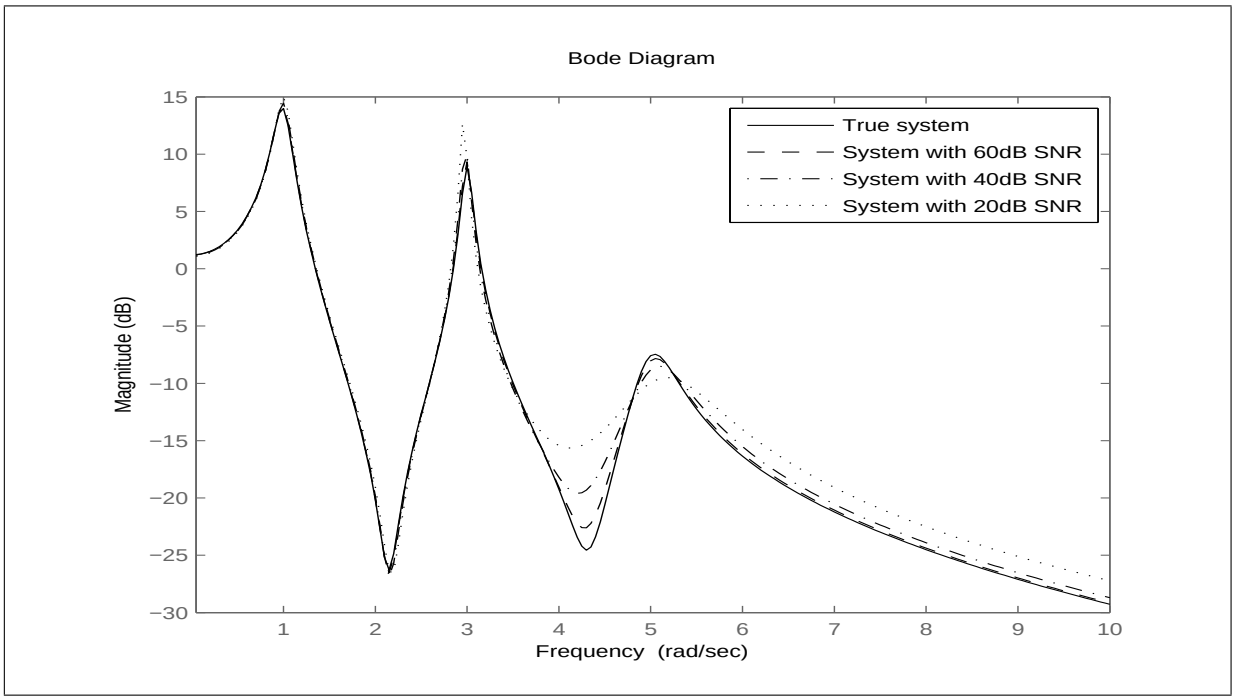

Figure 3.9: Superimposed of frequency response - SISO noise-added system

the row of the observability matrix, i is set equal to 10 and the model order, n is equal to 6. The subspace method to identify the noise-added system is shown in Figure (3.9). From this illustration, it shows that, for the noise-added system, the model can not identify the system closely anymore. We observed that Equation (3.35) will only produce a state space model with reasonable quality if the noise level in the system is sufficiently small. The model is still able to estimate the system at low frequency region but provide bias in the high frequency region. Therefore, another mechanism is needed in order to improve the model performance.

3.4 System Identification using Noisy Data

Consider again the state-space model represented by the following equations

$$\dot{x}(t) = Ax(t) + Bu(t) + h(t) \tag{3.43}$$

$$y(t) = Cx(t) + Du(t) + v(t) \tag{3.44}$$

where $x(t) \in R^n$ is the state-vector, $u(t) \in R^m$ is the measured input signals and $y(t) \in R^l$ is the measured output signals. The signals $h(t) \in R^n$ and $v(t) \in R^l$ represent the process and measurement noise respectively. $A \in R^{n \times n}$, $B \in R^{n \times m}$, $C \in R^{l \times n}$ and $D \in R^{l \times m}$ are the system

matrices. $\dot{x}$ means the time derivative of x. Notice now that, there are two terms added to the system model which represent the noise disturbance. Using Laplace transform, these state-space equations are defined as:

$$sX(s) = AX(s) + BU(s) + H(s) \tag{3.45}$$

$$Y(s) = CX(s) + DU(s) + V(s) \tag{3.46}$$

Now to adopt the $w-$oprator, substitute s with $p\frac{1+w}{1-w}$ in the state equation of (3.45) gives

$$\begin{aligned}
p\frac{1+w}{1-w}X(s) &= AX(s) + BU(s) + H(s) \\
p(1+w)X(s) &= A(1-w)X(s) + B(1-w)U(s) + (1-w)H(s) \\
pX(s) + pwX(s) &= AX(s) - AwX(s) + B(1-w)U(s) + (1-w)H(s) \\
pwX(s) + AwX(s) &= AX(s) - pX(s) + B(1-w)U(s) + (1-w)H(s) \\
w(A+pI_n)X(s) &= (A-pI_n)X(s) + B(1-w)U(s) + (1-w)H(s) \\
wX(s) &= (A+pI_n)^{-1}(A-pI_n)X(s) + (A+pI_n)^{-1}B(1-w)U(s) \\
&\quad + (A+pI_n)^{-1}(1-w)H(s) \\
&= (A+pI_n)^{-1}(A-pI_n)X(s) + \sqrt{2p}(A+pI_n)^{-1}Bw_0U(s) \\
&\quad + \sqrt{2p}(A+pI_n)^{-1}w_0H(s) \\
&= A_wX(s) + B_ww_0U(s) + w_0H_w(s)
\end{aligned}$$

where

$$H_w(s) = \sqrt{2p}(A+pI_n)^{-1}H(s)$$

Then, solve the output of state equation (3.46) as

$$\begin{aligned}
(1-w)Y(s) &= C(1-w)X(s) + D(1-w)U(s) + (1-w)V(s) \\
&= CX(s) - CwX(s) + D(1-w)U(s) + (1-w)V(s) \\
&= CX(s) - C[A_wX(s) + B_ww_0U(s) + w_0H_w(s)] + D(1-w)U(s) + (1-w)V(s) \\
&= CX(s) - CA_wX(s) - CB_ww_0U(s) - Cw_0H_w(s) + D(1-w)U(s) + (1-w)V(s) \\
\sqrt{2p}w_0Y(s) &= CX(s) - CA_wX(s) - CB_ww_0U(s) - Cw_0H_w(s) + \sqrt{2p}Dw_0U(s) + \sqrt{2p}w_0V(s) \\
&= (C-CA_w)X(s) + (\sqrt{2p}D - CB_w)w_0U(s) - Cw_0H_w(s) + \sqrt{2p}w_0V(s) \\
w_0Y(s) &= \frac{1}{\sqrt{2p}}(C-CA_w)X(s) + \frac{1}{\sqrt{2p}}(\sqrt{2p}D - CB_w)w_0U(s) - \frac{1}{\sqrt{2p}}Cw_0H_w(s) + w_0V(s) \\
&= C_wX(s) + D_ww_0U(s) + w_0V_w(s)
\end{aligned}$$

where

$$V_w(s) = \frac{1}{\sqrt{2p}} C H_w(s) + V(s)$$

Equation (3.43-3.44) is rewritten as

$$[wx](t) = A_w x(t) + B_w [w_0 u](t) + [w_0 h_w](t) \tag{3.47}$$

$$[w_0 y](t) = C_w x(t) + D_w [w_0 u](t) + [w_0 v_w](t) \tag{3.48}$$

Observing Equation (3.47-3.48) data equations are constructed as

$$\begin{aligned}
w_0 y(t) &= C_w x(t) + D_w w_0 u(t) + w_0 v_w(t) \\
w_0 w y(t) &= C_w w x(t) + D_w w_0 w u(t) + w_0 w v_w(t) \\
&= C_w [A_w x(t) + B_w w_0 u(t) + w_0 h_w(t)] + D_w w_0 w u(t) + w_0 w v_w(t) \\
&= C_w A_w x(t) + C_w B_w w_0 u(t) + C_w w_0 h_w(t) + D_w w_0 w u(t) + w_0 w v_w(t) \\
w_0 w^2 y(t) &= C_w A_w w x(t) + C_w B_w w_0 w u(t) + C_w w_0 w h_w(t) + D_w w_0 w^2 u(t) + w_0 w^2 v_w(t) \\
&= C_w A_w [A_w x(t) + B_w w_0 u(t) + w_0 h_w(t)] + C_w B_w w_0 w u(t) + C_w w_0 w h_w(t) \\
&+ D_w w_0 w^2 u(t) + w_0 w^2 v_w(t) \\
&= C_w A_w^2 x(t) + C_w A_w B_w w_0 u(t) + C_w A_w w_0 h_w(t) + C_w B_w w_0 w u(t) + C_w w_0 w h_w(t) \\
&+ D_w w_0 w^2 u(t) + w_0 w^2 v_w(t)
\end{aligned}$$

By repetitively multiplying with w, the data equations are rearranged as follows.

$$\begin{aligned}
\begin{bmatrix} [w_0 y](t) \\ [w_1 y](t) \\ \vdots \\ [w_{i-1} y](t) \end{bmatrix} &= \begin{bmatrix} C_w \\ C_w A_w \\ \vdots \\ C_w A_w^{i-1} \end{bmatrix} x(t) + \begin{bmatrix} D_w & 0 & \cdots & 0 \\ C_w B_w & D_w & \ddots & \vdots \\ \vdots & \ddots & \ddots & 0 \\ C_w A_w^{i-2} B_w & \cdots & C_w B_w & D_w \end{bmatrix} \begin{bmatrix} [w_0 u](t) \\ [w_1 u](t) \\ \vdots \\ [w_{i-1} u](t) \end{bmatrix} \\
&+ \begin{bmatrix} 0 & 0 & \cdots & 0 \\ C_w & 0 & \ddots & \vdots \\ \vdots & \ddots & \ddots & 0 \\ C_w A_w^{i-2} & \cdots & C_w & 0 \end{bmatrix} \begin{bmatrix} [w_0 h_w](t) \\ [w_1 h_w](t) \\ \vdots \\ [w_{i-1} h_w](t) \end{bmatrix} + \begin{bmatrix} [w_0 v_w](t) \\ [w_1 v_w](t) \\ \vdots \\ [w_{i-1} v_w](t) \end{bmatrix}
\end{aligned} \tag{3.49}$$

Introduce the new terms as

$$\Psi_j = \begin{bmatrix} 0 & 0 & \cdots & 0 \\ C_w & 0 & \ddots & \vdots \\ \vdots & \ddots & \ddots & 0 \\ C_w A_w^{j-2} & \cdots & C_w & 0 \end{bmatrix}; \quad H_{i,j}^f(t) = \begin{bmatrix} [w_i h_w](t) \\ [w_{i+1} h_w](t) \\ \vdots \\ [w_{i+j-1} h_w](t) \end{bmatrix}; \quad V_{i,j}^f(t) = \begin{bmatrix} [w_i v_w](t) \\ [w_{i+1} v_w](t) \\ \vdots \\ [w_{i+j-1} v_w](t) \end{bmatrix}$$

In compact form, Equation (3.49) can be rewritten as

$$Y_{i,j}^f(t) = \mathcal{O}_j \hat{X}(t) + \Gamma_j U_{i,j}^f(t) + \Psi_j H_{i,j}^f(t) + V_{i,j}^f(t) \tag{3.50}$$

Expanding the column matrices for N data samples, the equation becomes

$$Y_{i,j,N}^f(t) = \mathcal{O}_j \hat{X}_{i,N}(t) + \Gamma_j U_{i,j,N}^f(t) + \Psi_j H_{i,j,N}^f(t) + V_{i,j,N}^f(t) \tag{3.51}$$

where the data matrices of the two last terms in the equation are constructed as

$$H_{i,j,N}^f = \begin{bmatrix} [w_i h](t_1) & [w_i h](t_2) & \dots & [w_i h](t_N) \\ [w_{i+1} h](t_1) & [w_{i+1} h](t_2) & \dots & [w_{i+1} h](t_N) \\ \vdots & \vdots & \vdots & \vdots \\ [w_{i+j-1} h](t_1) & [w_{i+j-1} h](t_2) & \dots & [w_{i+j-1} h](t_N) \end{bmatrix} \tag{3.52}$$

$$V_{i,j,N}^f = \begin{bmatrix} [w_i v](t_1) & [w_i v](t_2) & \dots & [w_i v](t_N) \\ [w_{i+1} v](t_1) & [w_{i+1} v](t_2) & \dots & [w_{i+1} v](t_N) \\ \vdots & \vdots & \vdots & \vdots \\ [w_{i+j-1} v](t_1) & [w_{i+j-1} v](t_2) & \dots & [w_{i+j-1} v](t_N) \end{bmatrix} \tag{3.53}$$

In simplified notation, it becomes

$$\mathbf{Y} = \mathcal{O}_j \mathbf{X} + \Gamma_j \mathbf{U} + \Psi_j \mathbf{H} + \mathbf{V}$$

Now the second term of the right-hand side is removed by multiplying both side with $\Pi_{\mathbf{U}^\top}^\perp$ as defined by Equation (3.34). Therefore the equation reduces to

$$\mathbf{Y}\Pi_{\mathbf{U}^\top}^\perp = \mathcal{O}_j \mathbf{X}\Pi_{\mathbf{U}^\top}^\perp + \Psi_j \mathbf{H}\Pi_{\mathbf{U}^\top}^\perp + \mathbf{V}\Pi_{\mathbf{U}^\top}^\perp \tag{3.54}$$

The next task is to remove two noise terms on the right-hand side. This problem is solved by introducing the instrumental variables.

3.4.1 Instrumental Variable Method

The idea of using the instrumental variable (IV) in the subspace system identification has been proposed in more than a decade ago (see for examples in [10,93,168,174,175]). The instrumental variables are used as an instrument to remove the effect of the noise term, since the geometrical properties of the ordinary subspace equation was lost in the presence of noise term. Ideally, the instrumental variable approach lies on searching for one vector sequence that is correlated with the state/regression variable but uncorrelated with the noise term. Consider to multiply Equation (3.54) from the right by the instrumental variable define as P, and normalize by N such that

$$\frac{1}{N}\mathbf{Y}\Pi_{\mathbf{U}^\top}^{\perp}P^\top = \mathcal{O}_j\frac{1}{N}\mathbf{X}\Pi_{\mathbf{U}^\top}^{\perp}P^\top + \Psi_j\frac{1}{N}\mathbf{H}\Pi_{\mathbf{U}^\top}^{\perp}P^\top + \frac{1}{N}\mathbf{V}\Pi_{\mathbf{U}^\top}^{\perp}P^\top \tag{3.55}$$

The instrumental variable works to satisfy the following condition:

$$\lim_{N\to\infty}\frac{1}{N}\mathbf{H}\Pi_{\mathbf{U}^\top}^{\perp}P^\top = 0 \tag{3.56}$$

$$\lim_{N\to\infty}\frac{1}{N}\mathbf{V}\Pi_{\mathbf{U}^\top}^{\perp}P^\top = 0 \tag{3.57}$$

$$\operatorname{rank}\left(\lim_{N\to\infty}\frac{1}{N}\mathbf{X}\Pi_{\mathbf{U}^\top}^{\perp}P^\top\right) = n \tag{3.58}$$

In open-loop applications, the standard candidate of instrumental variable is the input signal, since it is uncorrelated with the noise and correlated with the state variable. Therefore, the three criteria for IV are met. However, in order to perform a direct estimate of the observability matrix $\mathcal{O}_j$, the instrumental variable should also be orthogonal to the input in Equation (3.51). Nevertheless, this requirement will mislead the compatibility of Equation (3.58).

A common approach to solve this problem is by dividing the data into two parts named as past and future terms. Past output horizon is obtained by constructing the data matrices from 0-th to $(i-1)$-th order and is represented by $Y_{0,i,N}$, while the future output horizon is obtained by constructing the data matrices from i-th to $(j-1)$-th order and is represented by $Y_{i,j,N}$. For instance, consider an output data matrices of discrete time systems. The block of Hankel matrix constructed for past and future output is defined as in Figure (3.10). Similar construction of data matrices is applied to past and future input and noise horizon, and will be represented as $U_{0,i,N}$, $U_{i,j,N}$, $H_{0,i,N}$, $H_{i,j,N}$, $V_{0,i,N}$ and $V_{i,j,N}$, respectively.

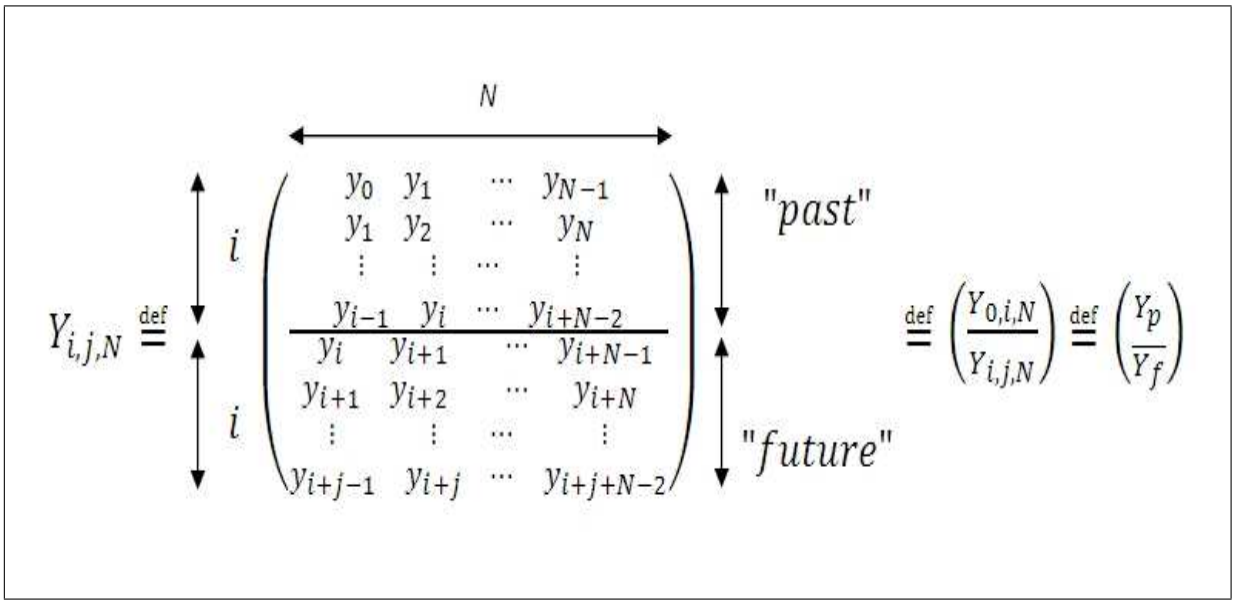

Figure 3.10: Data arrangement for past & future output [165]

There are three choices of instrumental variables defined as follows:

1. past/future input only
2. past/future output only
3. past/future input and output

The first choice is usually chosen for identification of a deterministic system. In broad definition, deterministic system is a system where both process or measurement noise is equal to zero. In circumstances where the noise-free real application sounds so impossible, this choice is still used if one is just interested to obtain the information regarding the transfer function and neglected the disturbance part.

The second choice is normally chosen for identification of a purely stochastic system, in which the system with only the output data is available ($u(t) = 0$). On the other hand, the third choice is chosen for the identification of a combined deterministic-stochastic system. This term represents most of the real application systems. In this system, the input and output data are available and the disturbance that may interrupt in the system is also acknowledged.

Discrete Time Subspace System Identification

In discrete time subspace system identification, the choice of instrumental variable is usually based on past data and the model is estimated over future outputs. This is due to the point that the discrete time subspace approach in $z-$operator is actually an anti-causal model, in which the output and the states is depended solely on future values. In the work by Verhaegen [171], the past inputs multi-variable output-error state space (PI-MOESP) was introduced. The first step of Verhaegen's PI-MOESP algorithm computes the following RQ factorization

$$\begin{bmatrix} U_{i,j,N} \\ U_{0,i,N} \\ Y_{i,j,N} \end{bmatrix} = \begin{bmatrix} R_{11} & 0 & 0 \\ R_{21} & R_{22} & 0 \\ R_{31} & R_{32} & R_{33} \end{bmatrix} \begin{bmatrix} Q_1 \\ Q_2 \\ Q_3 \end{bmatrix}$$

where the instrumental variable is defined as

$$P = \begin{bmatrix} U_{0,i,N} \end{bmatrix}$$

and the SVD is performed to the working matrix R_{32}.

$$[R_{32}] = USV^{\top}$$

However, this approach will only identify a purely deterministic system [175]. Any additional dynamics due to coloured disturbances are lost in the IV correlation.

In some applications, incorporating both deterministic and stochastic states is desired in order to form a complete state-space model. To fulfill the requirement of Equation (3.56) with n equals to the dimension of a complete state, the combination of past inputs and past outputs as instruments is proposed. This approach is proposed in [168, 174]. For instance, Verhaegen's PO (past outputs) MOESP algorithm computes the following RQ factorization

$$\begin{bmatrix} U_{i,j,N} \\ U_{0,i,N} \\ Y_{0,i,N} \\ Y_{i,j,N} \end{bmatrix} = \begin{bmatrix} R_{11} & 0 & 0 & 0 \\ R_{21} & R_{22} & 0 & 0 \\ R_{31} & R_{32} & R_{33} & 0 \\ R_{41} & R_{42} & R_{43} & R_{44} \end{bmatrix} \begin{bmatrix} Q_1 \\ Q_2 \\ Q_3 \\ Q_4 \end{bmatrix}$$

where the instrumental variable is defined as

$$P = \begin{bmatrix} U_{0,i,N} \\ Y_{0,i,N} \end{bmatrix}$$

and the SVD is performed to the working matrix $[\ R_{42} \quad R_{43}\ ]$.

$$[\ R_{42} \quad R_{43}\ ] = USV^{\top}$$

Continuous Time Subspace System Identification

In continuous time system identification where the Laguerre filters are adopted to overcome the derivatives problem in continuous time state-space model, the choice of instrumental variables requires some modifications. In here, two definition terms are involved, the causality and the stability. The system is said to be a causal system if the output at a certain time depends on the input up to that time only. In other words, the output and the states are depended only on the current and/or previous input values. Stability of the system is achieved when all poles are strictly on the left side of the $s-$plane.

The Laguerre filter is a causal model and the causality condition ($p > 0$) must be kept in order to remain its stability. As previously mentioned, the IVs that are based on past data are anti-causal. The problem now is how to solve the conflict between these two approaches. As discussed in [57, 58], the problem is solved by inverting the sequence of the samples data, therefore the anti-causal filter ($p < 0$) can be used. This work is possible for the off-line identification since the samples data are already recorded. From now on, the continuous time identification using anti-causal operator (both Laguerre and IVs) will be in close relation with the discrete time PO-MOESP algorithm in [174], where the $z-$operator is used, which is also an anti-causal operator.

In the extension of the approach in continuous time system, in which, if we want to keep the causal condition of the Laguerre filters, and without inverting the data sequence, the choice of output model and the IVs can be changed vice-versa. For instance, the regression matrix is developed based on the past input/output horizon and the instrumental variables are based on the future input/output horizon. This configuration will maintain the stability of a continuous time model which has been developed in parallel with the causality of the Laguerre filter.

Define the data matrices for the past and future filtered output as

$$
\begin{aligned}
Y^f_{0,i,N}(t) &= \begin{bmatrix} w_0 y(t_1) & w_0 y(t_2) & \cdots & w_0 y(t_N) \\ w_1 y(t_1) & w_1 y(t_2) & \cdots & w_1 y(t_N) \\ \vdots & \vdots & \cdots & \vdots \\ w_{i-1} y(t_1) & w_{i-1} y(t_2) & \cdots & w_{i-1} y(t_N) \end{bmatrix} \\
Y^f_{i,j,N}(t) &= \begin{bmatrix} w_i y(t_1) & w_i y(t_2) & \cdots & w_i y(t_N) \\ w_{i+1} y(t_1) & w_{i+1} y(t_2) & \cdots & w_{i+1} y(t_N) \\ \vdots & \vdots & \cdots & \vdots \\ w_{i+j-1} y(t_1) & w_{i+j-1} y(t_2) & \cdots & w_{i+j-1} y(t_N) \end{bmatrix}
\end{aligned} \tag{3.59}
$$

And the past and future filtered input as

$$
\begin{aligned}
U^f_{0,i,N}(t) &= \begin{bmatrix} w_0 u(t_1) & w_0 u(t_2) & \cdots & w_0 u(t_N) \\ w_1 u(t_1) & w_1 u(t_2) & \cdots & w_1 u(t_N) \\ \vdots & \vdots & \cdots & \vdots \\ w_{i-1} u(t_1) & w_{i-1} u(t_2) & \cdots & w_{i-1} u(t_N) \end{bmatrix} \\
U^f_{i,j,N}(t) &= \begin{bmatrix} w_i u(t_1) & w_i u(t_2) & \cdots & w_i u(t_N) \\ w_{i+1} u(t_1) & w_{i+1} u(t_2) & \cdots & w_{i+1} u(t_N) \\ \vdots & \vdots & \cdots & \vdots \\ w_{i+j-1} u(t_1) & w_{i+j-1} u(t_2) & \cdots & w_{i+j-1} u(t_N) \end{bmatrix}
\end{aligned} \tag{3.60}
$$

The instrumental variables constructed using future input and future output data are defined as

$$
P = \begin{bmatrix} U^f_{i,j,N} \\ Y^f_{i,j,N} \end{bmatrix} \tag{3.61}
$$

Now multiply again Equation (3.54) with the IV matrix, P will obtain

$$
\mathbf{Y}\Pi^{\perp}_{\mathbf{U}^\top} P^\top = \mathcal{O}_j \mathbf{X} \Pi^{\perp}_{\mathbf{U}^\top} P^\top \tag{3.62}
$$

since the IV term is independent of the noise terms, $\mathbf{H}$ and $\mathbf{V}$, therefore these noise terms disappeared.

$$
\Psi_j \mathbf{H} \Pi^{\perp}_{\mathbf{U}^\top} P^\top = 0
$$

$$
\mathbf{V}\Pi^{\perp}_{\mathbf{U}^\top} P^\top = 0
$$

From this point, the direct estimation of observability matrix can be obtained using SVD and the A, B, C and D matrices can be estimated after that.

3.4.2 Initial Condition, $x(0)$

In many cases, the initial condition of state variable of the state-space model is assumed not to influent much to the whole model development, therefore it is usually set to zero. In this chapter, the subspace methods have been developed with another additional term named as $\Phi_{0,i,N}$ in which the purpose is to filter the initial states condition. Consider again the state-space equations in Laplace domain

$$sX(s) = AX(s) + BU(s) + H(s) + x(0) \tag{3.63}$$

$$Y(s) = CX(s) + DU(s) + V(s) \tag{3.64}$$

Substitute $s = p\frac{1+w}{1-w}$ in the state equation gives

$$wX(s) = A_w X(s) + B_w w_0 U(s) + w_0 H_w(s) + K_1 w_0 x(0)$$

where

$$K_1 = \sqrt{2p}(A + pI_n)^{-1}$$

The output equation gives

$$w_0 Y(s) = C_w X(s) + D_w w_0 U(s) + w_0 V_w(s) + K_2 w_0 x(0)$$

where

$$K_2 = \sqrt{2p}C(A + pI_n)^{-1}$$

Translating back the result into time domain form gives

$$wx(t) = A_w x(t) + B_w w_0 u(t) + w_0 h_w(t) + K_1 x(0) w_0(t) \tag{3.65}$$

$$w_0 y(t) = C_w x(t) + D_w w_0 u(t) + w_0 v_w(t) + K_2 x(0) w_0(t) \tag{3.66}$$

Expanding the row by multiplying with $w-$operator results in the following continuous time

data equation

$$\begin{bmatrix} [w_0 y](t) \\ [w_1 y](t) \\ \vdots \\ [w_{i-1} y](t) \end{bmatrix} = \begin{bmatrix} C_w \\ C_w A_w \\ \vdots \\ C_w A_w^{i-1} \end{bmatrix} x(t) + \begin{bmatrix} D_w & 0 & \cdots & 0 \\ C_w B_w & D_w & \ddots & \vdots \\ \vdots & \ddots & \ddots & 0 \\ C_w A_w^{i-2} B_w & \cdots & C_w B_w & D_w \end{bmatrix} \begin{bmatrix} [w_0 u](t) \\ [w_1 u](t) \\ \vdots \\ [w_{i-1} u](t) \end{bmatrix}$$
$$+ \begin{bmatrix} 0 & 0 & \cdots & 0 \\ C_w & 0 & \ddots & \vdots \\ \vdots & \ddots & \ddots & 0 \\ C_w A_w^{i-2} & \cdots & C_w & 0 \end{bmatrix} \begin{bmatrix} [w_0 h_w](t) \\ [w_1 h_w](t) \\ \vdots \\ [w_{i-1} h_w](t) \end{bmatrix} + \begin{bmatrix} [w_0 v_w](t) \\ [w_1 v_w](t) \\ \vdots \\ [w_{i-1} v_w](t) \end{bmatrix}$$
$$+ \begin{bmatrix} K_2 x_0 & 0 & \cdots & 0 \\ C_w K_1 x_0 & K_2 x_0 & \ddots & \vdots \\ \vdots & \ddots & \ddots & 0 \\ C_w A_w^{i-2} K_1 x_0 & \cdots & C_w K_1 x_0 & K_2 x_0 \end{bmatrix} \begin{bmatrix} w_0(t) \\ w_1(t) \\ \vdots \\ w_{i-1}(t) \end{bmatrix} \tag{3.67}$$

Introduce the two new terms as

$$Z_j = \begin{bmatrix} K_2 x_0 & 0 & \cdots & 0 \\ C_w K_1 x_0 & K_2 x_0 & \ddots & \vdots \\ \vdots & \ddots & \ddots & 0 \\ C_w A_w^{j-2} K_1 x_0 & \cdots & C_w K_1 x_0 & K_2 x_0 \end{bmatrix} \qquad \Phi_{i,j}(t) = \begin{bmatrix} w_i(t) \\ w_{i+1}(t) \\ \vdots \\ w_{i+j-1}(t) \end{bmatrix}$$

In compact form, Equation (3.67) can be rewritten as

$$Y_{i,j}^f(t) = \mathcal{O}_j \hat{X}(t) + \Gamma_j U_{i,j}^f(t) + \Psi_j H_{i,j}^f(t) + V_{i,j}^f(t) + Z_j \Phi_{i,j}(t) \tag{3.68}$$

Expanding the column matrices of Equation (3.67) for N data samples, the equation becomes

$$Y_{i,j,N}^f(t) = \mathcal{O}_j \hat{X}_{i,N}(t) + \Gamma_j U_{i,j,N}^f(t) + \Psi_j H_{i,j,N}^f(t) + V_{i,j,N}^f(t) + Z_j \Phi_{i,j,N}(t) \tag{3.69}$$

where the Laguerre filter data equation is represented as

$$\Phi_{i,j,N} = \begin{bmatrix} w_i(t_1) & w_i(t_2) & \dots & w_i(t_N) \\ w_{i+1}(t_1) & w_{i+1}(t_2) & \dots & w_{i+1}(t_N) \\ \vdots & \vdots & \dots & \vdots \\ w_{i+j-1}(t_1) & w_{i+j-1}(t_2) & \dots & w_{i+j-1}(t_N) \end{bmatrix} \tag{3.70}$$

The past Laguerre filter bank is used for causal case and is denoted by $\Phi_{0,i,N}$. For the system where the initial condition is relatively small, the process of filtering the initial condition probably has no effect. However, the existence of this term in developing the model is good enough, just in case to reduce the influence of initial condition for certain state-space system.

3.4.3 Identification using A Causal IV

Let $L_i(s)$ be a bank of causal Laguerre filters ($p > 0$). Let $u(t)$ and $y(t)$ be the input and output plant data described in Equation (3.63) and Equation (3.64), respectively. Let $U^f_{0,i,N}$, $Y^f_{0,i,N}$, $U^f_{i,j,N}$ and $Y^f_{i,j,N}$ be constructed from $u(t)$ and $y(t)$, according to Equations (3.59-3.60) and $\Phi_{0,i,N}$ as in Equation (3.70).

Consider the RQ factorization

$$\begin{bmatrix} \Phi_{0,i,N} \\ U^f_{0,i,N} \\ U^f_{i,j,N} \\ Y^f_{i,j,N} \\ Y^f_{0,i,N} \end{bmatrix} = \begin{bmatrix} R_{11} & 0 & 0 & 0 & 0 \\ R_{21} & R_{22} & 0 & 0 & 0 \\ R_{31} & R_{32} & R_{33} & 0 & 0 \\ R_{41} & R_{42} & R_{43} & R_{44} & 0 \\ R_{51} & R_{52} & R_{53} & R_{54} & R_{55} \end{bmatrix} \begin{bmatrix} Q_1 \\ Q_2 \\ Q_3 \\ Q_4 \\ Q_5 \end{bmatrix} \tag{3.71}$$

Then the following holds

$$\lim_{N\to\infty} \frac{1}{\sqrt{N}} \begin{bmatrix} R_{53} & R_{54} \end{bmatrix} = \lim_{N\to\infty} \frac{1}{\sqrt{N}} \mathcal{O}_i \hat{X}_{0,N} \begin{bmatrix} Q_3 \\ Q_4 \end{bmatrix}^\top \tag{3.72}$$

Proof:

From the RQ factorization of Equation (3.71) we have

$$\lim_{N\to\infty} \frac{1}{\sqrt{N}} \begin{bmatrix} R_{53} & R_{54} \end{bmatrix} = \lim_{N\to\infty} \frac{1}{\sqrt{N}} Y^f_{0,i,N} \begin{bmatrix} Q_3 \\ Q_4 \end{bmatrix}^\top \tag{3.73}$$

From Equation (3.69) we have

$$\begin{aligned}\lim_{N\to\infty}\frac{1}{\sqrt{N}}Y^f_{0,i,N}\begin{bmatrix}Q_3\\Q_4\end{bmatrix}^\top &= \lim_{N\to\infty}\frac{1}{\sqrt{N}}\mathcal{O}_i\hat{X}_{0,N}\begin{bmatrix}Q_3\\Q_4\end{bmatrix}^\top + \lim_{N\to\infty}\frac{1}{\sqrt{N}}\Gamma_i U^f_{0,i,N}\begin{bmatrix}Q_3\\Q_4\end{bmatrix}^\top\\ &+ \lim_{N\to\infty}\frac{1}{\sqrt{N}}\Psi_i H^f_{0,i,N}\begin{bmatrix}Q_3\\Q_4\end{bmatrix}^\top + \lim_{N\to\infty}\frac{1}{\sqrt{N}}V^f_{0,i,N}\begin{bmatrix}Q_3\\Q_4\end{bmatrix}^\top\\ &+ \lim_{N\to\infty}\frac{1}{\sqrt{N}}Z_i\Phi_{0,i,N}\begin{bmatrix}Q_3\\Q_4\end{bmatrix}^\top \end{aligned} \tag{3.74}$$

As $\Phi_{0,i,N} = R_{11}Q_1$ *and* $U^f_{0,i,N} = R_{21}Q_1 + R_{22}Q_2$, *the second term and the fifth term on the right hand side goes to zero because of the orthogonality between* $\begin{bmatrix}Q_1\\Q_2\end{bmatrix}$ *and* $\begin{bmatrix}Q_3\\Q_4\end{bmatrix}$.

$$\lim_{N\to\infty}\frac{1}{\sqrt{N}}\Gamma_i U^f_{0,i,N}\begin{bmatrix}Q_3\\Q_4\end{bmatrix}^\top = 0 \tag{3.75}$$

$$\lim_{N\to\infty}\frac{1}{\sqrt{N}}Z_i\Phi_{0,i,N}\begin{bmatrix}Q_3\\Q_4\end{bmatrix}^\top = 0 \tag{3.76}$$

Next is to prove that the third and fourth term on the right hand side also goes to zero as N goes to infinity.

$$\lim_{N\to\infty}\frac{1}{\sqrt{N}}\Psi_i H^f_{0,i,N}Q_3^\top + \lim_{N\to\infty}\frac{1}{\sqrt{N}}V^f_{0,i,N}Q_3^\top = 0 \tag{3.77}$$

$$\lim_{N\to\infty}\frac{1}{\sqrt{N}}\Psi_i H^f_{0,i,N}Q_4^\top + \lim_{N\to\infty}\frac{1}{\sqrt{N}}V^f_{0,i,N}Q_4^\top = 0 \tag{3.78}$$

Since $h(t)$ *and* $v(t)$ *are independent from* $u(t)$, *therefore*

$$\lim_{N\to\infty}\frac{1}{\sqrt{N}}Q_1(\Psi_i H^f_{0,i,N})^\top = 0; \qquad \lim_{N\to\infty}\frac{1}{\sqrt{N}}Q_1(V^f_{0,i,N})^\top = 0$$

$$\lim_{N\to\infty}\frac{1}{\sqrt{N}}Q_2(\Psi_i H^f_{0,i,N})^\top = 0; \qquad \lim_{N\to\infty}\frac{1}{\sqrt{N}}Q_2(V^f_{0,i,N})^\top = 0$$

$$\lim_{N\to\infty}\frac{1}{\sqrt{N}}Q_3(\Psi_i H^f_{0,i,N})^\top = 0; \qquad \lim_{N\to\infty}\frac{1}{\sqrt{N}}Q_3(V^f_{0,i,N})^\top = 0$$

which proves Equation (3.77). Observe the fourth row of the RQ factorization leads to

$$\begin{aligned}
\lim_{N\to\infty}\frac{1}{N}Y^f_{i,j,N}(\Psi_i H^f_{0,i,n})^\top + \lim_{N\to\infty}\frac{1}{N}Y^f_{i,j,N}(V^f_{0,i,n})^\top &= 0\\
\lim_{N\to\infty}\frac{1}{N}(R_{41}Q_1 + R_{42}Q_2 + R_{43}Q_3 + R_{44}Q_4)(\Psi_i H^f_{0,i,n})^\top &= 0\\
\lim_{N\to\infty}\frac{1}{N}R_{44}Q_4(\Psi_i H^f_{0,i,n})^\top &= 0\\
\lim_{N\to\infty}\frac{1}{\sqrt{N}}Q_4(\Psi_i H^f_{0,i,n})^\top &= 0\\
\lim_{N\to\infty}\frac{1}{N}(R_{41}Q_1 + R_{42}Q_2 + R_{43}Q_3 + R_{44}Q_4)(V^f_{0,i,n})^\top &= 0\\
\lim_{N\to\infty}\frac{1}{N}R_{44}Q_4(V^f_{0,i,n})^\top &= 0\\
\lim_{N\to\infty}\frac{1}{\sqrt{N}}Q_4(V^f_{0,i,n})^\top &= 0
\end{aligned}$$

which is the transpose of Equation (3.78). Therefore now Equation (3.74) reduces to

$$\lim_{N\to\infty}\frac{1}{\sqrt{N}}Y^f_{0,i,N}\begin{bmatrix} Q_3 \\ Q_4 \end{bmatrix}^\top = \lim_{N\to\infty}\frac{1}{\sqrt{N}}\mathcal{O}_i\hat{X}_{0,N}\begin{bmatrix} Q_3 \\ Q_4 \end{bmatrix}^\top$$

The subspace algorithm in identifying the continuous time system can be described as below

1. Construct the filtered data matrices of $U^f_{0,i,N}$, $U^f_{i,j,N}$, $Y^f_{0,i,N}$ and $Y^f_{i,j,N}$ according to Equations (3.59-3.60), and $\Phi_{0,i,N}$ according to Equation (3.70).

2. Perform the RQ decomposition

$$\begin{bmatrix} \Phi_{0,i,N} \\ U^f_{0,i,N} \\ U^f_{i,j,N} \\ Y^f_{i,j,N} \\ Y^f_{0,i,N} \end{bmatrix} = \begin{bmatrix} R_{11} & 0 & 0 & 0 & 0 \\ R_{21} & R_{22} & 0 & 0 & 0 \\ R_{31} & R_{32} & R_{33} & 0 & 0 \\ R_{41} & R_{42} & R_{43} & R_{44} & 0 \\ R_{51} & R_{52} & R_{53} & R_{54} & R_{55} \end{bmatrix}\begin{bmatrix} Q_1 \\ Q_2 \\ Q_3 \\ Q_4 \\ Q_5 \end{bmatrix}$$

3. Perform the singular value decomposition (SVD) to the working matrix $\begin{bmatrix} R_{53} & R_{54} \end{bmatrix}$:

$$\begin{bmatrix} R_{53} & R_{54} \end{bmatrix} = USV^\top$$

4. Determine the model order n from the singular value in S.

5. Determine the system matrices (A_w, C_w).

$$
\begin{aligned}
A_w &= (J_1 U_n)^{\dagger} J_2 U_n \\
C_w &= J_3 U_n \\
J_1 &= \begin{bmatrix} I_{(i-1)l} & 0_{(i-1)l \times l} \end{bmatrix} \\
J_2 &= \begin{bmatrix} 0_{(i-1)l \times l} & I_{(i-1)l} \end{bmatrix} \\
J_3 &= \begin{bmatrix} I_{l \times l} & 0_{l \times (i-1)l} \end{bmatrix} \\
\Upsilon^{\dagger} &= (\Upsilon^{\top}\Upsilon)^{-1}\Upsilon^{\top}
\end{aligned}
$$

The A and C can be obtained using the relations:

$$
\begin{aligned}
A &= p(I_n + A_w)(I_n - A_w)^{-1} \\
C &= \sqrt{2p} C_w (I_n - A_w)^{-1}
\end{aligned}
$$

6. Solve least squares problem from model structure:

$$y(\ t \ \big|\ B, D\ ) = C(qI_n - A)^{-1}Bu(t) + Du(t)$$

7. Reconstruct B and D from $\begin{bmatrix} B \\ D \end{bmatrix}$

8. Generate the estimated output, $\hat{y}(t)$.

3.4.4 Simulation Results

In this section, the simulation results will be shown as to demonstrate the performance of the proposed approach in identifying a continuous time system. The results are categorized into SISO systems and MIMO systems, whereby the estimated output is compared with measured output. As a measure of accuracy of the proposed model, the *Variance Accounted For* (VAF), which is given by the following formula

$$\text{VAF} = \left(1 - \frac{\text{VAR}(y(t) - \hat{y}(t))}{\text{VAR}(y(t))}\right) \times 100$$

and the *Mean Square Errors* (MSE), which is given by the following formula

$$\text{MSE} = \frac{1}{N}\sum_{a=1}^{N} \mid y(t_a) - \hat{y}(t_a) \mid^2$$

are also calculated.

Table 3.2: System and model configuration - SISO noise-added system

Symbol	Description	Value
G_m	System response	$[A_m, B_m, C_m, D_m]$
p	Laguarre parameter	6
i	Expanding observability matrix	10
n	Model order	6
Δt	Sampling time	0.01
N	Number of sampled data	4000
N_{est}	Estimation data	2000
N_{val}	Validation data	2000
V & H	Noise disturbance	20dB SNR

Single Input Single Output Data System

The first data set is a simulated data based from the sixth order plant model example presented in [164, 188]. The state space model is developed based on the following set up.

$$A_m = \begin{bmatrix} 0 & 1 & 0 & 0 & 0 & 0 \\ -1 & -0.2 & 0 & 0 & 0 & 0 \\ 0 & 0 & 0 & 1 & 0 & 0 \\ 0 & 0 & -25 & -0.5 & 0 & 0 \\ 0 & 0 & 0 & 0 & 0 & 1 \\ 0 & 0 & 0 & 0 & -9 & -0.12 \end{bmatrix}; \; B_m = \begin{bmatrix} 0 \\ 1 \\ 0 \\ 1 \\ 0 \\ 1 \end{bmatrix}; \; C_m = \begin{bmatrix} 1 \\ 0 \\ 1 \\ 0 \\ 1 \\ 0 \end{bmatrix}^\top; \; D_m = [0];$$

The process noise, $h(t)$ and the measurement noise, $v(t)$ of about 20dB SNR are generated using random "seed" value according to the following condition

$$h(t) = v(t) = 0.07 \times e(t)$$

where $e(t)$ are unit variance, zero mean white Gaussian noise. The "seed" value to generate the process noise, $h(t)$ is set to 1, whereas the "seed" value to generate the measurement noise, $v(t)$

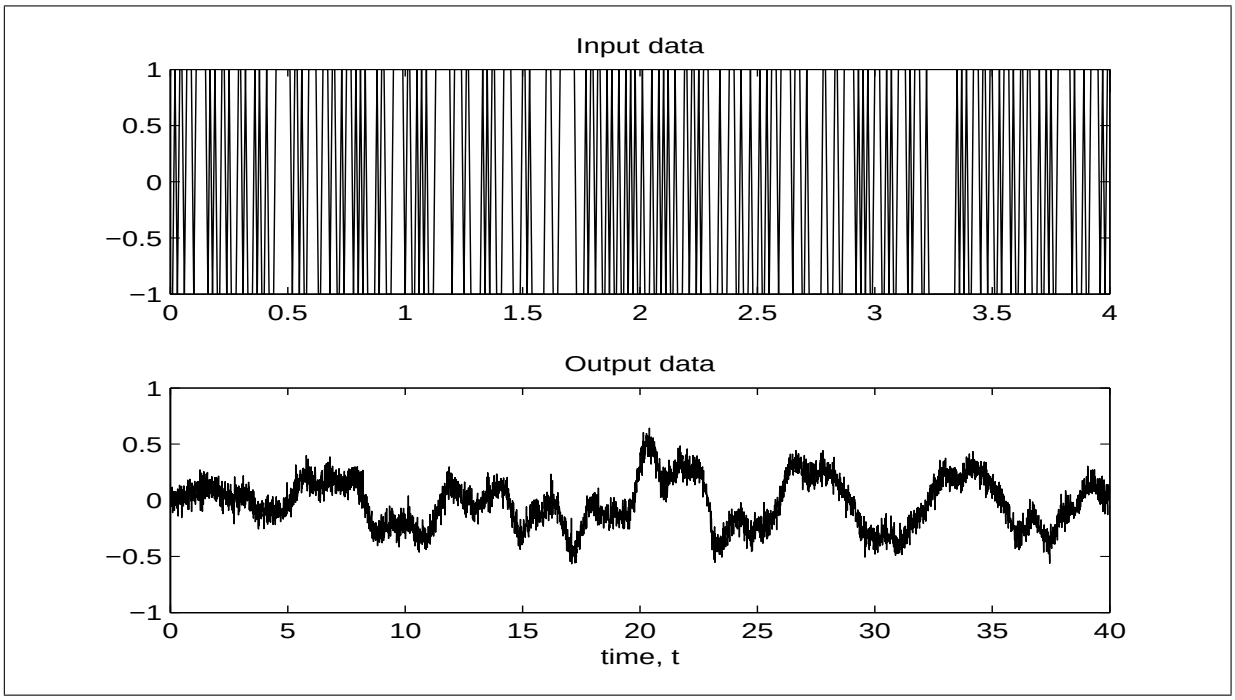

Figure 3.11: Plot of input & output - SISO noise-added system. (*Note*: The input data is re-scaled to only display 400 data points)

is set to 2. The identification process is run with system and model configuration details shown in Table 3.2. Again, the input signal, $u(t)$ is generated using GRBS sequences.

The plot of input and output data can be seen as in Figure (3.11). The comparison of estimation and validation data sets with the estimated outputs from the model obtained using subspace method is shown in Figure (3.12). The result shows that the model could describe the system closely. Further verification tests on MSE and VAF give a value of

$$\text{MSE}_{est} = 0.0051 \qquad \text{VAF}_{est} = 82.13\%$$

$$\text{MSE}_{val} = 0.0092 \qquad \text{VAF}_{val} = 85.37\%$$

This shows that the model is still able to identify the system with low MSE and good percentage of accuracy for both estimation and validation data set.

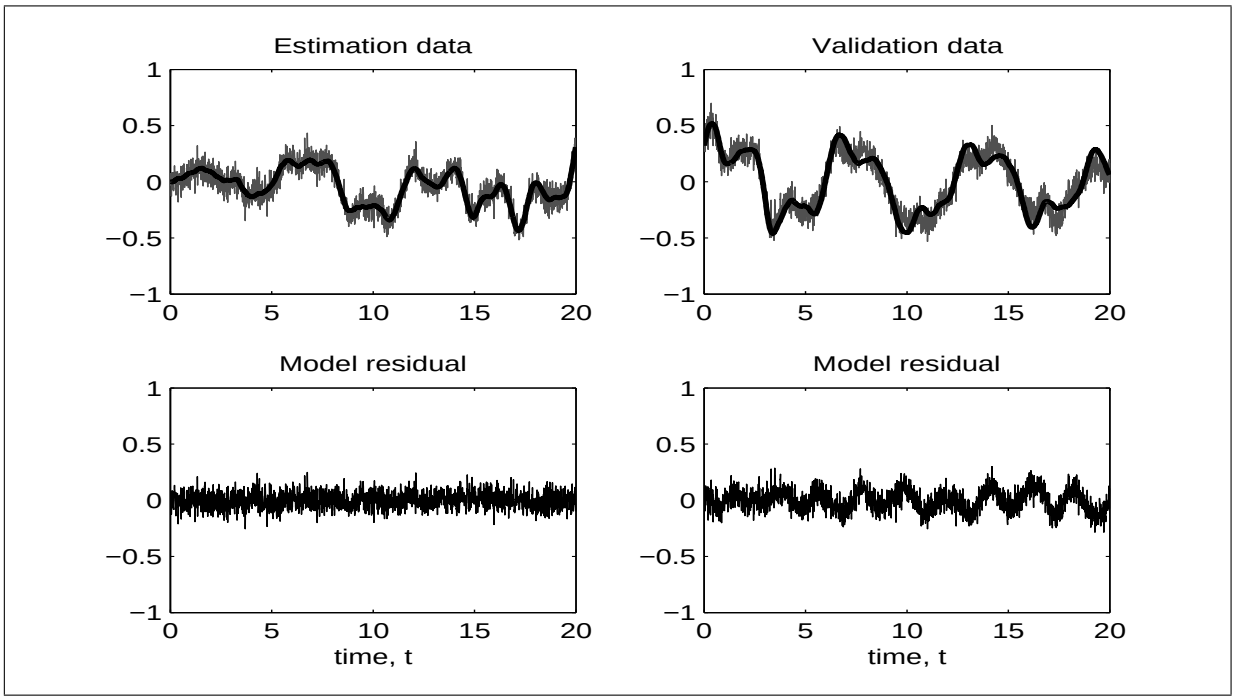

Figure 3.12: Superimposed of output data - SISO noise-added system. True system (solid grey) & estimated model (thick black)

The estimated of (A, B, C, D) matrices are obtained as

$$\hat{A} = \begin{bmatrix} -0.0562 & 1.0318 & -0.1990 & 0.4309 & 1.0012 & -0.2540 \\ -0.8637 & -0.0954 & 0.6541 & -0.1592 & -0.7232 & 0.2955 \\ 0.0041 & -0.4777 & -0.0598 & 3.0430 & 0.5820 & -0.6709 \\ -0.2832 & -0.1073 & -2.7003 & -0.0797 & -1.6749 & 0.0747 \\ -0.0673 & -0.0349 & -0.1723 & -0.0299 & -0.5201 & 6.3291 \\ 0.0751 & 0.0560 & 0.2012 & 0.0960 & -3.9643 & -0.0817 \end{bmatrix};$$

$$\hat{B} = \begin{bmatrix} -0.8891 \\ -1.0507 \\ -0.2053 \\ -0.2169 \\ 0.2374 \\ -0.0923 \end{bmatrix}; \qquad \hat{C} = \begin{bmatrix} -0.4967 \\ 0.3026 \\ -0.0261 \\ 0.9841 \\ -0.5010 \\ -1.4015 \end{bmatrix}^{\top}; \qquad \hat{D} = [0];$$

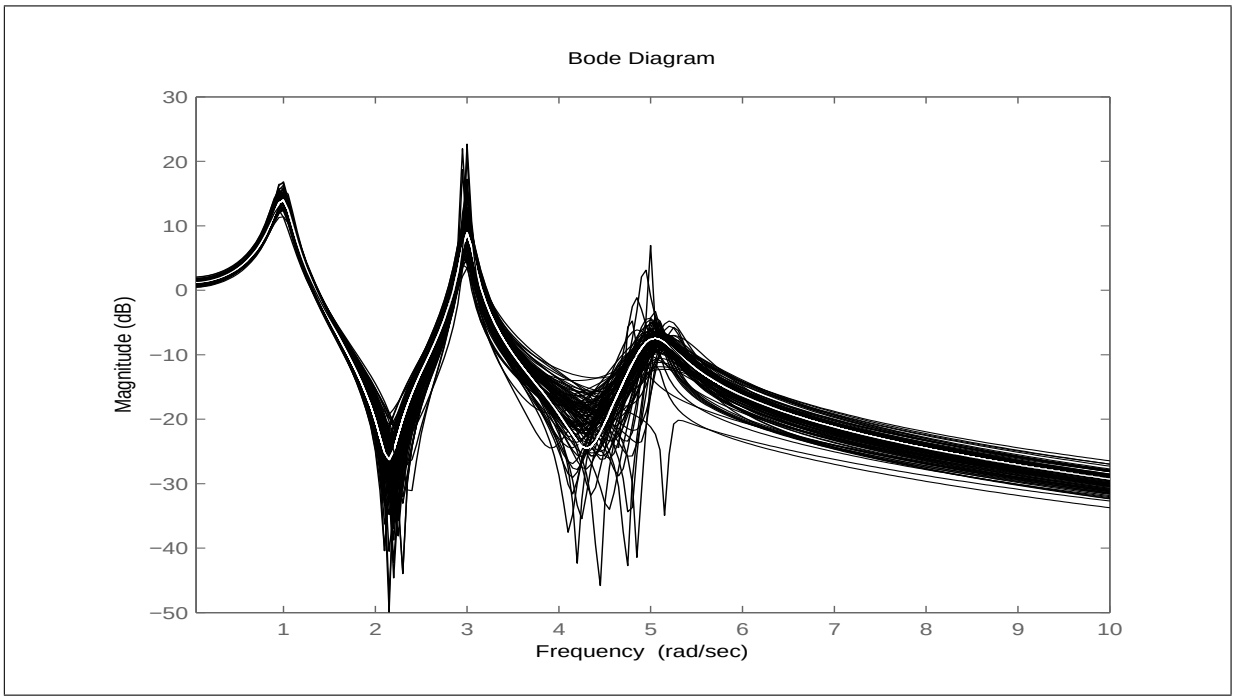

Figure 3.13: Frequency response over 100 runs - SISO simulated noise-added system

The transfer function of the system and the one generated from the estimated model is represented as

$$G_m(s) = \frac{3s^4 + 1.64s^3 + 70.184s^2 + 14.92s + 259}{s^6 + 0.82s^5 + 35.184s^4 + 14.932s^3 + 260.56s^2 + 52.5s + 225}$$

$$\hat{G}(s) = \frac{2.8951s^4 + 0.8457s^3 + 67.9062s^2 + 11.5326s + 255.7296}{s^6 + 0.8929s^5 + 35.0886s^4 + 14.2043s^3 + 257.5110s^2 + 46.7775s + 227.0661}$$

and the eigenvalues of A matrix give a result of

$$\text{eig}(A_m) = [-0.1000 \pm 0.9950j; -0.2500 \pm 4.9937j; -0.0600 \pm 2.9994j]$$

$$\text{eig}(\hat{A}) = [-0.0883 \pm 1.0089j; -0.3228 \pm 4.9951j; -0.0353 \pm 2.9723j]$$

which still gives a reasonable match to actual value. The Monte Carlo simulation for 100 runs is also performed in order to inspect the model capability in identifying with different noise level. The "seed" value is set in a range count of 1 to 100. Result from this simulation can be seen in Figure (3.13). The comparison is also made for a model with instrumental variable and model without instrumental variable. Result is shown in Figure (3.14). From this figure, it shows that the model with IV gives a better performance in estimating the noise-added systems.

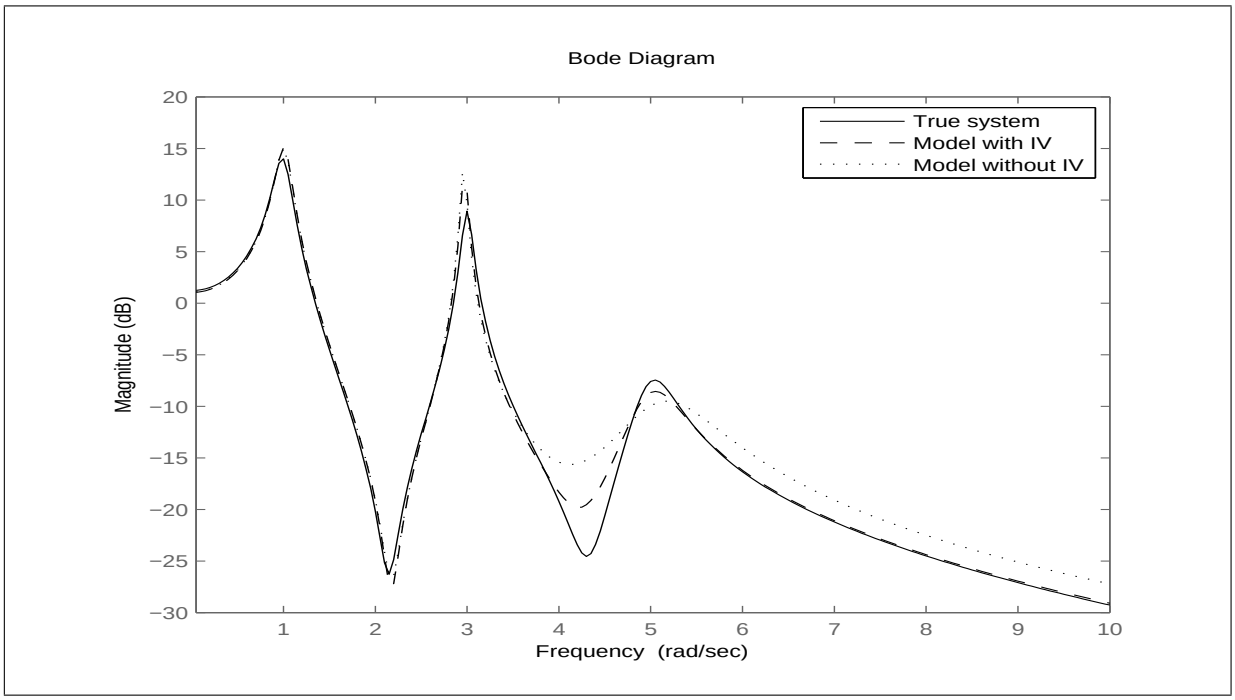

Figure 3.14: Frequency response with & without IV - SISO simulated noise-added system

Multi Input Multi Output Data Systems

Next in this section, the model is expanded to demonstrate its performance capability onto MIMO systems. The systems are represented as two inputs two outputs in this following form

$$\begin{bmatrix} y_1(t) \\ y_2(t) \end{bmatrix} = \begin{bmatrix} G_{11} & G_{12} \\ G_{21} & G_{22} \end{bmatrix} \begin{bmatrix} u_1(t) \\ u_2(t) \end{bmatrix}$$

The input signal, $u_1(t)$ and $u_2(t)$ are generated using a GRBS sequences. The measurement noise of about 30dB SNR is generated based on the following equation

$$v(t) = 0.02 \times e(t)$$

Table 3.3: System and model configuration - MIMO systems

Symbol	Description	Value
G	System response	$\begin{bmatrix} \frac{1}{s^2+2s+1} & \frac{1}{s^2+4s+3} \\ \frac{1}{s^2+3s+2} & \frac{1}{s^2+2s+1} \end{bmatrix}$
p	Laguarre parameter	15
i	Expanding observability matrix	10
n	Model order	4
Δt	Sampling time	0.01
N	Number of sampled data	2000
N_{est}	Estimation data	1000
N_{val}	Validation data	1000
V	Noise disturbance	30dB SNR

where $e(t)$ is unit variance, zero mean white Gaussian noise. The "seed" value is set equal to 1. The identification process is run with system and model configuration details shown in Table 3.3. The plot of output data, $y_1(t)$ and $y_2(t)$ can be seen as in Figure (3.15). This data set is further divided into estimation data set and validation data set. The performance of the estimated model is assessed based on the fit between the measured output and the estimated one.

The comparison of estimation and validation data sets with the estimated outputs from the model obtained using subspace method are shown in Figure (3.16) and Figure (3.17). Both results show that the model could describe the system closely. The verification test based on MSE and VAF calculation can be referred in Table 3.4. From the calculation, it shows that the model is still able to identify the MIMO noise-added systems with low MSE and good percentage of accuracy to both estimation and validation data set.

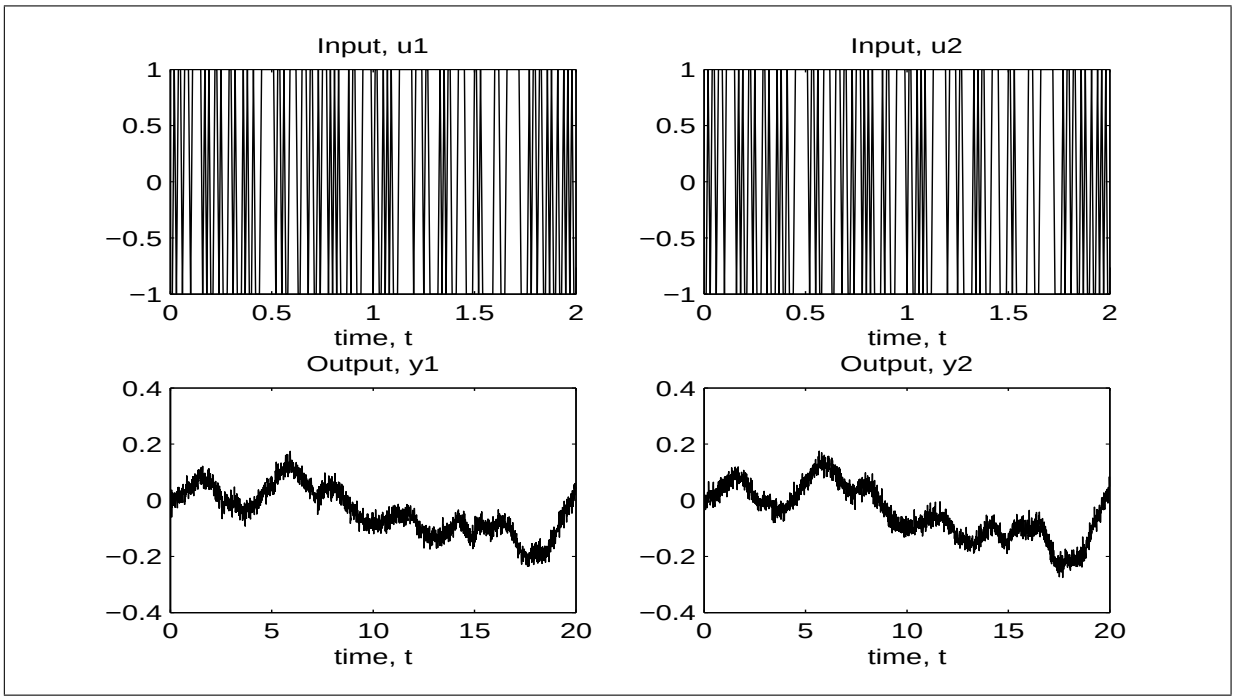

Figure 3.15: Plot of input & output - MIMO systems. (*Note*: The input data is re-scaled to only display 200 data points)

The estimated (A, B, C, D) matrices are obtained as

$$\hat{A} = \begin{bmatrix} -0.1212 & 3.1885 & -1.6029 & -7.3190 \\ -0.3503 & -3.1587 & 2.6036 & 21.4320 \\ 0.0242 & -0.6420 & -30.8828 & 29.0223 \\ 0.0519 & 1.8033 & -14.1142 & -37.9538 \end{bmatrix};$$

$$\hat{B} = \begin{bmatrix} 2.7782 & 2.7782 \\ -2.1165 & -2.1165 \\ 0.2455 & 0.2455 \\ -0.3770 & -0.3770 \end{bmatrix}; \qquad \hat{C} = \begin{bmatrix} -0.4425 & -0.5899 \\ 0.1957 & 0.0835 \\ -0.5200 & -0.6449 \\ 0.3780 & -0.1148 \end{bmatrix}^{\top}; \qquad \hat{D} = \begin{bmatrix} 0 & 0 \\ 0 & 0 \end{bmatrix};$$

and the eigenvalues is given as

$$\text{eig}(\hat{A}) = -0.7822; -1.5478; -34.8933 \pm 19.7766j;$$

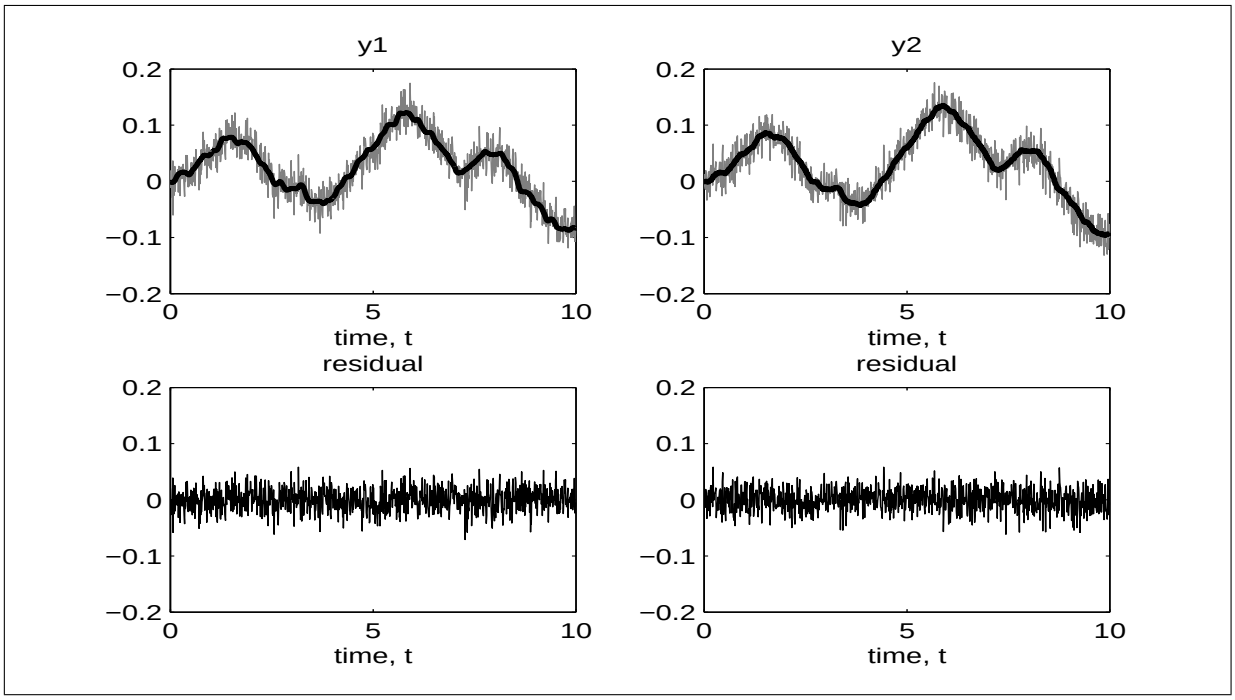

Figure 3.16: Measured (solid grey) & estimated (thick black) MIMO estimation data

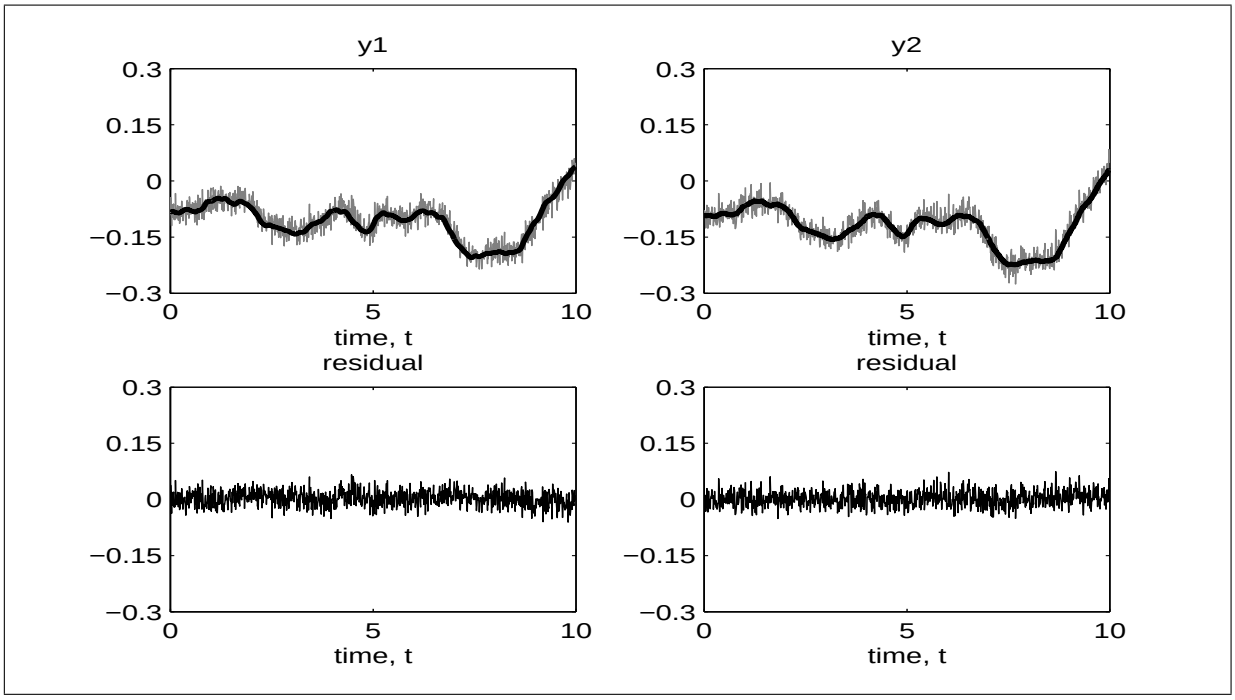

Figure 3.17: Measured (solid grey) & estimated (thick black) MIMO validation data

Table 3.4: MSE and VAF calculation - MIMO systems

Description	y_1	y_2
MSE - estimation data	4.1474×10^{-4}	4.0501×10^{-4}
MSE - validation data	4.2845×10^{-4}	4.1774×10^{-4}
VAF - estimation data	85.98%	88.75%
VAF - validation data	84.78%	87.93%

3.4.5 Case Study: Comparison with MATLAB Toolbox Model

As to further investigate the performance of the proposed model in identifying the systems, a comparative study is done with other linear parametric models available in MATLAB system identification toolbox. Those models are the ARX model, IV model, ARMAX model, OE model, BJ model, N4SID (CVA) model, N4SID (MOESP) model and the PEM model. The fit of the model as compared to the measured system can be calculated as

$$\text{BF} = \left(1 - \frac{|y - \hat{y}|}{|y - \bar{y}|}\right) \times 100\%$$

where y is a measured output, $\hat{y}$ is an estimated output from the model and $\bar{y}$ is a mean of y. The single input single output data systems discussed in previous section is used again for comparison. At sampling time of, $\Delta t = 0.01s$ and number of measured data, $N = 2000$, the first comparison are based on the noise-free data systems. Result based on the validation data systems can be seen as in Figure (3.18-3.20). The best fit calculation for each model can be seen in Table 3.5. From the plot and the fit calculation all models give excellent results in identifying the noise free systems.

Next, the comparison is done with the noise-added systems. The process and measurement noise of about 50dB SNR are added to the systems and is defined as

$$h(t) = v(t) = 0.01 \times e(t)$$

where $e(t)$ is unit variance, zero mean white Gaussian noise. The "seed" value for process noise, $h(t)$ is equal to 1 and the "seed" value for measurement noise, $v(t)$ is equal to 2. Again at

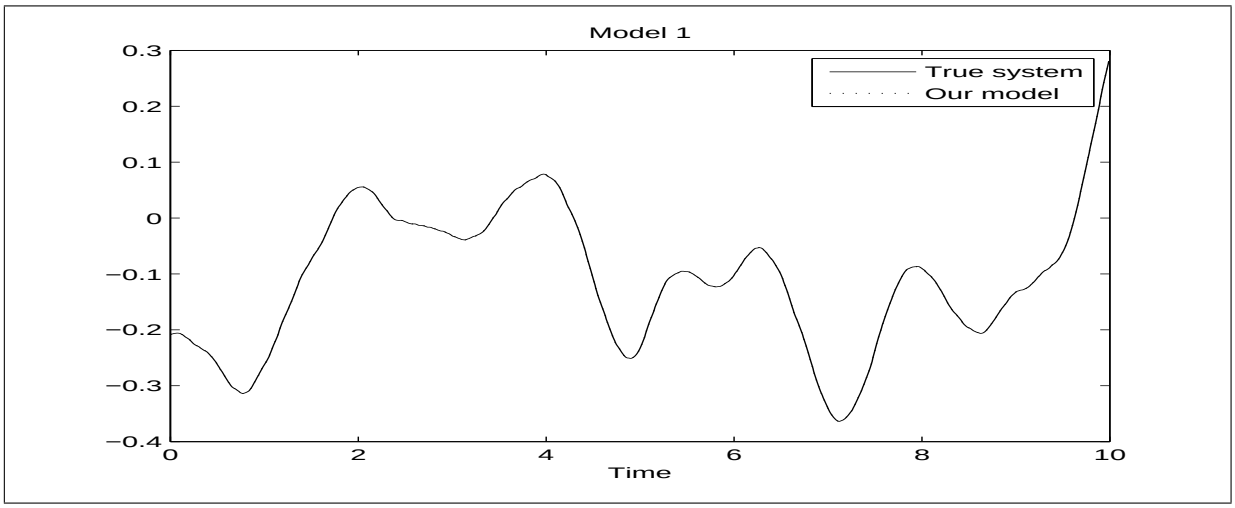

Figure 3.18: Comparison over noise-free SISO validation data systems (cont.) - 1: Our model

sampling time, $\Delta t = 0.01s$, about $N = 2000$ is sampled and those data is further divided into estimation data and validation data.

Table 3.5: Best fit calculation - Noise-free systems

Model	Model Order	Iteration	Estimation	Validation
ARX	[na=8; nb=5; nk=1]	-	100%	100%
IV	[na=8; nb=5; nk=1]	-	100%	100%
ARMAX	[na=8; nb=5; nc=1; nk=1]	60	100%	100%
OE	[nb=5; nf=8; nk=1]	60	100%	100%
BJ	[nb=5; nc=0; nd=0; nf=8; nk=1]	60	100%	100%
N4SID (CVA)	n=6	-	100%	100%
N4SID (MOESP)	n=6	-	100%	100%
PEM	n=6	1	100%	100%
Our Model	n=6	-	100%	100%

The plot for all models in identifying the noise-added simulated systems can be seen in Figure (3.21-3.23) for the estimation data and in Figure (3.24-3.26) for the validation data. From Figure (3.21-3.23), it shows that our model is able to identify the estimation data set closely. The ARMAX model, OE model and BJ model also show good performance. The rest of the

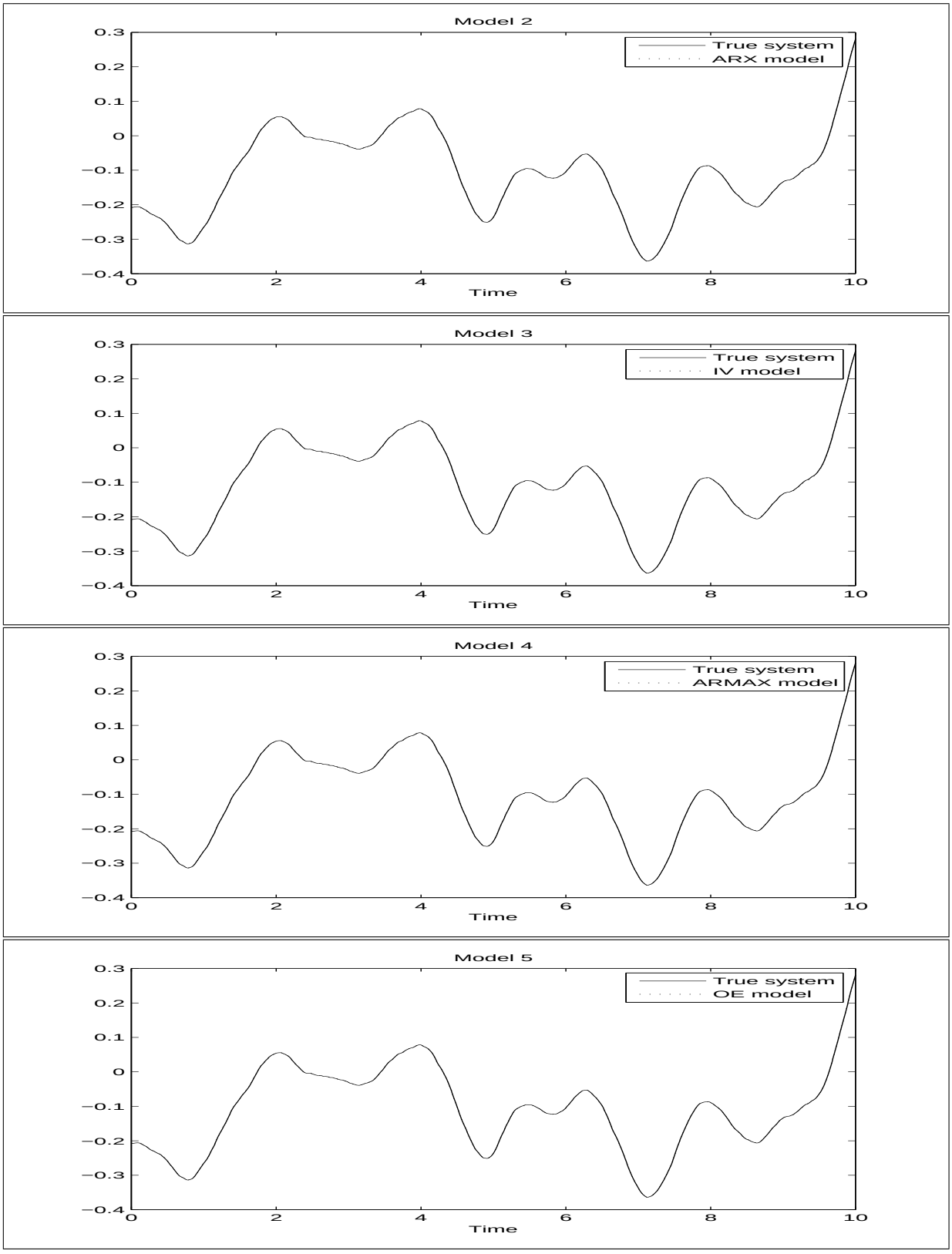

Figure 3.19: Comparison over noise-free SISO validation data systems (cont.) - 2: ARX model; 3: IV model; 4: ARMAX model; 5: OE model

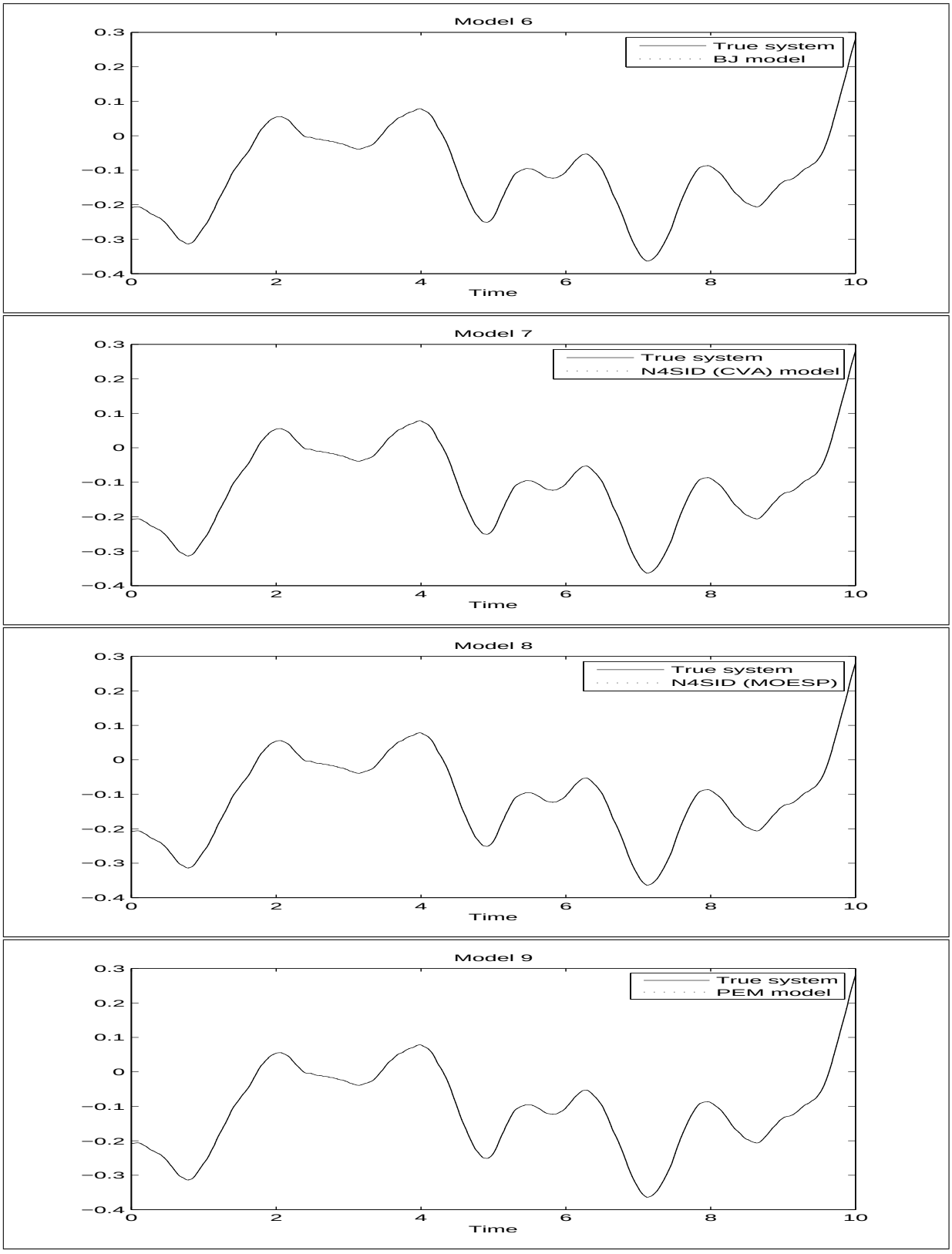

Figure 3.20: Comparison over noise-free SISO validation data systems - 6: BJ model; 7: N4SID(CVA) model; 8: N4SID(MOESP) model; 9: PEM model

Table 3.6: Best fit calculation - Noise-added systems

Model	Model Order	Iteration	Estimation	Validation
ARX	[na=10; nb=10; nk=1]	-	56.35%	29.33%
IV	[na=10; nb=10; nk=1]	-	56.35%	29.33%
ARMAX	[na=12; nb=8; nc=0; nk=1]	60	92.15%	91.30%
OE	[nb=12; nf=8; nk=1]	60	92.14%	91.70%
BJ	[nb=8; nc=0; nd=0; nf=8; nk=1]	40	92.17%	91.54%
N4SID (CVA)	n=8	-	30.38%	12.54%
N4SID (MOESP)	n=8	-	30.76%	11.07%
PEM	n=8	20	65.02%	26.26%
Our Model	n=8	-	90.78%	89.17%

model try to identify the systems with adequate performance. Next, refer to Figure (3.24-3.26) where the model is used to identify the validation data. Again, our model still shows an acceptable performance in identifying the validation data. The ARMAX model, OE model and BJ model give good performance. The rest of the models are poorly identify the system. Further verification test based on fit calculation can be referred in Table 3.6.

From this study, we found that all models are able to identify the systems successfully if the system is not perturbed by noise disturbances. When noise interferes the system, some of the models are unable to estimate the system closely especially when it comes to a test using validation data (data that are not used for modelling at all). Among 8 models that have been tested, the ARMAX model, the OE model and the BJ model have shown good performance in identifying the system closely. Our model also shows good competence in comparison with those models. This is due to the presence of Laguerre filter and the instrumental variables in our model that have shown ability to cope with process and measurement noise successfully.

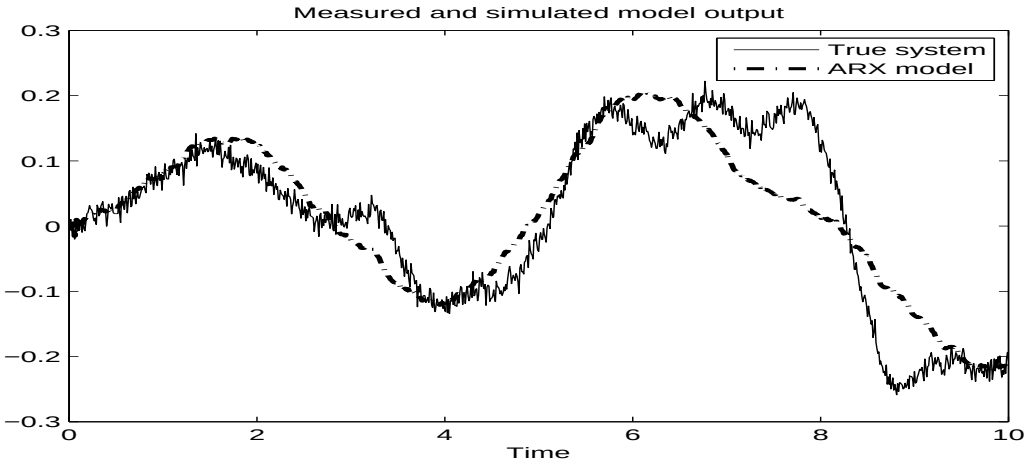

(a) -1. ARX model

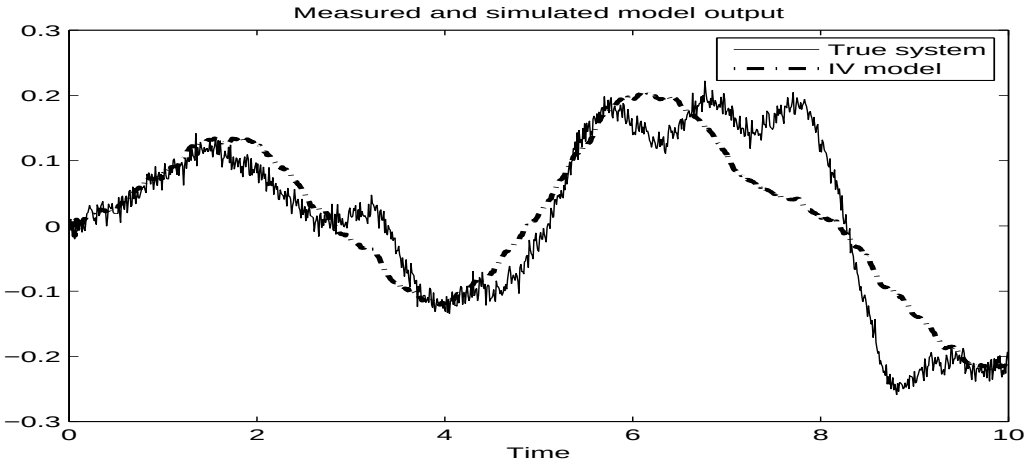

(b) -2. IV model

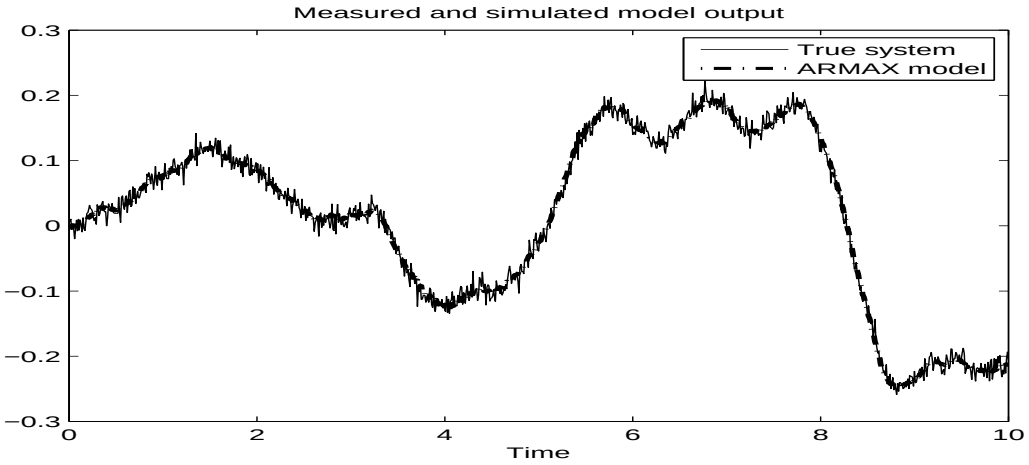

(c) -3. ARMAX model

Figure 3.21: Comparison over noise-added SISO estimation data systems (cont.)

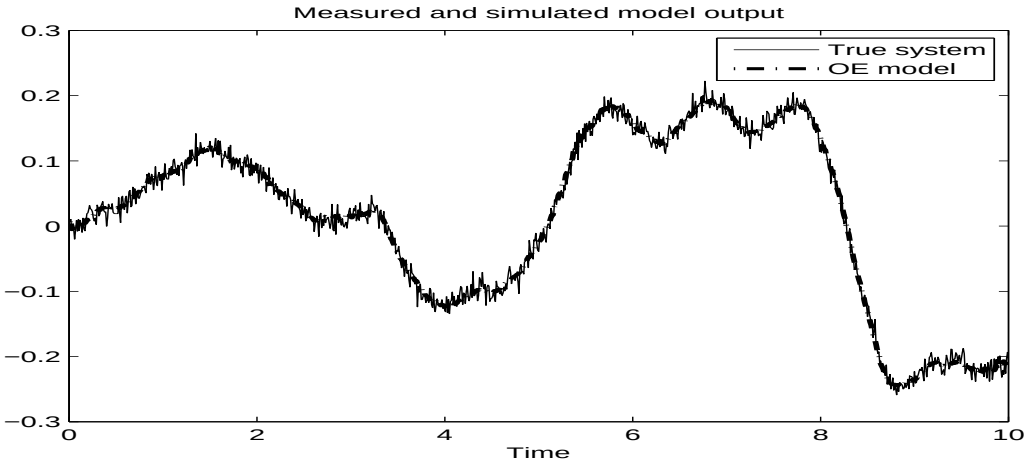

(a) -4. OE model

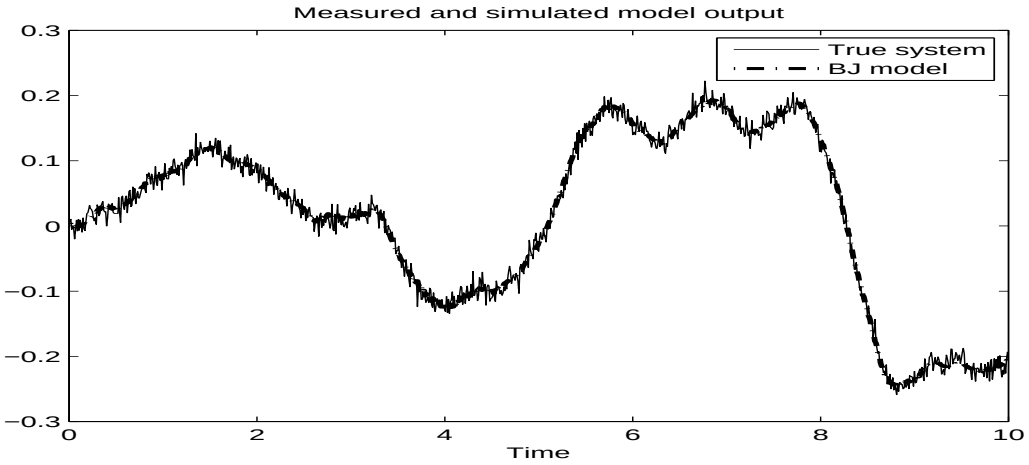

(b) -5. BJ model

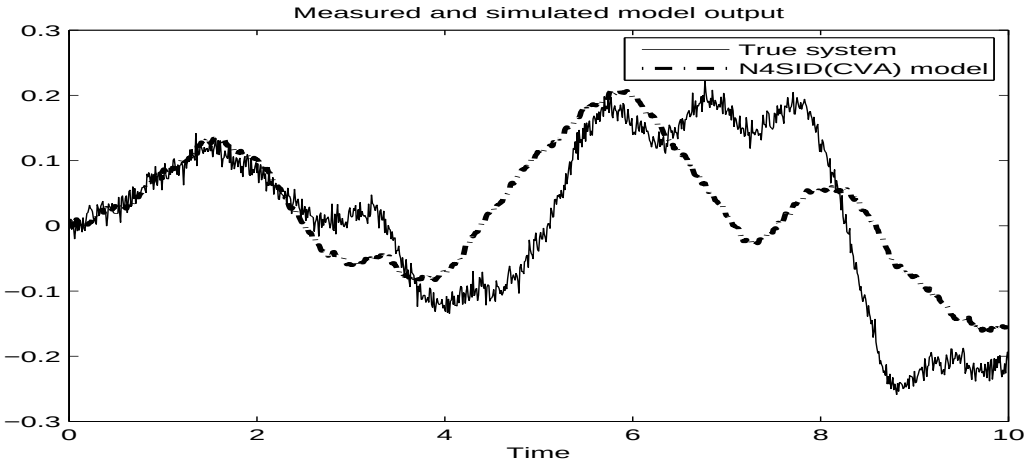

(c) -6. N4SID (CVA) model

Figure 3.22: Comparison over noise-added SISO estimation data systems (cont.)

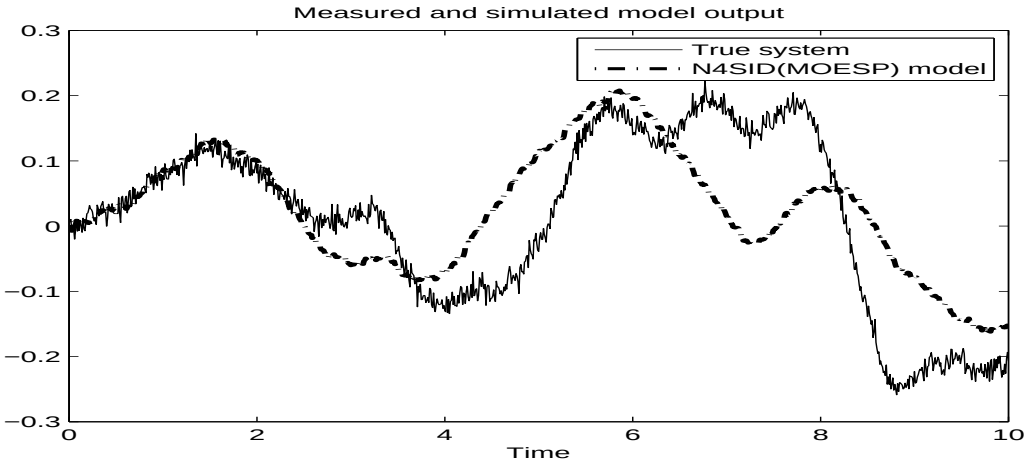

(a) -7. N4SID (MOESP) model

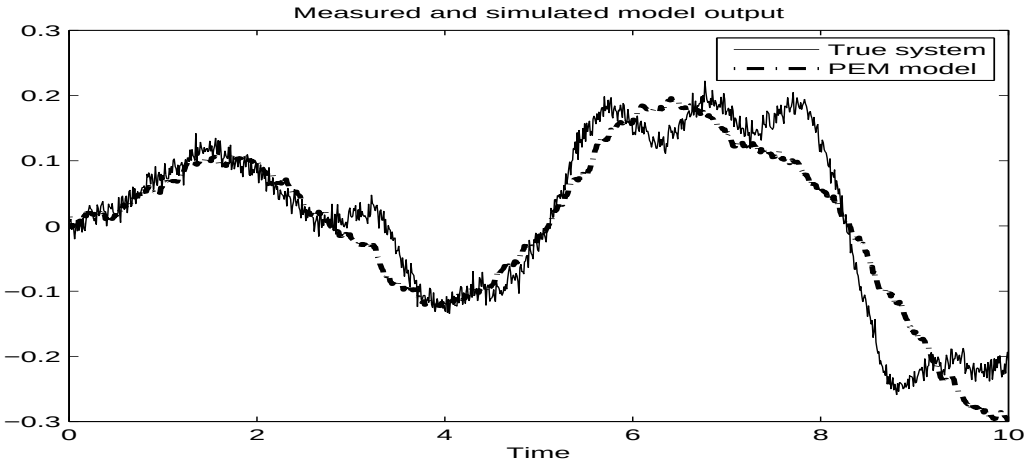

(b) -8. PEM model

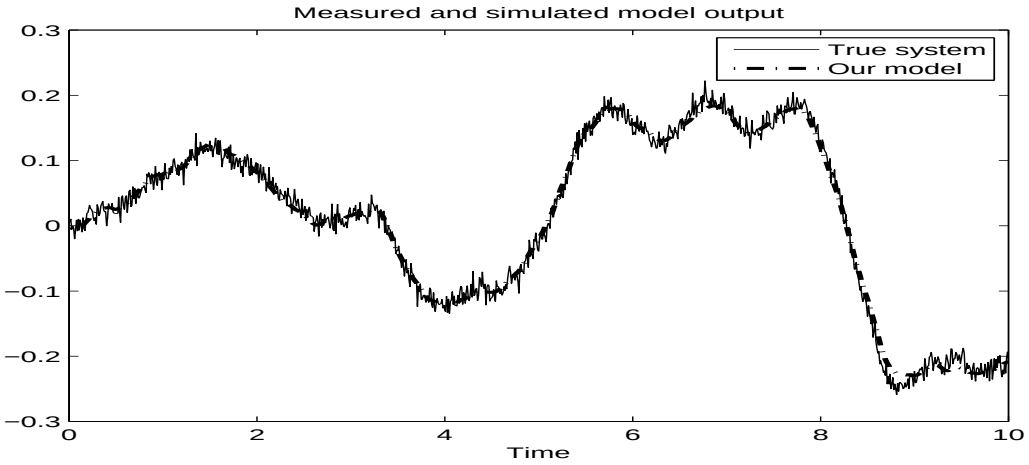

(c) -9. Our model

Figure 3.23: Comparison over noise-added SISO estimation data systems

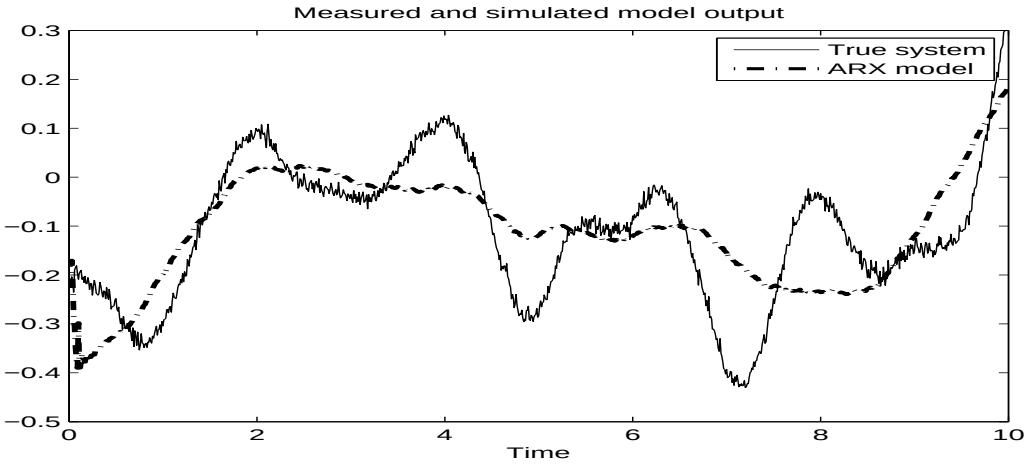

(a) - 1. ARX model

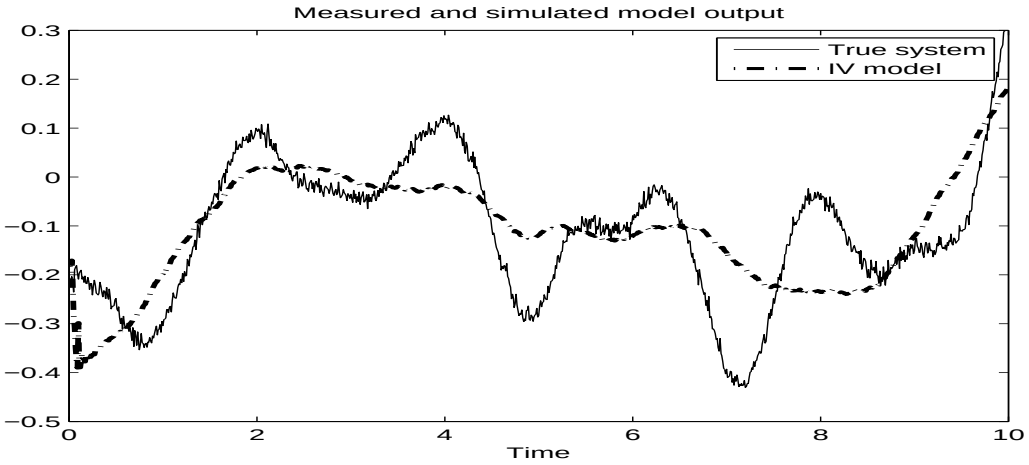

(b) - 2. IV model

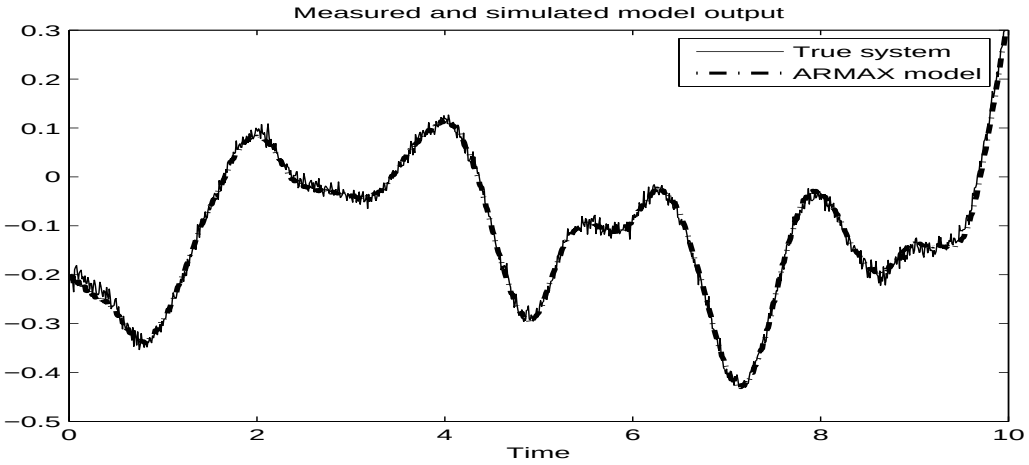

(c) - 3. ARMAX model

Figure 3.24: Comparison over noise-added SISO validation data systems (cont.)

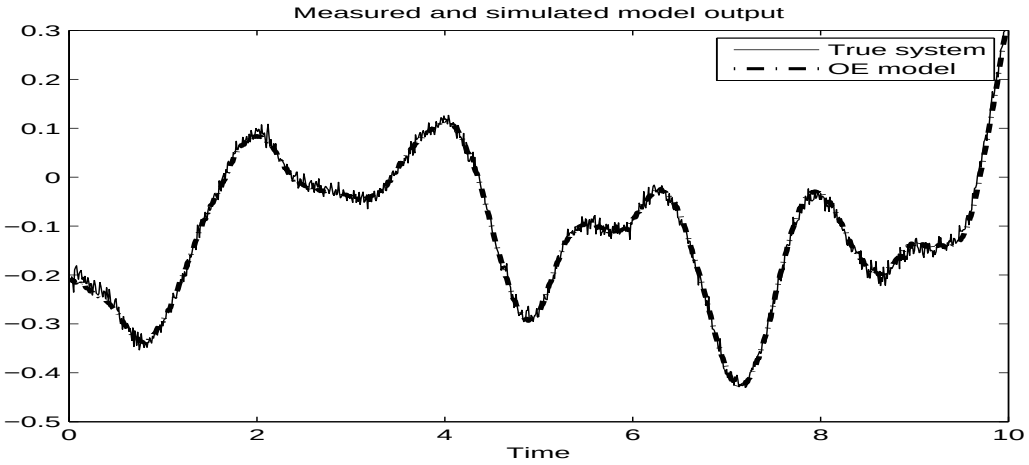

(a) - 4. OE model

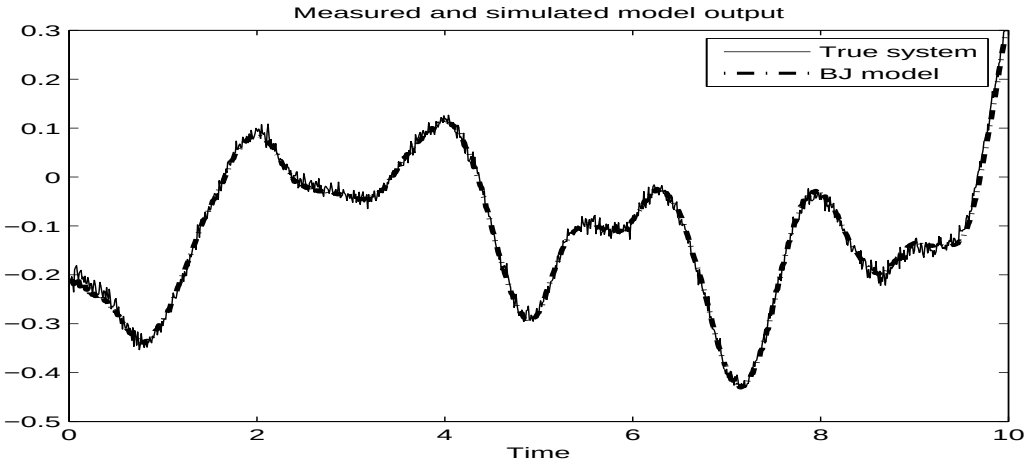

(b) - 5. BJ model

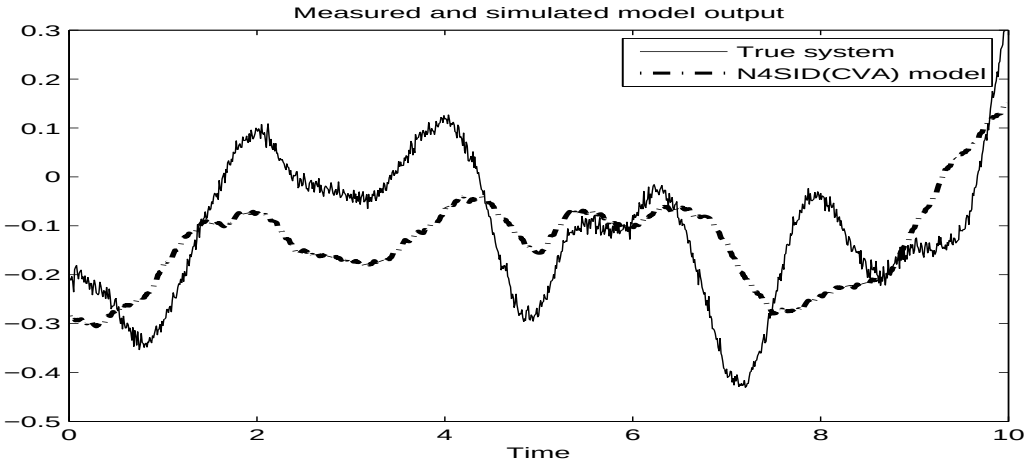

(c) - 6. N4SID (CVA) model

Figure 3.25: Comparison over noise-added SISO validation data systems (cont.)

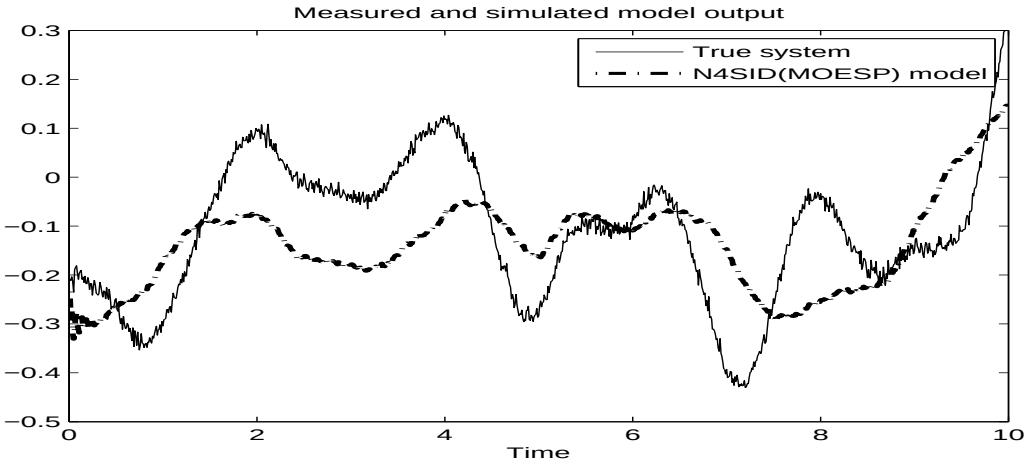

(a) - 7. N4SID (MOESP) model

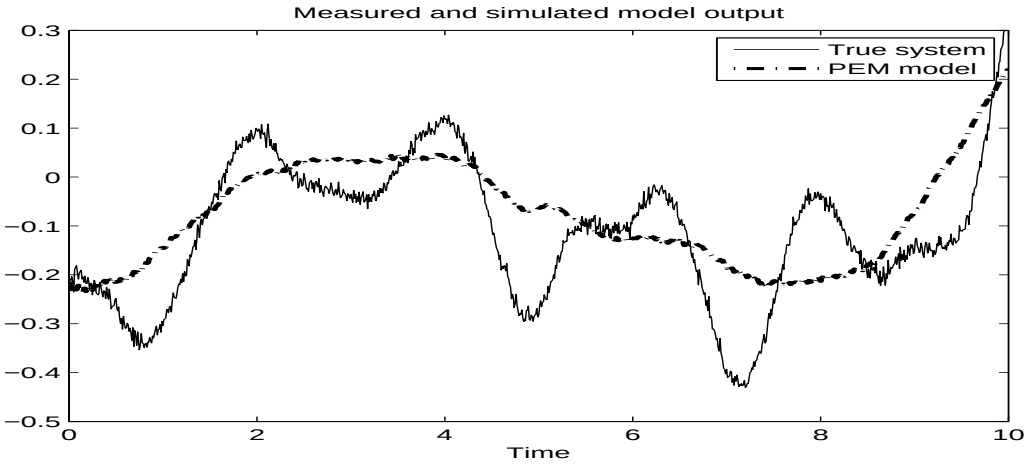

(b) - 8. PEM model

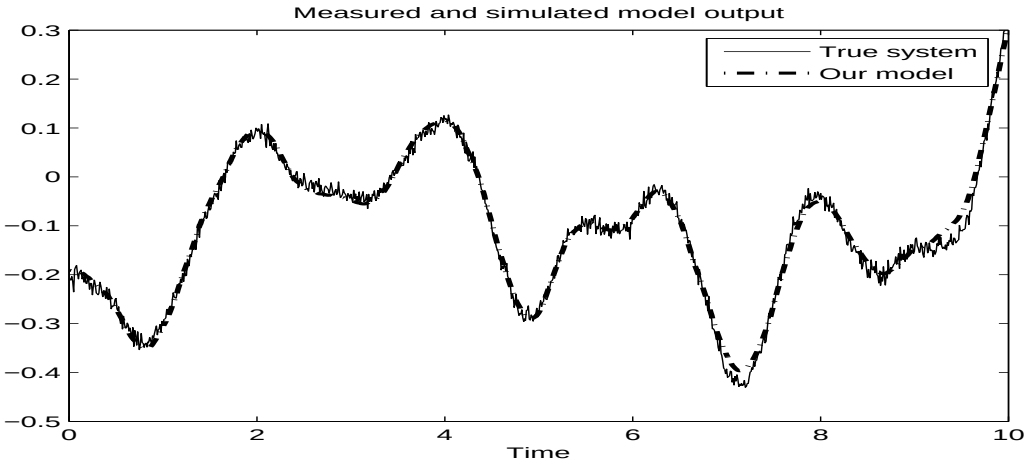

(c) - 9. Our model

Figure 3.26: Comparison over noise-added SISO validation data systems

3.5 Implementation Issues

In this section, the focus is aimed on performing an analysis and research on some of the implementation and performance issues that relate to the previously discussed system identification. The issues will be divided into two categories: First the issues that relate to subspace model identification and second the issues that relate to optimal selection of design parameters.

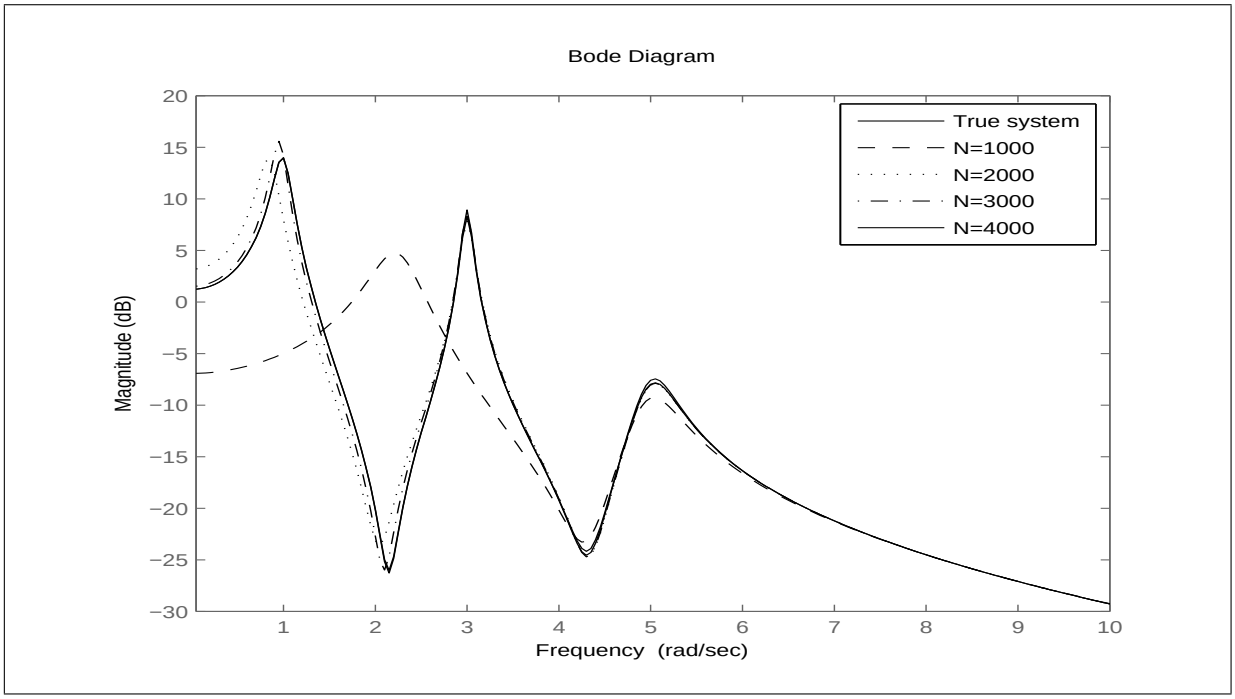

Figure 3.27: Comparison of different amount of data samples ($\Delta t = 0.001s$)

3.5.1 Subspace Model Identification

In the system identification using a subspace methods, there are few factors that have to be considered in order to guarantee a successful model development and the consistency and robustness of the identification process. In here, the focus is to only study and analyse some implementation issues that relates to the state-space model development and continuous time system identification that have been discussed in this chapter.

Sampling Time, Δt and Number of Data, N

In time domain system identification the sampling time plays a role in the continuous time subspace identification. It can be seen that a proper choice of sampling time will lead to a more accurate model development. The sampling time also depends on the models and the number of measured data, N. Precisely, the model performance depends on how much data that is available to describe the system and whether the sampling time is good enough to capture the information about the system.

Consider for example the simulation data for SISO system describes in state-space matrices as

$$A_m = \begin{bmatrix} 0 & 1 & 0 & 0 & 0 & 0 \\ -1 & -0.2 & 0 & 0 & 0 & 0 \\ 0 & 0 & 0 & 1 & 0 & 0 \\ 0 & 0 & -25 & -0.5 & 0 & 0 \\ 0 & 0 & 0 & 0 & 0 & 1 \\ 0 & 0 & 0 & 0 & -9 & -0.12 \end{bmatrix}; \; B_m = \begin{bmatrix} 0 \\ 1 \\ 0 \\ 1 \\ 0 \\ 1 \end{bmatrix}; \; C_m = \begin{bmatrix} 1 \\ 0 \\ 1 \\ 0 \\ 1 \\ 0 \end{bmatrix}^\top; \; D_m = [0];$$

For the noise-free system, we found that by setting the sampling time, $\Delta t = 0.001s$ gives good performance for the estimation data with N_{est} larger than 2000. For the modelling data below 2000, the estimation will be biased. Result from this analysis is shown in Figure (3.27). In that figure, it displays the total number of samples, N. These samples are further divided into two parts; estimation data set (N_{est}) and validation data set (N_{val}).

The eigenvalues obtained after running the identification with different number of sample data are given as

$$\begin{aligned} \text{eig}(A_m) &= [-0.1000 \pm 0.9950j; -0.2500 \pm 4.9937j; -0.0600 \pm 2.9994j] \\ \text{eig}(A_{500}) &= [1.1668; -3.9167; -0.3099 \pm 4.9593j; -0.2819 \pm 2.2390j] \\ \text{eig}(A_{1000}) &= [-0.1114 \pm 0.8451j; -0.2625 \pm 4.9927; -0.0735 \pm 3.0011j] \\ \text{eig}(A_{1500}) &= [-0.0831 \pm 0.9575j; -0.2624 \pm 4.9925; -0.0651 \pm 2.9986j] \\ \text{eig}(A_{2000}) &= [-0.1005 \pm 0.9948j; -0.2624 \pm 4.9925; -0.0645 \pm 2.9992j] \end{aligned}$$

For the eigenvalue of A_{500}, it contains two wrong poles. When the data is not enough, the model is unable to identify the correct poles that represent the system. Therefore, it tends to capture

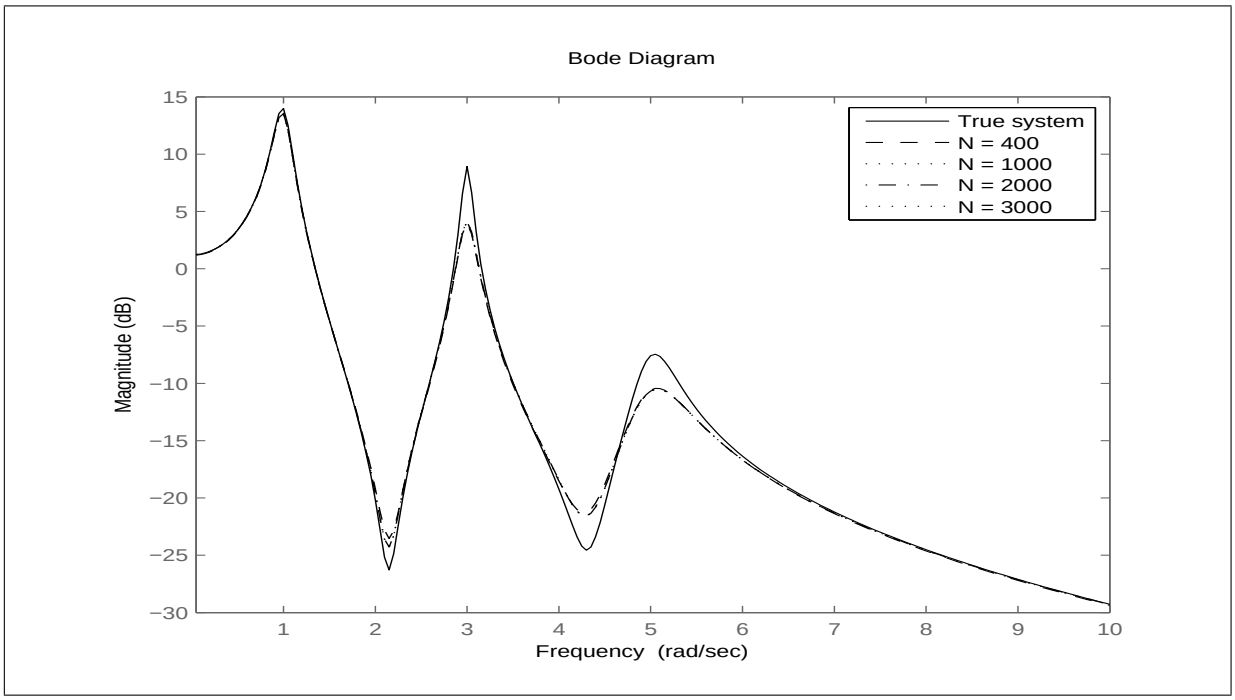

Figure 3.28: Comparison of different amount of data samples ($\Delta t = 0.01s$)

dummy poles (the first two poles) in order to fulfil the requirement of $n = 6$ (actual order of the system). This will also make the system looks unstable since there is one pole that is located on the right-hand plane. Analysis shows that for N greater than 1500 ($N_{est} \geq 750$), then only the model is able to capture the correct poles.

The analysis is also performed by decreasing the sampling time to $\Delta t = 0.01s$. The result from this analysis is shown in Figure (3.28). The result gives similar performance even though the data samples are increased. This also results in similar eigenvalues for all tested data samples which is given as

$$\text{eig}(A_m) = [-0.1000 \pm 0.9950j; -0.2500 \pm 4.9937j; -0.0600 \pm 2.9994j]$$

$$\text{eig}(A_{200}) = [-0.1049 \pm 0.9940j; -0.3740 \pm 4.9792j; -0.1049 \pm 2.9972j]$$

$$\text{eig}(A_{500}) = [-0.1049 \pm 0.9940j; -0.3740 \pm 4.9792j; -0.1049 \pm 2.9972j]$$

$$\text{eig}(A_{1000}) = [-0.1049 \pm 0.9940j; -0.3740 \pm 4.9792j; -0.1049 \pm 2.9972j]$$

$$\text{eig}(A_{1500}) = [-0.1049 \pm 0.9940j; -0.3740 \pm 4.9792j; -0.1049 \pm 2.9972j]$$

In contrast, the analysis is also performed by increasing the sampling rate to $\Delta t = 0.0001s$. As the sampling process getting faster, therefore small data samples are not enough to describe the system. For $\Delta t = 0.0001s$, about $N_{est} = 20000$ is needed for the model to describe the system

successfully. In summary, the data samples needed based on different sampling time is given as in Table 3.7.

Table 3.7: Requirement for data samples of noise-free system

Sampling time, Δt	Estimation data, N_{est}	Sampling period, T
0.1 sec	20	2 sec
0.01 sec	200	2 sec
0.001 sec	2000	2 sec
0.0001 sec	20000	2 sec
0.00001 sec	200000	2 sec

Based on the information obtained from Table 3.7, by setting the sampling time $\Delta t = 0.0001s$ or lower, very large amount of data is needed, in which will require a very long computational time. On the other hand, by setting the sampling time $\Delta t = 0.01s$, less data is needed and also reduced the computational time. However, the accuracy of the model in identifying the system is decreased. Therefore, to find the optimal balance between the accuracy and the computational time, the sampling time $\Delta t = 0.001s$ is chosen.

Next, the analysis is run when the system is added with noise. As for $\Delta t = 0.001s$, with noise is added in the system, by using $N_{est} = 2000$ is no longer hold the good performance. Therefore, longer sampling period is required. For instance, as the amount of sample data are increased and up to $N_{est} = 5000$, then only the model shows reasonable performance but to a low level of noise only. In summary, the analysis run over a system with 20dB SNR disturbance provides with the result as in Table 3.8. At this time, in order to reduce the computational load and at the same time to maintain the model accuracy within reasonable performance, the sampling time of $\Delta t = 0.01s$ is chosen.

Table 3.8: Requirement for data samples of noise-added system

Sampling time, Δt	Estimation data, N_{est}	Sampling period, T
0.1 sec	200	20 sec
0.01 sec	2000	20 sec
0.001 sec	20000	20 sec
0.0001 sec	200000	20 sec

In conclusion, the chances for successful identification are very much relied on the system, amount of data available and the proper time sampling setup. Therefore, proper judgement and preliminary analysis before running the identification may provide better understanding of the system behaviour.

3.5.2 Optimal Selection for Design Parameters

In the subspace identification algorithm, there are three main adjustable parameters that play an important role in developing the state space model. First parameter is the p parameter, which plays a role in tuning the Laguerre filter network. Second is the i parameter, which determines the length of row for the extended observability matrix and the Hankel matrix. Third is the n parameter, which determines the model order.

The optimal search for these parameters are necessary in order to obtain a reliable and correct model to represent the systems. However, there is no significant way to determine the absolutely correct value for these parameters since most of the system dynamic is unknown. As for the p parameter, the only information that can be put under consideration is that p must be greater than zero in order to maintain the stability of the Laguerre filter. Therefore, one possible way to choose the value for parameter p is by calculating its mean square error with the assumption that, a good model will provide a better prediction of the system behaviour with minimum mean square error. The MSE formula is given as

$$\text{MSE} = \frac{1}{N}\sum_{a=1}^{N} \mid y(t_a) - \hat{y}(t_a) \mid^2$$

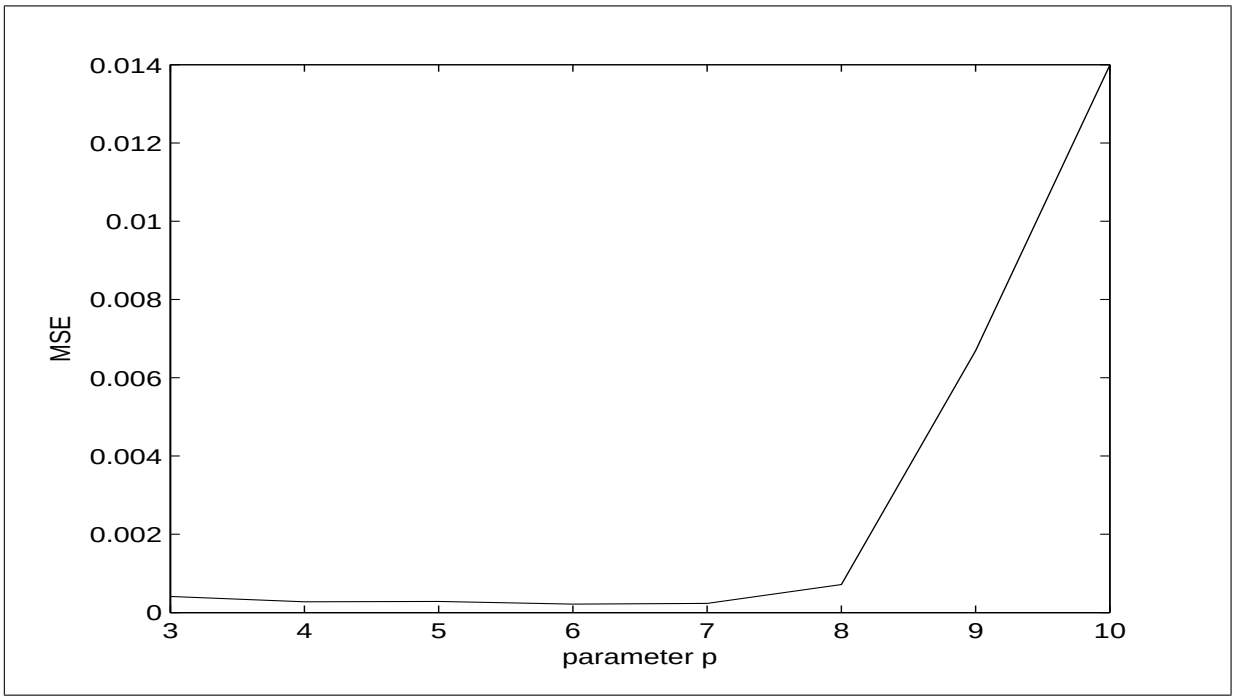

Figure 3.29: MSE run for optimal p

Consider analysing the identification over SISO simulated data systems discussed in previous section. With $N = 4000$, $\Delta t = 0.01s$, $i = 10$ and $n = 6$, the MSE test for this analysis is shown in Figure (3.29). From this figure, it shows that the model has low MSE when the value of ($p < 8$). Based on the analysis, we observed that tuning the parameter p of Laguerre filter plays an important role in improving the subspace model. However, the model is quite sensitive towards the change of parameter p especially when is applied to the noisy data systems. By manipulating the parameter p of the Laguerre network, the model is able to identify the system if moderate noise is perturbed with the system.

Next parameter on test is the i-parameter. This variable determines the number of terms for the observability matrix as well as represents how many block of rows constructed after filtering the data with Laguerre filter network. The number of block of rows is basically a user-defined index which is sufficiently large, at least larger than the maximum order of the system to be identified. Theoretically, the number of block rows should only be larger than the largest observability index, but since this index is unknown, so an assumption is made that $i > n$ [99, 165]. The result from this analysis of the system with a model order, $n = 6$ can be seen as in Figure (3.30). This figure shows that the model has low MSE for $i < 11$.

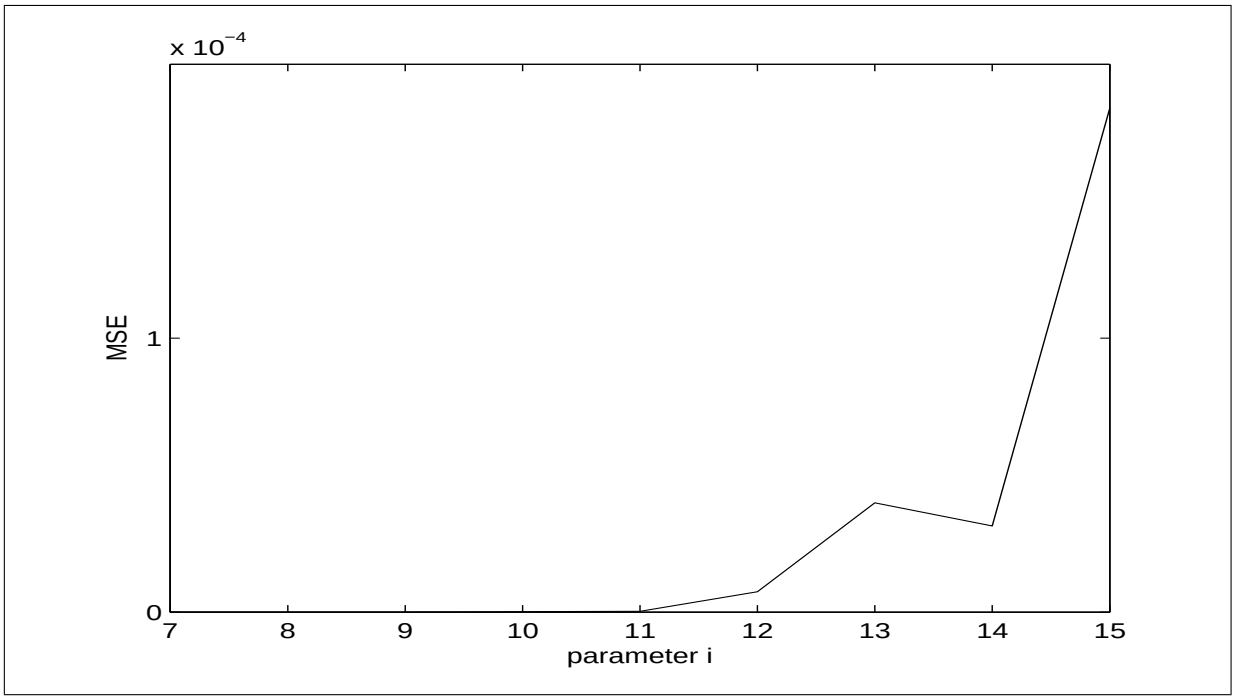

Figure 3.30: MSE run for optimal i

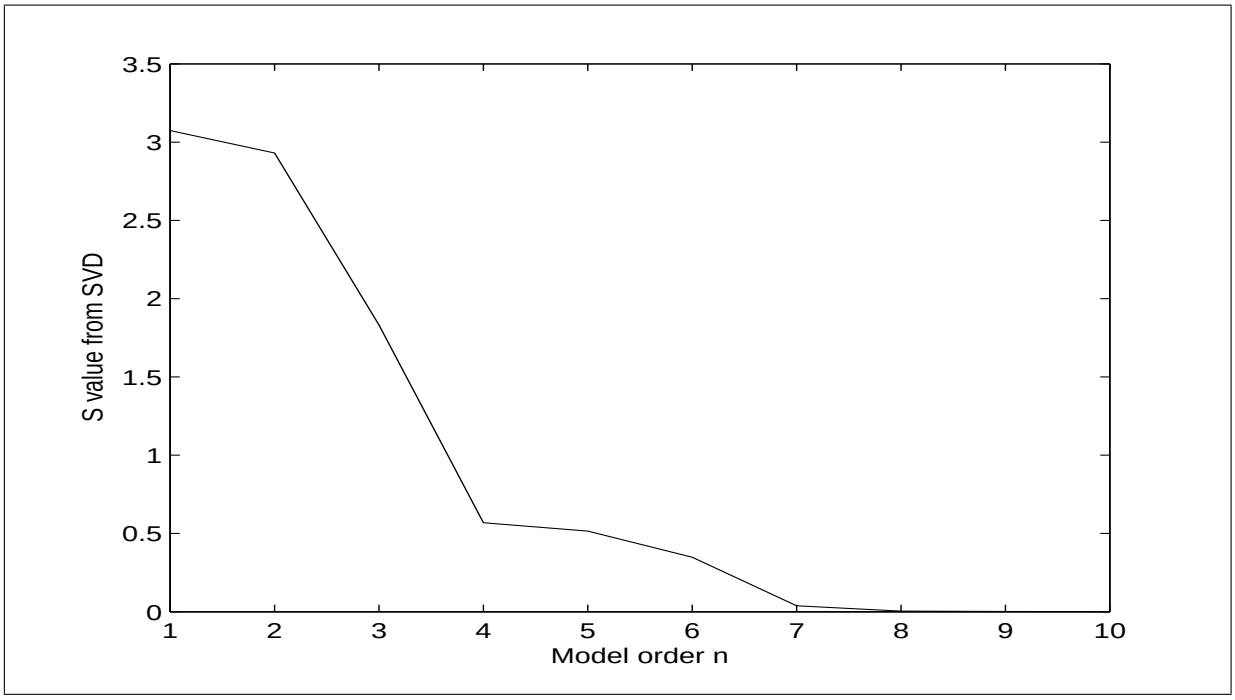

Figure 3.31: Diagonal plot of S matrix - simulated time domain data

The third parameter is the $n-$parameter. It represents the model order of the estimated system. For the subspace methods, a common approach to determine the model order is based on the diagonal plot of S matrix after performing the SVD. The diagonal plot obtained from the model identification can be seen as in Figure (3.31).

3.6 Summary

This chapter has presented a subspace method to identify a continuous time state space model using Laguerre filter network and the instrumental variables. The first part of this chapter has introduced the bilinear transformation in which finally leads to the use of Laguerre filter network. The innovation of constructing filtered data matrices using differential equations provides better computation and easily maintainable parametrization. The second part of this chapter has explained the role of instrumental variable in coping with process and measurement noise. The simulation results are demonstrated to identify both SISO and MIMO systems. Results have shown a good performance of the subspace method to estimate the continuous time system closely. In addition, the performance comparison with other available models in MATLAB system identification toolbox is also carried out. The implementation issues that relate to the subspace state-space model identification are also justified. This will become a useful guideline for the usage of the subspace identification approach in the later chapters.

Chapter 4

Continuous Time Closed-loop System Identification

4.1 Introduction

In closed-loop system, the correlation between the input signal and the output noise may occur since the output and the noise output are fed back to the system. Thus, the subspace identification methods presented in open-loop approach will give bias in closed-loop operating system. Fortunately, with special modifications, the subspace methods are able to perform the task as well. The idea of implementing the subspace method for identification of a closed-loop system has been studied in early 90s (see for examples in [30,85,100,166,170]). Recent examples can be referred in [29,84,96,132,133]. In some cases, an assumption that the input is not correlated with the output noise is always made or if any, it will be in at least in one sample delay. However, in state-space model identification, most of the subspace approaches are proposed in discrete time model and the choice of either the regression or prediction matrix is based on future horizon variables.

In contrast, this chapter will study the subspace methods in estimating a state-space model for a continuous time closed-loop systems. The research into identification of a closed-loop system starts with the problem of identifying a system in a noisy input and noisy output condition. This phenomena is known as the error in variables (EIV) problem. There are two approaches

that will be studied in this chapter.

The first approach adopting the idea of using subspace method to identify a closed-loop system for EIV models by Chou and Verhaegen [30]. However, the approach in this chapter handles the closed-loop systems in a different way. As a continuous time closed-loop identification is the prime subject, the Laguerre filter network is used in the identification procedure. The regression matrix is based on past horizon. Furthermore, to maintain the stability and causality of the filter, the extended future horizon is used as instrumental variables and the matrix configurations are manipulated in such a way to satisfy the closed-loop conditions. This configuration will give consistent estimates for the deterministic part of the state space model (i.e. (A,B,C) matrices).

Second approach considers the idea by Zhao and Westwick in which the subspace methods were used to identify a closed-loop system of Wiener models [192]. The similarity with their approach is on setting the choice of instrumental variables in which the reference signal is used as an instrument. However, in this chapter, the future reference is used instead of the past reference signal. This approach is also used to identify a continuous time closed-loop systems. The use of Laguerre filter network in the identification will definitely give different viewpoint from them.

The content for this chapter is partially taken from a paper by author as can be referred in [118]. This chapter starts with the formulation of error in variable problem discussed in Section 4.2. The step by step approach in solving this identification problem leads to the development of closed-loop system identification. With the idea gathered from the discrete time problem formulation, the new continuous time subspace identification approach is developed. The simulation results of SISO and MIMO system identification are shown as to demonstrate the performance of the proposed model. In Section 4.3, another approach based on a reference signal as a choice of instrumental variable is studied. The experimental results are also shown as to demonstrate the performance of the proposed model in identifying systems, from simulated data to real data taken from the magnetic bearing apparatus. Finally, Section 4.4 concludes the chapter.

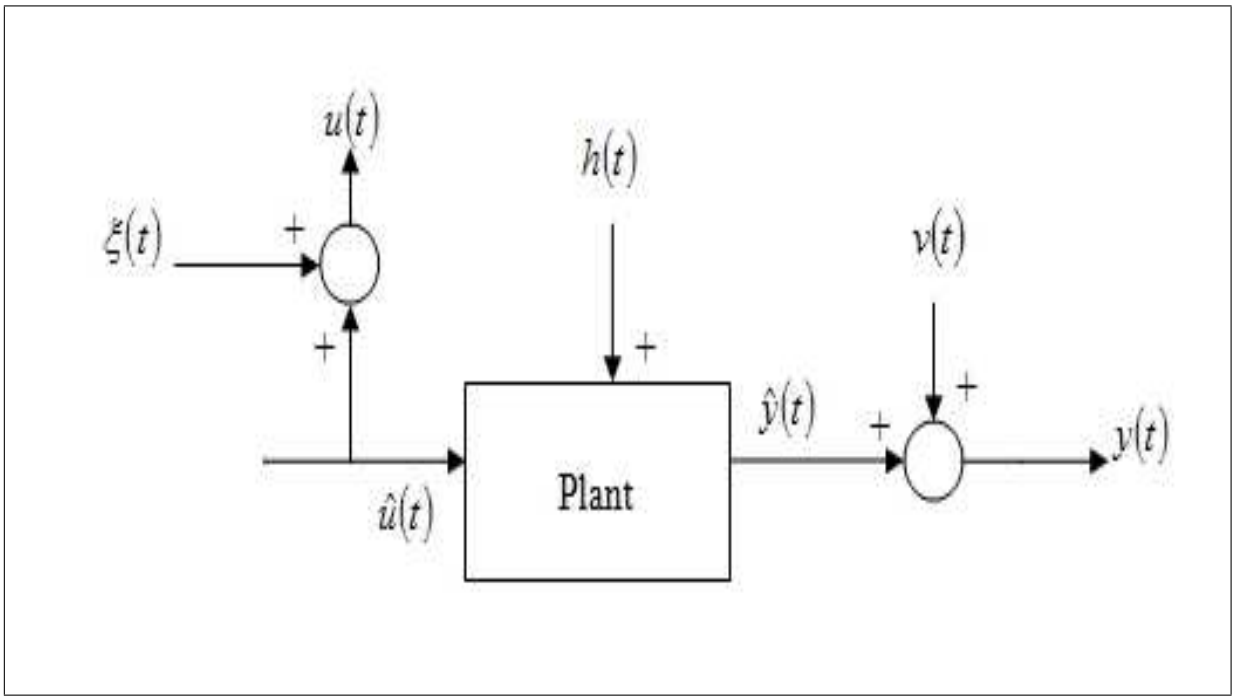

Figure 4.1: Schematic representation of the EIV identification problem

4.2 Error in Variable Problem Formulation

In broad definition, the error in variable (EIV) problem actually refers to the problem of identifying a model in a noisy input-output environment. In this case, an assumption is made that every variable can have error or noise. In system modelling perspective, this means that both the input and output variables are perturbed by noise. The scenario of this problem is illustrated in Figure (4.1). The system can be modelled by the following state-space equations

$$\dot{x}(t) = Ax(t) + B\hat{u}(t) + h(t) \tag{4.1}$$

$$y(t) = Cx(t) + D\hat{u}(t) + v(t) \tag{4.2}$$

$$u(t) = \hat{u}(t) + \xi(t) \tag{4.3}$$

In general, the problem is to determine the system characteristics, such as the transfer function. In doing so, there are three different categories of reported estimation algorithms for EIV problem.

1. Using the covariance matrix. This category includes the instrumental variable (IV) method [30, 149, 152], total least squares (TLS) method [68–70], bias eliminating least squares (BELS) method [51, 104, 193] and the Frisch scheme [18, 24, 148].

2. Using the input-output spectrum and the frequency domain data [17, 127, 128].

3. Using the original time series data. This category includes the prediction error method (PEM) and the maximum likelihood (ML) techniques [128, 129].

A survey paper by Soderstrom gives an excellent explanation regarding all the method described above [146]. In judging the phenomena of EIV problem, there are two classifications that have normally been made by the researchers. The first class assumes that the input and the output systems are both disturbed by the white noise. On the other hand, the second class defines the input measurement noise is to be either white or moving average (MA) process while the output measurement noise is assumed to be coloured.

In this thesis, the research interest is emphasized on the subspace identification algorithm with the adoption of instrumental variable estimators to solve the EIV problem proposed by Chou and Verhaegen [30]. In their work, they employed instrumental variables and subspace model identification [165,172] to identify a discrete time linear time-invariant state-space models under the EIV formulation. Two estimation methods are given. One is to solve the EIV problem for open loop case in which the assumption is made that the input and output noise are white noise disturbance. The other one is on estimation when the input noise is not a white noise. The second estimation also leads to the estimation of closed-loop problem, which will become our interest in this chapter.

4.2.1 EIV in the Closed-loop System

Consider a discrete time model describing the open-loop system of EIV problem. In mathematical formulation, the model can be described by the following state-space equations

$$x(k+1) = Ax(k) + B\hat{u}(k) + h(k) \tag{4.4}$$

$$y(k) = Cx(k) + D\hat{u}(k) + v(k) \tag{4.5}$$

$$u(k) = \hat{u}(k) + \xi(k) \tag{4.6}$$

where $x(k) \in R^n$ is the state-vector, $u(k) \in R^m$ is the measured input signals, $\hat{u}(k) \in R^m$ is the noise-free input and $y(k) \in R^l$ is the measured output signals. $A \in R^{n\times n}$, $B \in R^{n\times m}$, $C \in R^{l\times n}$ and $D \in R^{l\times m}$ are the system matrices. The input is added with measurement noise, $\xi(t)$ while

the output is added with process noise, $h(t)$ and measurement noise, $v(t)$. Let the input and output data set be declared as $u(k), y(k), k \in [1, N]$.

The EIV identification problem works with an assumption that,

1. The $\xi(k)$, $h(k)$ and $v(k)$ are assumed to be discrete time, zero mean, white noise.
2. These disturbances are assumed to be statistically independent of the past noise-free input, $\hat{u}(k)$.

$$\mathbf{E}[\hat{u}(k)h(j)^\top] = \mathbf{E}[\hat{u}(k)v(j)^\top] = \mathbf{E}[\hat{u}(k)\xi(j)^\top] = 0 \qquad \text{for all} \qquad j \geq k$$

   where $\mathbf{E}$ denotes the expectation operator.
3. $\xi(k)$ and $v(k)$ are independent of the state sequence, $x(k)$ and the process noise $h(k)$ (with $k \geq 1$) is independent of the initial state $x(1)$.
4. The three disturbances are assumed to be correlated and their covariance is given by the following unknown matrix

$$\mathbf{E}\left[\begin{pmatrix} h(k) \\ \xi(k) \\ v(k) \end{pmatrix} \begin{pmatrix} h(j)^\top & \xi(j)^\top & v(j)^\top \end{pmatrix}\right] = \begin{bmatrix} \sum(h) & \sum(h\xi) & \sum(hv) \\ \sum(h\xi)^\top & \sum(\xi) & \sum(\xi v) \\ \sum(hv)^\top & \sum(\xi v)^\top & \sum(v) \end{bmatrix} \delta(kj) \geq 0$$

   where $\delta(kj)$ denotes the Kronecker delta.
5. The signals in the identification problem to be the realizations of ergodic stochastic processes such that, for $N \to \infty$, $[u(1), \ldots, u(N)]$ and $[v(1), \ldots, v(N)]$ are realizations of u and v respectively.

Then, the identification problem is to consistently estimate:

1. The system order, n.
2. The extended observability matrix, $\mathcal{O}_j$ based on the availability of input signal $u(k)$ and output signal $y(k)$.
3. The (A, B, C, D) matrices.

The data equation is constructed as

$$Y_{i,j,N} = \mathcal{O}_j X_{i,N} + \Gamma_j U_{i,j,N} - \Gamma_j F_{i,j,N} + \Psi_j H_{i,j,N} + V_{i,j,N} \tag{4.7}$$

where $\mathcal{O}_j$ is the extended observability matrix and both Γ_j and Ψ_j are Toeplitz matrices. Define $U_{i,j,N}$ and $Y_{i,j,N}$ as the future input and future output, and $U_{0,i,N}$ and $Y_{0,i,N}$ as the past input and past output. The instrumental variable is based on the past input and past output. Post-multiply the data equation (4.7) with the IV is expressed as

$$\begin{aligned}
\frac{1}{N} Y_{i,j,N} \begin{bmatrix} U_{0,i,N}^\top & Y_{0,i,N}^\top \end{bmatrix} &= \mathcal{O}_j \frac{1}{N} X_{i,N} \begin{bmatrix} U_{0,i,N}^\top & Y_{0,i,N}^\top \end{bmatrix} + \Gamma_j \frac{1}{N} U_{i,j,N} \begin{bmatrix} U_{0,i,N}^\top & Y_{0,i,N}^\top \end{bmatrix} \\
&- \Gamma_j \frac{1}{N} F_{i,j,N} \begin{bmatrix} U_{0,i,N}^\top & Y_{0,i,N}^\top \end{bmatrix} + \Psi_j \frac{1}{N} H_{i,j,N} \begin{bmatrix} U_{0,i,N}^\top & Y_{0,i,N}^\top \end{bmatrix} \\
&+ \frac{1}{N} V_{i,j,N} \begin{bmatrix} U_{0,i,N}^\top & Y_{0,i,N}^\top \end{bmatrix}
\end{aligned} \tag{4.8}$$

For the case where the noise-free input $\hat{u}(k)$ is a white noise sequence, post-multiplying the data Equation (4.7) with the instrumental variable will eliminate the second, third, fourth and fifth term on the right-hand side as $N \to \infty$ (Third, fourth and fifth term tend to zero as $N \to \infty$ since $F_{i,j,N}$, $H_{i,j,N}$ and $V_{i,j,N}$ are uncorrelated with the instruments, whereas the second term tend to zero as $N \to \infty$ due to white noise property of $\hat{u}(k)$). However, if the noise-free input $\hat{u}(k)$ is not a white noise sequence, the third, fourth and fifth terms tend to zero due to uncorrelated condition with the instruments but, the second term remains non-zero.

To solve this problem, the following solution is introduced. Let the following RQ factorization be given as

$$\begin{aligned}
\begin{bmatrix} U_{i,j,N} \\ Y_{i,j,N} \end{bmatrix} \begin{bmatrix} U_{0,i,N}^\top & Y_{0,i,N}^\top \end{bmatrix} &= \begin{bmatrix} R_{11} & 0 \\ R_{21} & R_{22} \end{bmatrix} \begin{bmatrix} Q_1 \\ Q_2 \end{bmatrix} \\
\begin{bmatrix} U_{i,j,N} U_{0,i,N}^\top & U_{i,j,N} Y_{0,i,N}^\top \\ Y_{i,j,N} U_{0,i,N}^\top & Y_{i,j,N} Y_{0,i,N}^\top \end{bmatrix} &= \begin{bmatrix} R_{11} & 0 \\ R_{21} & R_{22} \end{bmatrix} \begin{bmatrix} Q_1 \\ Q_2 \end{bmatrix}
\end{aligned} \tag{4.9}$$

By using the RQ factorization given in Equation (4.9), Equation (4.8) can be rewritten as

$$R_{21} Q_1 + R_{22} Q_2 = \mathcal{O}_j X_{i,N} \begin{bmatrix} U_{0,i,N}^\top & Y_{0,i,N}^\top \end{bmatrix} + \Gamma_j R_{11} Q_1 + \zeta \tag{4.10}$$

where ζ contains the three terms in Equation (4.8) which will be disappeared as $N \to \infty$.

Post-multiply both sides of Equation (4.10) by $\frac{1}{\sqrt{N}}Q_1^\top$ and taking the limit, then

$$\lim_{N\to\infty}\frac{1}{\sqrt{N}}R_{21} = \lim_{N\to\infty}\frac{1}{\sqrt{N}}\times\left(\mathcal{O}_j X_{i,N}\left[\begin{array}{cc} U_{0,i,N}^\top & Y_{0,i,N}^\top \end{array}\right]Q_1^\top + \Gamma_j R_{11}\right) \tag{4.11}$$

And post-multiply both sides of Equation (4.10) by $\frac{1}{\sqrt{N}}Q_2^\top$ and taking the limit, then

$$\lim_{N\to\infty}\frac{1}{\sqrt{N}}R_{22} = \lim_{N\to\infty}\frac{1}{\sqrt{N}}\mathcal{O}_j X_{i,N}\times\left[\begin{array}{cc} U_{0,i,N}^\top & Y_{0,i,N}^\top \end{array}\right]Q_2^\top \tag{4.12}$$

Let $\rho(M)$ denotes the rank of the matrix M, then under the condition that

$$\rho\left(\lim_{N\to\infty}\frac{1}{\sqrt{N}}X_{i,N}\left[\begin{array}{cc} U_{0,i,N}^\top & Y_{0,i,N}^\top \end{array}\right]Q_2^\top\right) = n$$

Therefore, Equation (4.12) gives a consistent estimate of the extended observability matrix, $\mathcal{O}_j$, and is represented by the matrix R_{22} in Equation (4.9).

This algorithm is also applicable to identify the closed-loop system since the only requirement is to have $\hat{u}(k)$ that is uncorrelated with the future $h(k)$, $v(k)$ and $\xi(k)$. Thus, the significant advantage of this algorithm will be extended to identify the continuous time closed-loop system.

4.2.2 Continuous Time Closed-loop Identification

The continuous time closed-loop identification system is described with the help of Figure (4.2). In mathematical formulation, the continuous time closed-loop system is given by the following state-space model equations

$$\dot{x}(t) = Ax(t) + B\hat{u}(t) + h(t) \tag{4.13}$$

$$y(t) = Cx(t) + D\hat{u}(t) + v(t) \tag{4.14}$$

$$\hat{u}(t) = r(t) - u_c(t) \tag{4.15}$$

$$u(t) = \hat{u}(t) + \xi(t) \tag{4.16}$$

The controller model is defined as

$$\dot{x}_c(t) = A_c x_c(t) + B_c y(t) \tag{4.17}$$

$$u_c(t) = C_c x_c(t) \tag{4.18}$$

Here, $x(t) \in R^n$ is the state-vector, $u(t) \in R^m$ is the measured input signals, $y(t) \in R^l$ is the measured output signals and $r(t)$ is the reference signal. $A \in R^{n\times n}$, $B \in R^{n\times m}$, $C \in R^{l\times n}$ and

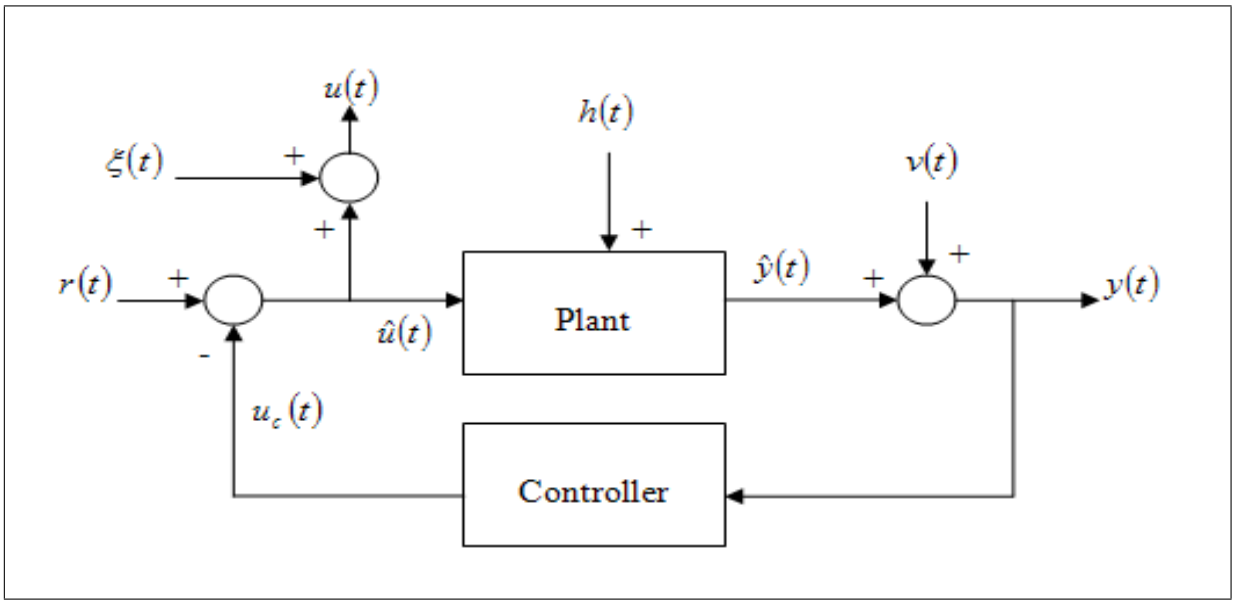

Figure 4.2: Schematic representation of the closed-loop model

$D \in R^{l \times m}$ are the system matrices. $u_c(t)$ is the control signal from the feedback controller. The input is added with measurement noise, $\xi(t)$ while the output is added with process noise, $h(t)$ and measurement noise, $v(t)$.

Let the input and output data set declared as $u(t_k), y(t_k), k \in [1, N]$ and its sampling time is t_k. The noise term $h(t)$, $v(t)$ and $\xi(t)$ are denoted as zero mean white noise. There are few assumptions need to be made in order to solve this identification problem.

1. The reference input, $r(t)$, the input, $\hat{u}(t)$ and the initial states are assumed to be uncorrelated with future value of noise.
2. The controller is assumed to be stabilizing and causal.
3. The system is assumed to be minimal and to have at least one delay.

Since the closed-loop system is stable, therefore $\hat{u}(t)$ is a stationary signal. And if, there is at least a delay in the controller, the requirement for $\hat{u}(t)$ to be uncorrelated with future noise is hold since $\hat{u}(t)$ depends only on the past values of $y(t)$ and also past value of noise. Then, the problem is to consistently estimate:

1. The system order, n.

2. The extended observability matrix, $\mathcal{O}_j$ based on the availability of input signal $u(t)$ and output signal $y(t)$.

3. The $\hat{A}$ and $\hat{C}$ matrices obtained from the extended observability matrix

$$\mathcal{O}_j = \begin{bmatrix} C_w \\ C_w A_w \\ \vdots \\ C_w A_w^{j-1} \end{bmatrix}$$

4. The $\hat{B}$ and $\hat{D}$ matrices by using a least squares solution of

$$\hat{y}(\ t \ \Big|\ B, D\ ) = \hat{C}(qI_n - \hat{A})^{-1}\hat{B}u(t) + \hat{D}u(t)$$

The state-space equations in Laplace domain are defined as

$$sX(s) = AX(s) + BU(s) - BF(s) + H(s) \tag{4.19}$$

$$Y(s) = CX(s) + DU(s) - DF(s) + V(s) \tag{4.20}$$

where $F(s)$ denotes the matrices represent the input noise, $\xi(t)$. The filtering process of input and output data system using the Laguerre filter are similar to the one that has been discussed in Chapter 3. Therefore, the model description in Equations (4.19-4.20) is transformed into:

$$[wx](t) = A_w x(t) + B_w[w_0 u](t) - B_w[w_0 \xi](t) + [w_0 h_w](t) \tag{4.21}$$

$$[w_0 y](t) = C_w x(t) + D_w[w_0 u](t) - D_w[w_0 \xi](t) + [w_0 v_w](t) \tag{4.22}$$

where

$$\begin{aligned} h_w(t) &= \sqrt{2p}(A + pI_n)^{-1}h(t) \\ v_w(t) &= \frac{1}{\sqrt{2p}}Ch_w(t) + v(t) \end{aligned} \tag{4.23}$$

Observing Equations (4.21-4.22), data equations are constructed as

$$
\begin{aligned}
w_0 y(t) &= C_w x(t) + D_w w_0 u(t) - D_w w_0 \xi(t) + w_0 v_w(t) \\
w_0 w y(t) &= C_w w x(t) + D_w w_0 w u(t) - D_w w_0 w \xi(t) + w_0 w v_w(t) \\
&= C_w [A_w x(t) + B_w w_0 u(t) - B_w w_0 \xi(t) + w_0 h_w(t)] + D_w w_0 w u(t) \\
&- D_w w_0 w \xi(t) + w_0 w v_w(t) \\
&= C_w A_w x(t) + C_w B_w w_0 u(t) - C_w B_w w_0 \xi(t) + C_w w_0 h_w(t) + D_w w_0 w u(t) \\
&- D_w w_0 w \xi(t) + w_0 w v_w(t) \\
w_0 w^2 y(t) &= C_w A_w w x(t) + C_w B_w w_0 w u(t) - C_w B_w w_0 w \xi(t) + C_w w_0 w h_w(t) + D_w w_0 w^2 u(t) \\
&- D_w w_0 w^2 \xi(t) + w_0 w^2 v_w(t) \\
&= C_w A_w [A_w x(t) + B_w w_0 u(t) - B_w w_0 \xi(t) + w_0 h_w(t)] + C_w B_w w_0 w u(t) \\
&- C_w B_w w_0 w \xi(t) + C_w w_0 w h_w(t) + D_w w_0 w^2 u(t) - D_w w_0 w^2 \xi(t) + w_0 w^2 v_w(t) \\
&= C_w A_w^2 x(t) + C_w A_w B_w w_0 u(t) - C_w A_w B_w w_0 \xi(t) + C_w A_w w_0 h_w(t) + C_w B_w w_0 w u(t) \\
&- C_w B_w w_0 w \xi(t) + C_w w_0 w h_w(t) + D_w w_0 w^2 u(t) - D_w w_0 w^2 \xi(t) + w_0 w^2 v_w(t)
\end{aligned}
$$

By repetitively multiplying with w, the continuous time data equations are rearranged as

$$
\begin{aligned}
\begin{bmatrix} [w_0 y](t) \\ [w_1 y](t) \\ \vdots \\ [w_{i-1} y](t) \end{bmatrix} &= \begin{bmatrix} C_w \\ C_w A_w \\ \vdots \\ C_w A_w^{i-1} \end{bmatrix} x(t) + \begin{bmatrix} D_w & 0 & \cdots & 0 \\ C_w B_w & D_w & \ddots & \vdots \\ \vdots & \ddots & \ddots & 0 \\ C_w A_w^{i-2} B_w & \cdots & C_w B_w & D_w \end{bmatrix} \begin{bmatrix} [w_0 u](t) \\ [w_1 u](t) \\ \vdots \\ [w_{i-1} u](t) \end{bmatrix} \\
&- \begin{bmatrix} D_w & 0 & \cdots & 0 \\ C_w B_w & D_w & \ddots & \vdots \\ \vdots & \ddots & \ddots & 0 \\ C_w A_w^{i-2} B_w & \cdots & C_w B_w & D_w \end{bmatrix} \begin{bmatrix} [w_0 \xi](t) \\ [w_1 \xi](t) \\ \vdots \\ [w_{i-1} \xi](t) \end{bmatrix} \\
&+ \begin{bmatrix} 0 & 0 & \cdots & 0 \\ C_w & 0 & \ddots & \vdots \\ \vdots & \ddots & \ddots & 0 \\ C_w A_w^{i-2} & \cdots & C_w & 0 \end{bmatrix} \begin{bmatrix} [w_0 h_w](t) \\ [w_1 h_w](t) \\ \vdots \\ [w_{i-1} h_w](t) \end{bmatrix} + \begin{bmatrix} [w_0 v_w](t) \\ [w_1 v_w](t) \\ \vdots \\ [w_{i-1} v_w](t) \end{bmatrix}
\end{aligned} \tag{4.24}
$$

Introduce the new noise disturbance as

$$F_{i,j}^{f}(t) = \begin{bmatrix} [w_i\xi](t) \\ [w_{i+1}\xi](t) \\ \vdots \\ [w_{i+j-1}\xi](t) \end{bmatrix}$$

Therefore, the continuous time data equation can be written in a compact form as follows

$$Y_{i,j}^{f}(t) = \mathcal{O}_j\hat{X}(t) + \Gamma_j U_{i,j}^{f}(t) - \Gamma_j F_{i,j}^{f}(t) + \Psi_j H_{i,j}^{f}(t) + V_{i,j}^{f}(t) \tag{4.25}$$

Expanding the column matrices for N data samples, the equation becomes

$$Y_{i,j,N}^{f}(t) = \mathcal{O}_j\hat{X}_{i,N}(t) + \Gamma_j U_{i,j,N}^{f}(t) - \Gamma_j F_{i,j,N}^{f}(t) + \Psi_j H_{i,j,N}^{f}(t) + V_{i,j,N}^{f}(t) \tag{4.26}$$

where the data matrices for a new term in the equation is constructed as

$$F_{i,j,N}^{f} = \begin{bmatrix} [w_i\xi](t_1) & [w_i\xi](t_2) & \dots & [w_i\xi](t_N) \\ [w_{i+1}\xi](t_1) & [w_{i+1}\xi](t_2) & \dots & [w_{i+1}\xi](t_N) \\ \vdots & \vdots & \vdots & \vdots \\ [w_{i+j-1}\xi](t_1) & [w_{i+j-1}\xi](t_2) & \dots & [w_{i+j-1}\xi](t_N) \end{bmatrix} \tag{4.27}$$

In this situation, the input is added with measurement noise, just like the output is added with process and measurement noise. For this case, the subspace method discussed in Chapter 3 will not give consistent estimate anymore, since the disturbance is correlated with the input. This scenario is very common for a system that is operated in closed-loop, as the noise that enters the system at any point in the loop tends to influence the input or the output signal.

Thus, in the continuous time closed-loop system identification, the identification solution similar to the discrete time EIV problem defined in Equation (4.9) is considered. The differences are on the adoption of Laguerre filter and the instrumental variables, in which are based on future input and output horizon.

4.2.3 Identification Procedure

Let $u(t)$ and $y(t)$ be the input and output plant data described in Equations (4.13-4.16). Let $U_{0,i,N}^{f}$, $Y_{0,i,N}^{f}$, $U_{i,j,N}^{f}$ and $Y_{i,j,N}^{f}$ be the filtered data matrices constructed from $u(t)$ and $y(t)$. The

continuous time closed-loop identification considers the following RQ factorization.

$$\begin{bmatrix} U^f_{0,i,N} \\ Y^f_{0,i,N} \end{bmatrix} P^\top = \begin{bmatrix} R_{11} & 0 \\ R_{21} & R_{22} \end{bmatrix} \begin{bmatrix} Q_1 \\ Q_2 \end{bmatrix} \tag{4.28}$$

where

$$P = \begin{bmatrix} U^f_{i,j,N} \\ Y^f_{i,j,N} \end{bmatrix}$$

Then the following holds

$$\lim_{N\to\infty} \frac{1}{\sqrt{N}} R_{22} = \lim_{N\to\infty} \mathcal{O}_i \hat{X}^f_{0,N} P^\top Q_2^\top \tag{4.29}$$

Proof:

From the RQ factorization of Equation (4.28) we have

$$\lim_{N\to\infty} \frac{1}{\sqrt{N}} R_{22} = \lim_{N\to\infty} \frac{1}{\sqrt{N}} Y^f_{0,i,N} P^\top Q_2^\top \tag{4.30}$$

From Equation (4.25) we have

$$\begin{aligned} \lim_{N\to\infty} \frac{1}{\sqrt{N}} Y^f_{0,i,N} P^\top Q_2^\top &= \lim_{N\to\infty} \frac{1}{\sqrt{N}} \mathcal{O}_i \hat{X}^f_{0,N} P^\top Q_2^\top + \lim_{N\to\infty} \frac{1}{\sqrt{N}} \Gamma_i U^f_{0,i,N} P^\top Q_2^\top \\ &- \lim_{N\to\infty} \frac{1}{\sqrt{N}} \Gamma_i F^f_{0,i,N} P^\top Q_2^\top + \lim_{N\to\infty} \frac{1}{\sqrt{N}} \Psi_i H^f_{0,i,N} P^\top Q_2^\top \\ &+ \lim_{N\to\infty} \frac{1}{\sqrt{N}} V^f_{0,i,N} P^\top Q_2^\top \end{aligned} \tag{4.31}$$

As $U^f_{0,i,N} P^\top = R_{11} Q_1$, the second term on the right hand side goes to zero because of the post-multiplication between Q_1 and Q_2.

$$\lim_{N\to\infty} \frac{1}{\sqrt{N}} \Gamma_i U^f_{0,i,N} P^\top Q_2^\top = 0 \tag{4.32}$$

Next is to prove that the third, fourth and fifth term on the right hand side also goes to zero as N goes to infinity

$$\lim_{N\to\infty} \frac{1}{\sqrt{N}} \Gamma_i F^f_{0,i,N} P^\top Q_2^\top + \lim_{N\to\infty} \frac{1}{\sqrt{N}} \Psi_i H^f_{0,i,N} P^\top Q_2^\top + \lim_{N\to\infty} \frac{1}{\sqrt{N}} V^f_{0,i,N} P^\top Q_2^\top = 0 \tag{4.33}$$

With the assumption that there is at least a delay in the controller, therefore the future input and output are independent of the noise sources $\xi(t)$, $h(t)$ and $v(t)$, therefore

$$\lim_{N\to\infty} \frac{1}{N} F^f_{0,i,N} P^\top = 0$$

$$\lim_{N\to\infty} \frac{1}{N} H^f_{0,i,N} P^\top = 0$$

$$\lim_{N\to\infty}\frac{1}{N}V^f_{0,i,N}P^\top = 0$$

Equation (4.31) reduces to

$$\lim_{N\to\infty}\frac{1}{\sqrt{N}}Y^f_{0,i,N}P^\top Q_2^\top = \lim_{N\to\infty}\frac{1}{\sqrt{N}}\mathcal{O}_i\hat{X}^f_{0,N}P^\top Q_2^\top$$

From computation point of view, the straightforward implementation of Equation (4.28) that involves multiplication of data matrices will normally lead to a loss of precision [30]. The required matrix that has the same column space as of R_{22} can be computed without explicitly forming the matrix product given in Equation (4.28). This can be done by stacking the instrumental variable in the middle of the past input and the past output.

$$\begin{bmatrix} U^f_{0,i,N} \\ \begin{bmatrix} U^f_{i,j,N} \\ Y^f_{i,j,N} \end{bmatrix} \\ Y^f_{0,i,N} \end{bmatrix} = \begin{bmatrix} \hat{R}_{11} & 0 & 0 \\ \hat{R}_{21} & \hat{R}_{22} & 0 \\ \hat{R}_{31} & \hat{R}_{32} & \hat{R}_{33} \end{bmatrix} \begin{bmatrix} \hat{Q}_1 \\ \hat{Q}_2 \\ \hat{Q}_3 \end{bmatrix} \tag{4.34}$$

Then rearrange the matrix as

$$\begin{bmatrix} U^f_{0,i,N} \\ Y^f_{0,i,N} \end{bmatrix} \begin{bmatrix} (P^f_{i,j,N})^\top \end{bmatrix} = \begin{bmatrix} \hat{R}_{11} & 0 & 0 \\ \hat{R}_{31} & \hat{R}_{32} & \hat{R}_{33} \end{bmatrix} \begin{bmatrix} \hat{Q}_1 \\ \hat{Q}_2 \\ \hat{Q}_3 \end{bmatrix} \begin{bmatrix} \hat{Q}_1^\top & \hat{Q}_2^\top & \hat{Q}_3^\top \end{bmatrix} \begin{bmatrix} \hat{R}_{21}^\top \\ \hat{R}_{22}^\top \\ 0 \end{bmatrix}$$

$$= \begin{bmatrix} \hat{R}_{11} & 0 \\ \hat{R}_{31} & \hat{R}_{32} \end{bmatrix} \begin{bmatrix} \hat{R}_{21}^\top \\ \hat{R}_{22}^\top \end{bmatrix}$$

Perform another RQ factorization to the second matrix on the right-hand side will give

$$= \begin{bmatrix} \hat{R}_{11} & 0 \\ \hat{R}_{31} & \hat{R}_{32} \end{bmatrix} \begin{bmatrix} \tilde{R}_{11} & 0 \\ \tilde{R}_{21} & \tilde{R}_{22} \end{bmatrix} \begin{bmatrix} \tilde{Q}_1^\top \\ \tilde{Q}_2^\top \end{bmatrix}$$

By comparing the final result of these transformations with (4.28), thus

$$R_{22} = \hat{R}_{32}\tilde{R}_{22}$$

For easy recognition in this chapter, the model that has been developed based on the idea of system identification for EIV problem will be defined as the CEIV where the capital "C" stands for the continuous time. In summary, the subspace method in identifying the continuous time state space model for a closed-loop system can be described as follow.

1. Construct the filtered data matrices of $U^f_{0,i,N}$, $U^f_{i,j,N}$, $Y^f_{0,i,N}$ and $Y^f_{i,j,N}$.

2. Perform the RQ decomposition

$$\begin{bmatrix} U^f_{0,i,N} \\ Y^f_{0,i,N} \end{bmatrix} P^\top = \begin{bmatrix} R_{11} & 0 \\ R_{21} & R_{22} \end{bmatrix} \begin{bmatrix} Q_1 \\ Q_2 \end{bmatrix}$$
$$\begin{bmatrix} U^f_{0,i,N} \\ Y^f_{0,i,N} \end{bmatrix} P^\top = \begin{bmatrix} \hat{R}_{11} & 0 \\ \hat{R}_{31} & \hat{R}_{32} \end{bmatrix} \begin{bmatrix} \tilde{R}_{11} & 0 \\ \tilde{R}_{21} & \tilde{R}_{22} \end{bmatrix} \begin{bmatrix} \tilde{Q}_1^\top \\ \tilde{Q}_2^\top \end{bmatrix}$$

   where $P = [(U^f_{i,j,N})^\top (Y^f_{i,j,N})^\top]$ for the CEIV method.

3. Perform the SVD to the working matrix $\hat{R}_{32}\tilde{R}_{22}$:

$$\hat{R}_{32}\tilde{R}_{22} = USV^\top$$

4. Determine the model order n from the singular value in S.

5. Determine the system matrices (A_w, C_w).

$$A_w = (J_1 U_n)^\dagger J_2 U_n$$
$$C_w = J_3 U_n$$
$$J_1 = \begin{bmatrix} I_{(i-1)l} & 0_{(i-1)l \times l} \end{bmatrix}$$
$$J_2 = \begin{bmatrix} 0_{(i-1)l \times l} & I_{(i-1)l} \end{bmatrix}$$
$$J_3 = \begin{bmatrix} I_{l \times l} & 0_{l \times (i-1)l} \end{bmatrix}$$
$$\Upsilon^\dagger = (\Upsilon^\top \Upsilon)^{-1} \Upsilon^\top$$

   The A and C matrices can be obtained using the relations:

$$\begin{aligned} A &= p(I_n + A_w)(I_n - A_w)^{-1} \\ C &= \sqrt{2p} C_w (I_n - A_w)^{-1} \end{aligned}$$

6. Solve least squares problem from model structure:

$$y(\ t \ \Big|\ B, D\ ) = C(qI_n - A)^{-1}Bu(t) + Du(t)$$

7. Reconstruct B and D from $\begin{bmatrix} B \\ D \end{bmatrix}$

8. Generate the estimated output, $\hat{y}(t)$.

4.2.4 Simulation Results

In this section, the simulation results will be shown in which the estimated output will be compared with the measured output. As a measure of accuracy of the proposed model, the VAF and MSE test is also calculated. There are two data sets provided for observation. One is the simulated data set and the other is the real data set taken from magnetic bearing system apparatus. To verify model capability, the data set is divided into two parts: First is the estimation data in which the data that is used to develop the model and second is the validation data that has not been used during the modelling process. The proposed model is used to identify the SISO systems and the MIMO systems.

Single Input Single Output Data System

The SISO system under investigation has provided with two different examples. The first example is the simulation data and the second example is an experimental data from magnetic bearing system apparatus.

Example 1: Simulated Data System

The first data set is a simple mass, spring and damper simulated system presented in [3], and is given by the following transfer function

$$G(s) = \frac{1}{Ms^2 + bs + k}$$

where M = 1kg, b = 10N.s/m and k = 20N/m. The *Proportional-Integral* (PI) controller is used as to reduce the rise time, increase the overshoot and eliminate the steady-state error. The proportional and integral gains are respectively set to Kp=30 and Ki=70. The reference signal, $r(t)$ is generated using a GRBS sequences. The output measurement noise and input measurement noise of about 25dB SNR are added while we obtained the closed-loop input and output data. The reference signal, input signal and output signal of the system can be seen in Figure (4.3). The identification process for CEIV model is run under the configuration as can be referred in Table 4.1. The superimposed of the estimated output over the measured output can be seen in Figure (4.4).

Table 4.1: System and model configuration - SISO simulated data

Symbol	Description	Value
p	Laguarre parameter	10
i	Expanding observability matrix	10
n	Model order	2
Δt	Sampling time	0.01
N	Number of sampled data	4000
N_{est}	Estimation data	2000
N_{val}	Validation data	2000
F, V, H	Input & output noise	25 dB SNR

Further verification test by MSE and VAF calculation is given a value of

$$\begin{aligned} \text{CEIV}: \qquad & \text{MSE}_{est} = 9.9474 \times 10^{-7} \qquad && \text{VAF}_{est} = 92.56\% \\ & \text{MSE}_{val} = 1.0279 \times 10^{-6} && \text{VAF}_{val} = 90.91\% \end{aligned}$$

Performance measures based on the plots show that both models are able to identify the systems closely. The MSE values are also small and the VAF indicates an acceptable accuracy. The estimated (A, B, C, D) system matrices are given as

$$\hat{A} = \begin{bmatrix} -0.3242 & 6.3192 \\ -2.7471 & -9.8113 \end{bmatrix}; \quad \hat{B} = \begin{bmatrix} -76.7437 \\ 67.9789 \end{bmatrix}; \quad \hat{C} = \begin{bmatrix} -0.0175 \\ -0.0199 \end{bmatrix}^{\top}; \quad \hat{D} = [0];$$

and the eigenvalues are given as

$$\text{eig}(\hat{A}) = -2.8003; \quad -7.3352$$

The transfer function of the estimated CEIV model is

$$\hat{G}_{CEIV}(s) = \frac{1.0215}{s^2 + 10.1355s + 20.5407}$$

which still shows a close match in comparison with the actual transfer function.

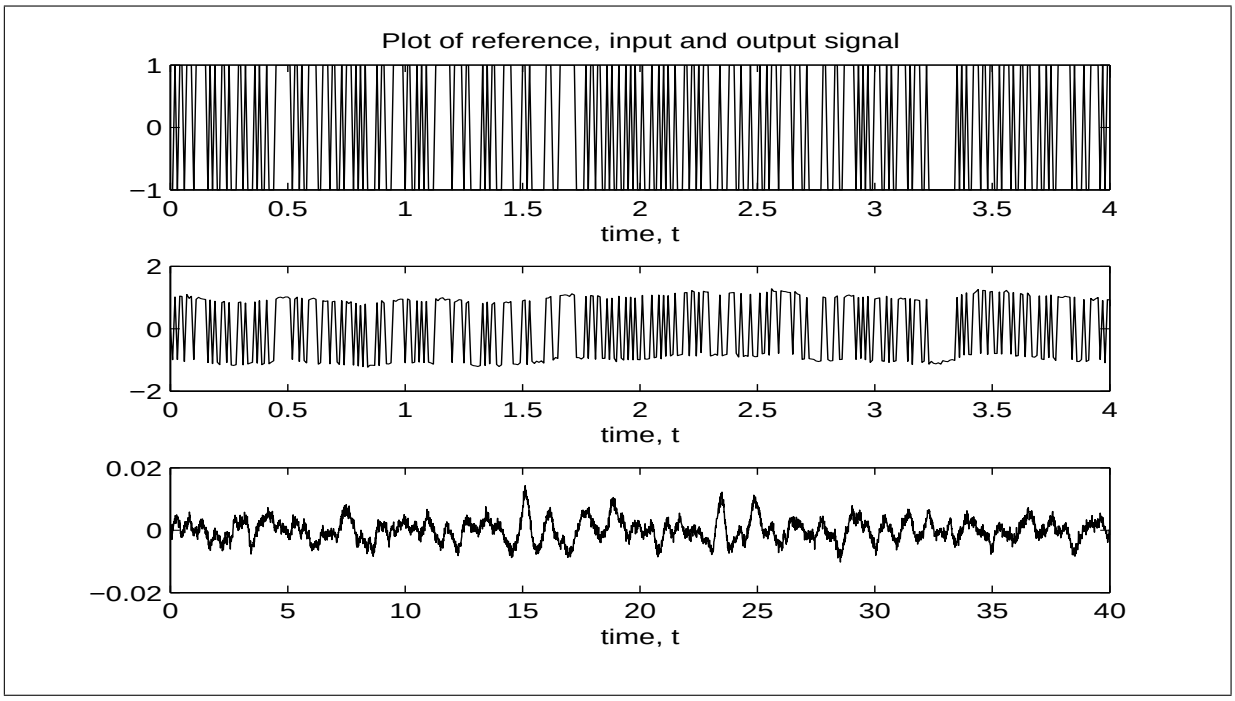

Figure 4.3: Plot of reference, input & output signal - SISO simulated data. (*Note*: The reference & input data are re-scaled to only display 400 data points)

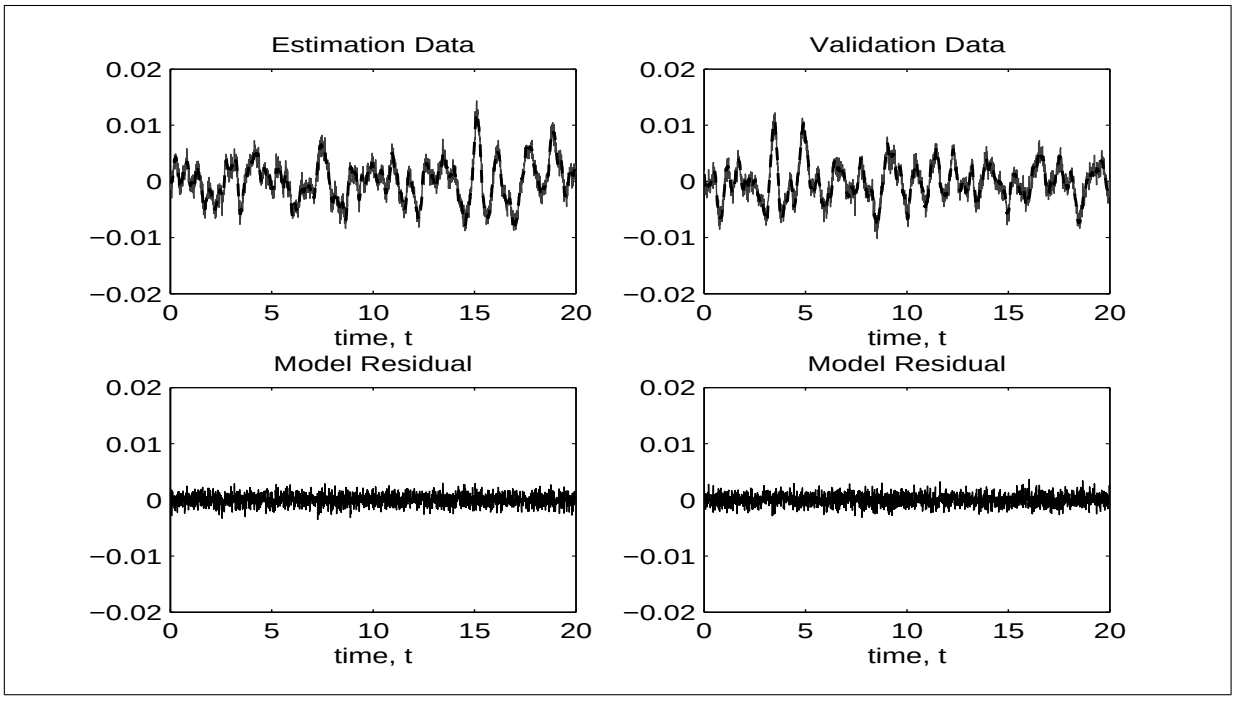

Figure 4.4: Measured (solid) & estimated (dashed) - SISO simulated data (CEIV)

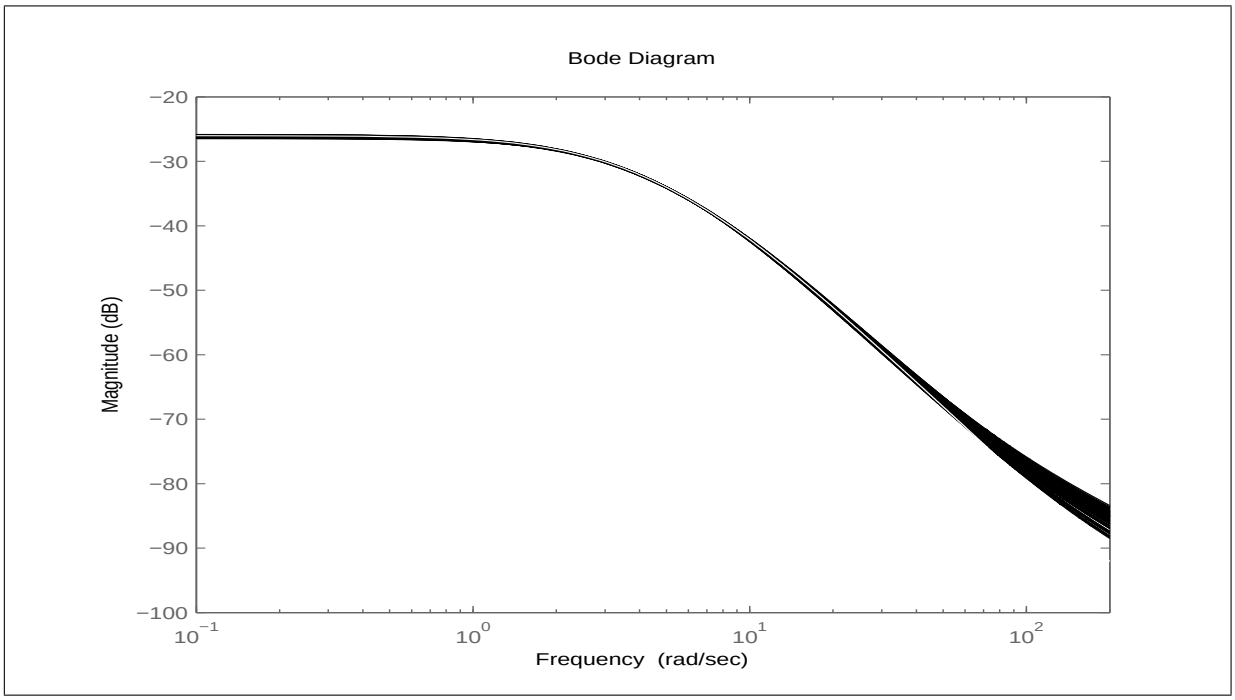

Figure 4.5: Frequency response over 100 runs - SISO simulated data (CEIV)

In order to see the difference when different types of noise are added to the system, the Monte Carlo simulation is performed based on 100 runs. The choice of different random "seed" specifies the noise added to the input and output signal. The result from this analysis can be seen in Figure (4.5). From this figure, it shows that with different types of noise, the proposed identification technique is still able to identify the system closely.

Example 2: Real Data of MB systems

The second data set is a real data set taken from magnetic bearing apparatus. Since the magnetic bearing system is an open-loop unstable system, therefore the *Proportional-Derivative* (PD) controllers are embedded to the bearing system in order to suspend the shaft and to facilitate a closed-loop data collection. The experiment setup for data acquisition can be referred in Appendix B. There are two sets of data available. The first set is measured from the $x-z$ plane, left and right bearing and will be labelled as (x_L&x_R). Second set is measured from the $y-z$ plane, left and right bearing and will be labelled as (y_L&y_R). For the SISO system identification, only the data taken from the x_R plane is demonstrated in this section. The illustration results for the SISO system identification using the data of x_L, y_L and y_R are omitted. However, the MSE and VAF test for all sets of data are calculated.

Table 4.2: System and model configuration - SISO real data

Symbol	Description	CEIV model (x_L&x_R)	CEIV model (y_L&y_R)
p	Laguarre parameter	100	260
i	Expanding observability matrix	10	10
n	Model order	6	6
Δt	Sampling time	0.002	0.002
N	Number of sampled data	1000	1000
N_{est}	Estimation data	500	500
N_{val}	Validation data	500	500

Table 4.3: MSE and VAF calculation - SISO MB systems

Description	MSE_{est}	MSE_{val}	VAF_{est}	VAF_{val}
EIV model: x_L	0.0087	0.0077	83.57%	88.55%
EIV model: x_R	0.0114	0.0063	90.16%	92.54%
EIV model: y_L	0.0114	0.0082	85.12%	87.11%
EIV model: y_R	0.0152	0.0146	81.12%	73.59%

The configuration of the model can be referred in Table 4.2. The plot of input and output data for x_R can been seen as in Figure (4.6). The comparison results of estimation and validation data sets with the estimated output from the proposed model can be seen in Figure (4.7). The VAF and MSE calculation over the model can be seen in Table 4.3. From observation, it shows that the model can identify the system closely for both estimation and validation data set. Calculations on VAF show that the model has provided with acceptable level of quality. The model also gives low value of MSE.

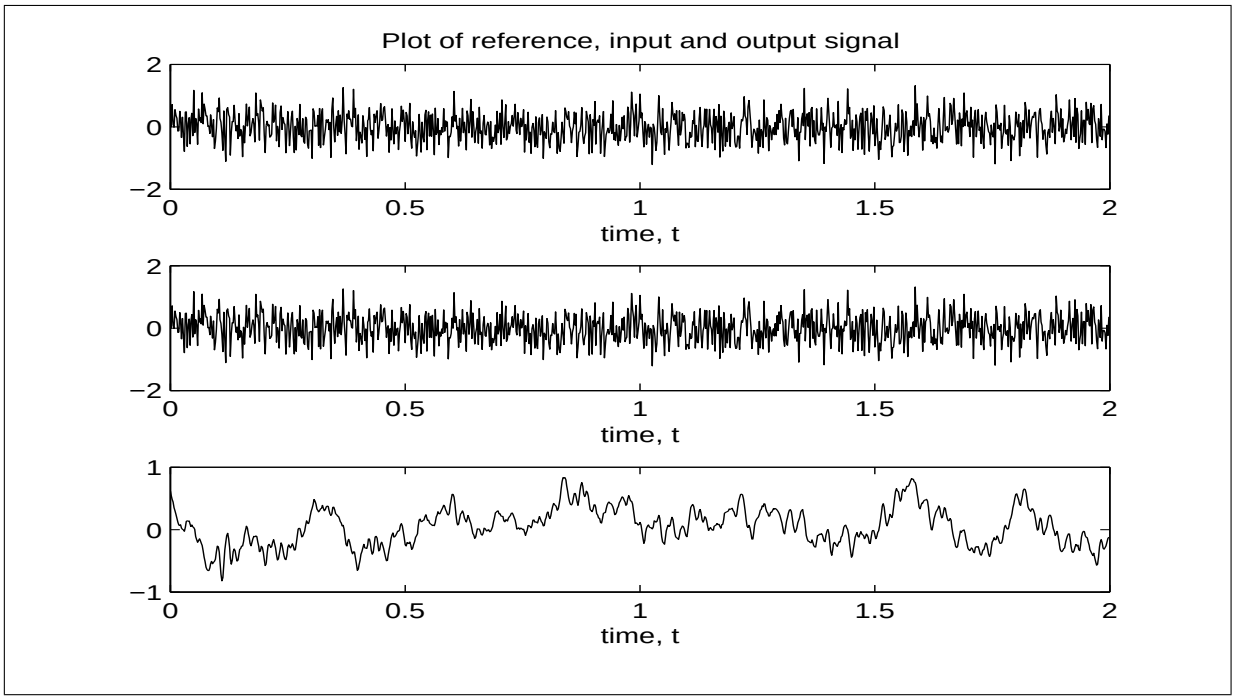

Figure 4.6: Plot of input & output - SISO MB System, x_R

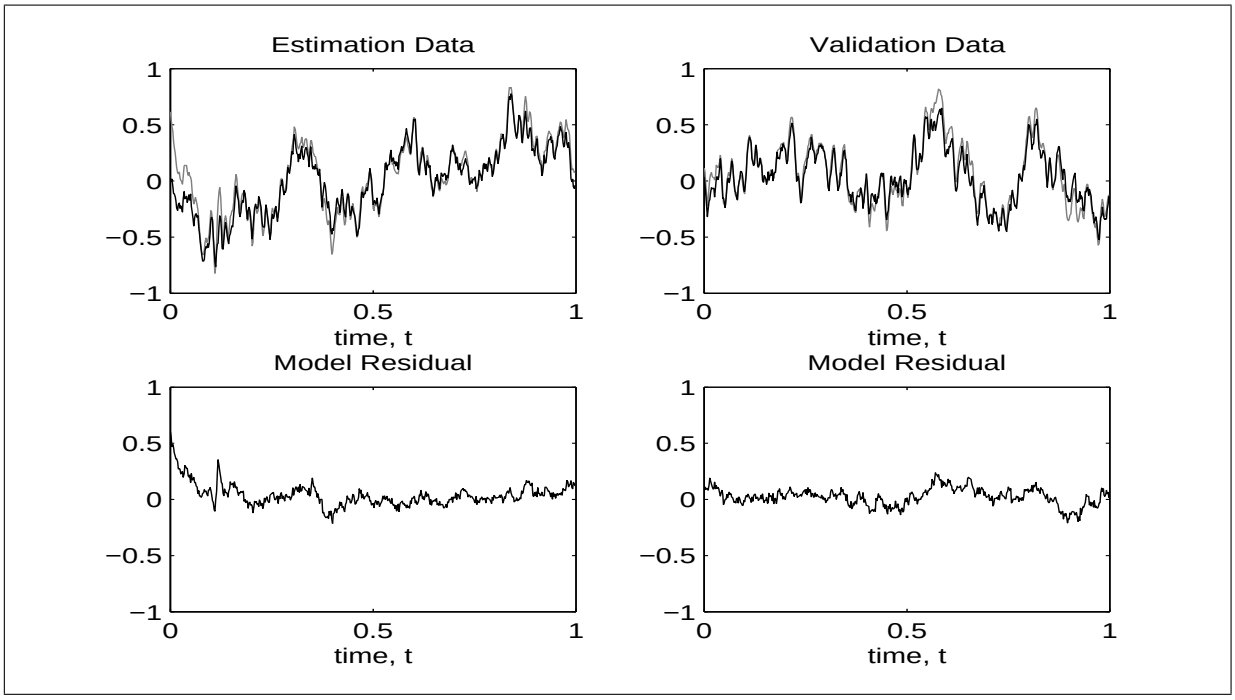

Figure 4.7: Measured (solid-line) & estimated (thick-line) output - SISO MB x_R (CEIV)

The estimated (A, B, C, D) system matrices are obtained as

$$\hat{A} = \begin{bmatrix} -8.5633 & 44.1788 & -105.9845 & -69.8583 & -57.8388 & 37.0082 \\ -12.0474 & -28.5021 & 93.1495 & 39.4584 & 123.8526 & -79.7434 \\ 16.9914 & 72.3601 & -230.5504 & -299.5824 & -382.4434 & 204.2352 \\ 15.7272 & 61.3710 & 19.1457 & -85.2620 & -222.9352 & 112.0583 \\ 0.9856 & -20.8887 & 88.4328 & 43.6879 & -86.7905 & 135.2260 \\ 0.2685 & 7.9745 & -4.3819 & 10.4485 & -21.5309 & -14.1040 \end{bmatrix};$$

$$\hat{B} = \begin{bmatrix} -1.2913 \\ -0.0955 \\ 0.2644 \\ 0.2320 \\ -0.1007 \\ -0.1040 \end{bmatrix} \times 10^3; \quad \hat{C} = \begin{bmatrix} -0.1631 \\ -1.4554 \\ -0.0898 \\ -0.1243 \\ 0.6956 \\ 1.9022 \end{bmatrix}^\top; \quad \hat{D} = [0];$$

and the eigenvalues is given as

$$\text{eig}(\hat{A}) = \begin{bmatrix} -2.0123 \pm 2.2722j \\ -0.1535 \pm 0.1499j \\ -0.1031 \pm 0.6271j \end{bmatrix} \times 10^2$$

Multi Input Multi Output Data Systems

In this section, the two input two output systems of MB systems are given by the following equation

$$\begin{bmatrix} y_1(t) \\ y_2(t) \end{bmatrix} = \begin{bmatrix} G_{11} & G_{12} \\ G_{21} & G_{22} \end{bmatrix} \begin{bmatrix} u_1(t) \\ u_2(t) \end{bmatrix}$$

Table 4.4: System and model configuration - MIMO real data

Symbol	Description	CEIV model (x_L&x_R)	CEIV model (y_L&y_R)
p	Laguarre parameter	190	260
i	Expanding observability matrix	10	10
n	Model order	8	8
Δt	Sampling time	0.002	0.002
N	Number of sampled data	1000	1000
N_{est}	Estimation data	500	500
N_{val}	Validation data	500	500

Table 4.5: MSE and VAF calculation - MIMO MB systems

Description	MSE_{est}	MSE_{val}	VAF_{est}	VAF_{val}
EIV model: x_L	0.0140	0.0124	74.07%	79.26%
EIV model: x_R	0.0148	0.0106	86.64%	87.35%
EIV model: y_L	0.0188	0.0241	75.53%	62.12%
EIV model: y_R	0.0133	0.0135	83.45%	75.26%

For the MIMO systems, the same data sets that were used in SISO identification are used again, however, it is implemented together to build the MIMO systems. So in this case, there are two sets of two-input-two-output data available. First case is the data for $x - z$ plane and second case is the $y - z$ plane of the MB systems. The identification results for the $x - z$ plane are shown in this section. The illustration results for $y - z$ plane are omitted, however, the MSE and VAF are calculated and mentioned.

The identification is run under the configuration as it can be referred in Table 4.4. The data is also divided into estimation data and validation data. The performance is compared based on the fit between the measured output and the estimated output. The measured and estimated output are superimposed which can be seen in Figure (4.8). The VAF and MSE calculations

can be referred as in Table 4.5. Based on the fit between the measured and estimated, it can be said that the CEIV model is able to identify the multi-variable MB systems with reasonable performance. The MSE and VAF calculations also show that the model gives a reasonable level of accuracy.

The estimated (A, B, C, D) system matrices are obtained as

$$\hat{A} = \begin{bmatrix} -62.3673 & -161.3267 & 128.9896 & 45.7793 & 170.1881 & 180.3723 & 61.2045 & -14.2145 \\ 10.4701 & -218.3041 & -57.6564 & 225.0433 & 338.4266 & -11.4315 & 238.2461 & 63.1461 \\ 26.6006 & -10.0305 & -224.1275 & 161.8549 & -51.5358 & -449.0338 & 97.4713 & 97.7111 \\ -7.4738 & -49.1065 & -79.3349 & -38.2803 & -93.6023 & 20.1898 & -88.4323 & -27.8315 \\ -38.5862 & -68.2114 & -1.1466 & 0.5722 & -79.4305 & -31.2021 & -105.1535 & 16.9795 \\ -40.1581 & -6.2026 & 85.3495 & 30.3985 & -40.8994 & -137.2292 & 48.1287 & 99.4318 \\ -7.7679 & -20.7251 & -10.0528 & -3.0828 & 1.6215 & -4.5332 & -49.9029 & -13.3173 \\ -1.6943 & -4.2189 & -0.3700 & -4.5311 & -14.0608 & -27.3381 & -13.1566 & -5.4132 \end{bmatrix}$$

$$\hat{B} = \begin{bmatrix} -40.1936 & 132.0502 \\ 74.8633 & 58.4370 \\ 73.7068 & -76.2532 \\ -63.9399 & -32.3884 \\ 1.7233 & 6.1884 \\ -14.6589 & 14.7230 \\ 3.8460 & 2.6565 \\ -12.6273 & -31.9061 \end{bmatrix}; \quad \hat{C} = \begin{bmatrix} 0.1300 & -0.2706 \\ 0.4564 & 0.5508 \\ 0.3558 & -0.5793 \\ 0.5751 & -0.0620 \\ -0.4664 & 0.6534 \\ 0.2385 & 0.5040 \\ -0.5360 & -0.0363 \\ -0.5158 & 0.6843 \end{bmatrix}^{\top}; \quad \hat{D} = \begin{bmatrix} 0 & 0 \\ 0 & 0 \end{bmatrix};$$

The eigenvalues is given as

$$\text{eig}(\hat{A}) = \begin{bmatrix} -1.9658 \pm 2.3756j \\ -1.8138 \pm 2.3259j \\ -0.0959 \pm 0.1152j \\ -0.1997 \pm 0.2289j \end{bmatrix} \times 10^2$$

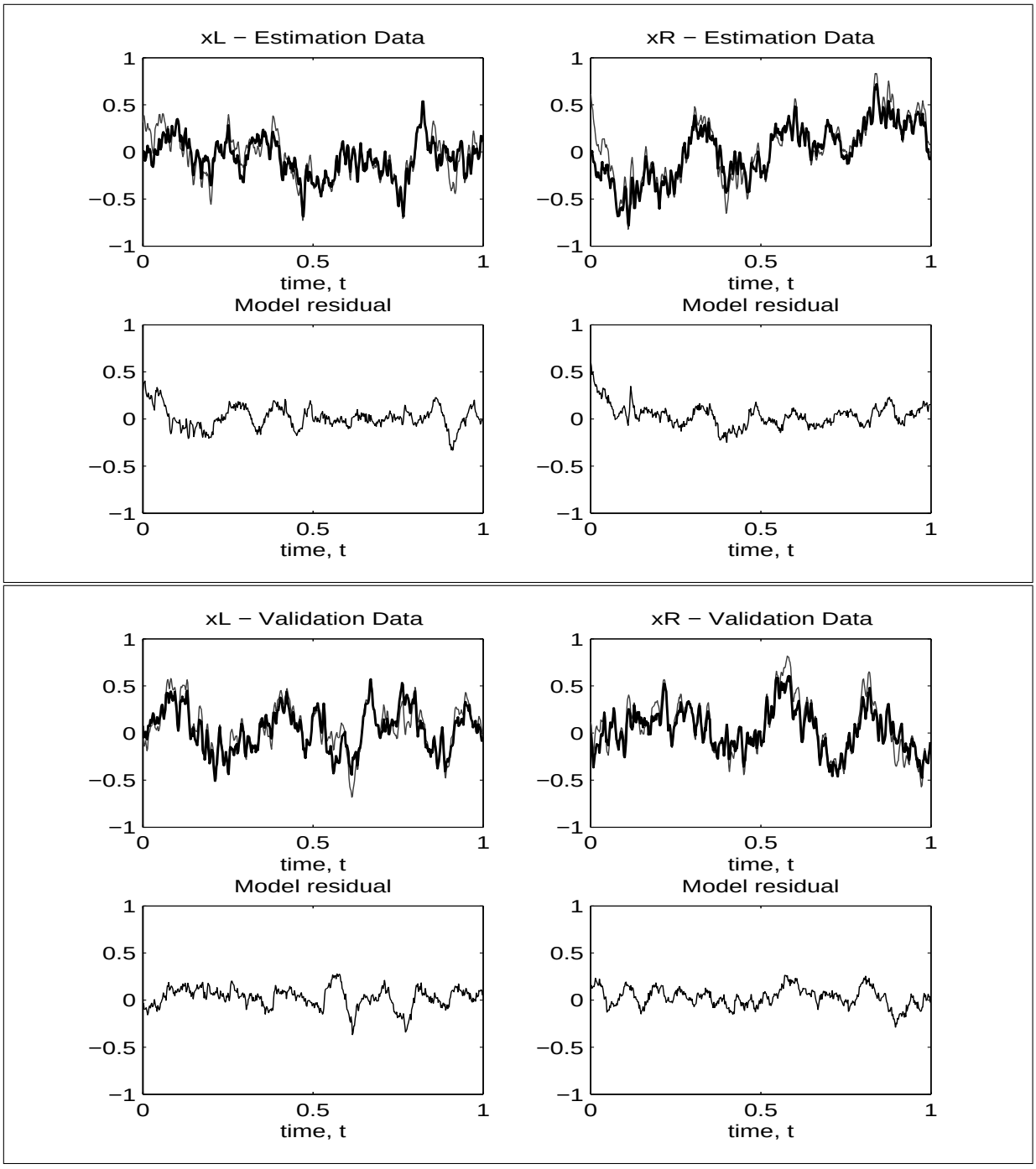

Figure 4.8: Measured (solid-line) & estimated (thick-line) MIMO MB $x-$plane (CEIV)

4.3 Reference Signal As IV Formulation

The idea of using reference signal as a choice of instrumental variable was influenced by Zhao and Westwick to identify the Wiener system [192]. This approach is inherited since certain nonlinear systems will not have the input signal, $\hat{u}(t)$ to be Gaussian distributed due to feedback in the system. Thus, by collecting only the input signal will not provide enough information about the systems. Therefore in order to perform the algorithm to closed-loop data, the two Gaussian signals must be obtained. The Gaussian output and the Gaussian reference signal.

The classical choice to determine the Gaussianity of the output data is by measuring its Gaussianity according to the Kurtosis calculation defines as

$$\text{Kurt}(x) = \mathbf{E}\left(x^4\right) - 3\left(\mathbf{E}\left(x^2\right)\right)^2 \tag{4.35}$$

For a sample data defines as $x = [x_1, x_2, \ldots, x_N]$, the calculation goes as

$$K1 = \mathbf{E}\left(x^4\right) = \frac{1}{N}\sum_{a=1}^{N}(x_a - \bar{x})^4$$

$$K2 = \mathbf{E}\left(x^2\right) = \frac{1}{N}\sum_{a=1}^{N}(x_a - \bar{x})^2$$

$$\text{Kurt}(x) = K1 - 3(K2)^2$$

where $\bar{x}$ is a mean value of the sample x.

If the random sequence is Gaussian, its Kurtosis should be equal to zero. The signal with smaller value of Kurtosis is more Gaussian than with larger value of Kurtosis. The Kurtosis can be positive or negative. Random variables that have a negative kurtosis are called subgaussian, and those with positive kurtosis are called supergaussian. Now that the Gaussianity condition is satisfied, the same algorithm and assumption for the continuous time closed-loop identification that have been discussed in previous section can be used again in this section, however, the instrumental variable is constructed from the reference signal, $r(t)$.

$$P = \left[\ \mathcal{R}^f_{i,j,N}\ \right]$$

where

$$\mathcal{R}^f_{i,j,N}(t) = \begin{bmatrix} [w_i r](t_1) & [w_i r](t_2) & \ldots & [w_i r](t_N) \\ [w_{i+1} r](t_1) & [w_{i+1} r](t_2) & \ldots & [w_{i+1} r](t_N) \\ \vdots & \vdots & \vdots & \vdots \\ [w_{i+j-1} r](t_1) & [w_{i+j-1} r](t_2) & \ldots & [w_{i+j-1} r](t_N) \end{bmatrix}$$

For easy recognition of this model, it will be named as "CREF" in which capital "C" represents the continuous time and "REF" for reference signal.

4.3.1 Identification Procedure

Let $u(t)$ and $y(t)$ be the input and output plant data described in Equations (4.13-4.16). Let $U^f_{0,i,N}$ and $Y^f_{0,i,N}$ be the filtered data matrices constructed from $u(t)$ and $y(t)$, and $\mathcal{R}^f_{i,j,N}$ be the filtered data matrices constructed from $r(t)$, this method consider the following RQ factorization.

$$\begin{bmatrix} U^f_{0,i,N} \\ Y^f_{0,i,N} \end{bmatrix} P^\top = \begin{bmatrix} R_{11} & 0 \\ R_{21} & R_{22} \end{bmatrix} \begin{bmatrix} Q_1 \\ Q_2 \end{bmatrix} \tag{4.36}$$

where

$$P = \begin{bmatrix} \mathcal{R}^f_{i,j,N} \end{bmatrix}$$

1. Perform the RQ decomposition

$$\begin{bmatrix} U^f_{0,i,N} \\ Y^f_{0,i,N} \end{bmatrix} P^\top = \begin{bmatrix} R_{11} & 0 \\ R_{21} & R_{22} \end{bmatrix} \begin{bmatrix} Q_1 \\ Q_2 \end{bmatrix}$$

$$\begin{bmatrix} U^f_{0,i,N} \\ Y^f_{0,i,N} \end{bmatrix} P^\top = \begin{bmatrix} \hat{R}_{11} & 0 \\ \hat{R}_{31} & \hat{R}_{32} \end{bmatrix} \begin{bmatrix} \tilde{R}_{11} & 0 \\ \tilde{R}_{21} & \tilde{R}_{22} \end{bmatrix} \begin{bmatrix} \tilde{Q}_1^\top \\ \tilde{Q}_2^\top \end{bmatrix}$$

   where $P = [\mathcal{R}^f_{i,j,N}]^\top$ for the CREF method.

2. Perform the SVD to the working matrix $\hat{R}_{32}\tilde{R}_{22}$:

$$\hat{R}_{32}\tilde{R}_{22} = USV^\top$$

3. Determine the model order n from the singular value in S.

4. Determine the system matrices (A_w, C_w).

   $A_w = (J_1U_n)^\dagger J_2U_n$

   $C_w = J_3U_n$

   $J_1 = \begin{bmatrix} I_{(i-1)l} & 0_{(i-1)l\times l} \end{bmatrix}$

   $J_2 = \begin{bmatrix} 0_{(i-1)l\times l} & I_{(i-1)l} \end{bmatrix}$

   $J_3 = \begin{bmatrix} I_{l\times l} & 0_{l\times(i-1)l} \end{bmatrix}$

   $\Upsilon^\dagger = (\Upsilon^\top\Upsilon)^{-1}\Upsilon^\top$

The A and C matrices can be obtained using the relations:

$$\begin{aligned} A &= p(I_n + A_w)(I_n - A_w)^{-1} \\ C &= \sqrt{2p}C_w(I_n - A_w)^{-1} \end{aligned}$$

5. Solve least squares problem from model structure:

$$y(\ t \mid B, D\ ) = C(qI_n - A)^{-1}Bu(t) + Du(t)$$

6. Reconstruct B and D from $\begin{bmatrix} B \\ D \end{bmatrix}$

7. Generate the estimated output, $\hat{y}(t)$.

4.3.2 Simulation Results

In this section, the simulation results will be shown and the estimated output will be compared with the measured output. As a measure of accuracy of the proposed model, the VAF and MSE tests are also calculated. There are two data sets provided for the study. One is the simulated data set and the other is the real data set taken from magnetic bearing system apparatus. To verify the model capability, the data set is divided into two parts: First is the estimation data in which the data that is used to develop the model and second is the validation data that has not been used during the modelling process. The proposed model is used to identify the SISO systems and the MIMO systems.

Single Input Single Output Data System

The SISO system under investigation has provided two examples. First example is based on a set of simulation data and second example is based on a set of experimental data taken from magnetic bearing system apparatus.

Example 1: Simulated Data System

The first data set is a simple mass, spring and damper simulated system given by the following transfer function [3]

$$G(s) = \frac{1}{Ms^2 + bs + k}$$

where M = 1kg, b = 10N.s/m and k = 20N/m. The *Proportional-Integral* (PI) controller is used as to reduce the rise time, increase the overshoot and eliminate the steady-state error. The proportional and integral gains are respectively set to Kp=30 and Ki=70. The reference signal, $r(t)$ is generated using a Gaussian random generator. The output measurement noise and input measurement noise of about 25dB SNR are added while we obtained the closed-loop input and output data. Plot for reference signal, input signal and output signal of the system can be seen in Figure (4.9).

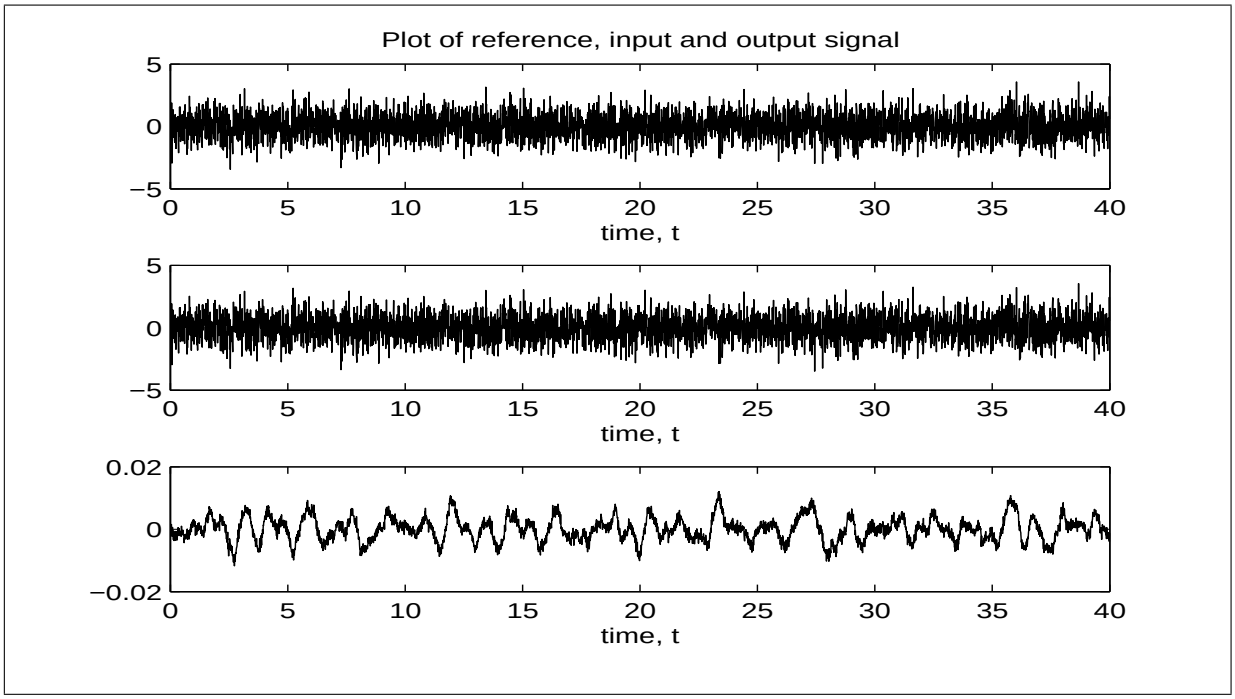

Figure 4.9: Plot of reference, input & output signal - SISO simulated data

The Kurtosis calculated for reference signal, input signal and output signal are given as

$$\text{Kurt}(r) = -0.0658$$
$$\text{Kurt}(u) = -0.0760$$
$$\text{Kurt}(y) = -3.2351 \times 10^{-11}$$

The identification process for CREF model is run under the configuration as can be referred in Table 4.6. The superimposed of the estimated output over the measured output can be seen in Figure (4.10). Further verification test by MSE and VAF calculation have given a value of

$$\text{CREF}: \qquad \text{MSE}_{est} = 1.0364 \times 10^{-6} \qquad \text{VAF}_{est} = 92.59\%$$
$$\text{MSE}_{val} = 1.0532 \times 10^{-6} \qquad \text{VAF}_{val} = 92.56\%$$

Performance measure based on the plot shows that the model is able to identify the systems closely. The MSE value is also small and the VAFs indicate an acceptable accuracy. The estimated (A, B, C, D) system matrices are given as

$$\hat{A} = \begin{bmatrix} -0.1655 & 5.7803 \\ -3.2148 & -9.9343 \end{bmatrix}; \quad \hat{B} = \begin{bmatrix} 37.9829 \\ -1.6615 \end{bmatrix}; \quad \hat{C} = \begin{bmatrix} -0.0007 \\ -0.0104 \end{bmatrix}^{\top}; \quad \hat{D} = [0];$$

The eigenvalue is obtained as

$$\text{eig}(\hat{A}) = -2.7532; \quad -7.3465;$$

The transfer function of the estimated CREF model is obtained as

$$\hat{G}_{CREF}(s) = \frac{1.0127}{s^2 + 10.0998s + 20.2265}$$

which still shows a close match in comparison with the actual transfer function.

In order to see the differences when different types of noise are added to the system, Monte Carlo simulation is performed based on 100 runs. The choice of different random "seed" specifies the noise adding to the input and output signal. The result from this analysis can be seen in Figure (4.11). From this figure, it shows that with different types of noise, both models are still able to identify the system closely.

Table 4.6: System and model configuration - SISO simulated data

Symbol	Description	Value
p	Laguarre parameter	10
i	Expanding observability matrix	10
n	Model order	2
Δt	Sampling time	0.01
N	Number of sampled data	4000
N_{est}	Estimation data	2000
N_{val}	Validation data	2000
F, H, V	Input & output noise	25 dB SNR

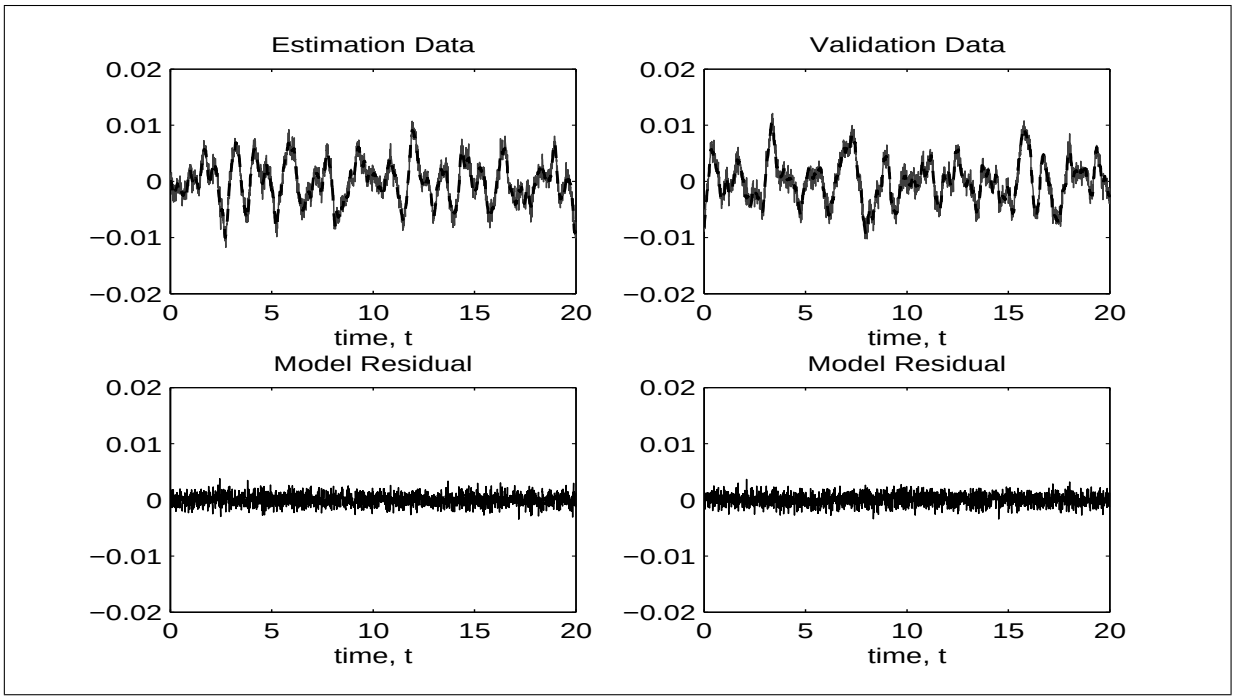

Figure 4.10: Measured (solid) & estimated (dashed) - SISO simulated data (CREF)

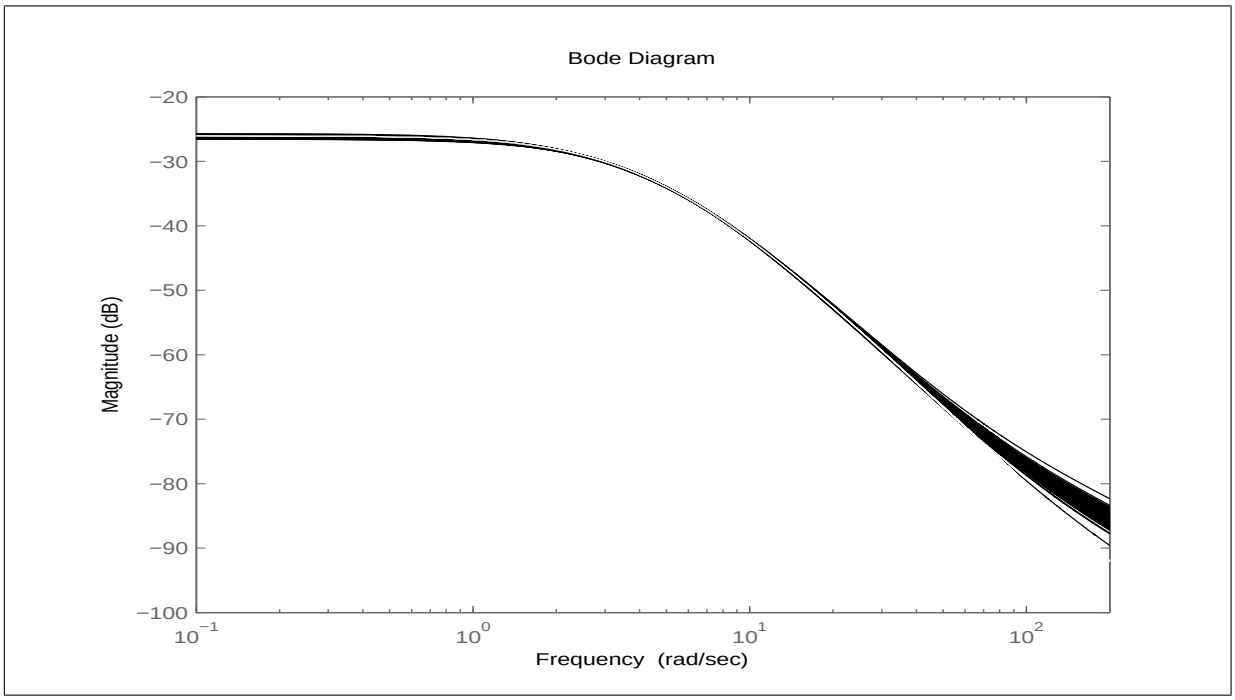

Figure 4.11: Frequency response over 100 runs - SISO simulated data (CREF)

Example 2: Real Data of MB systems

The second data set is a real data set taken from magnetic bearing apparatus. Since the magnetic bearing system is an open-loop unstable system, therefore the *Proportional-Derivative* (PD) controllers are embedded to the bearing system in order to suspend the shaft and to facilitate a closed-loop data collection. There are two sets of data available. The first set is measured from the $x - z$ plane, left and right bearing and will be labelled as $(x_L \& x_R)$. Second set is measured from the $y - z$ plane, left and right bearing and will be labelled as $(y_L \& y_R)$. For the SISO system identification, these data will be identified individually. However, in this section only the data taken from the x_R will be demonstrated. The illustration results for other set of plane are omitted, however, the MSE and VAF are calculated and mentioned.

The Kurtosis calculated for the signal is given in Table 4.7. The configuration of the model can be referred in Table 4.8. The plot of input and output data for x_R can been seen as in Figure (4.12). The comparison results of estimation and validation data sets with the estimated output from the proposed model can be seen in Figure (4.13). The VAF and MSE values can be seen in Table 4.9. From observation, the results show that the model can identify the system closely for both estimation and validation data set.

Table 4.7: Kurtosis of the input & output signal - SISO real data

Description	Kurtosis of input	Kurtosis of output
x_L	-0.0185	-4.4184×10^{-4}
x_R	-0.0107	-0.0031
y_L	-0.0240	-0.0017
y_R	-0.0147	-0.0012

Table 4.8: System and model configuration - SISO real data

Symbol	Description	CREF model (x_L&x_R)	CREF model (y_L&y_R)
p	Laguarre parameter	230	230
i	Expanding observability matrix	10	10
n	Model order	6	6
Δt	Sampling time	0.002	0.002
N	Number of sampled data	1000	1000
N_{est}	Estimation data	500	500
N_{val}	Validation data	500	500

Table 4.9: MSE and VAF calculation - SISO MB systems

Description	MSE_{est}	MSE_{val}	VAF_{est}	VAF_{val}
CREF model: x_L	0.0074	0.0073	86.21%	88.55%
CREF model: x_R	0.0103	0.0067	91.71%	91.61%
CREF model: y_L	0.0063	0.0063	87.16%	90.06%
CREF model: y_R	0.0144	0.0144	89.28%	73.13%

Calculation on VAF also show that the model has demonstrated an acceptable level of quality. The model also gives low value of MSE.

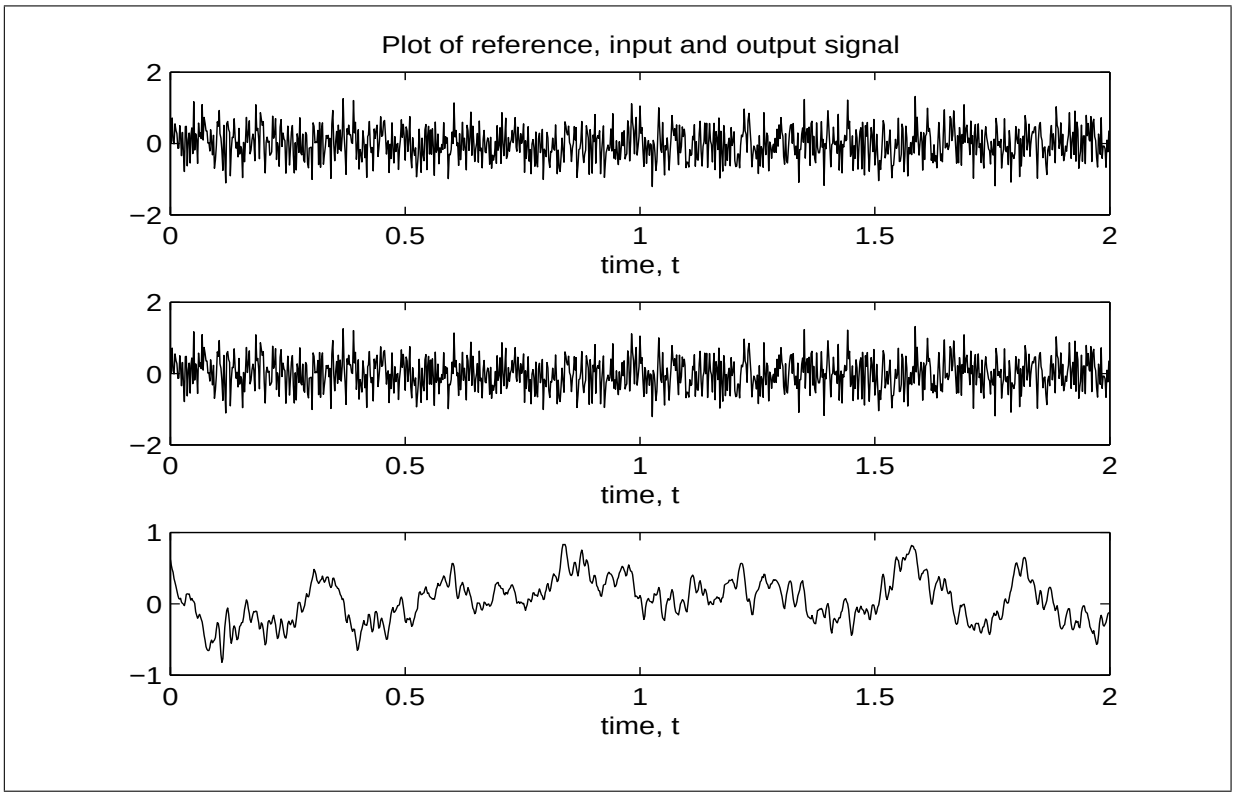

Figure 4.12: Plot of input & output - SISO MB System, x_R

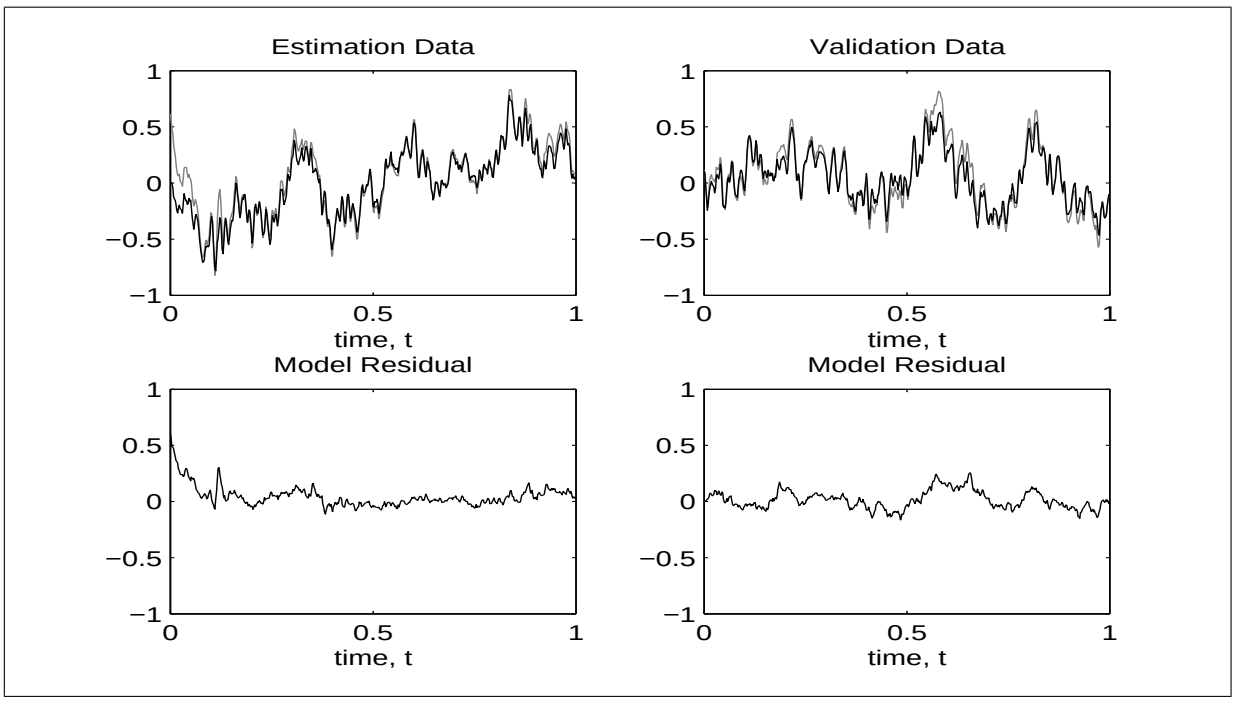

Figure 4.13: Measured (solid-line) & estimated (thick-line) output - SISO MB x_R (CREF)

The estimated (A, B, C, D) system matrices are obtained as

$$\hat{A} = \begin{bmatrix} -218.5893 & 152.2021 & -529.4181 & 56.2305 & -495.4974 & -775.6968 \\ -55.6609 & -9.6979 & 89.5740 & -20.8493 & 112.3898 & 167.3354 \\ 102.5845 & 4.7648 & -208.2802 & 11.0533 & -469.9023 & -788.8309 \\ -5.8212 & 2.6146 & 37.7181 & 10.5029 & -25.9838 & 99.1283 \\ -2.1953 & 2.2948 & -15.6177 & 63.8423 & -274.0887 & -737.6722 \\ -7.9211 & 0.6857 & 22.7917 & 6.9395 & -154.9759 & -681.0978 \end{bmatrix}$$

$$\hat{B} = \begin{bmatrix} -2.6228 \\ -0.1589 \\ -0.0188 \\ 0.0054 \\ -0.0659 \\ 0.0589 \end{bmatrix} \times 10^3; \quad \hat{C} = \begin{bmatrix} -0.2744 \\ 1.4474 \\ -0.2051 \\ -5.0999 \\ 3.1628 \\ -4.0820 \end{bmatrix}^\top; \quad \hat{D} = [0];$$

The eigenvalue is given as

$$\text{eig}(\hat{A}) = \begin{bmatrix} -8.7489 \\ -2.2853 \pm 2.6403j \\ -0.1346 \pm 0.4975j \\ -0.2237 \end{bmatrix} \times 10^2$$

Multi Input Multi Output Data Systems

In this section, the two inputs two outputs systems are investigated. The data taken from the $x-z$ plane of the MB apparatus will be used for multi-variable closed-loop system identification. The identification is run under the configuration as can be referred in Table 4.10. The data is also divided into estimation data and validation data. The performance is compared based on the fit between the measured output and the estimated output. The superimposed of measured and estimated output can be seen as in Figure (4.14). The VAF and MSE calculation can be referred as in Table 4.11. Based on the fit between the measured and estimated, it can be said that the model is still able to identify the multi-variable MB systems with reasonable performance. The MSE and VAF calculation also show that the model gives reasonable level of accuracy.

Table 4.10: System and model configuration - MIMO real data

Symbol	Description	CREF model (x_L&x_R)	CREF model (y_L&y_R)
p	Laguarre parameter	210	200
i	Expanding observability matrix	10	10
n	Model order	6	6
Δt	Sampling time	0.002	0.002
N	Number of sampled data	1000	1000
N_{est}	Estimation data	500	500
N_{val}	Validation data	500	500

Table 4.11: MSE and VAF calculation - MIMO MB systems

Description	MSE_{est}	MSE_{val}	VAF_{est}	VAF_{val}
CREF model: x_L	0.0167	0.0148	69.98%	75.02%
CREF model: x_R	0.0192	0.0143	84.27%	81.65%
CREF model: y_L	0.0218	0.0204	71.27%	67.66%
CREF model: y_R	0.0211	0.0170	74.17%	69.44%

The estimated (A, B, C, D) system matrices are obtained as

$$\hat{A} = \begin{bmatrix} -224.5888 & -81.3482 & -124.7197 & -150.6280 & 490.9242 & -147.2753 \\ 18.2897 & -200.3484 & 120.4889 & -209.8670 & -160.5393 & -439.4549 \\ 31.6193 & 51.7443 & -52.9217 & 72.1994 & 197.9366 & 174.2963 \\ 35.7413 & 78.8937 & -41.6793 & -30.3442 & 53.1054 & -103.8757 \\ -97.0787 & 35.7693 & -29.5466 & -11.9255 & -187.6419 & -39.3412 \\ 18.1400 & 72.4412 & -34.7701 & -21.2507 & -23.0873 & -138.9825 \end{bmatrix}$$

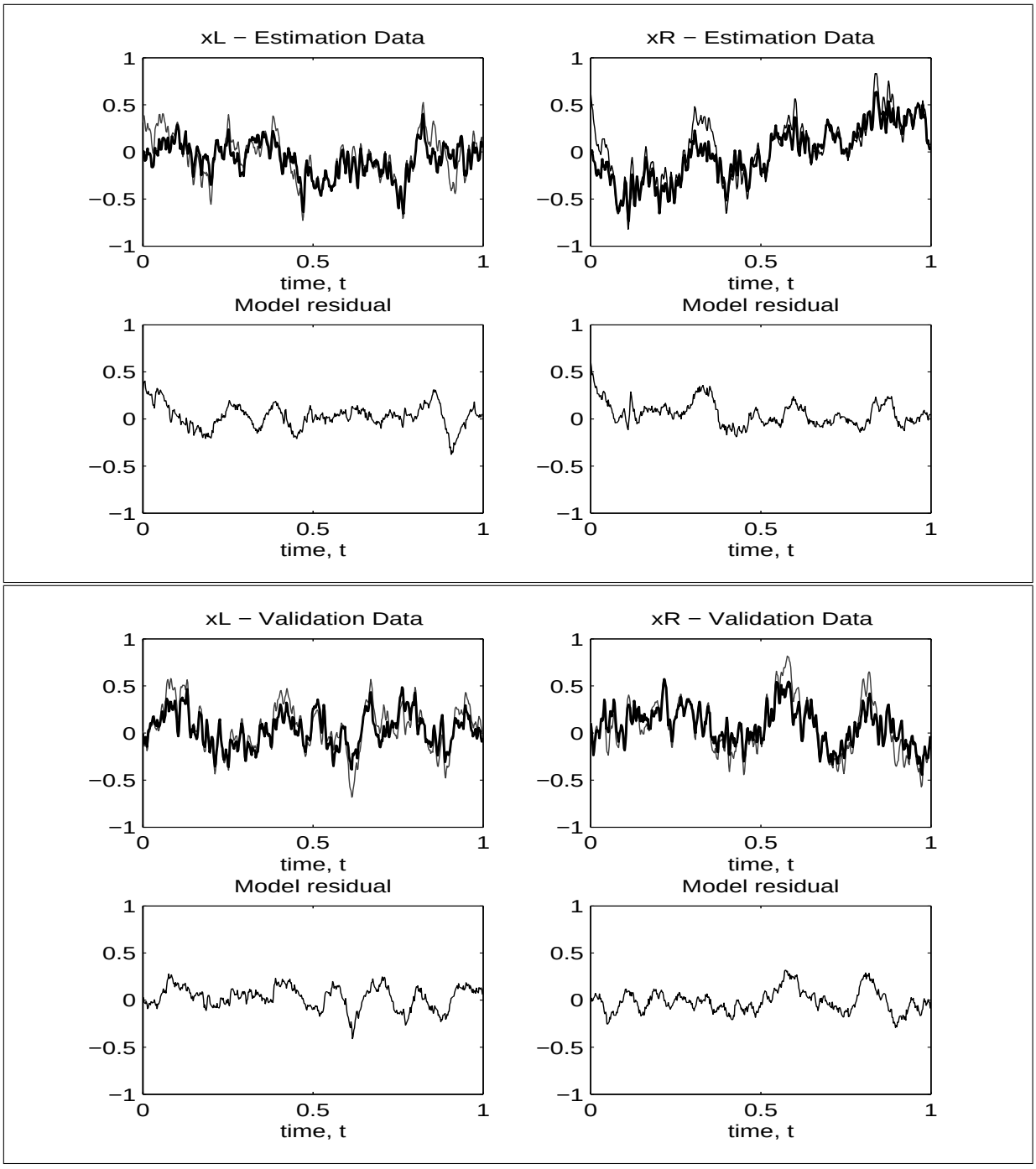

Figure 4.14: Measured (solid-line) & estimated (thick-line) MIMO MB $x-$plane (CREF)

$$\hat{B} = \begin{bmatrix} -1.5992 & -112.8881 \\ -78.2819 & 70.6188 \\ 4.3564 & 34.1773 \\ -72.5089 & -16.8690 \\ 6.7836 & -16.5156 \\ 21.9138 & 0.6673 \end{bmatrix}; \quad \hat{C} = \begin{bmatrix} -0.4132 & -0.5718 \\ -0.6045 & -0.2215 \\ 0.2517 & -1.0635 \\ 0.3737 & 0.0022 \\ 0.1384 & -1.1496 \\ -0.1839 & -0.2359 \end{bmatrix}^{\top}; \quad \hat{D} = \begin{bmatrix} 0 & 0 \\ 0 & 0 \end{bmatrix}$$

The eigenvalue is given as

$$\text{eig}(\hat{A}) = \begin{bmatrix} -2.1184 \pm 2.6391j \\ -1.9202 \pm 2.4363j \\ -0.1137 \\ -0.1574 \end{bmatrix} \times 10^2$$

4.4 Summary

This chapter has demonstrated an approach based on subspace method to identify a continuous time state-space model for closed-loop data. Two approaches have been studied and the performance capability of each approach in identifying the systems are investigated. The first approach is an extension of the existing approach in discrete time system identification for "error in variable" problem into the continuous time closed-loop system identification. Second approach is an extension of the existing approach in discrete time system identification using the reference signal as an instrumental variable into the continuous time closed-loop system identification. These two approaches are tested to identify the SISO and MIMO systems; for simulated data systems and real data of magnetic bearing systems. These two models have successfully identified the simulated systems and also give acceptable performance in identifying the MB systems. In comparison among models, both models show quite a similar performance in identifying the system closely.

Chapter 5

Subspace System Identification Through Data Compression

5.1 Introduction

In previous chapters, the subspace identification method is used to develop a continuous time state-space model for open-loop and closed-loop systems, in which it has been demonstrated based on a direct periodic input signal to produce output as time domain data. Overall, the identifications have demonstrated a promising performance. There is another good data viewpoint that one might consider; a step response data. The step response of a dynamical system provides information regarding the stability of the system and its ability to reach a stationary state. It also has a transparent representation in terms of gain, time delay and time constant. At some points, it is widely viewed as a precursor to the design of further experiments, as an indicator to the collection of more input-output data, and as a subsequent for regression-based techniques to obtain more accurate model [180].

In this chapter the identification procedure involves two steps. The first step is the identification of the system step response from the experimental data using the *Frequency Sampling Filter* (FSF) approach of Wang and Cluett [179, 180]. This first stage is also referred as data compression stage in which the raw data will be analysed, the noise will be eliminated and the data is finally compressed into an empirical model of the analysed data. The second step is the

identification of a continuous time state space model using subspace methods from the identified step response. The subspace method that will be used is similar to that one that has already discussed in Chapter 3. The contribution of this chapter is rather the combination of the two stages in a novel way and to verify the approach in a real application context. The main content of this chapter has been written in a conference paper and submitted to IEEE International Conference on Systems, Man and Cybernetics to be held in Singapore in October 2008 [117].

The two stage system identification demonstrated in this chapter involves both a discrete time model and a continuous time model. The first stage of identification involves the discrete time model. However, the step response that is obtained from the first stage is invariant in both discrete time and continuous time. Therefore, the applicability remains in continuous time model during the second stage of system identification.

As a reminder to readers, some of the mathematical symbol presented in this chapter may have the same character as the one represented for subspace identification equations in previous chapters. Therefore, confusion due to redundancy usage may arise. The author will try her best to indicate and declare the meaning of each symbol after each equation presented. Overall, this chapter will go as follows. Section 5.2 elaborates the data compression using the FSF approach. The key ingredients behind the FSF model are justified and the use of PRESS statistic and the orthogonal decomposition algorithm are also stated. Next in Section 5.3, the step response estimates obtained from FSF model are justified. Then, Section 5.4 visualizes the continuous time state space model identification using the identified step response estimates. To show the performance capability of the proposed model, the simulation and experimental data systems are used, in which the SISO and multi-variable systems are observed. These examples are shown in Section 5.5. Finally, Section 5.6 concludes the chapter.

5.2 Data Compression using Frequency Sampling Filters

Data acquisition process from real system typically yields large amounts of data. This particular raw data may contain complex system disturbance information which may require a sophisticated optimization algorithm to achieve desirable results [48, 49]. Thus, there must be a certain mechanism that can utilize the measured data by encapsulating the important features and compressing it into a few parameters within an empirical system model. As discussed in [48,49],

there are many possible empirical models available but one of interest is the FSF model approach [179, 180].

5.2.1 Frequency Sampling Filter Model

Introduce the *Finite Impulse Response* (FIR) transfer function model as

$$G(z) = \sum_{i=0}^{n-1} h_i z^{-i} \tag{5.1}$$

where n is the model order chosen such that the FIR model coefficients $h_i \approx 0$ for all $i \geq n$, and z^{-1} is the backward shift operator. The model order n can be determined from an estimate of the process settling time T_s, where $n = \frac{T_s}{\Delta t}$ and Δt is the sampling interval [180]. Under the assumption that n is an odd number, the relationship between the process frequency response and its impulse response of the *Inverse Discrete Fourier Transform* (IDFT) can be defined as

$$h_i = \frac{1}{n} \sum_{l=-\frac{n-1}{2}}^{\frac{n-1}{2}} G\left(e^{j\frac{2\pi l}{n}}\right) e^{j\frac{2\pi l i}{n}} \tag{5.2}$$

This relationship maps a set of discrete time frequency response coefficients, $G\left(e^{j\frac{2\pi l}{n}}\right)$, $l = 0, \pm 1, \pm 2, \ldots, \pm\frac{n-1}{2}$ into the set of discrete time unit impulse response coefficients, h_i, $i = 0, \ldots, n-1$. Substituting Equation (5.2) into Equation (5.1) gives

$$G(z) = \sum_{i=0}^{n-1} \frac{1}{n} \sum_{l=-\frac{n-1}{2}}^{\frac{n-1}{2}} G\left(e^{j\frac{2\pi l}{n}}\right) e^{j\frac{2\pi l i}{n}} z^{-i} \tag{5.3}$$

Interchanging the summations in Equation (5.3) gives the transfer function in its FSF model form

$$G(z) = \sum_{l=-\frac{n-1}{2}}^{\frac{n-1}{2}} G\left(e^{j\frac{2\pi l}{n}}\right) \frac{1}{n} \frac{1 - z^{-n}}{1 - e^{j\frac{2\pi l}{n}} z^{-1}} \tag{5.4}$$

where

$$\sum_{i=0}^{n-1} e^{j\frac{2\pi l i}{n}} z^{-i} = \frac{1 - z^{-n}}{1 - e^{j\frac{2\pi l}{n}} z^{-1}} \tag{5.5}$$

Define a set of transfer functions extracting from Equation (5.4)

$$H^l(z) = \frac{1}{n} \frac{1 - z^{-n}}{1 - e^{j\frac{2\pi l}{n}} z^{-1}} \tag{5.6}$$

for $l = 0, \pm 1, \pm 2, \ldots, \pm\frac{n-1}{2}$, the above equation is referred as the $l-$th FSF with the centre frequency of the $l-$th filter is at $\frac{2\pi l}{n}$ radians. Let $z = e^{j\omega}$, Equation (5.4) will become

$$G\left(e^{j\omega}\right) = \sum_{l=-\frac{n-1}{2}}^{\frac{n-1}{2}} G\left(e^{j\frac{2\pi l}{n}}\right) \frac{1}{n} \frac{1 - e^{-j\omega n}}{1 - e^{j\frac{2\pi l}{n}} e^{-j\omega}} \tag{5.7}$$

At $\omega = \omega_l$, the following condition holds

$$H^a\left(e^{j\omega}\right) = 0 \qquad \text{for} \qquad a \neq l$$

$$H^a\left(e^{j\omega}\right) = 1 \qquad \text{for} \qquad a = l$$

where a is an integer like l in the range $\left[-\frac{n-1}{2}, \frac{n-1}{2}\right]$. In this case, the value of the process frequency response in Equation (5.7) reduces to the value of the process frequency response coefficient $G\left(e^{j\frac{2\pi l}{n}}\right)$.

Given the discrete time input signal, $u(k)$, the discrete time measured output signal, $y(k)$, and the disturbance $v(k)$, the FSF model can be explained in block diagram as shown in Figure (5.1). The FSF filters are narrow band-limited around their respective centre frequencies [180]. All the filters have identical frequency responses except for the location of their centre frequencies. Some of the FSF model characteristics are listed below [180].

1. FSF model only requires prior information about the process settling time expressed in terms of n.
2. The number of unknown parameters in the FSF model is equal to the number of unknown parameters in the FIR model.
3. FSF model corresponds to the discrete time frequency response coefficients.
4. The elements of the regressor vector for estimating the frequency response coefficients are formed by passing the process input through the set of narrow band-limited frequency sampling filters.

Therefore, with the arbitrary input, $u(k)$ and the measured output, $y(k)$, the FSF model system can be identified as

$$y(k) = G(z)u(k) + v(k) \tag{5.8}$$

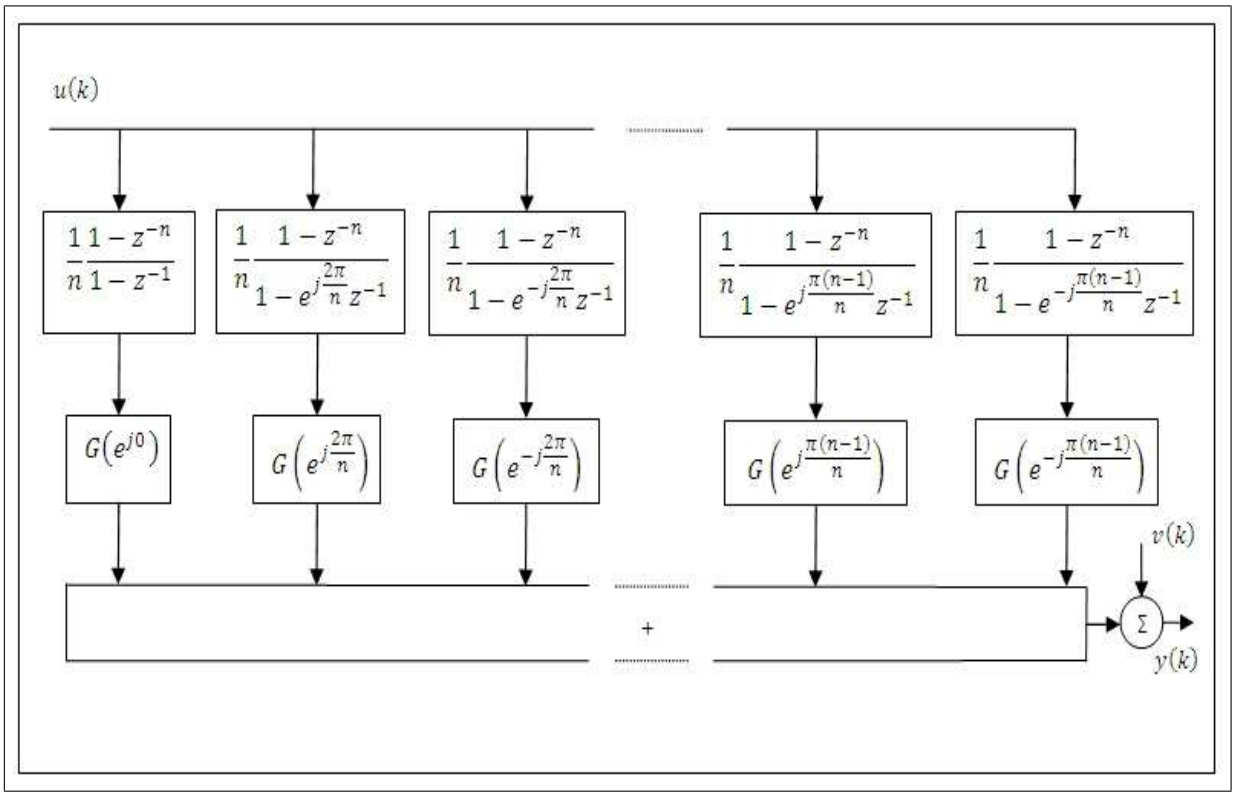

Figure 5.1: Frequency sampling filter model structure [180]

where $G(z)$ is given by Equation (5.4) and $v(k)$ is the zero mean disturbance term. Define the parameter vector as

$$\theta = \left[\begin{array}{ccccccc} G(0) & G\left(e^{j\left(\frac{2\pi}{n}\right)}\right) & G\left(e^{-j\left(\frac{2\pi}{n}\right)}\right) & \dots & G\left(e^{j\left(\frac{(n-1)\pi}{n}\right)}\right) & G\left(e^{-j\left(\frac{(n-1)\pi}{n}\right)}\right) \end{array} \right]^{\top} \tag{5.9}$$

and its corresponding regressor vector as

$$\phi(k) = \left[\begin{array}{ccccccc} f_0(k) * u(k) & f_1(k) * u(k) & f_{-1}(k) * u(k) & \dots & f_{\frac{n-1}{2}}(k) * u(k) & f_{-\frac{n-1}{2}}(k) * u(k) \end{array} \right]^{\top} \tag{5.10}$$

where $f_l(k)$ is defined according to Equation (5.6). Thus, Equation (5.8) can be rewritten as

$$y(k) = \theta^{\top}\phi(k) + v(k) \tag{5.11}$$

For N data measurements, Equation (5.11) can also be written in matrix form as

$$Y = \Theta\Phi + V \tag{5.12}$$

where

$$Y^\top = \begin{bmatrix} y(1) & y(2) & \dots & y(N) \end{bmatrix}$$

$$V^\top = \begin{bmatrix} v(1) & v(2) & \dots & v(N) \end{bmatrix}$$

$$\Phi = \begin{bmatrix} f_0(1) & f_1(1) & f_{-1}(1) & \dots & f_{-\frac{n-1}{2}}(1) \\ f_0(2) & f_1(2) & f_{-1}(2) & \dots & f_{-\frac{n-1}{2}}(2) \\ \vdots & \vdots & \vdots & \dots & \vdots \\ f_0(N) & f_1(N) & f_{-1}(N) & \dots & f_{-\frac{n-1}{2}}(N) \end{bmatrix}$$

Equation (5.12) can then be used to solve the least squares estimate of Θ given by

$$\hat{\Theta} = (\Phi_N^\top \Phi_N)^{-1} \Phi_N^\top Y_N \tag{5.13}$$

which minimize the performance index of the form

$$J(N, \hat{\Theta}) = \sum_{a=0}^{N} |Y - \Theta\Phi|^2 \tag{5.14}$$

The matrix $\Phi_N^\top \Phi_N$ is called the correlation matrix and the invertibility condition on this matrix is sometimes called the sufficient excitation condition for parameter estimation [180]. In order to obtain a proper FSF parameter optimization, the least squares model estimates based on PRESS computation is used. The PRESS criterion will ensure that the FSF model has the greatest predictive capability among all its candidate models.

5.2.2 The PRESS Criterion

In the statistical literature, the sum of squared prediction errors is defined as the PRESS (An abbreviation of *Predicted REsidual Sums of Square*) [178–180]. The idea of PRESS is to set aside each data point, estimate a model using the rest of the data, and then evaluate the prediction error at the point that was removed [121]. Instead of its usage in minimizing the prediction error, the PRESS statistic can be applied as a criterion for model structure detection in dynamic system identification [178]. The PRESS computation is based on the orthogonal decomposition algorithm proposed by Korenberg et al. [90]. The orthogonal decomposition algorithm can be referred as in Appendix A.

Define the prediction error as

$$\begin{aligned} e_{-k}(k) &= y(k) - \hat{\theta}^\top \phi(k) \\ &= y(k) - \hat{y}_{-k}(k) \end{aligned} \tag{5.15}$$

where $e_{-k}(k), k = 1, 2, \ldots, N$ are called the PRESS residuals and $\hat{\theta}$ has been estimated according to Equation (5.13) without including $\phi(k)$ and $y(k)$. The PRESS residuals $e_{-k}(k)$ represent the true prediction errors, since $y(k)$ and $\hat{y}_{-k}(k)$ are independent. Based on the Shermon-Morrison-Woodbury theorem (see e.g. in [121]), the PRESS residuals $e_{-k}(k)$ can be calculated according to the following equation

$$e_{-k}(k) = \frac{e(k)}{1 - \phi(k)^\top (\Phi^\top \Phi)^{-1} \phi(k)} \tag{5.16}$$

The PRESS statistic is defined as

$$\text{PRESS} = \sum_{k=1}^{N} e_{-k}(k)^2 \tag{5.17}$$

The average PRESS is calculated as

$$\text{PRESS}_{av} = \sqrt{\frac{\sum_{k=1}^{N} e_{-k}(k)^2}{N-1}} \tag{5.18}$$

Equations (5.17) and (5.18) both provide measures of the predictive capability of the estimated model. In terms of model structure selection, the chosen structures are based on the smallest PRESS value.

5.2.3 Computation of the PRESS statistic

Let $w_i(\cdot)$ denote the ith column of W and $\hat{g}_i$ represent the ith estimated auxiliary parameter (Refer to Appendix A on elaboration of these two terms). The PRESS residuals $e_{-k}(k)$, $k = 1, 2, \ldots, N$ defined in Equation (5.15) for the original model with n parameters are given by

$$e_{-k}(k) = \frac{y(k) - \sum_{i=1}^{n} w_i(k)\hat{g}_i}{1 - \sum_{i=1}^{n} \frac{w_i(k)^2}{\|w_i\|^2}} \tag{5.19}$$

where $\|w_i\| = \sqrt{\sum_{k=1}^{N} w_i(k)^2}$ is the norm of w_i.

Proof:

The ordinary residuals can be written in terms of orthogonalized data matrix and the auxiliary parameter estimates [180]

$$e(k) = y(k) - \sum_{i=1}^{n} w_i(k)\hat{g}_i \tag{5.20}$$

From definitions of $\phi(t)$ and Φ in Equations (5.9-5.12), it becomes

$$\phi(k)^\top(\Phi^\top\Phi)^{-1}\phi(k) = diag_k[\Phi(\Phi^\top\Phi)^{-1}\Phi^\top] \tag{5.21}$$

Using $\Phi = WT$ gives

$$\begin{aligned}\Phi(\Phi^\top\Phi)^{-1}\Phi^\top &= WT(T^\top W^\top WT)^{-1}T^\top W^\top \\ &= W(W^\top W)^{-1}W^\top \end{aligned} \tag{5.22}$$

Hence

$$\begin{aligned}\phi(k)^\top(\Phi^\top\Phi)^{-1}\phi(k) &= diag_k[W(W^\top W)^{-1}W^\top] \\ &= \sum_{i=1}^{n}\frac{w_i(k)^2}{\|w_i\|^2}\end{aligned} \tag{5.23}$$

From the expression for the PRESS residuals $e_k(k)$ in Equation (5.16), the result in Equation (5.19) dictates as follows [180].

1. The sum of squares of the ordinary residuals for a model with n parameters is given by

$$J_n = \sum_{k=1}^{N} y(k)^2 - \sum_{i=1}^{n}\hat{g}_i^2\|w_i\|^2 \tag{5.24}$$

   Therefore, for a model of order, $n+1$

$$J_n - J_{n+1} = \hat{g}_{n+1}^2\|w_{n+1}\|^2 \tag{5.25}$$

   which indicates that the sum of squares of the ordinary residuals is non-increasing with respect to model order. However, if a term is added to the model and the PRESS increases, this indicates that the predictive capability of the model is better without that term.

2. The true prediction errors $e_k(k)$ are actually a weighted version of the ordinary residuals. The weighting factor $[1-\sum_{i=1}^{n}\frac{w_i(k)^2}{\|w_i\|^2}]^{-1}$ gives large weights to ordinary residuals associated with data points where prediction is poor.

3. The computation of the PRESS residuals $e_k(k)$ using Equation (5.19) only requires the orthogonal matrix W and the auxiliary parameter vector $\hat{g}$. Hence, the value of the PRESS can be used to detect the significance of each additional term in the original model without actually having to compute $\hat{\theta}$.

5.3 Step Response Estimation using Frequency Sampling Filters

In the estimation of step response, the description of the system using frequency sampling filters can be described as follow.

$$y(k) = \sum_{l=-\frac{n-1}{2}}^{\frac{n-1}{2}} G\left(e^{j\frac{2\pi l}{n}}\right) H^l(z)u(k) + v(k) \tag{5.26}$$

where for a suitable choice of $G\left(e^{j\frac{2\pi l}{n}}\right)$ and $H^l(z)$ defined as in Equation (5.3) and (5.6), respectively, $u(k)$ is the input signal, y(k) is the output signal and $v(k)$ is the disturbance signal. Upon obtaining the estimate of the frequency response parameters (according to FSF model and PRESS criterion), the estimate of the step response at sampling instant, m can be expressed by

$$\hat{g}_m = \sum_{i=0}^{m-1} \hat{h}_i \tag{5.27}$$

where the estimated impulse response coefficients $\hat{h}_0, \hat{h}_1, \hat{h}_2, \ldots, \hat{h}_{m-1}$ are related to frequency response via

$$\hat{h}_i = \frac{1}{n} \sum_{l=-\frac{n-1}{2}}^{\frac{n-1}{2}} \hat{G}\left(e^{j\frac{2\pi l}{n}}\right) e^{j\frac{2\pi li}{n}} \tag{5.28}$$

Substituting Equation (5.28) into (5.27), the estimated step response coefficient can be rewritten as

$$\hat{g}_m = \sum_{l=-\frac{n-1}{2}}^{\frac{n-1}{2}} \hat{G}\left(e^{j\frac{2\pi l}{n}}\right) \frac{1}{n} \frac{1 - e^{j\frac{2\pi 1}{n}(m+1)}}{1 - e^{j\frac{2\pi l}{n}}} \tag{5.29}$$

Although the FSF approach is cast in the discrete time domain and the corresponding z-transform domain, the resultant model can be used to obtain continuous time step response [180]. The system impulse response $\hat{g}(t)$ can be approximately computed using the continuous time equivalent as

$$\hat{g}(t) \approx \hat{g}_{fsf}(t) = \sum_{l=-\frac{n-1}{2}}^{\frac{n-1}{2}} \hat{\theta}_l \hat{h}_l(t) \tag{5.30}$$

and

$$\hat{h}_l(t) = \frac{1}{T} e^{j\frac{2\pi l t}{T}} \qquad \text{for} \qquad t < T\triangle \tag{5.31}$$

where T is a sampling period. The step response is determined as

$$y_s(t) = \int_0^t \hat{g}(\tau)\mathrm{d}\tau \tag{5.32}$$

5.4 Continuous Time Model Identification using Step Response Estimates

As discussed in Section 5.2 and Section 5.3, the first stage of the two-stage identification involved a process of data compression in which the system step response in non-parametric form is obtained. The significant of this approximation lies in the fact that

1. Large amount of data that have been collected from the system can be deduced or compressed into fewer number of data.
2. The process frequency parameters correspond to higher frequency region of the system are neglected as the information contain from that region normally has severe noise corruption.
3. The relatively noise-free step response is obtained as compared to an actual step response test. Thus, it can be intuitively judged by the process engineer.

Next in this section, the second stage of the identification is discussed in which the continuous time state space model is developed based on the estimated step response. In here, the open-loop identification technique is possible to be used as to deal with the closed-loop data from closed-loop system. Since the procedure in the first stage involves the usage of the FIR model and the maximum likelihood method (based on PRESS calculation) as to remove the noise effects, the estimated data used for identification in second stage will give unbiased estimation.

Consider the state-space model of the continuous time system in the Laplace domain

$$\begin{aligned} sX(s) &= AX(s) + BU(s) \\ Y(s) &= CX(s) + DU(s) \end{aligned} \tag{5.33}$$

where $U(s) \in R^m$, $Y(s) \in R^l$, $X(s) \in R^n$ are the Laplace transforms of the system inputs, outputs and state variables respectively, and $A \in R^{n\times n}$, $B \in R^{n\times m}$, $C \in R^{l\times n}$ and $D \in R^{l\times m}$ are the system matrices. The transfer function can be expressed as

$$G(s) = C(sI_n - A)^{-1}B + D \tag{5.34}$$

For a given plant input signal $u(t)$, the plant output response is described by [182]

$$y(t) = G(p)u(t) + \eta(t) \tag{5.35}$$

where $G(p)$ is an operator corresponding to the transfer function $G(s)$ and $\eta(t)$ is a continuous time disturbance. In this indirect approach, the input to the plant is a unit step and the output is the step response resulting from stage 1 as discussed in previous section. Thus,

$$y(t_i) = \hat{g}(t_i) = g(t_i) + \eta(t_i) \tag{5.36}$$

It can be regarded this way as at the sampling instant t_i, of the step response are equivalent in both continuous time and discrete time cases, and the disturbance $\eta(t_i)$ is the error contained in the estimated step response. The disturbance is a discrete sequence with known statistical properties that

$$\mathbf{E}[\eta(t_i)] = 0$$
$$\mathbf{E}[\eta(t_i)^2] = \delta(i)^2$$

If $\delta(i)$ is approximately constant for all i, the discrete disturbance sequence is a near white noise in the discrete time. In general, $\eta(\cdot)$ has a "flat" spectrum in the low and medium frequency region and its amplitude is relatively small [182]. In the second stage of the identification procedure, the subspace method with the adoption of Laguerre filter and Instrumental Variable methods discussed in Chapter 3 will be used again here. The overall identification process can be referred as in Figure 5.2.

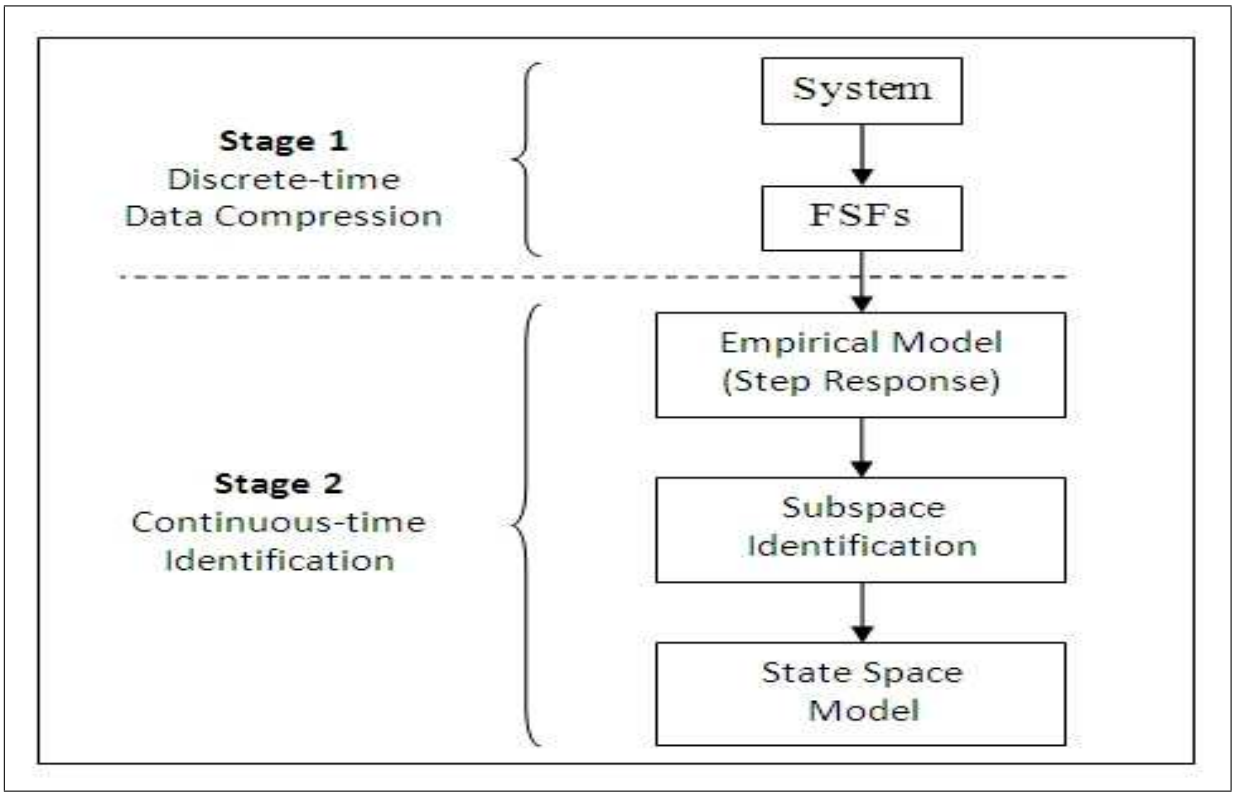

Figure 5.2: 2-stage identification procedure

5.5 Simulation and Experimental Examples

In this section the results from the 2-stage identification will be demonstrated. The system under investigation is divided into two categories: A simulated system and the actual magnetic bearing apparatus. As for the simulated system, a simple stable system is generated according to the following transfer function

$$G(s) = \frac{1}{(s+1)(s+3)}$$

The GRBS is used to generate the input signal, $u(t)$. At sampling time of $\Delta t = 0.05s$, about $Nm = 3000$ set of output signal $y(t)$ is generated. To see the difference when the system is corrupted with measurement noise, $v(t)$, three sets of noise are added to the system. The added sets of noise are labelled according to the *Signal to Noise Ratio* (SNR); 25dB, 50dB and 75dB SNR. The output signal of these systems are shown in Figure (5.3). The step response estimates with confidence bounds obtained from the 1-stage identification can be seen as in Figure (5.4).

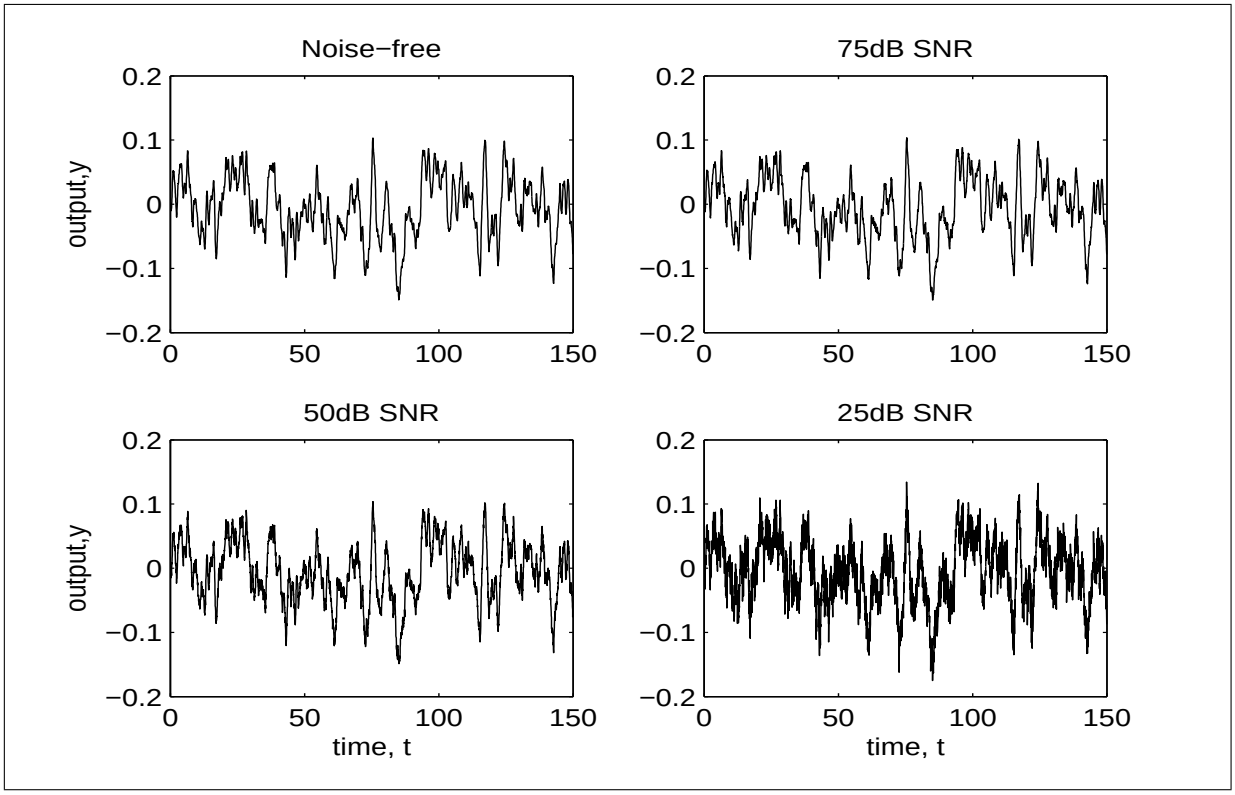

Figure 5.3: The output system for different noise level

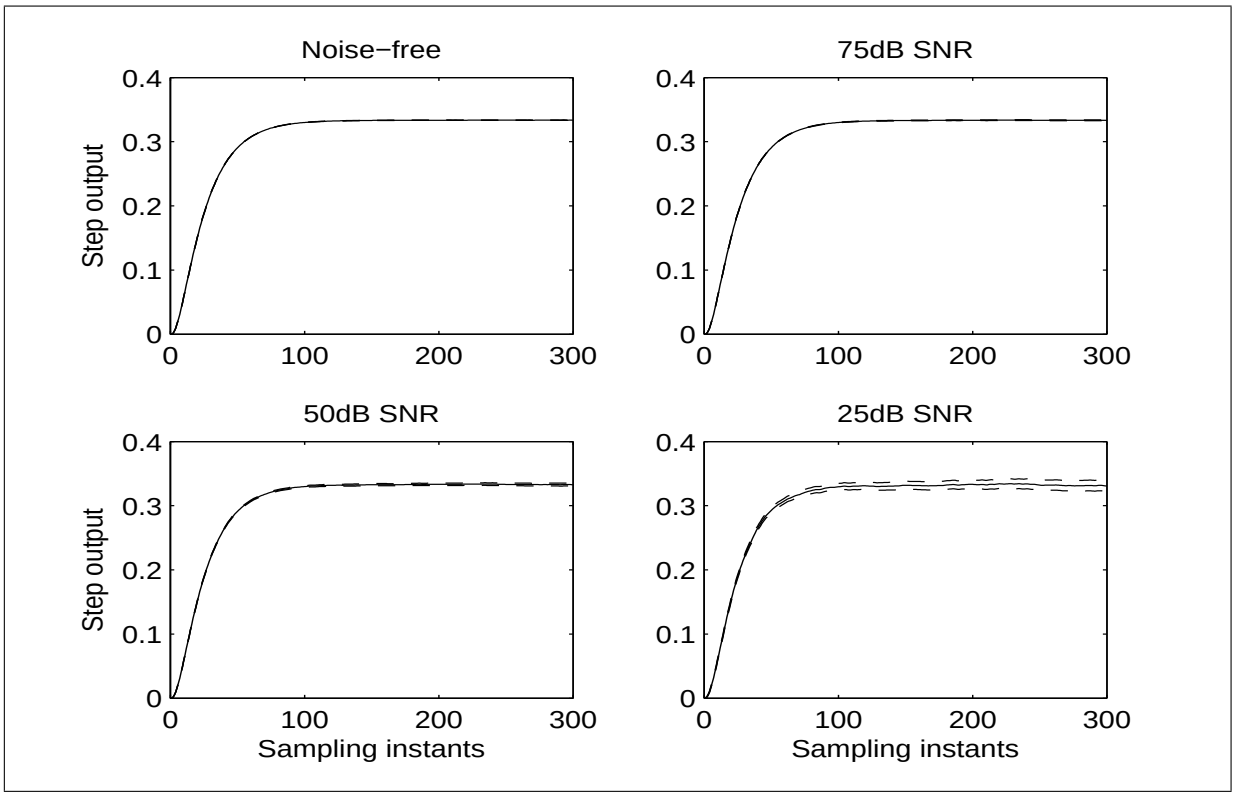

Figure 5.4: The step response estimate with confidence bounds - simulated data

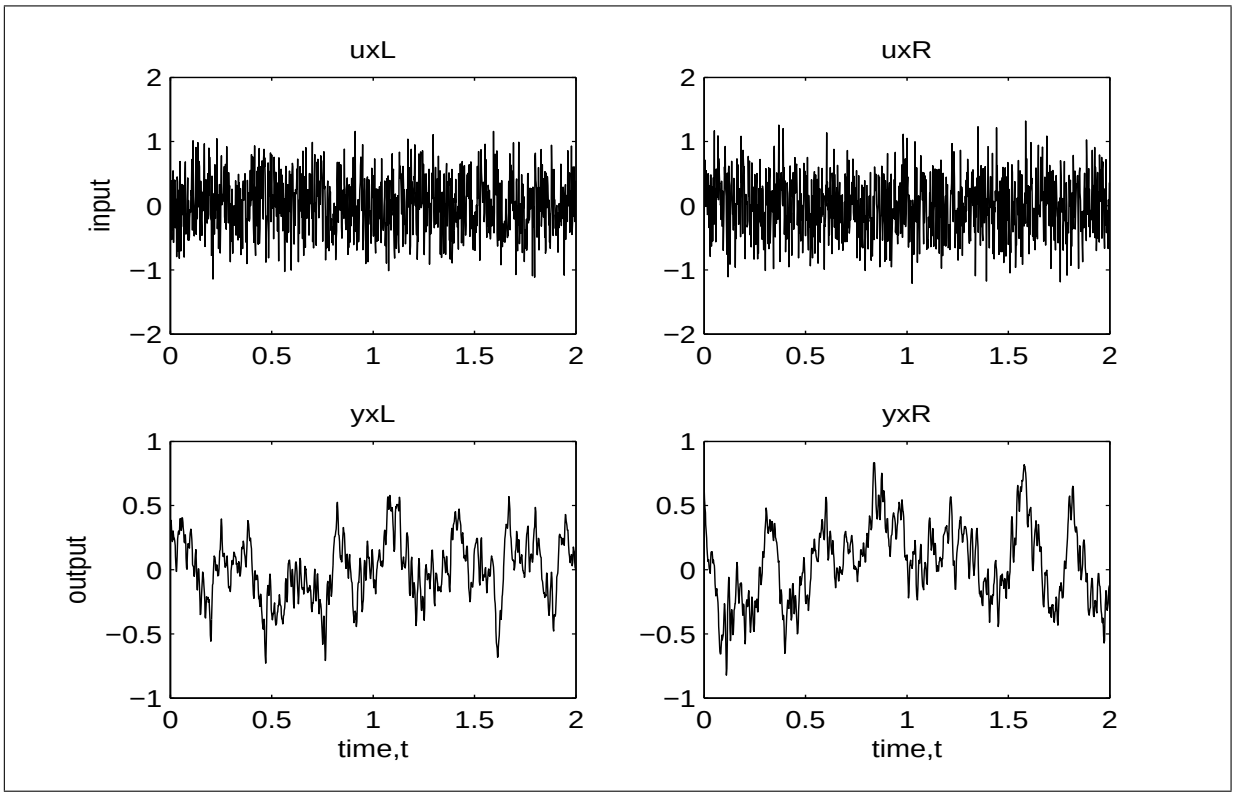

Figure 5.5: The MB input-output systems $x - z$ plane

For the real magnetic bearing data systems, the plot of input and output signal obtained from the $x - z$ of left and right plane and the $y - z$ of left and right plane can be seen as in Figures (5.5) and (5.6) respectively. The step response estimates with confidence bounds obtained from the 1-stage identification of MB systems can be seen as in Figure (5.7). From the step response plots, it shows that the confidence bounds are relatively wider, especially in the steady state parts of the 25dB step response plot. This indicates that the plant disturbances have frequency contents that are concentrated in the low frequency regions.

Upon obtaining the continuous time step response data from the first stage of the identification, the second stage of the identification takes part in which the state-space model is developed based on the subspace methods. During this stage, the input signal $u(t)$ is a unit step input signal and the output signal $y(t)$ is based on the step response output data from first stage. The model is developed for both SISO and MIMO systems. The performance capability of the proposed model is further demonstrated by measuring its accuracy based on VAF and MSE calculation.

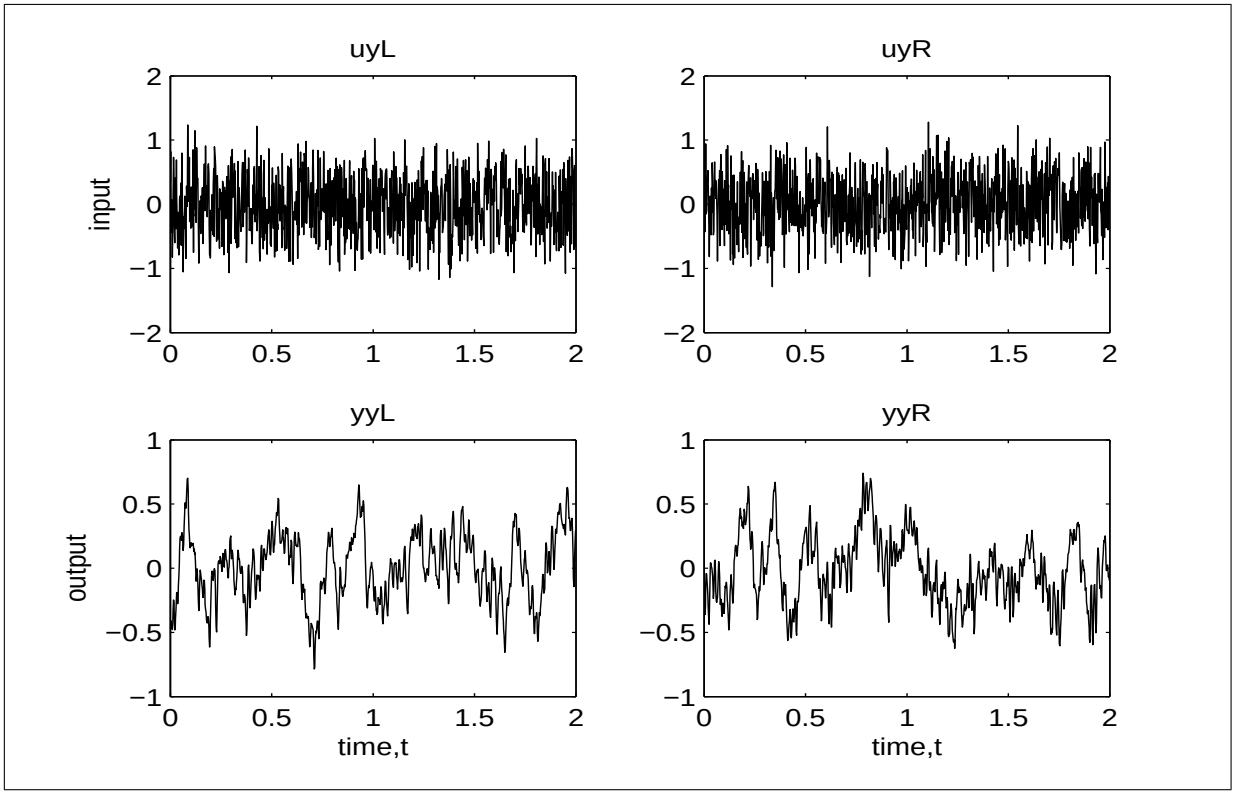

Figure 5.6: The MB input-output systems $y - z$ plane

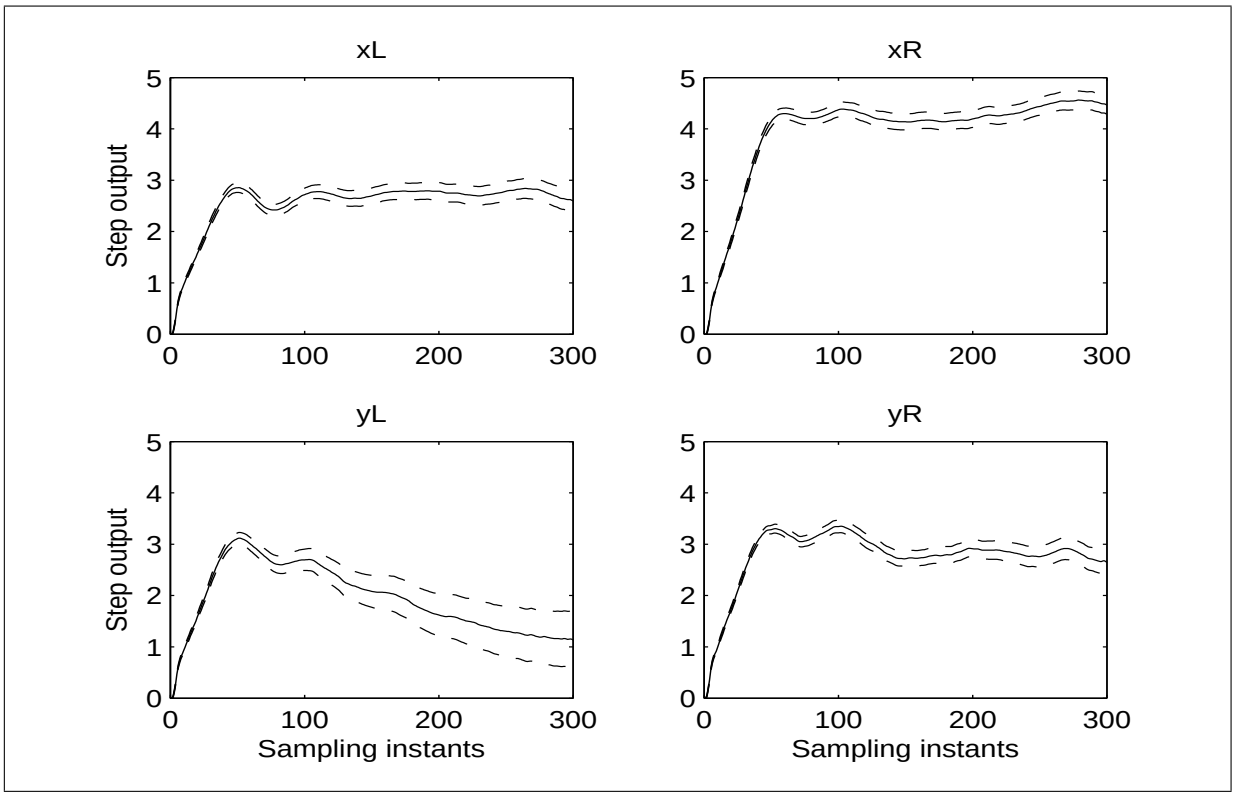

Figure 5.7: The step response estimate with confidence bounds - MB data

Table 5.1: Model configuration - SISO simulated data

Symbol	Description	Noise-free	75dB SNR	50dB SNR	25dB SNR
p	Laguarre parameter	2	2	2	2
i	Expanding observability matrix	10	10	10	10
n	Model order	2	2	2	2
Δt	Sampling time	0.05	0.05	0.05	0.05
N	Number of sampled data	3000	3000	3000	3000
Ns	Number of step response data	300	300	300	300

5.5.1 Single Input Single Output System

Observation over single input single output system is divided into two examples: A simulated data and a real MB data.

Example 1 - Simulated Data

The parameter used in developing the model can be referred as in Table 5.1. The step responses of the continuous time models are compared to their respective responses as in Figure (5.8). From the step response plot of each systems, it shows that the subspace model can identify the step response data successfully. The VAF percentage and MSE calculation can be referred in Table 5.2. From this calculation, it shows that even though the actual data has different noise level, after running through the first identification stage, the subspace model can identify the systems with approximately the same accuracy.

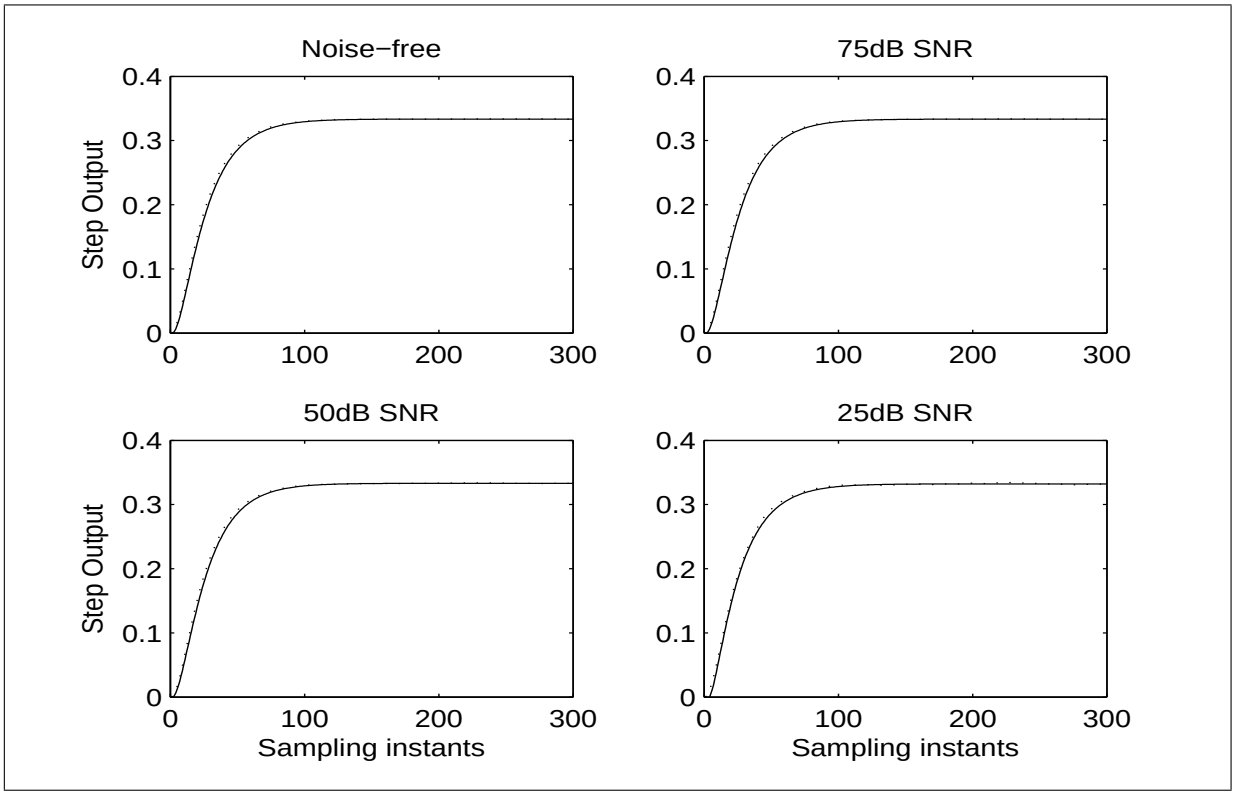

Figure 5.8: System (dotted) & model (solid) step response - SISO simulated data

Table 5.2: VAF & MSE - SISO simulated data

Description	Noise-free	75dB SNR	50dB SNR	25dB SNR
VAF	99.8283%	99.8282%	99.8281%	99.8219%
MSE	1.1631×10^{-5}	1.1623×10^{-5}	1.1595×10^{-5}	1.1976×10^{-5}

The estimated (A, B, C, D) system matrices are given as

$$\hat{A}_{nf} = \begin{bmatrix} -0.7288 & -3.1316 \\ 0.1620 & -3.0249 \end{bmatrix}; \hat{B}_{nf} = \begin{bmatrix} -9.1469 \\ -3.2984 \end{bmatrix} \times 10^3; \hat{C}_{nf} = \begin{bmatrix} -0.1415 \\ 0.3986 \end{bmatrix}^\top \times 10^3; \hat{D}_{nf} = [0];$$

$$\hat{A}_{75dB} = \begin{bmatrix} -0.7300 & -3.1287 \\ 0.1626 & -3.0128 \end{bmatrix}; \hat{B}_{75dB} = \begin{bmatrix} 6.5746 \\ 0.9635 \end{bmatrix} \times 10^3; \hat{C}_{75dB} = \begin{bmatrix} 0.0002 \\ -0.0014 \end{bmatrix}^\top; \hat{D}_{75dB} = [0];$$

$$\hat{A}_{50dB} = \begin{bmatrix} -0.7328 & 3.1445 \\ -0.1647 & -3.0249 \end{bmatrix}; \hat{B}_{50dB} = \begin{bmatrix} -1.0399 \\ 0.1913 \end{bmatrix} \times 10^3; \hat{C}_{50dB} = \begin{bmatrix} -0.0011 \\ -0.0062 \end{bmatrix}^\top; \hat{D}_{50dB} = [0];$$

$$\hat{A}_{25dB} = \begin{bmatrix} -0.7352 & 3.8288 \\ -0.1889 & -4.2267 \end{bmatrix}; \hat{B}_{25dB} = \begin{bmatrix} -223.3228 \\ 24.8873 \end{bmatrix}; \hat{C}_{25dB} = \begin{bmatrix} -0.0050 \\ -0.0497 \end{bmatrix}^\top; \hat{D}_{25dB} = [0];$$

The eigenvalues are obtained as

$$\text{eig}(\hat{A}_{nf}) = \begin{bmatrix} -0.9764 \\ -2.7773 \end{bmatrix}; \qquad \text{eig}(\hat{A}_{75dB}) = \begin{bmatrix} -0.9802 \\ -2.7625 \end{bmatrix};$$

$$\text{eig}(\hat{A}_{50dB}) = \begin{bmatrix} -0.9869 \\ -2.7708 \end{bmatrix}; \qquad \text{eig}(\hat{A}_{25dB}) = \begin{bmatrix} -0.9564 \\ -4.0055 \end{bmatrix};$$

Next, the comparison is made as to see any significant improvement in system identification by using fresh measured data direct apply to the subspace model and by using the estimated data obtained from first stage of 2-stage identification method. Since the same subspace identification algorithms are used, the parameters involved are equally set for this comparison.

The result of the comparison can be seen in Table 5.3. From this table, first obvious improvement is on number of sampled data, in which it has been compressed from 3000 to 300 data. Second improvement can be observed as the noise level adding to the system is increased. This will degrade the performance of the subspace model in identifying the systems. However, the performance remain almost the same for the 2-stage identification, as the noise effects in the systems have been cleared during the first stage.

Example 2 - MB Data

For the SISO system identification, the four sets of MB data will be identified individually. The parameter used in developing the model can be referred as in Table 5.4. The step responses of

Table 5.3: Performance comparison - SISO simulated data

Symbol	Description	Direct Identification	2-stage Identification
p	Laguarre parameter	2	2
i	Expanding observability matrix	10	10
n	Model order	2	2
Δt	Sampling time	0.05	0.05
N	Number of sampled data	3000	300
	VAF for noise-free data	99.95%	99.83%
	VAF for 75dB data	99.89%	99.83%
	VAF for 50dB data	99.23%	99.83%
	VAF for 25dB data	90.74%	99.82%

Table 5.4: Model configuration - SISO MB data

Symbol	Description	x_L	x_R	y_L	y_R
p	Laguarre parameter	60	60	100	60
i	Expanding observability matrix	10	10	10	10
n	Model order	8	8	8	8
Δt	Sampling time	0.002	0.002	0.002	0.002
N	Number of sampled data	1000	1000	1000	1000
Ns	Number of step response data	300	300	300	300

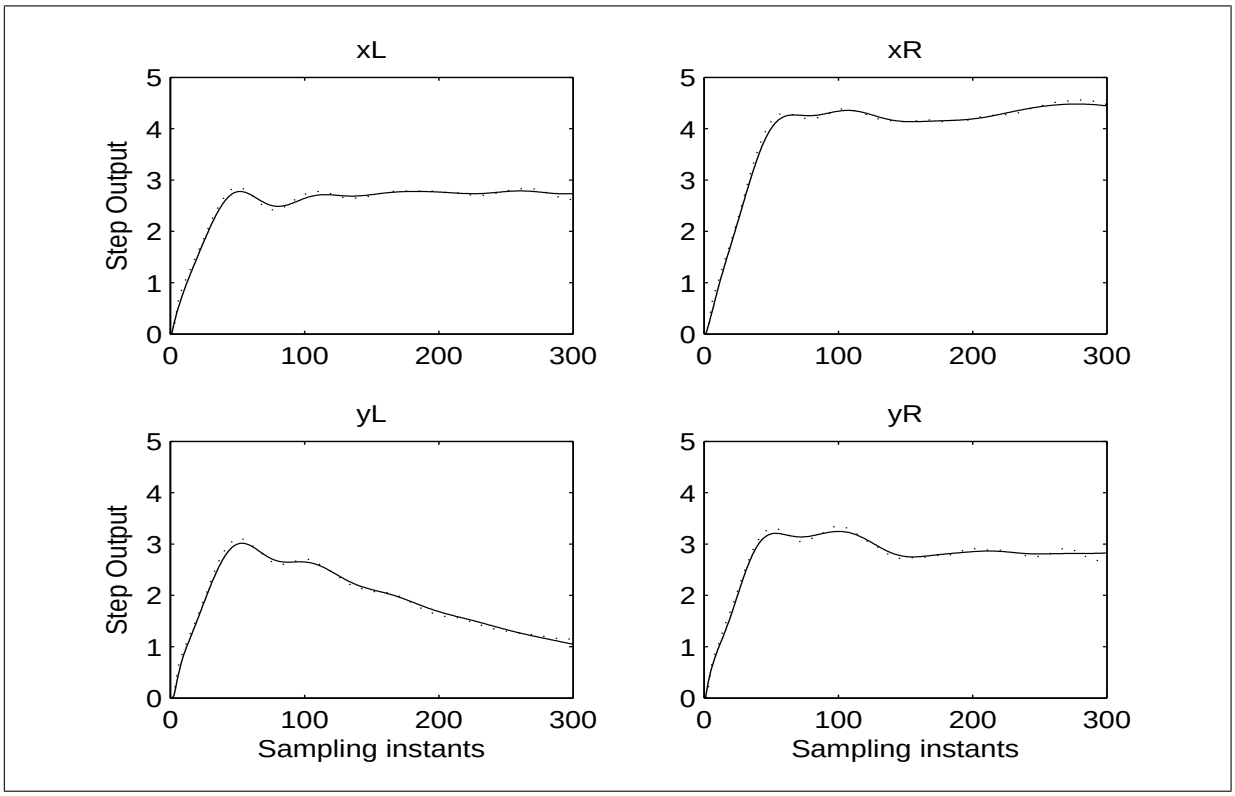

Figure 5.9: System (dotted) & model (solid) step response - SISO MB data

the continuous time models are compared to their respective responses as in Figure (5.9). From this figure, it shows that the subspace model can identify the step response for each of the MB systems closely.

The VAF percentage and MSE calculation can be referred in Table 5.5. These calculation also give low MSE and good performance of accuracy according to VAF. The example of the

Table 5.5: VAF & MSE - SISO MB data

Description	y_{xL}	y_{xR}	y_{yL}	y_{yR}
VAF	98.8437%	99.6518%	99.3985%	98.7117%
MSE	0.0030	0.0035	0.0027	0.0041

estimated (A, B, C, D) system matrices for the x_L data are given as

$$\hat{A}_{xL} = \begin{bmatrix} -20.7652 & 36.3213 & -42.0148 & 24.7938 & 3.8734 & -46.3922 & 13.2676 & 106.3437 \\ -15.4431 & -5.1447 & 59.0697 & -16.6568 & -4.9293 & 32.1206 & -4.7140 & -53.3310 \\ -4.5090 & -36.5395 & -24.2739 & 23.3503 & 1.2529 & -56.9782 & 15.1193 & 106.0079 \\ 1.9955 & 3.8430 & 3.9400 & -7.6038 & 11.5437 & 46.1725 & -12.7770 & -56.0640 \\ 1.5582 & 1.6780 & 6.9961 & -16.6960 & 0.3012 & -31.4479 & -8.8977 & -16.9652 \\ -1.7037 & -5.5373 & -6.8972 & -7.5324 & 31.6759 & -13.8510 & 33.5567 & 146.2488 \\ -0.4849 & -1.4467 & -1.9126 & 5.3835 & 6.5553 & -15.6471 & -1.7769 & -57.8724 \\ 0.9421 & 1.7715 & 4.2056 & -5.5019 & -3.0691 & 5.8146 & 28.3058 & -122.8657 \end{bmatrix}$$

$$\hat{B}_{xL} = \begin{bmatrix} -651.0776 \\ -324.7180 \\ -301.4940 \\ -418.6805 \\ 45.4888 \\ 138.6734 \\ -135.1435 \\ -82.8360 \end{bmatrix}; \quad \hat{C}_{xL} = \begin{bmatrix} -0.3230 \\ -0.2925 \\ 1.5299 \\ -1.2331 \\ 1.1892 \\ -5.6717 \\ -0.4905 \\ -4.4514 \end{bmatrix}^{\top}; \quad \hat{D}_{xL} = [0];$$

The eigenvalue is given as

$$\text{eig}(\hat{A}_{xL}) = \begin{bmatrix} -1.3619 \\ -0.0773 \pm 0.5590j \\ -0.1514 \\ -0.1423 \pm 0.2506j \\ -0.0037 \pm 0.4521j \end{bmatrix} \times 10^2$$

Next, the comparison is made based on direct open-loop subspace identification, closed-loop subspace identification and the 2-stage identification. Results from this analysis can be referred in Table 5.6. From this table, the 2-stage identification has given better performance in comparison with others. The analysis also shows that the subspace model becomes more stable and is not so sensitive towards the change of the design parameter p and i when is identifying the step response data. This is probably due to the "clean" step response data that make the model identification run successfully.

Table 5.6: Performance comparison - SISO MB data

Description	Direct Identification	Closed-loop CEIV model	Closed-loop CREF model	2-stage Identification
Sampling time, Δt	0.002	0.002	0.002	0.002
Number of data, N	1000	1000	1000	300
VAF for x_L data	[p=60,i=10,n=8] 86.66%	[p=100,i=10,n=6] 83.57%	[p=230,i=10,n=6] 86.21%	[p=60,i=10,n=8] 98.84%
VAF for x_R data	[p=230,i=10,n=8] 91.72%	[p=100,i=10,n=6] 90.16%	[p=230,i=10,n=6] 91.71%	[p=60,i=10,n=8] 99.65%
VAF for y_L data	[p=230,i=10,n=8] 87.05%	[p=260,i=10,n=6] 85.12%	[p=230,i=10,n=6] 87.16%	[p=100,i=10,n=8] 99.40%
VAF for y_R data	[p=100,i=10,n=8] 92.80%	[p=260,i=10,n=6] 81.12%	[p=230,i=10,n=6] 89.28%	[p=60,i=10,n=8] 98.71%

5.5.2 Multi Input Multi Output Systems

Observation over multi input multi output systems are divided into three examples: A two-input-two-output simulated data, a two-input-two-output MB data and a four-input-four-output MB data.

Example 1 - 2 in 2 out simulated data

The two-input-two-output systems are defined by the following configuration

$$\begin{bmatrix} y_1(t) \\ y_2(t) \end{bmatrix} = \begin{bmatrix} \frac{1}{s+1} & \frac{1}{s+3} \\ \frac{1}{s+2} & \frac{1}{s+1} \end{bmatrix} \begin{bmatrix} u_1(t) \\ u_2(t) \end{bmatrix}$$

At sampling time, $\Delta t = 0.01s$, about $N = 4000$ data is sampled. The input and output data with different noise level are then processed in the first stage to obtain about $Ns = 400$ step response data. The parameter used in developing the model can be referred as in Table 5.7. The step responses of the continuous time models are compared to their respective responses

Table 5.7: Model configuration - MIMO simulated data

Symbol	Description	Noise-free	75dB SNR	50dB SNR	25dB SNR
p	Laguarre parameter	16	14	16	14
i	Expanding observability matrix	10	10	10	10
n	Model order	4	4	4	4
Δt	Sampling time	0.01	0.01	0.01	0.01
N	Number of sampled data	4000	4000	4000	4000
Ns	Number of step response data	400	400	400	400

Table 5.8: VAF & MSE - MIMO simulated data

Description	Noise-free	75dB SNR	50dB SNR	25dB SNR
VAF - y_1	99.7677%	99.5581%	99.2758%	99.6785%
VAF - y_2	99.9263%	99.5167%	99.6985%	99.3817%
MSE - y_1	4.5943×10^{-4}	4.5532×10^{-4}	0.0011	0.0029
MSE - y_2	1.6507×10^{-4}	6.3879×10^{-4}	9.2808×10^{-4}	0.0019

as in Figure (5.10). The results show very good performance for all the data tested. The VAF percentage and MSE calculation can be referred in Table 5.8. These calculations also give low MSE and good level of accuracy.

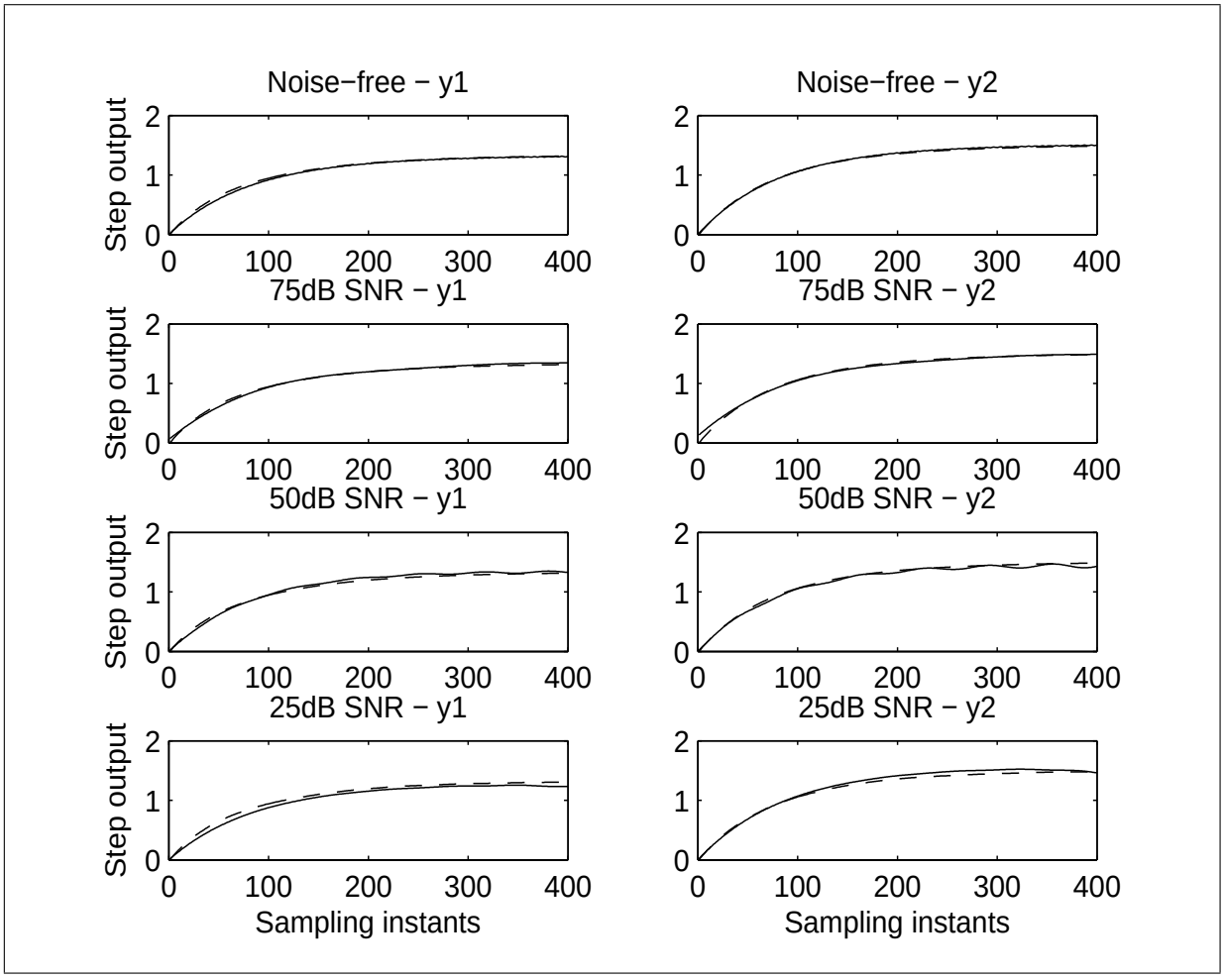

Figure 5.10: System (dashed) & model (solid) step response - MIMO simulated data

The example of estimated (A, B, C, D) system matrices for the identification of 50dB SNR data are given by

$$\hat{A}_{50dB} = \begin{bmatrix} -1.0914 & 1.6321 & -3.7023 & 0.2767 \\ 0.0200 & -0.4697 & 4.4103 & 2.6245 \\ 0.0242 & -0.6541 & -1.4724 & 9.4458 \\ -0.0147 & -0.8310 & -9.7561 & 0.9137 \end{bmatrix};$$

$$\hat{B}_{50dB} = \begin{bmatrix} -3.3168 & -3.3168 \\ 0.1123 & 0.1123 \\ -0.0089 & -0.0089 \\ -0.0463 & -0.0463 \end{bmatrix}; \quad \hat{C}_{50dB} = \begin{bmatrix} -0.2635 & -0.2856 \\ 0.6555 & -0.8424 \\ 0.6217 & -0.6924 \\ -0.0548 & 0.0017 \end{bmatrix}^{\top}; \quad \hat{D}_{50dB} = \begin{bmatrix} 0 & 0 \\ 0 & 0 \end{bmatrix};$$

The eigenvalue is given by

$$\text{eig}(\hat{A}_{50dB}) = \begin{bmatrix} -0.1996 \pm 9.7934j \\ -1.1001 \\ -0.6204 \end{bmatrix}$$

Example 2 - 2 in 2 out MB data

The two inputs two outputs MB systems are defined by the following configuration

$$\begin{bmatrix} y_{xL}(t) \\ y_{xR}(t) \end{bmatrix} = \begin{bmatrix} G_{11} & G_{12} \\ G_{21} & G_{22} \end{bmatrix} \begin{bmatrix} u_{xL}(t) \\ u_{xR}(t) \end{bmatrix}$$

and

$$\begin{bmatrix} y_{yL}(t) \\ y_{yR}(t) \end{bmatrix} = \begin{bmatrix} G_{11} & G_{12} \\ G_{21} & G_{22} \end{bmatrix} \begin{bmatrix} u_{yL}(t) \\ u_{yR}(t) \end{bmatrix}$$

The system identification for $x - z$ plane is treated separately from $y - z$ plane. The parameter used in developing the model can be referred as in Table 5.9. The step responses of the continuous time models are compared to their respective response as in Figure (5.11). From this figure, it shows that for the $x - z$ plane data and $y - z$ plane data, the subspace models are still able to identify the step response data closely. The VAF and MSE calculation also give good percentage and low MSE value. The result from the calculation can be referred in Table 5.10.

Table 5.9: Model configuration - 2in2out MB data

Symbol	Description	$x-z$	$y-z$
p	Laguarre parameter	440	440
i	Expanding observability matrix	10	10
n	Model order	8	8
Δt	Sampling time	0.002	0.002
N	Number of sampled data	1000	1000
Ns	Number of step response data	300	300

Table 5.10: VAF & MSE - 2in2out MB data

Description	y_{xL}	y_{xR}	y_{yL}	y_{yR}
VAF	90.8608%	95.5858%	97.5811%	94.8730%
MSE	0.0242	0.0378	0.0107	0.0158

The example of the estimated (A, B, C, D) system matrices for $x-z$ plane data are obtained as

$$\hat{A}_{xz} = \begin{bmatrix} -22.4907 & 94.4261 & 144.8680 & -100.3611 & 158.0706 & -15.0460 & -60.5002 & -86.5977 \\ -5.9929 & -76.7282 & -112.5933 & 265.0370 & -282.2011 & 95.8136 & 46.7170 & 241.1249 \\ 1.0407 & -104.4179 & -242.3469 & 448.9313 & -561.0103 & -42.1161 & 369.0528 & 107.5494 \\ -1.6883 & -50.7986 & -142.2114 & -119.8108 & 340.4446 & -74.5834 & -86.5572 & -266.8047 \\ -3.3409 & 39.7773 & 161.1324 & 23.1792 & -195.4469 & 49.5041 & 105.6253 & 328.8940 \\ -0.4993 & -19.4826 & -39.3356 & 5.3463 & 30.8667 & -65.7358 & 276.6391 & -325.4345 \\ 0.7978 & -14.4095 & -49.1758 & 11.2010 & 23.5728 & -14.9632 & -209.7371 & 463.8943 \\ 0.0846 & -19.1350 & -4.2794 & 18.8740 & -17.0796 & 89.6570 & -209.8264 & -232.1297 \end{bmatrix};$$

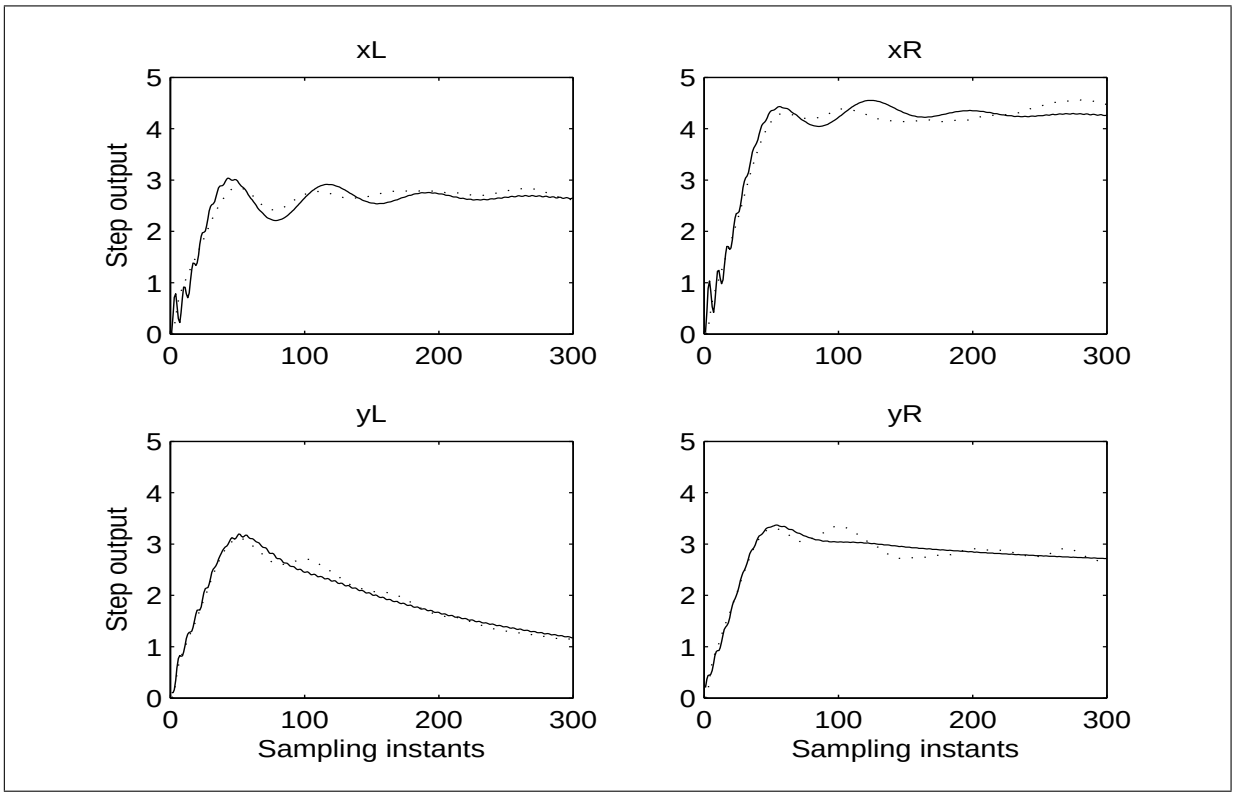

Figure 5.11: System (dotted) & model (solid) step response - 2in2out MB data

$$\hat{B}_{xz} = \begin{bmatrix} 100.4897 & 100.4897 \\ 5.9133 & 5.9133 \\ -370.2224 & -370.2224 \\ -142.5527 & -142.5527 \\ 118.0908 & 118.0908 \\ -297.7573 & -297.7573 \\ 160.3891 & 160.3891 \\ 163.6160 & 163.6160 \end{bmatrix}; \quad \hat{C}_{xz} = \begin{bmatrix} -0.4309 & -2.1302 \\ -1.8894 & -1.1540 \\ 0.9752 & -1.1796 \\ -1.9071 & -4.9300 \\ -4.2980 & -3.9139 \\ 5.9112 & 2.5031 \\ -3.3507 & 2.1924 \\ -3.4569 & -0.3461 \end{bmatrix}^{\top}; \quad \hat{D}_{xz} = \begin{bmatrix} 0 & 0 \\ 0 & 0 \end{bmatrix};$$

The eigenvalue is given as

$$\text{eig}(\hat{A}_{xz}) = \begin{bmatrix} -3.2756 \pm 4.7399j \\ -2.3340 \pm 3.8535j \\ -0.0867 \pm 0.4146j \\ -0.1258 \pm 0.0773j \end{bmatrix} \times 10^2$$

Table 5.11: Model configuration - 4in4out MB data

Symbol	Description	Value
p	Laguarre parameter	640
i	Expanding observability matrix	10
n	Model order	8
Δt	Sampling time	0.002
N	Number of sampled data	1000
Ns	Number of step response data	300

Example 3 - 4 in 4 out MB data

The four inputs four outputs MB systems are defined by the following configuration

$$\begin{bmatrix} y_{xL}(t) \\ y_{xR}(t) \\ y_{yL}(t) \\ y_{yR}(t) \end{bmatrix} = \begin{bmatrix} G_{11} & G_{12} & G_{13} & G_{14} \\ G_{21} & G_{22} & G_{23} & G_{24} \\ G_{31} & G_{32} & G_{33} & G_{34} \\ G_{41} & G_{42} & G_{43} & G_{44} \end{bmatrix} \begin{bmatrix} u_{xL}(t) \\ u_{xR}(t) \\ u_{yL}(t) \\ u_{yR}(t) \end{bmatrix}$$

The parameter used in developing the model can be referred as in Table 5.11. The step responses of the continuous time models are compared to their respective response as in Figure (5.12). For the four inputs four outputs systems, it shows that the subspace model is still able to identify the system closely. The VAF percentage and MSE calculation can be referred in Table 5.12. From this multi-variable identification results, in which the model has been developed to identify for up to four inputs and outputs signals, represent the strong contribution of the first stage identification in diminishing the noise effects that occurred in the data systems. Thus, the subspace identification is able to develop a state-space model with high chances of good performance and excellent accuracy.

Table 5.12: VAF & MSE - 4in4out MB data

Description	y_{xL}	y_{xR}	y_{yL}	y_{yR}
VAF	93.8496%	97.9419%	93.1036%	87.3999%
MSE	0.0153	0.0178	0.0304	0.0389

The estimated (A, B, C, D) system matrices are given as

$$\hat{A} = \begin{bmatrix} -1.6882 & 1.2788 & -2.5298 & 18.0770 & -21.5398 & 33.6565 & 22.0558 & -114.5656 \\ -19.7703 & -26.0653 & -200.5672 & 145.5981 & -61.1684 & 106.7317 & -93.1105 & -2.1850 \\ -3.1778 & 1.5481 & -316.2057 & 674.6397 & -271.4468 & 420.5493 & -264.7590 & 79.9086 \\ 1.6769 & 1.7037 & -151.5716 & -199.2238 & 143.7993 & -260.4409 & 217.4410 & -41.3422 \\ 2.6859 & 5.7584 & 108.5820 & -2.8537 & -44.7762 & 48.4710 & -67.6132 & 99.5774 \\ -1.3526 & -4.0713 & -119.3756 & 2.7179 & 53.6197 & -140.4750 & -146.5774 & -139.0323 \\ -0.4252 & 1.7930 & 52.1407 & -2.6976 & -12.0736 & 2.8736 & -240.0895 & -272.2605 \\ -1.8397 & -3.8484 & -16.1018 & 14.9791 & 1.4585 & 103.1877 & 249.9907 & -249.1268 \end{bmatrix};$$

$$\hat{B} = \begin{bmatrix} -50.5297 & -50.5297 & -50.5297 & -50.5297 \\ -12.8267 & -12.8267 & -12.8267 & -12.8267 \\ -11.3887 & -11.3887 & -11.3887 & -11.3887 \\ 21.5039 & 21.5039 & 21.5039 & 21.5039 \\ 38.6656 & 38.6656 & 38.6656 & 38.6656 \\ -81.6739 & -81.6739 & -81.6739 & -81.6739 \\ -156.9741 & -156.9741 & -156.9741 & -156.9741 \\ -90.0863 & -90.0863 & -90.0863 & -90.0863 \end{bmatrix};$$

$$\hat{C} = \begin{bmatrix} -0.6116 & -0.5839 & 0.8383 & 2.4955 & 3.9557 & -0.0529 & 0.9094 & 0.7470 \\ -2.0006 & -2.4017 & 1.2398 & 2.0675 & -0.7498 & -1.4914 & 1.6280 & -0.3750 \\ 5.2039 & -1.7414 & 0.6871 & 1.3952 & -0.5589 & -0.5394 & 0.6183 & -2.2174 \\ 0.9092 & -1.3441 & 1.1632 & 2.9194 & -1.2504 & -3.7543 & 3.2109 & -1.5084 \end{bmatrix};$$

$$\hat{D} = \begin{bmatrix} 0 & 0 & 0 & 0 \\ 0 & 0 & 0 & 0 \\ 0 & 0 & 0 & 0 \\ 0 & 0 & 0 & 0 \end{bmatrix};$$

The eigenvalue is given by

$$\text{eig}(\hat{A}) = \begin{bmatrix} -3.2678 \pm 4.7439j \\ -2.5695 \pm 2.9351j \\ -0.2075 \pm 0.2615j \\ -0.0165 \\ -0.0704 \end{bmatrix} \times 10^2$$

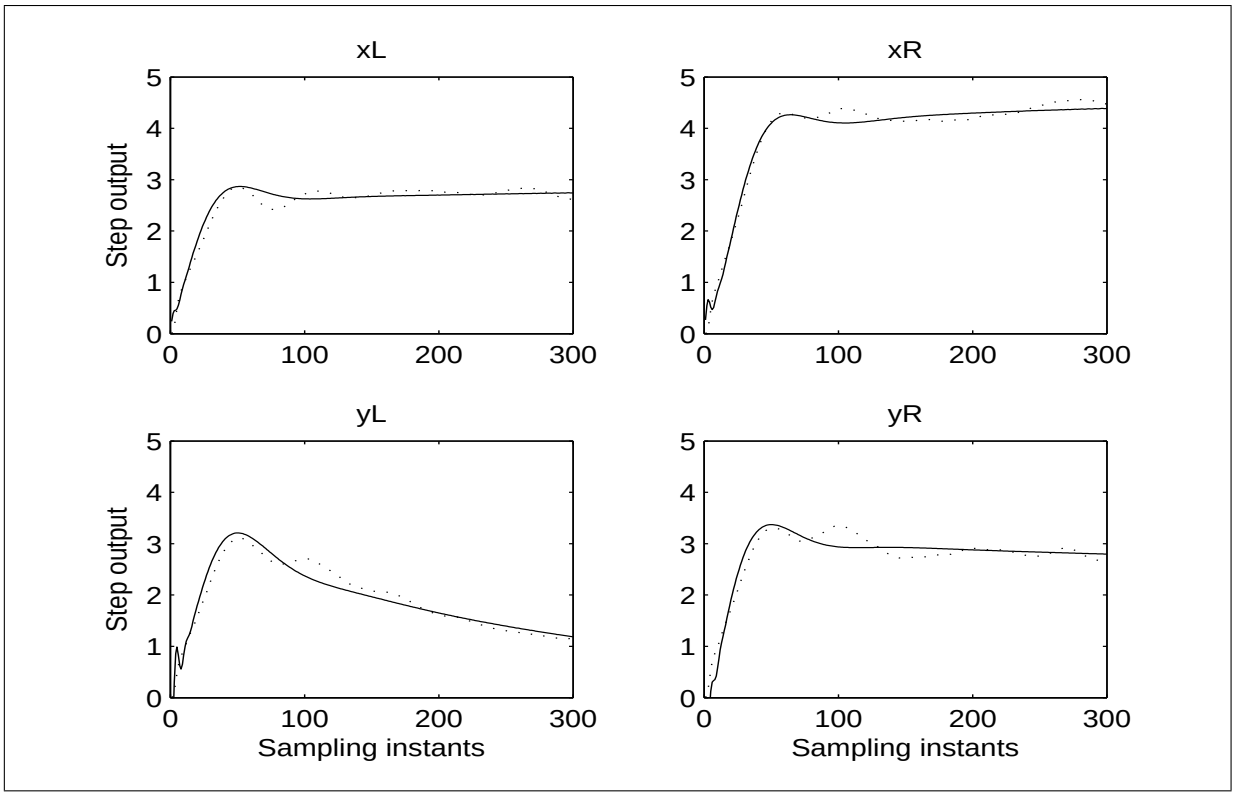

Figure 5.12: System (dotted) & model (solid) step response - 4in4out MB data

5.6 Summary

In this chapter the 2-stage system identification is performed. The first stage includes a process of compressing the data and perform a non-parametric identification of the system step response by using the FSF filters approach. The second stage involves a parametric model fitting of the identified step response by using the subspace methods. The contribution of this research is to combine these two approaches in a novel way and perform the indirect continuous time identification method. This method has been evaluated on identifying a simulated data system and an experimental data system from magnetic bearing apparatus. The performance results based on SISO and multi-variable systems have shown that this proposed identification method is capable of identifying the systems closely. The role play by the first stage identification has contributed to huge improvement in diminishing the noise that appear in the system. By running the first stage identification as well, the closed-loop data can next be treated using open-loop subspace identification method in which the problem of biased estimation (if direct identification is applied) is finally solved.

Chapter 6

Continuous Time Identification using Frequency Response Data

6.1 Introduction

This chapter discusses on continuous time state space model identification using subspace approach with respect to frequency response data. Subspace-based identification methods in the frequency domain have been proposed by McKelvey and colleagues in [107, 109], in addition to the work by De Moor and Vandewalle [120], and Liu et.al [97]. In McKelvey et al. [109], a bilinear transformation was used in deriving a continuous time state-space model of the form $\frac{s-1}{s+1}$. In Haverkamp et al. [59], a Laguerre network was proposed in subspace continuous time system identification whereby the scaling factor in the Laguerre network plays a role in the model estimation. This work was further extended by Yang [188] to subspace continuous time using frequency response data.

The strategy of implementing the subspace methods with additional $w-$operator has improved system performance and stability, as well as providing better conditioning in regards to all the data matrices employed in the identification algorithm. In addition, the instrumental variable method is adopted to the algorithm with the goal to cope with measurement noise. It has shown a successful result in identifying a single input single output system based on frequency response data. In this chapter, the proposed algorithm by Yang [188] is further extended for

multi-input-multi-output systems. Perhaps the subspace frequency response approach is not new in terms of methodology. However, the use of the subspace method with additional operator and strategy to identify the continuous time state-space model of MIMO magnetic bearing system will demonstrate another new real application for the methodology of subspace frequency response methods.

This chapter is an expandable and detail elaborated version of two published papers by the author in [115, 119]. The Chapter starts with the subspace identification approach in frequency domain form. In Section 6.2 the $w-$operator method, instrumental variable method and other approaches are explained. As the aim here is to apply the subspace identification approach to the MB systems, therefore Section 6.3 demonstrates on how to obtain frequency response estimates using FSF filters. This procedure is necessary in order to perform unbiased estimation to the closed-loop MB data. To evaluate the performance capability of the proposed identification algorithm, an analysis on SISO and MIMO data system is presented in Section 6.4. The performance is measured by identifying the models using two sets of data: Noise-added data and a real data from MB systems. Finally, Section 6.5 concludes the chapter.

6.2 Subspace Identification Approach in Frequency Domain

Consider the state-space model of the continuous time system in the Laplace domain

$$\begin{aligned} sX(s) &= AX(s) + BU(s) \\ Y(s) &= CX(s) + DU(s) \end{aligned} \tag{6.1}$$

where $U(s) \in R^m$, $Y(s) \in R^l$, $X(s) \in R^n$ are the Laplace transforms of the system inputs, outputs and state variables respectively, and $A \in R^{n\times n}$, $B \in R^{n\times m}$, $C \in R^{l\times n}$ and $D \in R^{l\times m}$ are the system matrices. The transfer function can be expressed as

$$G(s) = C(sI_n - A)^{-1}B + D \tag{6.2}$$

Define $U(s) = I_m$ (as I_m denotes $m \times m$ identity matrix), Equation (6.1) can be rewritten as

$$\begin{aligned} s\hat{X}(s) &= A\hat{X}(s) + BI_m \\ G(s) &= C\hat{X}(s) + DI_m \end{aligned} \tag{6.3}$$

where $\hat{X}(s)$ is an $n \times m$ matrix in which the k-th column corresponds to the state variable when the k-th impulse input is activated. For a single input and single output system with the input signal being a unit impulse, therefore $U(s) = I_m = 1$. Traditionally, the N frequency response samples are measured at frequencies $\omega_k (k = 1, \ldots, N)$ for each individual element giving the frequency response data matrices

$$G_m(j\omega_k) = G(j\omega_k) + V(j\omega_k), \quad k = 1, \ldots, N \tag{6.4}$$

where $V(j\omega_k)$ is a stochastic noise of zero mean.

6.2.1 w-operator and Laguerre filters

In similarity with the continuous time system identification using time domain data, the Laguerre filters will be adopted again in the frequency response system identification. Thus, define again the $w-$operator corresponds to the all-pass filter as

$$w(s) = \frac{s-p}{s+p} \tag{6.5}$$

where

$$\begin{aligned} w &= \frac{s-p}{s+p} \\ w(s+p) &= s-p \\ ws + wp &= s-p \\ ws - s &= -p - wp \\ -s(1-w) &= -p(1+w) \\ s &= p\frac{1+w}{1-w} \end{aligned}$$

The notation of Laguerre filters in the form of $w-$operator is given by

$$L_\sigma(s) = w_0(s) w_\sigma(s), \qquad (\sigma = 1, \ldots, i-1) \tag{6.6}$$

where

$$w_0 = \frac{\sqrt{2p}}{s+p}$$

$p > 0$ is a design parameter to ensure that the filters are stable. With the all-pass filter described by Equation (6.5), a bank of Laguerre filters can be generated by multiplying the first order

of Laguerre filter repetitively with the all-pass filter. In the frequency domain, the w-operator with respect to the Laguerre filter bank can be expressed as

$$w_\sigma(j\omega) = \sqrt{2p}\frac{(j\omega - p)^\sigma}{(j\omega + p)^{\sigma+1}}, \qquad (\sigma = 0, 1, \ldots, i-1) \tag{6.7}$$

With $w-$operator been described as in Equation (6.5), now, substitute s with $p\frac{1+w}{1-w}$ in the state equation of (6.3) gives

$$\begin{aligned}
p\frac{1+w}{1-w}\hat{X}(s) &= A\hat{X}(s) + BI_m \\
p(1+w)\hat{X}(s) &= A(1-w)\hat{X}(s) + B(1-w)I_m \\
p\hat{X}(s) + pw\hat{X}(s) &= A\hat{X}(s) - Aw\hat{X}(s) + B(1-w)I_m \\
pw\hat{X}(s) + Aw\hat{X}(s) &= A\hat{X}(s) - p\hat{X}(s) + B(1-w)I_m \\
w(A + pI_n)\hat{X}(s) &= (A - pI_n)\hat{X}(s) + B(1-w)I_m \\
w\hat{X}(s) &= (A + pI_n)^{-1}(A - pI_n)\hat{X}(s) + (A + pI_n)^{-1}B(1-w)I_m
\end{aligned}$$

Using Equation (6.5),

$$\begin{aligned}
1 - w &= 1 - \left(\frac{s-p}{s+p}\right) \\
&= \frac{s+p-s+p}{s+p} \\
&= \frac{2p}{s+p}
\end{aligned}$$

Substituting $w_0 = \frac{\sqrt{2p}}{s+p}$ into the solution gives

$$\begin{aligned}
1 - w &= \frac{2p}{s+p} \\
&= \frac{2p}{\frac{\sqrt{2p}}{w_0}} \\
&= \sqrt{2p}w_0
\end{aligned}$$

Therefore now the state equation becomes

$$\begin{aligned}
w\hat{X}(s) &= (A + pI_n)^{-1}(A - pI_n)\hat{X}(s) + \sqrt{2p}(A + pI_n)^{-1}Bw_0I_m \\
w\hat{X}(s) &= A_w\hat{X}(s) + B_ww_0I_m
\end{aligned}$$

Thus, the A_w and B_w are obtained as

$$\begin{aligned}
A_w &= (A + pI_n)^{-1}(A - pI_n) \\
B_w &= \sqrt{2p}(A + pI_n)^{-1}B
\end{aligned}$$

Then, solve the output of state equation (6.3) as

$$\begin{aligned}
(1-w)G_m(s) &= C(1-w)\hat{X}(s) + D(1-w)I_m + (1-w)V(s) \\
&= C\hat{X}(s) - Cw\hat{X}(s) + D(1-w)I_m + (1-w)V(s) \\
&= C\hat{X}(s) - C[A_w\hat{X}(s) + B_w w_0 I_m] + D(1-w)I_m + (1-w)V(s) \\
&= C\hat{X}(s) - CA_w\hat{X}(s) - CB_w w_0 I_m + D(1-w)I_m + (1-w)V(s) \\
\sqrt{2p}w_0 G_m(s) &= C\hat{X}(s) - CA_w\hat{X}(s) - CB_w w_0 I_m + \sqrt{2p}Dw_0 I_m + \sqrt{2p}w_0 V(s) \\
&= (C - CA_w)\hat{X}(s) + (\sqrt{2p}D - CB_w)w_0 I_m + \sqrt{2p}w_0 V(s) \\
w_0 G_m(s) &= \frac{1}{\sqrt{2p}}(C - CA_w)\hat{X}(s) + \frac{1}{\sqrt{2p}}(\sqrt{2p}D - CB_w)w_0 I_m + w_0 V(s) \\
&= C_w\hat{X}(s) + D_w w_0 I_m + w_0 V(s)
\end{aligned}$$

which results in

$$\begin{aligned}
C_w &= \frac{1}{\sqrt{2p}}(C - CA_w) \\
&= \frac{1}{\sqrt{2p}}(C - C(A + pI_n)^{-1}(A - pI_n)) \\
&= \frac{1}{\sqrt{2p}}(C(A + pI_n)^{-1}(A + pI_n) - C(A + pI_n)^{-1}(A - pI_n)) \\
&= \frac{1}{\sqrt{2p}}(2pC(A + pI_n)^{-1}) \\
&= \sqrt{2p}C(A + pI_n)^{-1}
\end{aligned}$$

and,

$$\begin{aligned}
D_w &= \frac{1}{\sqrt{2p}}(\sqrt{2p}D - CB_w) \\
&= \frac{1}{\sqrt{2p}}(\sqrt{2p}D - C\sqrt{2p}(A + pI_n)^{-1}B) \\
&= D - C(A + pI_n)^{-1}B
\end{aligned}$$

The corresponding state-space models therefore can be transformed into the following form

$$w\hat{X}(s) = A_w\hat{X}(s) + B_w w_0 I_m \tag{6.8}$$

$$w_0 G_m(s) = C_w\hat{X}(s) + D_w w_0 I_m + w_0 V(s) \tag{6.9}$$

where

$$\begin{aligned}
A_w &= (A + pI_n)^{-1}(A - pI_n) \\
B_w &= \sqrt{2p}(A + pI_n)^{-1}B \\
C_w &= \sqrt{2p}C(A + pI_n)^{-1} \\
D_w &= D - C(A + pI_n)^{-1}B
\end{aligned} \tag{6.10}$$

and

$$\begin{aligned} A &= p(I_n - A_w)^{-1}(I_n + A_w) \\ B &= \sqrt{2p}(I_n - A_w)^{-1}B_w \\ C &= \sqrt{2p}C_w(I_n - A_w)^{-1} \\ D &= D_w + C_w(I_n - A_w)^{-1}B_w \end{aligned} \tag{6.11}$$

In frequency domain, Equation (6.8-6.9) with the $w-$operator model can be expressed as

$$\begin{aligned} w(j\omega)\hat{X}_w(j\omega) &= A_w\hat{X}_w(j\omega) + B_w w_0(j\omega)I_m \\ w_0(j\omega)G_m(j\omega) &= C_w\hat{X}_w(j\omega) + D_w w_0(j\omega)I_m + w_0(j\omega)V(j\omega) \end{aligned} \tag{6.12}$$

6.2.2 Constructing Data Matrices

Based on the model description given in Equation (6.12), data equations are constructed as

$$\begin{aligned} w_0(j\omega)G_m(j\omega) &= C_w\hat{X}_w(j\omega) + D_w w_0(j\omega)I_m + w_0(j\omega)V(j\omega) \\ w_0(j\omega)w(j\omega)G_m(j\omega) &= C_w w(j\omega)\hat{X}_w(j\omega) + D_w w_0(j\omega)w(j\omega)I_m + w_0(j\omega)w(j\omega)V(j\omega) \\ &= C_w[A_w\hat{X}_w(j\omega) + B_w w_0(j\omega)I_m] + D_w w_0(j\omega)w(j\omega)I_m \\ &\quad + w_0(j\omega)w(j\omega)V(j\omega) \\ &= C_w A_w\hat{X}_w(j\omega) + C_w B_w w_0(j\omega)I_m + D_w w_0(j\omega)w(j\omega)I_m \\ &\quad + w_0(j\omega)w(j\omega)V(j\omega) \\ w_0(j\omega)w^2(j\omega)G_m(j\omega) &= C_w A_w w(j\omega)\hat{X}_w(j\omega) + C_w B_w w_0(j\omega)w(j\omega)I_m \\ &\quad + D_w w_0(j\omega)w^2(j\omega)I_m + w_0(j\omega)w^2(j\omega)V(j\omega) \\ &= C_w A_w[A_w\hat{X}_w(j\omega) + B_w w_0(j\omega)I_m] + C_w B_w w_0(j\omega)w(j\omega)I_m \\ &\quad + D_w w_0(j\omega)w^2(j\omega)I_m + w_0(j\omega)w^2(j\omega)V(j\omega) \\ &= C_w A_w^2(j\omega)\hat{X}_w(j\omega) + C_w A_w B_w w_0(j\omega)I_m \\ &\quad + C_w B_w w_0(j\omega)w(j\omega)I_m + D_w w_0(j\omega)w^2(j\omega)I_m \\ &\quad + w_0(j\omega)w^2(j\omega)V(j\omega) \end{aligned}$$

By repetitively multiplying with w, the impulse response is related to the measured frequency response as follows

$$\begin{bmatrix} w_0(j\omega)G_m^f(j\omega) \\ w_1(j\omega)G_m^f(j\omega) \\ w_2(j\omega)G_m^f(j\omega) \\ \vdots \\ w_{i-1}(j\omega)G_m^f(j\omega) \end{bmatrix} = \mathcal{O}_i\hat{X}_w(j\omega) + \Gamma_i \begin{bmatrix} w_0(j\omega)I_m \\ w_1(j\omega)I_m \\ w_2(j\omega)I_m \\ \vdots \\ w_{i-1}(j\omega)I_m \end{bmatrix} + \begin{bmatrix} w_0(j\omega)V^f(j\omega) \\ w_1(j\omega)V^f(j\omega) \\ w_2(j\omega)V^f(j\omega) \\ \vdots \\ w_{i-1}(j\omega)V^f(j\omega) \end{bmatrix} \tag{6.13}$$

where the extended observability matrix, $\mathcal{O}_i$ is defined as

$$\mathcal{O}_i = \begin{bmatrix} C_w \\ C_wA_w \\ C_wA_w^2 \\ \vdots \\ C_wA_w^{i-1} \end{bmatrix} \tag{6.14}$$

And the Toeplitz matrix, Γ_i is defined as

$$\Gamma_i = \begin{bmatrix} D_w & 0 & 0 & \dots & 0 \\ C_wB_w & D_w & 0 & \dots & 0 \\ C_wA_wB_w & C_wB_w & D_w & \dots & 0 \\ \vdots & \ddots & \ddots & \ddots & \vdots \\ C_wA_w^{i-2}B_w & \dots & C_wA_wB_w & C_wB_w & D_w \end{bmatrix} \tag{6.15}$$

and i is the number of term for the observability matrix. Given frequency response data at $\omega_k(k = 1, \dots, N)$, expanding the row matrix will produce the extended model formulation as

$$G_{i,N}^f = \mathcal{O}_i\hat{X}_{wN} + \Gamma_i\Omega_{i,N}^f + V_{i,N}^f \tag{6.16}$$

where

$$G_{i,N}^f = \begin{bmatrix} w_0(j\omega_1)G_m^f(j\omega_1) & \dots & w_0(j\omega_N)G_m^f(j\omega_N) \\ w_1(j\omega_1)G_m^f(j\omega_1) & \dots & w_1(j\omega_N)G_m^f(j\omega_N) \\ w_2(j\omega_1)G_m^f(j\omega_1) & \dots & w_2(j\omega_N)G_m^f(j\omega_N) \\ \vdots & \vdots & \vdots \\ w_{i-1}(j\omega_1)G_m^f(j\omega_1) & \dots & w_{i-1}(j\omega_N)G_m^f(j\omega_N) \end{bmatrix} \tag{6.17}$$

$$\hat{X}_{wN} = \begin{bmatrix} \hat{X}_w(j\omega_1) & \hat{X}_w(j\omega_2) & \dots & \hat{X}_w(j\omega_N) \end{bmatrix} \tag{6.18}$$

$$\Omega_{i,N}^{f} = \begin{bmatrix} w_0(j\omega_1)I_m & \dots & w_0(j\omega_N)I_m \\ w_1(j\omega_1)I_m & \dots & w_1(j\omega_N)I_m \\ w_2(j\omega_1)I_m & \dots & w_2(j\omega_N)I_m \\ \vdots & \vdots & \vdots \\ w_{i-1}(j\omega_1)I_m & \dots & w_{i-1}(j\omega_N)I_m \end{bmatrix} \tag{6.19}$$

$$V_{i,N}^{f} = \begin{bmatrix} w_0(j\omega_1)V^f(j\omega_1) & \dots & w_0(j\omega_N)V^f(j\omega_N) \\ w_1(j\omega_1)V^f(j\omega_1) & \dots & w_1(j\omega_N)V^f(j\omega_N) \\ w_2(j\omega_1)V^f(j\omega_1) & \dots & w_2(j\omega_N)V^f(j\omega_N) \\ \vdots & \vdots & \vdots \\ w_{i-1}(j\omega_1)V^f(j\omega_1) & \dots & w_{i-1}(j\omega_N)V^f(j\omega_N) \end{bmatrix} \tag{6.20}$$

6.2.3 State-space Model Identification

Consider now a problem to estimate the system matrices A, B, C and D in the state-space model. With the assumption that the state-space representation is a minimal realization, the transfer function and state-space model of the system defined in the form of $w-$operator as

$$G_w(w) = C_w(wI_n - A_w)^{-1}B_w + D_w \tag{6.21}$$

$$wx_w(t) = A_w x_w(t) + B_w u(t) \tag{6.22}$$

$$y(t) = C_w x_w(t) + D_w u(t) \tag{6.23}$$

The identification algorithm is therefore developed to consistently estimate:

- The system order, n.
- The extended observability matrix, $\mathcal{O}_i$ based on the availability of a transfer function data, $G_m(j\omega)$.
- The A_w and C_w matrices from the extended observability matrix, $\mathcal{O}_i$.

$$\mathcal{O}_i = \begin{bmatrix} C_w \\ C_w A_w \\ \vdots \\ C_w A_w^{i-1} \end{bmatrix}$$

- The matrices B_w and D_w with the knowledge of A_w and C_w using a least squares solution from

$$G_m(\ j\omega \ \Big|\ B_w, D_w\ ) = C_w(w(j\omega)I_n - A_w)^{-1}B_wI_m + D_wI_m$$

- The A, B, C and D matrices from A_w, B_w, C_w and D_w.

Refer back to the Equation (6.16) of

$$G^f_{i,N} = \mathcal{O}_i\hat{X}_{wN} + \Gamma_i\Omega^f_{i,N} + V^f_{i,N}$$

The next step is to isolate the $\mathcal{O}_i$ term using known data structures. Before doing so, the data equation notation is simplified for easier recognition and is defined as

$$\mathbf{G} = \mathcal{O}_i\mathbf{X} + \Gamma_i\mathbf{\Omega} + \mathbf{V} \tag{6.24}$$

The second term on the right-hand side can be removed by introducing a projection on the null space of $\mathbf{\Omega}$ which is defined as

$$\Pi^{\perp}_{\mathbf{\Omega}^\top} = I - \mathbf{\Omega}^\top(\mathbf{\Omega}\mathbf{\Omega}^\top)^{-1}\mathbf{\Omega} \tag{6.25}$$

where I is the identity matrix. If $\mathbf{\Omega}\mathbf{\Omega}^\top$ is singular, then the Moore-Penrose pseudo-inverse of $\mathbf{\Omega}^\top$ (denotes as $(\mathbf{\Omega}^\top)^\dagger$) can be taken. Mathematically, it is equivalent to

$$\Upsilon^\dagger = (\Upsilon^\top\Upsilon)^{-1}\Upsilon^\top$$

The pseudo-inverse is computed recursively using singular value decomposition (SVD) describes as [53]

$$\Upsilon = USV^\top$$
$$\Upsilon^\dagger = VS^\dagger U^\top$$

Therefore equation (6.25) can be written as

$$\Pi^{\perp}_{\mathbf{\Omega}^\top} = I - \mathbf{\Omega}^\top(\mathbf{\Omega}^\top)^\dagger$$

Multiply this projection on $\mathbf{\Omega}$ gives

$$\begin{aligned}\mathbf{\Omega}\Pi^{\perp}_{\mathbf{\Omega}^\top} &= \mathbf{\Omega} - (\mathbf{\Omega}\mathbf{\Omega}^\top(\mathbf{\Omega}\mathbf{\Omega}^\top)^{-1})\mathbf{\Omega}\\ &= \mathbf{\Omega} - I\mathbf{\Omega}\\ &= 0\end{aligned}$$

Thus, by multiplying Equation (6.25) to both side of Equation (6.24), the term Γ_i will be removed as $\mathbf{\Omega}\Pi^{\perp}_{\mathbf{\Omega}^\top} = 0$. Therefore, the data equation reduces to

$$\mathbf{G}\Pi^{\perp}_{\mathbf{\Omega}^\top} = \mathcal{O}_i\mathbf{X}\Pi^{\perp}_{\mathbf{\Omega}^\top} + \mathbf{V}\Pi^{\perp}_{\mathbf{\Omega}^\top} \tag{6.26}$$

For a general case where noise effect to the system can be omitted ($\mathbf{V} = 0$), the data equation of (6.26) is reduced to

$$\mathbf{G}\Pi^{\perp}_{\mathbf{\Omega}^\top} = \mathcal{O}_i\mathbf{X}\Pi^{\perp}_{\mathbf{\Omega}^\top} \tag{6.27}$$

From the above equation, the identification goes as according to MOESP method that can be referred in [172, 175]. However, in many practical systems, the effect of noise either from measurement or process noise is somehow unavoidable. Therefore, a new mechanism needs to be implemented or improved as to overcome those disturbances.

6.2.4 Instrumental Variable Method

The instrumental variable method is used here to handle the measurement noise that may exist in the system. Defining instrumental variable matrix as $P(j\omega)$, Equation (6.16) can be rewritten as

$$\frac{1}{N}G^f_{i,N}(P^f_{\beta,N})^\top = \frac{1}{N}\mathcal{O}_i\hat{X}_{wN}(P^f_{\beta,N})^\top + \frac{1}{N}\Gamma_i\Omega^f_{i,N}(P^f_{\beta,N})^\top + \frac{1}{N}V^f_{i,N}(P^f_{\beta,N})^\top \tag{6.28}$$

where

$$P^f_{\beta,N} = \begin{bmatrix} w^i(j\omega_1)I_m & \dots & w^i(j\omega_N)I_m \\ w^{i+1}(j\omega_1)I_m & \dots & w^{i+1}(j\omega_N)I_m \\ w^{i+2}(j\omega_1)I_m & \dots & w^{i+2}(j\omega_N)I_m \\ \vdots & \vdots & \vdots \\ w^{i+\beta-1}(j\omega_1)I_m & \dots & w^{i+\beta-1}(j\omega_N)I_m \end{bmatrix} \tag{6.29}$$

Again, multiplying the projection matrix, $\Pi^{\perp}_{\Omega^\top}$ to Equation (6.28) will give the following expression

$$\frac{1}{N}G^f_{i,N}\Pi^{\perp}_{\Omega^\top}(P^f_{\beta,N})^\top = \frac{1}{N}\mathcal{O}_i\hat{X}^f_{wN}\Pi^{\perp}_{\Omega^\top}(P^f_{\beta,N})^\top \tag{6.30}$$

And it can give consistent estimation if it satisfies the following conditions

$$\lim_{N\to\infty}\frac{1}{N}V^f_{i,N}\Pi^{\perp}_{\Omega^\top}(P^f_{\beta,N})^\top = 0 \tag{6.31}$$

$$\operatorname{rank}(\lim_{N\to\infty}\frac{1}{N}\mathcal{O}_i\hat{X}_{wN}\Pi^{\perp}_{\Omega^\top}(P^f_{\beta,N})^\top) = n \tag{6.32}$$

Up to this far, the formulation can now be used to model the systems. Nevertheless, the algorithm can also be implemented by performing the *linear quadratic* (LQ) factorization and *singular value decomposition* (SVD) to the working matrices. Here, the *recursive quadratic* (RQ) factorization using the modified Gram-Schmidt algorithm is used.

6.2.5 Identification Algorithm

Let $w_i(j\omega)$ be an operator developed from Laguerre filters ($p > 0$). Let $G_m(j\omega)$ be the measured frequency response data described in Equation (6.4). For N frequency response samples measured at frequencies $\omega_k(k = 1, \ldots, N)$, construct $G^f_{i,N}$, $\Omega^f_{i,N}$ and $P^f_{\beta,N}$ according to Equations (6.17), (6.19) and (6.29) respectively.

Consider the RQ factorization

$$\begin{bmatrix} \Omega^f_{i,N} \\ G^f_{i,N} \\ P^f_{\beta,N} \end{bmatrix} = \begin{bmatrix} R_{11} & 0 & 0 \\ R_{21} & R_{22} & 0 \\ R_{31} & R_{32} & R_{33} \end{bmatrix} \begin{bmatrix} Q_1 \\ Q_2 \\ Q_3 \end{bmatrix} \tag{6.33}$$

Then the following holds:

$$\lim_{N\to\infty} \frac{1}{\sqrt{N}} R_{22} R_{32}^\top = \lim_{N\to\infty} \frac{1}{\sqrt{N}} \mathcal{O}_i \hat{X}_{wN} (P^f_{\beta,N})^\top \begin{bmatrix} Q_2 \\ Q_3 \end{bmatrix}^\top \tag{6.34}$$

Proof:

From the RQ factorization of Equation (6.33)*, we have*

$$\lim_{N\to\infty} \frac{1}{\sqrt{N}} R_{22} R_{32}^\top = \lim_{N\to\infty} \frac{1}{\sqrt{N}} G^f_{i,N} (P^f_{\beta,N})^\top \begin{bmatrix} Q_2 \\ Q_3 \end{bmatrix}^\top \tag{6.35}$$

From Equation (6.28) *we have*

$$\begin{aligned} \lim_{N\to\infty} \frac{1}{\sqrt{N}} G^f_{i,N} (P^f_{\beta,N})^\top \begin{bmatrix} Q_2 \\ Q_3 \end{bmatrix}^\top &= \lim_{N\to\infty} \frac{1}{\sqrt{N}} \mathcal{O}_i \hat{X}_{wN} (P^f_{\beta,N})^\top \begin{bmatrix} Q_2 \\ Q_3 \end{bmatrix}^\top \\ &+ \lim_{N\to\infty} \frac{1}{\sqrt{N}} \Gamma_i \Omega^f_{i,N} (P^f_{\beta,N})^\top \begin{bmatrix} Q_2 \\ Q_3 \end{bmatrix}^\top \\ &+ \lim_{N\to\infty} \frac{1}{\sqrt{N}} V^f_{i,N} (P^f_{\beta,N})^\top \begin{bmatrix} Q_2 \\ Q_3 \end{bmatrix}^\top \end{aligned} \tag{6.36}$$

As $\Omega^f_{i,N} = R_{11}Q_1$*, the second term on the right hand side goes to zero as* $Q_1 \begin{bmatrix} Q_2 \\ Q_3 \end{bmatrix}^\top = 0$

$$\lim_{N\to\infty} \frac{1}{\sqrt{N}} \Gamma_i \Omega^f_{i,N} (P^f_{\beta,N})^\top \begin{bmatrix} Q_2 \\ Q_3 \end{bmatrix}^\top = 0$$

Next is to prove that the third term on the right hand side also goes to zero as N *goes to infinity.*

$$\lim_{N\to\infty} \frac{1}{\sqrt{N}} V^f_{i,N} Q_2^\top = 0 \tag{6.37}$$

$$\lim_{N\to\infty} \frac{1}{\sqrt{N}} V^f_{i,N} Q_3^\top = 0 \tag{6.38}$$

Observe the first row of the RQ factorization leads to

$$\begin{aligned} \lim_{N\to\infty} \frac{1}{N} \Omega^f_{i,N} (V^f_{i,N})^\top &= 0 \\ \lim_{N\to\infty} \frac{1}{N} R_{11} Q_1 (V^f_{i,N})^\top &= 0 \\ \lim_{N\to\infty} \frac{1}{\sqrt{N}} Q_1 (V^f_{i,N})^\top &= 0 \end{aligned}$$

in which Equations (6.37) *and* (6.38) *goes to zero as* $Q_1 \begin{bmatrix} Q_2 \\ Q_3 \end{bmatrix}^\top = 0$*. Then, observe the second row of the RQ factorization leads to*

$$\begin{aligned} \lim_{N\to\infty} \frac{1}{N} G^f_{i,N} (V^f_{i,N})^\top &= 0 \\ \lim_{N\to\infty} \frac{1}{N} (R_{21}Q_1 + R_{22}Q_2) (V^f_{i,N})^\top &= 0 \\ \lim_{N\to\infty} \frac{1}{N} R_{22} Q_2 (V^f_{i,N})^\top &= 0 \\ \lim_{N\to\infty} \frac{1}{\sqrt{N}} Q_2 (V^f_{i,N})^\top &= 0 \end{aligned}$$

which is the transpose of Equation (6.37)*. Similarly, observe the third row of the RQ factorization leads to*

$$\begin{aligned} \lim_{N\to\infty} \frac{1}{N} P^f_{\beta,N} (V^f_{i,N})^\top &= 0 \\ \lim_{N\to\infty} \frac{1}{N} (R_{31}Q_1 + R_{32}Q_2 + R_{33}Q_3) (V^f_{i,N})^\top &= 0 \\ \lim_{N\to\infty} \frac{1}{N} R_{33} Q_3 (V^f_{i,N})^\top &= 0 \\ \lim_{N\to\infty} \frac{1}{\sqrt{N}} Q_3 (V^f_{i,N})^\top &= 0 \end{aligned}$$

which is the transpose of Equation (6.38)*. Therefore now Equation* (6.36) *reduces to*

$$\lim_{N\to\infty}\frac{1}{\sqrt{N}}G^f_{i,N}(P^f_{\beta,N})^\top\begin{bmatrix}Q_2\\Q_3\end{bmatrix}^\top=\lim_{N\to\infty}\frac{1}{\sqrt{N}}\mathcal{O}_i\hat{X}_{wN}(P^f_{\beta,N})^\top\begin{bmatrix}Q_2\\Q_3\end{bmatrix}^\top$$

The subspace algorithm with the aid of $w-$operator and instrumental variable used to identify the continuous time systems can be summarized as follows

1. Construct the filtered data matrices of $G^f_{i,N}$, $\Omega^f_{i,N}$ and $P^f_{\beta,N}$ according to Equations (6.17), (6.19) and (6.29) respectively.

2. Divide matrices into real and imaginary part

$$G^f_{i,N}=\begin{bmatrix}\mathbf{Re}(G^f_{i,N}) & \mathbf{Im}(G^f_{i,N})\end{bmatrix}$$
$$\Omega^f_{i,N}=\begin{bmatrix}\mathbf{Re}(\Omega^f_{i,N}) & \mathbf{Im}(\Omega^f_{i,N})\end{bmatrix}$$
$$P^f_{\beta,N}=\begin{bmatrix}\mathbf{Re}(P^f_{\beta,N}) & \mathbf{Im}(P^f_{\beta,N})\end{bmatrix}$$

3. Perform the RQ factorization

$$\begin{bmatrix}\Omega^f_{i,N}\\G^f_{i,N}\\P^f_{\beta,N}\end{bmatrix}=\begin{bmatrix}R_{11}&0&0\\R_{21}&R_{22}&0\\R_{31}&R_{32}&R_{33}\end{bmatrix}\begin{bmatrix}Q_1\\Q_2\\Q_3\end{bmatrix}$$

4. Perform the SVD to the working matrix $R_{22}R_{32}^\top$.

$$R_{22}R_{32}^\top=\begin{bmatrix}U_n & U_0\end{bmatrix}\begin{bmatrix}S_n&0\\0&S_0\end{bmatrix}\begin{bmatrix}V_n\\V_0\end{bmatrix}^\top$$

5. Determine the model order n from the singular value in S.

6. Determine the system matrices (A_w, C_w).

$$
\begin{aligned}
A_w &= (J_1 U_n)^{\dagger} J_2 U_n \\
C_w &= J_3 U_n \\
J_1 &= \begin{bmatrix} I_{(i-1)l} & 0_{(i-1)l \times l} \end{bmatrix} \\
J_2 &= \begin{bmatrix} 0_{(i-1)l \times l} & I_{(i-1)l} \end{bmatrix} \\
J_3 &= \begin{bmatrix} I_{l \times l} & 0_{l \times (i-1)l} \end{bmatrix} \\
\Upsilon^{\dagger} &= (\Upsilon^{\top} \Upsilon)^{-1} \Upsilon^{\top}
\end{aligned}
$$

7. Solve least squares problem to determine (B_w, D_w).

$$
\begin{bmatrix} \mathbf{Re}(Z) \\ \mathbf{Im}(Z) \end{bmatrix} = \begin{bmatrix} \mathbf{Re}(\bar{Z}) \\ \mathbf{Im}(\bar{Z}) \end{bmatrix} \begin{bmatrix} B_w \\ D_w \end{bmatrix}
$$

$$
Z = \begin{bmatrix} G_m(j\omega_1) \\ G_m(j\omega_2 \\ \vdots \\ G_m(j\omega_N) \end{bmatrix}
$$

$$
\bar{Z} = \begin{bmatrix} C_w(w(j\omega_1) I_n - A_w)^{-1} & I_l \\ C_w(w(j\omega_2) I_n - A_w)^{-1} & I_l \\ \vdots & \vdots \\ C_w(w(j\omega_N) I_n - A_w)^{-1} & I_l \end{bmatrix}
$$

8. Reconstruct B_w and D_w from $\begin{bmatrix} B_w \\ D_w \end{bmatrix}$

9. Compute the matrices A, B, C and D.

10. Generate the estimated transfer function.

$$
\hat{G}(s) = C(sI_n - A)^{-1} B + D
$$

6.2.6 Data Arrangement for MIMO Identification

For the single input single output system identification, the data matrices for $G^f_{i,N}$, $\Omega^f_{i,N}$ and $P^f_{\beta,N}$ are constructed in straightforward way according to Equations (6.17), (6.19) and (6.29). However, for the MIMO system, the matrix expansion is arranged as follows. For instance, consider the two-input-two-output system identification, the data matrices of $G^f_{i,N}$, $\Omega^f_{i,N}$ and $P^f_{\beta,N}$ are arranged as

$$G^f_{i,N} = \begin{bmatrix} w_0(j\omega_1)\begin{bmatrix} G^f_{11}(j\omega_1) & G^f_{12}(j\omega_1) \\ G^f_{21}(j\omega_1) & G^f_{22}(j\omega_1) \end{bmatrix} & \dots & w_0(j\omega_N)\begin{bmatrix} G^f_{11}(j\omega_N) & G^f_{12}(j\omega_N) \\ G^f_{21}(j\omega_N) & G^f_{22}(j\omega_N) \end{bmatrix} \\ w_1(j\omega_1)\begin{bmatrix} G^f_{11}(j\omega_1) & G^f_{12}(j\omega_1) \\ G^f_{21}(j\omega_1) & G^f_{22}(j\omega_1) \end{bmatrix} & \dots & w_1(j\omega_N)\begin{bmatrix} G^f_{11}(j\omega_N) & G^f_{12}(j\omega_N) \\ G^f_{21}(j\omega_N) & G^f_{22}(j\omega_N) \end{bmatrix} \\ w_2(j\omega_1)\begin{bmatrix} G^f_{11}(j\omega_1) & G^f_{12}(j\omega_1) \\ G^f_{21}(j\omega_1) & G^f_{22}(j\omega_1) \end{bmatrix} & \dots & w_2(j\omega_N)\begin{bmatrix} G^f_{11}(j\omega_N) & G^f_{12}(j\omega_N) \\ G^f_{21}(j\omega_N) & G^f_{22}(j\omega_N) \end{bmatrix} \\ \vdots & \vdots & \vdots \\ w_{i-1}(j\omega_1)\begin{bmatrix} G^f_{11}(j\omega_1) & G^f_{12}(j\omega_1) \\ G^f_{21}(j\omega_1) & G^f_{22}(j\omega_1) \end{bmatrix} & \dots & w_{i-1}(j\omega_N)\begin{bmatrix} G^f_{11}(j\omega_N) & G^f_{12}(j\omega_N) \\ G^f_{21}(j\omega_N) & G^f_{22}(j\omega_N) \end{bmatrix} \end{bmatrix}$$

$$\Omega^f_{i,N} = \begin{bmatrix} w_0(j\omega_1)I_2 & \dots & w_0(j\omega_N)I_2 \\ w_1(j\omega_1)I_2 & \dots & w_1(j\omega_N)I_2 \\ w_2(j\omega_1)I_2 & \dots & w_2(j\omega_N)I_2 \\ \vdots & \vdots & \vdots \\ w_{i-1}(j\omega_1)I_2 & \dots & w_{i-1}(j\omega_N)I_2 \end{bmatrix}$$

$$P^f_{\beta,N} = \begin{bmatrix} w_i(j\omega_1)I_2 & \dots & w_i(j\omega_N)I_2 \\ w_{i+1}(j\omega_1)I_2 & \dots & w_{i+1}(j\omega_N)I_2 \\ w_{i+2}(j\omega_1)I_2 & \dots & w_{i+2}(j\omega_N)I_2 \\ \vdots & \vdots & \vdots \\ w_{i+\beta-1}(j\omega_1)I_2 & \dots & w_{i+\beta-1}(j\omega_N)I_2 \end{bmatrix}$$

6.3 Frequency Response Estimates

Measured frequency response data come in two forms, either as samples of the transfer function [106]

$$G_k = G_m(j\omega_k), \qquad k = 1, \ldots, N$$

or as samples of the input and output Fourier transforms

$$Y_k = Y_m(j\omega_k), \qquad U_k = U_m(j\omega_k), \qquad k = 1, \ldots, N$$

If the method requires samples of the frequency response, the common way is to form as

$$G_k = \frac{Y_k}{U_k}$$

For the case where the noise level on the input signal is low and can be omitted, the notation as above is still valid. However, if noise disturbance is high, two distinctions must be put into consideration [106].

- If U_k is small or zero, the input signal $u(k)$ contains little or no power at the frequency and the samples should be discarded to reduce the noise influence.
- If the inputs are corrupted by noise of known character, it is favourable to use the input and output samples directly in the identification.

It has been noted that the direct frequency response measurement based on Fast Fourier Transforms (FFT) usually will provide biased measurement of the transfer function for a closed-loop system. In consideration of the noise influence in the closed-loop MB systems, the second distinction will be followed. To overcome biased measurement, the FSF filters approach will be used to process the measured input and output samples and obtained the frequency response estimates.

The FSF approach approximates the transfer function $\bar{G}(z)$ as [49]

$$\bar{G}_{fsf}(z) = \sum_{k=-\frac{n-1}{2}}^{\frac{n-1}{2}} \theta_k \bar{H}_k(z) \tag{6.39}$$

$$\bar{H}_k(z) = \frac{1}{\mathcal{N}} \frac{1 - z^{-\mathcal{N}}}{1 - e^{j\Omega k} z^{-1}} \tag{6.40}$$

where n is odd and the frequency sampling interval $\Omega = \frac{2\pi}{T}$, $\bar{H}_k(z)$ is the kth FSF and θ_k is the corresponding (complex) parameter. For the frequency range of $0 \leq \omega \leq \mathcal{N}\Omega$, choosing $n = \mathcal{N}$ gives an exact match $\bar{G}_{fsf}(z) = \bar{G}(z)$ and choosing $n < \mathcal{N}$ gives an approximate match $\bar{G}_{fsf}(z) \approx \bar{G}(z)$ [179, 180].

The FSF Equation (6.39) can be rewritten in a compact form as [49]

$$\bar{G}_{fsf}(z) = \theta^{\top} \bar{F}(z) \tag{6.41}$$

where

$$\bar{F}(z) = \begin{bmatrix} \bar{H}_0(z) \\ \bar{H}_{-1}(z) \\ \bar{H}_1(z) \\ \vdots \\ \bar{H}_{-\frac{n-1}{2}}(z) \\ \bar{H}_{\frac{n-1}{2}}(z) \end{bmatrix}; \qquad \theta = \begin{bmatrix} \theta_0 \\ \theta_{-1} \\ \theta_1 \\ \vdots \\ \theta_{-\frac{n-1}{2}} \\ \theta_{\frac{n-1}{2}} \end{bmatrix}$$

Although the FSF approach is cast in the discrete time domain and the corresponding $z-$transform domain, the resultant model can be used to obtain frequency responses [180]. Using $z = e^{j\omega\Delta}$, Equation (6.39) and Equation (6.40) can be rewritten in frequency domain form as

$$G(j\omega) \approx G_{fsf}(j\omega) = \sum_{k=-\frac{n-1}{2}}^{\frac{n-1}{2}} \theta_k H_k(j\omega) \tag{6.42}$$

$$H_k(j\omega) = \bar{H}_k(e^{j\omega\Delta}) \qquad \text{for} \qquad \omega < \mathcal{N}\Omega \tag{6.43}$$

6.4 Simulation Results

In this section, the simulation results will be shown in which the magnitude and phase of the estimated response will be compared with the measured response. As a measure of accuracy of the proposed model, the *Variance Accounted For* (VAF), which is given by the following formula

$$\text{VAF} = \left(1 - \frac{\text{VAR}(G_m - \hat{G})}{\text{VAR}(G_m)}\right) \times 100$$

and the *Mean Square Errors* (MSE), which is given by the following formula

$$\text{MSE} = \frac{1}{N}\sum_{a=1}^{N} \mid G_m(j\omega_a) - \hat{G}(j\omega_a) \mid^2$$

is also calculated. The Bode Plot that demonstrate the performance comparison of the systems is further categorized into identification of a simulated data and a real data taken from magnetic bearing system apparatus.

6.4.1 Single Input Single Output Data System

For SISO systems, two different sets of data are observed: a simulated data and a real data taken from magnetic bearing system apparatus.

Simulated Data System

The first data set is a simulated data. The sixth order plant model example presented in [164,188] will be used here. The state space model is developed based on the following set up.

$$A_m = \begin{bmatrix} 0 & 1 & 0 & 0 & 0 & 0 \\ -1 & -0.2 & 0 & 0 & 0 & 0 \\ 0 & 0 & 0 & 1 & 0 & 0 \\ 0 & 0 & -25 & -0.5 & 0 & 0 \\ 0 & 0 & 0 & 0 & 0 & 1 \\ 0 & 0 & 0 & 0 & -9 & -0.12 \end{bmatrix}; \quad B_m = \begin{bmatrix} 0 \\ 1 \\ 0 \\ 1 \\ 0 \\ 1 \end{bmatrix}; \quad C_m = \begin{bmatrix} 1 \\ 0 \\ 1 \\ 0 \\ 1 \\ 0 \end{bmatrix}^\top; \quad D_m = [0];$$

At a frequency of ($\omega = 0.01, 0.02, \ldots, 10$ rad/s), about $N = 1000$ frequency response data is generated according to the following function

$$G_m(j\omega) = C_m(j\omega I_n - A_m)^{-1}B_m + D_m$$

The disturbance is generated according to the following condition

$$V(j\omega_k) = 0.15 \times [e_R(j\omega_k) + je_I(j\omega_k)]$$

where $e_R(j\omega_k)$ and $e_I(j\omega_k)$ are unit variance, zero mean white Gaussian noises. The model is developed using model parameters listed in Table 6.1.

Table 6.1: Model parameter - Simulated data system

Symbol	Description	Value
p	Laguarre parameter	5
i	Expanding observability matrix	30
n	Model order	6

The Bode Plot of magnitude and phase of the measured and estimated systems are shown in Figure (6.1). From this figure, it can be said that the model is able to identify the systems successfully. The verification test gives a value of MSE = 0.0249 and VAF = 95.0997%. Again, this shows that, for a noise added data, the model is still able to identify the system with low MSE and good percentage of accuracy. The transfer function of frequency response estimated from the model is given by

$$G_m(s) = \frac{3s^4 + 1.64s^3 + 70.184s^2 + 14.92s + 259}{s^6 + 0.82s^5 + 35.184s^4 + 14.932s^3 + 260.56s^2 + 52.5s + 225}$$

$$\hat{G}(s) = \frac{2.8781s^4 + 1.8810s^3 + 69.6337s^2 + 16.1777s + 261.7167}{s^6 + 0.7748s^5 + 35.4423s^4 + 14.4575s^3 + 262.8496s^2 + 52.5750s + 226.5904}$$

and the eigenvalues of A matrix is given by

$$\text{eig}(A_m) = [-0.1000 \pm 0.9950j; -0.2500 \pm 4.9937j; -0.0600 \pm 2.9994j]$$

$$\text{eig}(\hat{A}) = [-0.1003 \pm 0.9936j; -0.2307 \pm 5.0242j; -0.0563 \pm 2.9965j]$$

which still shows a good match. The Monte Carlo simulations are also performed based on 100 runs. The choice of different random "seed" specifies the measurement noise adding to the signal. The result from this analysis can be seen in Figure (6.2). From this figure, it shows that with different types of noise, the model is still able to represent the system closely.

The estimated (A, B, C, D) system matrices are given as

$$\hat{A} = \begin{bmatrix} -0.1496 & 1.1008 & 0.1345 & -0.1207 & -0.4572 & -0.3548 \\ -0.9104 & -0.0397 & -0.3402 & 0.1929 & 0.3082 & 0.2919 \\ 0.0570 & 0.1813 & -0.0447 & -2.8925 & 0.2762 & 0.1662 \\ -0.1023 & -0.1015 & 3.0803 & -0.0523 & -0.4894 & -0.2698 \\ 0.0412 & 0.0232 & -0.0701 & 0.0971 & -0.2327 & -5.2924 \\ -0.0409 & -0.0257 & 0.0743 & -0.0413 & 4.7606 & -0.2557 \end{bmatrix}$$

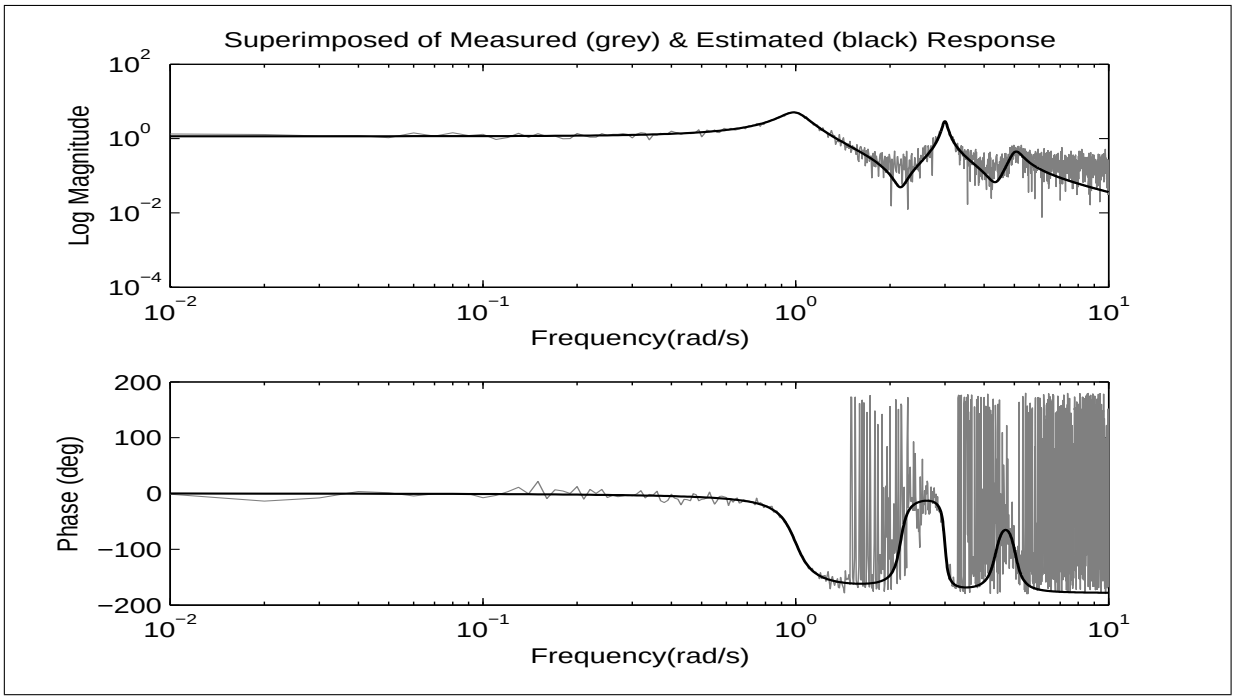

Figure 6.1: Bode plot of magnitude & phase - SISO simulated data system

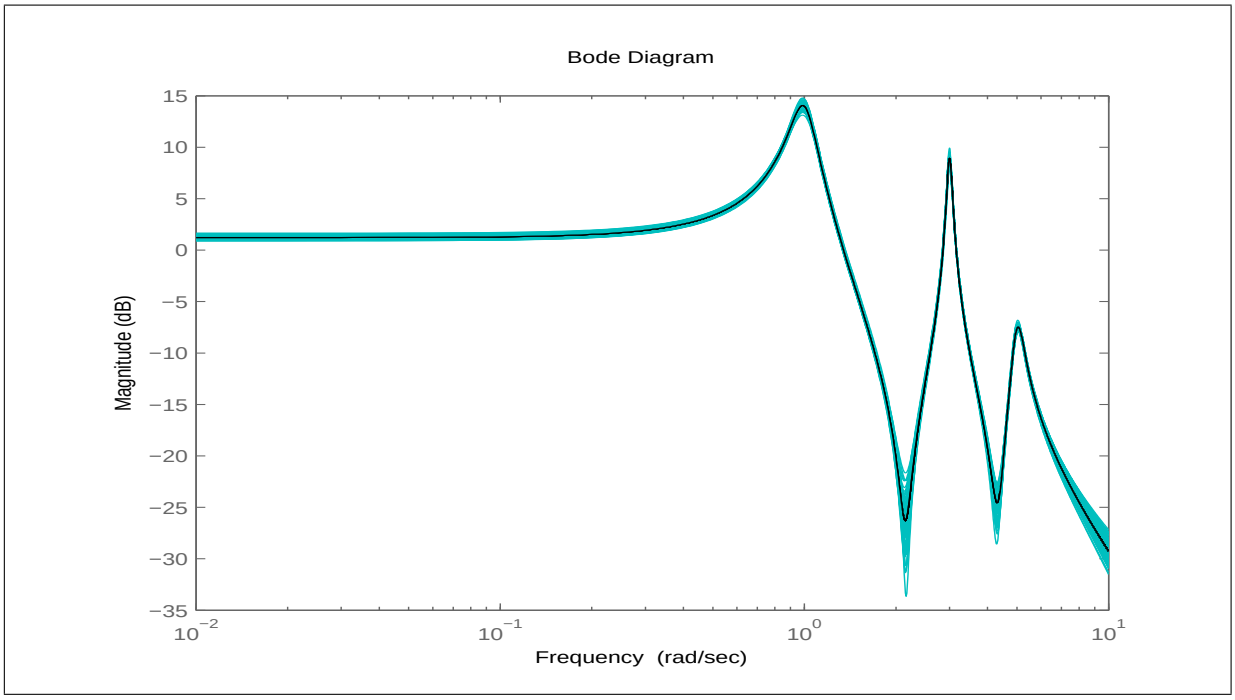

Figure 6.2: Frequency response over 100 runs - SISO simulated data system

$$\hat{B} = \begin{bmatrix} 4.9286 \\ 1.3855 \\ 0.9868 \\ -0.2960 \\ -0.1223 \\ 0.6963 \end{bmatrix}; \quad \hat{C} = \begin{bmatrix} 0.0480 \\ -0.2351 \\ 0.1521 \\ 0.2845 \\ -0.2645 \\ -0.0056 \end{bmatrix}^{\top}; \quad \hat{D} = [-0.0024];$$

Real Data - MB System

The second data set is a real input and output data measured from the MB apparatus. The frequency response estimates of the measured data are obtained using the FSF approach. There are $N = 1000$ samples of input and output is processed at $\Delta t = 0.002s$. The model order, n is determined by the singular value of S after the SVD evaluation. The model parameters can be referred as in Table 6.2.

Table 6.2: Model configuration - MB data system

Symbol	Description	G_{xL}	G_{xR}	G_{yL}	G_{yR}
p	Laguarre parameter	20	20	20	10
i	Expanding observability matrix	40	30	50	40
n	Model order	30	23	29	25

The Bode Plots of magnitude and phase of the measured and estimated systems for data G_{xL} are illustrated in Figure (6.3). The other illustration results for G_{xR}, G_{yL} and G_{yR} transfer function are omitted, however, the MSE and VAF of the systems are calculated and mentioned. Based on the figure, the model is still able to identify the systems successfully. The verification test give a value of

G_{xL}: MSE= 0.0016; VAF= 99.3751%

G_{xR}: MSE= 0.0026; VAF= 99.4044%

G_{yL}: MSE= 0.0035; VAF= 98.9081%

G_{yR}: MSE= 0.0042; VAF= 98.7160%

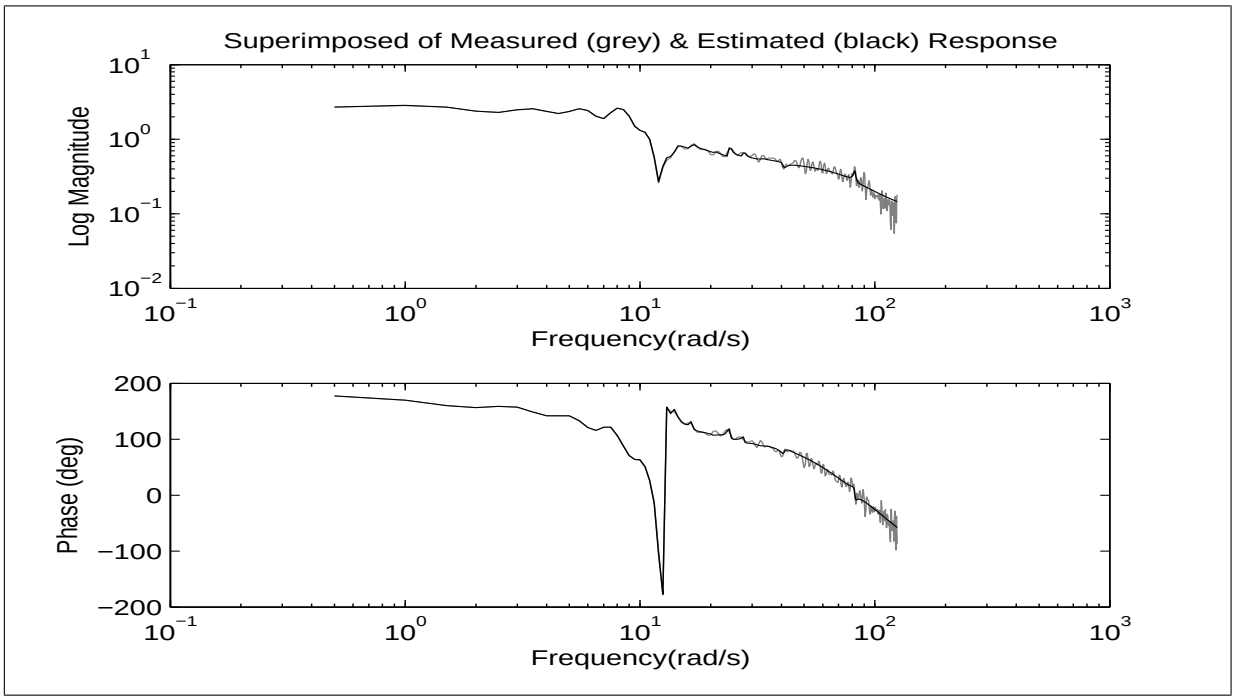

Figure 6.3: Bode plot of magnitude & phase - MB system G_{xL}

Based on the calculations, the model is able to identify the system with low MSE and good percentage of accuracy.

6.4.2 Multi Input Multi Output Data Systems

Next in this section, the model is demonstrated onto MIMO systems. In here, the identification will run for a two-input-two-output systems in which it will provide with 2×2 transfer function.

Table 6.3: Model parameter - MIMO simulated data systems

Symbol	Description	Value
p	Laguarre parameter	5
i	Expanding observability matrix	10
n	Model order	6

The system transfer function is defined as

$$G_m = \begin{bmatrix} \frac{1}{s+1} & \frac{1}{s^2+0.2s+1} \\ \frac{1}{s^2+0.5s+1} & \frac{1}{s+2} \end{bmatrix}$$

At a frequency of $(\omega = 0.01, 0.02, \ldots, 10)$ rad/s, about $N = 1000$ frequency responses are generated using a Matlab function "freqs". The measurement noise is generated according to the following condition

$$V(j\omega_k) = 0.01 * [e_R(j\omega_k) + je_I(j\omega_k)]$$

where $e_R(j\omega_k)$ and $e_I(j\omega_k)$ are unit variance, zero mean white Gaussian noise. The model parameter can be referred in Table 6.3. Figures (6.4) and (6.5) show the superimposed of magnitude and phase for the measured and estimated response respectively. From this figure, it shows that the model can identify the MIMO systems closely. The verification test also give an average value of MSE $= 4.1409 \times 10^{-4}$ and VAF $= 99.6883\%$. This shows that the model is able to identify the system with low MSE and good percentage of accuracy.

The poles location calculated from the system is given by

$$s = [-1; -2; -0.25 \pm 0.9682j; -0.1 \pm j]$$

The poles obtained from the eigenvalues of the A matrix of the model is given by

$$s = [-0.9980; -1.9762; -0.2484 \pm 0.9687j; -0.0994 \pm 0.9950j]$$

which are also almost identical to the actual pole of the systems.

The estimated (A, B, C, D) system matrices are obtained as

$$\hat{A} = \begin{bmatrix} -0.1508 & 0.9361 & -0.7001 & -0.4115 & 1.0675 & -0.8789 \\ -0.7111 & -0.1562 & 0.4927 & -0.4609 & -0.9850 & -0.3591 \\ 0.1652 & -0.3946 & -0.1093 & -1.1094 & -0.1386 & -1.2831 \\ 0.1615 & 0.2215 & 0.6823 & -0.3292 & -0.2203 & -1.6114 \\ 0.0152 & 0.0327 & 0.1738 & -0.2947 & -1.0799 & -0.5432 \\ -0.0749 & -0.0767 & 0.0385 & 0.0432 & -0.2512 & -1.8346 \end{bmatrix}$$

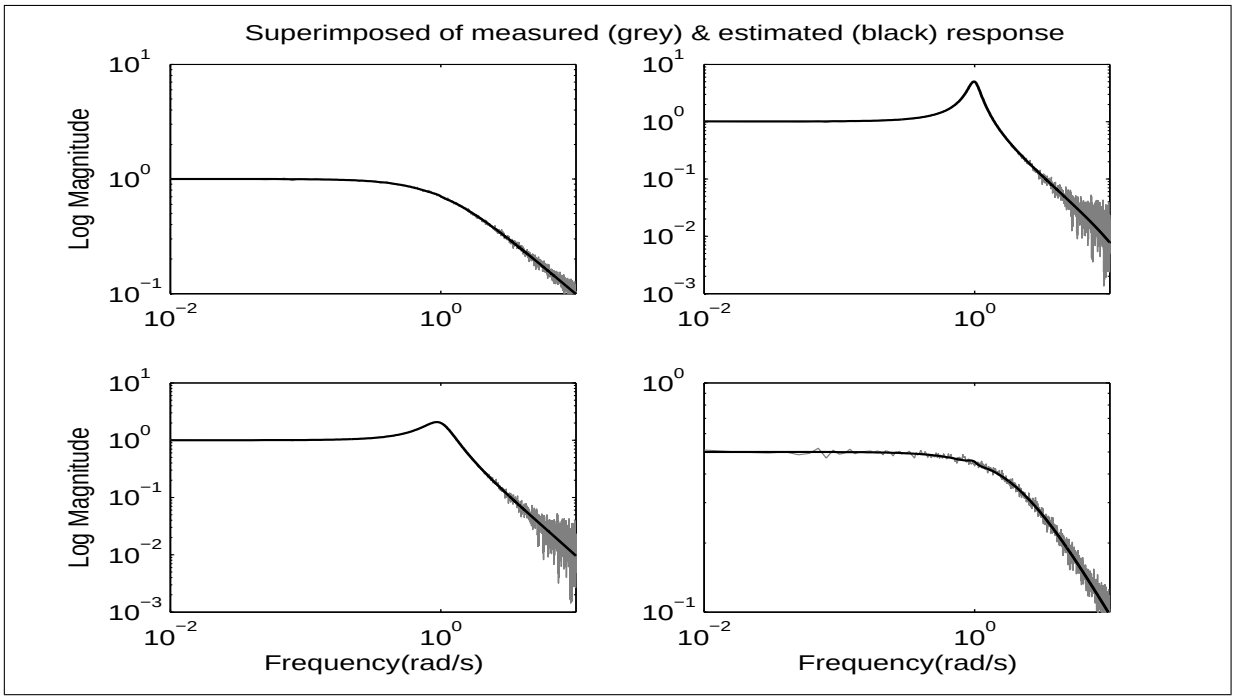

Figure 6.4: Bode plot for magnitude of MIMO simulated data systems

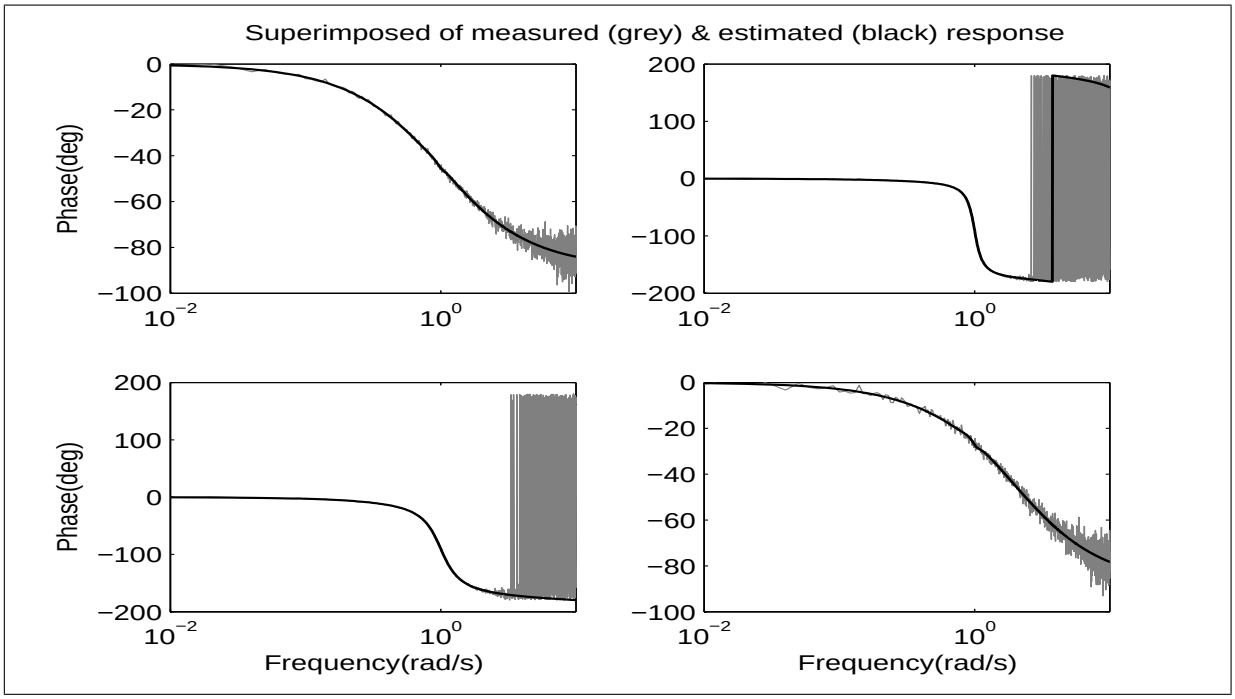

Figure 6.5: Bode plot for phase of MIMO simulated systems

$$\hat{B} = \begin{bmatrix} -24.6695 & -261.0673 \\ 5.2628 & -284.0706 \\ 17.9844 & -630.7181 \\ 5.1694 & -285.9333 \\ 31.0169 & -308.2670 \\ 8.4441 & -582.3992 \end{bmatrix}; \hat{C} = \begin{bmatrix} 0.4659 & 0.0953 \\ -0.0535 & 0.1275 \\ -0.3208 & 0.3228 \\ -0.0048 & -0.0128 \\ 0.6462 & -0.0100 \\ -0.1749 & -0.4446 \end{bmatrix}^{\top}; \hat{D} = \begin{bmatrix} 0.0005 & 0.0040 \\ 0.0006 & 0.0010 \end{bmatrix}$$

6.4.3 Optimal Selection for Design Parameter

When the subspace identification algorithm is applied to frequency domain data, the roles played by the parameter p, i and n are important. Therefore, in this section, an analysis is undertaken in order to find optimal values of these three design parameters. Optimal search for these parameters is necessary in order to obtain a reliable and correct model to represent the system. For this analysis, the MSE calculation is used as a guide for selecting the optimal value of parameter p and i. The formula to determine the MSE is given as

$$\text{MSE} = \frac{1}{N} \sum_{a=1}^{N} \mid G_m(j\omega_a) - \hat{G}(j\omega_a) \mid^2$$

With the assumption that a good model will provide a better prediction of the system behaviour, optimal selection of parameter p and i are based on the lowest value of mean square error. In this analysis, the SISO simulated data system and the MB system that have been discussed in previous section are investigated. In general, the information from the SISO system identification can be used as a guideline for the MIMO system identification as well.

Choice of Laguerre Design Parameter, p

For the frequency domain data, the model shows its consistency in modeling the system with respect towards the change of parameter p. For instance, the result for the first run using the noise added simulated data can be seen as in Figure (6.6). From this figure, it is seen that the model gives good performance when the value is set to ($p < 12$). Second test run is done for the magnetic bearing data. The result from the analysis can be seen as in Figure (6.7). For the MB data, it gives good performance for the value to be ($20 < p < 160$).

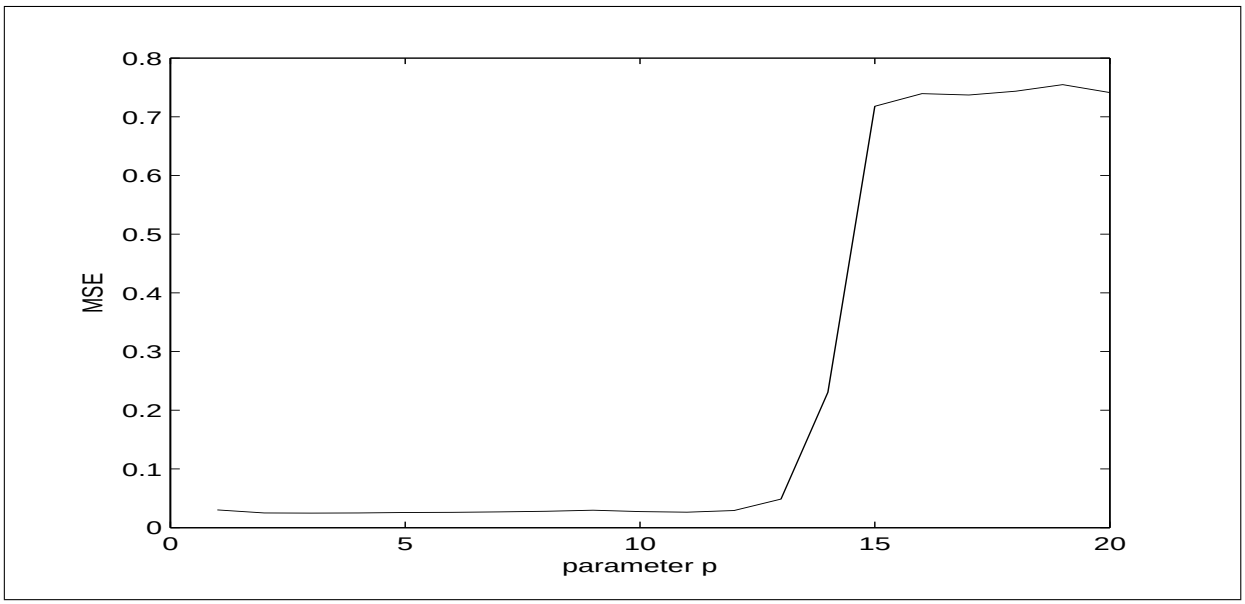

Figure 6.6: MSE run for optimal p - simulated frequency domain data

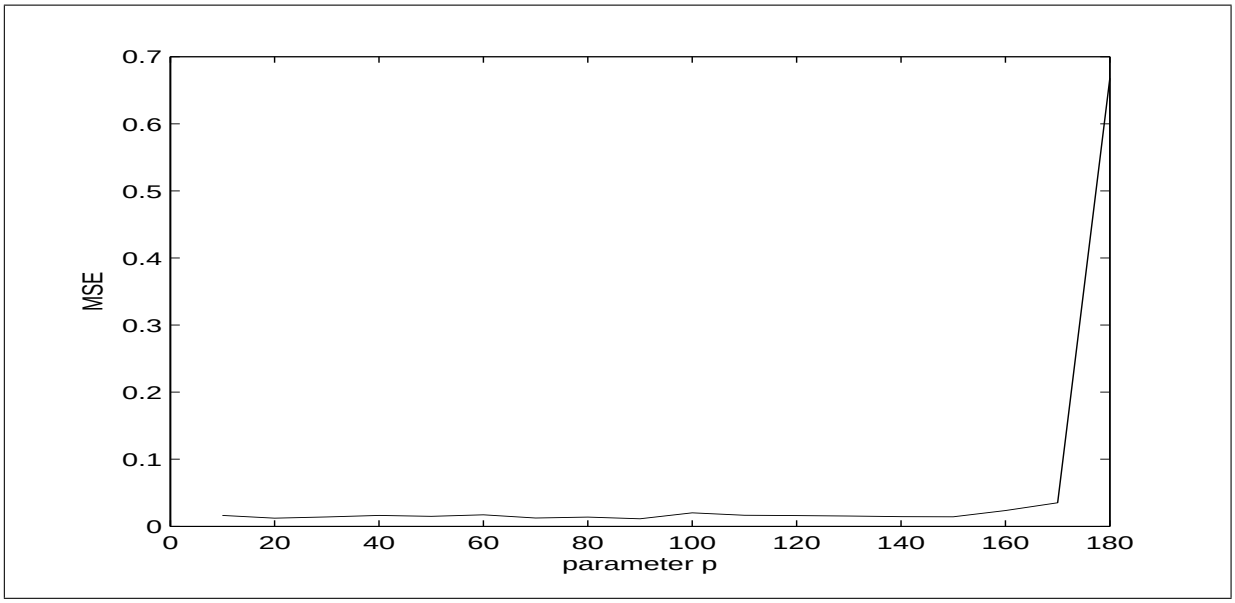

Figure 6.7: MSE run for optimal p - MB frequency domain data

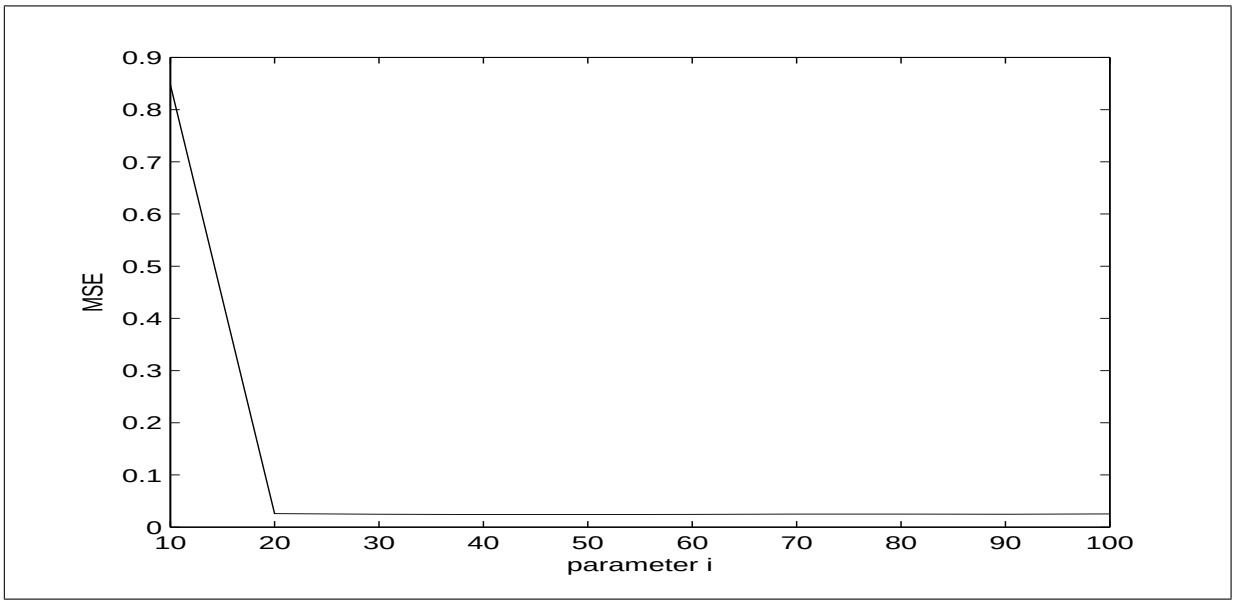

Figure 6.8: MSE run for optimal i - simulated frequency domain data

Choice on Expanding the Observability Matrix, i

Next parameter is i-parameter, the variable that determines the number of terms for the observability matrix as well as the representation of how many block rows constructed after filtering the data with Laguerre filter network. Increasing the i value will improve the performance accuracy. However, this trend will only hold for ($i \leq 100$) for the examples shown. Increasing the value of i more than 100 will add more complexity and increase running time, in which also will results in numerical condition problem. Analysis based on the simulated data can be referred in Figure (6.8). The analysis based on the real data using frequency domain data can be referred in Figure (6.9).

Choice of Model Order, n

Similar to implementation to time domain, the choice of model order for frequency domain model is also based on the diagonal plot of S matrix after performing the SVD. The diagonal plot obtained using the frequency domain data can be seen in Figure (6.10) and Figure (6.11).

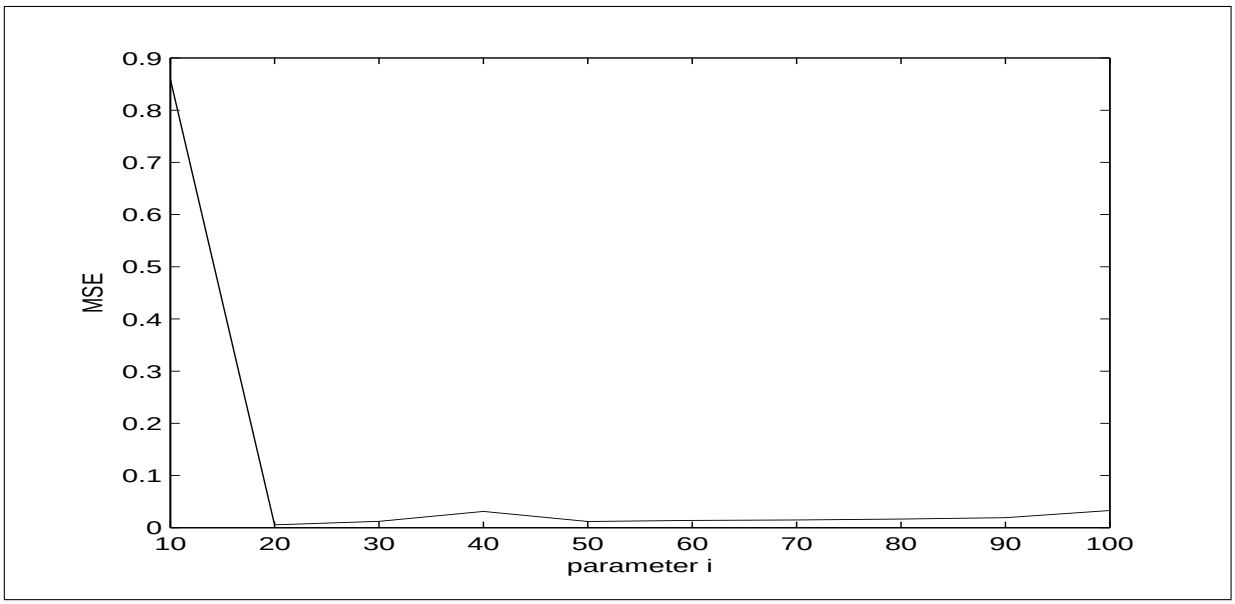

Figure 6.9: MSE run for optimal i - MB frequency domain data

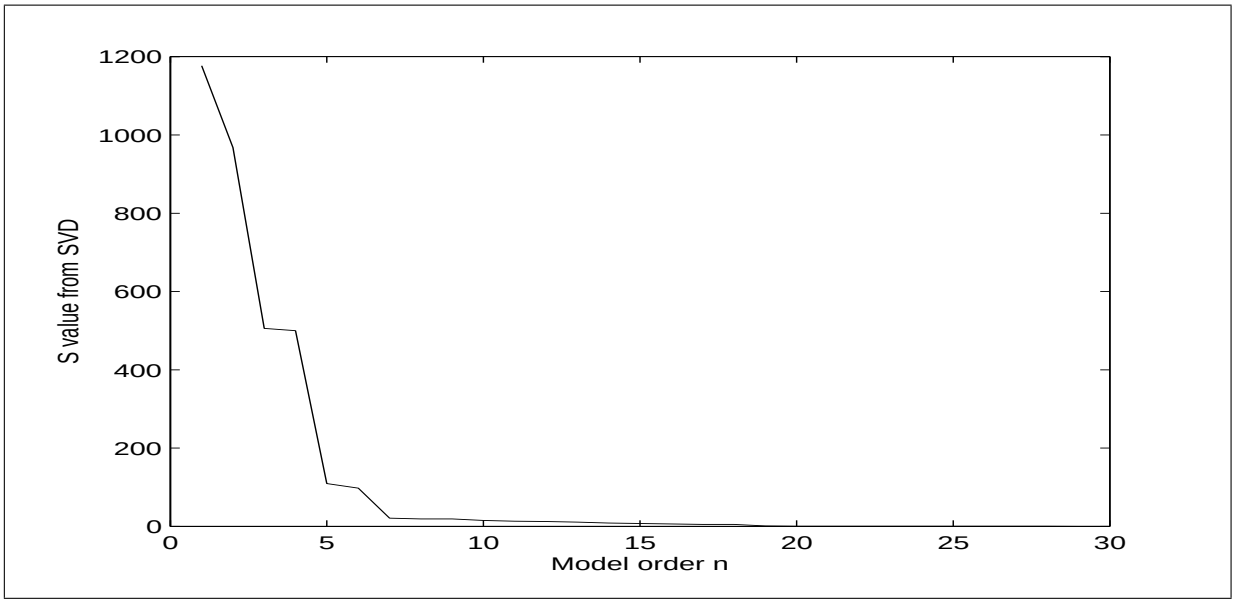

Figure 6.10: Diagonal plot of S matrix - simulated frequency domain data

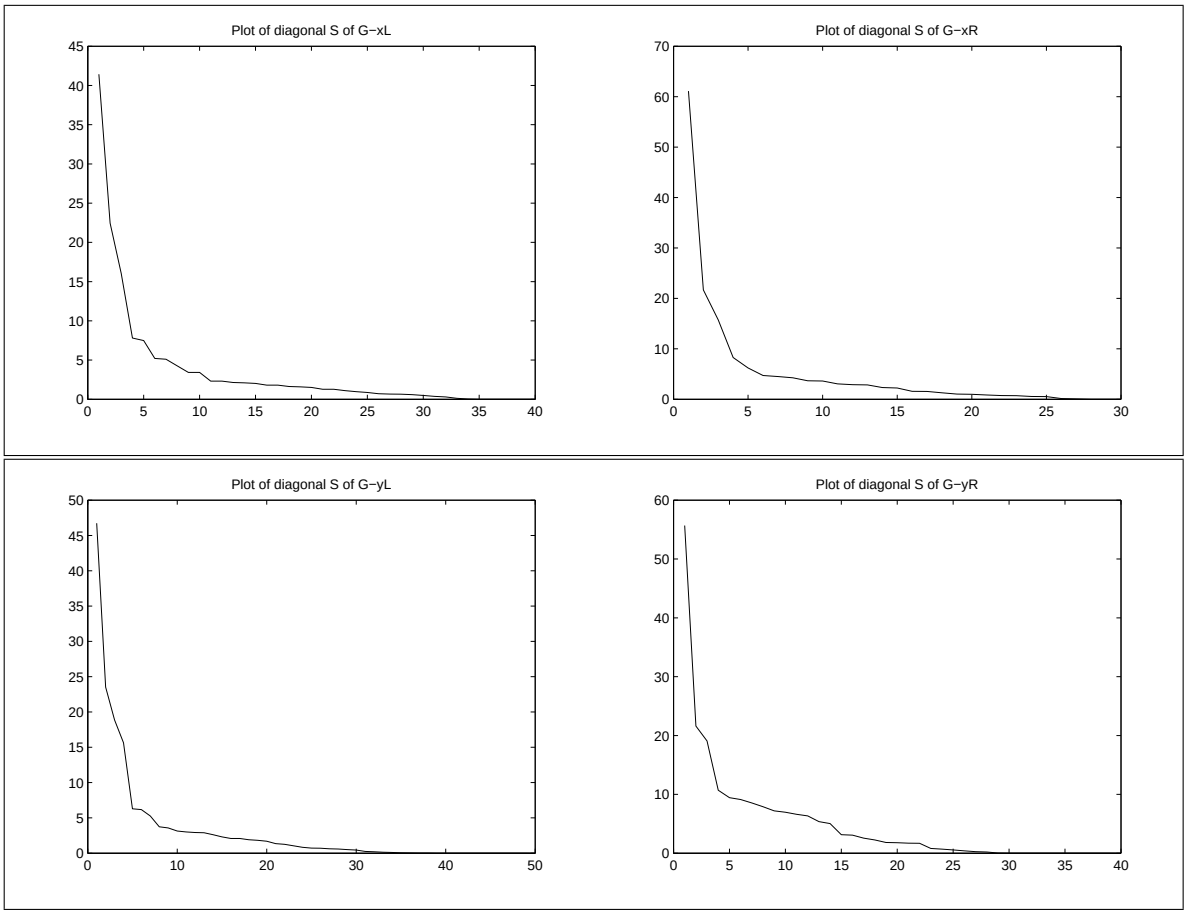

Figure 6.11: Diagonal plot of S matrix - MB frequency domain data

6.5 Summary

This chapter has presented a subspace identification approach in the frequency domain with an adoption of Laguerre filter network and an instrumental variable method. Based on observations, the design parameters, p and i play an important role in improving the model performance. For the noise-free system, small values of design parameters, p and i, are sufficient enough to identify the system successfully. However, when the system is corrupted with noise, higher values of both parameters are desired in the examples. As for the magnetic bearing system data, it can be seen that the model could identify the system nicely. The frequency response estimates obtained over the frequency sampling filter approach have provided with "clean" and unbiased closed-loop data, therefore the direct closed-loop identification using the open-loop system identification approach can be done successfully. Proper selection of parameters, p and i will also improve the model performance. The only drawback can be seen on MB data is that the model requires high order to present the system closely.

Chapter 7

Conclusions

7.1 Conclusions

This thesis mainly studies in four subjects: the subspace methods, the state space models, the continuous time systems and the magnetic bearing application. The subspace identification algorithms do not require an explicit parametrization. The only parameter needed for user specification is the system order, in which it can be explicitly determined by inspection of a singular value spectrum. The subspace identification algorithm also requires no nonlinear parametric optimization and no iterative procedures, thus, is abolishing the problems of local minima and model convergence. This method is also convenient for optimal estimation and control. In this thesis, the development of subspace methods is investigated in both open-loop and closed-loop systems. The performance evaluation is performed over time domain data, step response data and frequency response data. In all different environments, the subspace approach is properly developed as to suit with its purpose of identification.

In summary, the subspace approach on continuous time domain data has built the model catering with input signal and output signal, targeting to cope with process and measurement noise. The approach to closed-loop system has built the model catering with two signals (input/reference signal and output signal) coping with noises that interfere in both input and output point. On the other hand, the approach using step response data tries to compress the raw data and provide a better subspace identification model. Similar purposes apply to frequency response

data. In all of the subspace identification approaches, the main purpose is to generate accurate state space model.

In system identification, models that describe the systems may be in various forms and one of the possibilities is a state space model formulation. The state space mathematical modelling involves vectors and matrices in a unique geometrical framework. It offers the key advantages on providing low parameter sensitivity with respect to perturbation for high order systems and also has shown its ability to present the multi-variable systems with minimal state dimensions. Significantly, the aim is to search for accurate A, B, C and D matrices of the state space model as to ensure that the constructed model can closely mimic the actual system as well as provide information for the purpose of control system design. In this thesis, the subspace methods are carried out in developing a good state space model. Eventually, this state space model has been used to identify the continuous time system closely.

Even though the environment of "go digital" has widely influenced many researchers, this thesis has targeted its arrow towards continuous time systems. Yet, the identification performance over continuous time systems are more challenging as compared to discrete time systems. Fortunately, the combinations of Laguerre filter network, the instrumental variables and the frequency sampling filters have contributed to excellent performance of the continuous time system identification overall. The Laguerre filters used in this thesis are utilized to filter the input and output signals. The advantage of these filters lies in that they do not alter the frequency content of the signals but only influence the phase of the frequency contents. The transformed parameter model requires only simple algebraic relations and its orthogonality helps to cope with both process and measurement noise.

The instrumental variables adopted in the model are to cope with process and measurement noise. In this thesis, the choices of instrumental variables are based on future horizon which provide different approach from existing reported literature. This consideration is taken in-line with the properties of Laguerre filter network that require the causality in order to keep stability. This causal condition however can only solve the deterministic part of the systems (i.e obtain A,B and C matrices). The stochastic part which usually involved with noise models can not be utilized since the condition of the stochastic part is anti-causal. The only possible way to apply the anti-causal part for the continuous time system is by working in reverse for the batch recorded data. Apparently, this will only work if the identification is handled off-line.

The use of frequency sampling filter in this thesis also benefits in enhancing the performance capability and stability of subspace identification approach. In spite of its usage on compressing the data, the step response estimates and the frequency response estimates obtained from the frequency sampling filter also help in removing the noise contained in the measured data. This will give unbiased estimation for the data taken from the closed-loop systems. Thus, the "clean" step response and frequency response data has successfully identified using the subspace methods.

The final subject is where all the proposed approaches are used to identify the magnetic bearing system. As the successful rate of system identification relies on the quality of the acquired data from the plant, the identification over magnetic bearing system is seemly so challenging. However, with the proposed approaches it has shown that the subspace approaches are able to identify the magnetic bearing system closely. All the results have shown the efficacy of the proposed algorithms with acceptable accuracy.

7.2 Future Work

As the purpose of identification is to obtain an accurate model which therefore will be used in control system design, therefore the extension of this research primarily towards the implementation of this model to apply with suitable design controller. In general controller design, the model normally obtained from the already available model in system identification toolbox. Thus, using this model to develop a controller would be another advantage. The comparison of controller performance among models will be also something of interest. Other than that, the research viewpoint on step response data and frequency response data can be utilized in understanding and enhancing the controller performance.

In addition, the causal setup environment of subspace methods and Laguerre filter has allowed for possible online identification. Further study on online identification using this approach will contribute to useful research in regards towards real time modelling, controlling, diagnosing and monitoring the systems.

In discrete time systems, the subspace methods are successfully employed to identify both the deterministic part and stochastic part of the systems. This is due to the fact that the model

and identification procedure in discrete time systems are all anti-causal. As to the continuous time subspace identification, the only possible way to retrieve the stochastic part is by working with off-line identification in which the recorded data has to be identified back-ward in time. Thus, further research can be done as to solve the stochastic part and at the same time working in real time identification.

The 2-stage identification which involved the frequency sampling filters, Laguerre filters and instrumental variables has shown such a promising achievement in identification performance. By applying the first stage of identification using FSF approach, followed by the second stage of subspace identification become more consistent in identifying the noisy multi-variable data systems. However, the usage of the FSF model in this thesis is limited to single input single output system. The extension of its capability for data compression of multi-variable systems will definitely open for wider multi-variable system identification procedures. This will probably become a useful tool for process engineers in which any possible applications may be employed.

Appendix A

Algorithm

A.1 Orthogonal Decomposition Algorithm (Chapter 5)

The orthogonal decomposition algorithm was originally proposed by Korenberg et.al. [90]. The computation of the PRESS residuals can be viewed as a by-product of their proposed algorithm [180]. Here the data matrix is decomposed as

$$\Phi = WT$$

where W is a $N \times n$ matrix with N refers to number of data and n refers to the dimensionality of the parameter vector θ. T is a unit upper triangular $n \times n$ matrix and W is arranged such that

$$W_d = W^\top W$$

with $W_d(n \times n)$ being a diagonal matrix. Inserting $T^{-1}T$ into a general system model

$$\begin{aligned} Y &= \Phi(T^{-1}T)\theta + V \\ &= Wg + V \end{aligned}$$

where $g = T\theta$ is the auxiliary model parameter vector and $W = \Phi T^{-1}$ is the transformed data matrix. The vector g can now be estimated from the least squares solution as

$$\hat{g} = W_d^{-1} W^\top Y$$

which minimizes the loss function

$$J_n = (Y - Wg)^\top (Y - Wg)$$

The least squares estimate of the original parameter vector $\hat{\theta}$ is then obtained using the relation

$$\hat{\theta} = T^{-1}\hat{g}$$

Appendix B

Data Acquisition

B.1 Experimental Setup for MB Data Acquisition (Chapter 4)

As one of the objectives in this thesis is to implement a subspace model identification with application to magnetic bearing systems data, therefore, this section explains the data acquisition procedures that run for MB system apparatus available in the laboratory. For zero shaft speed (levitating mode machine), the dynamics in the $x-z$ and $y-z$ planes are decoupled, leading to two separate dynamic systems. Each of the two systems has two inputs and two outputs. Therefore, can be modelled by a 2×2 transfer matrix. As MB systems are open-loop unstable, feedback control systems are required to stabilize the system and to suspend the shafts so as to facilitate the closed-loop data acquisition. It has been noted that decentralized PD control system is usually sufficient for this purpose and is used here as shown in Figure (B.1).

Another important task needs to be done before running the experiment is to inject the exciting signal. In real process industry, the information content of the input and output data measured under steady state conditions usually insufficient for identification purposes. This is due to the fact that, for certain systems the input does not excite the system enough to be able to identify the system uniquely. Thus, the statistical information content from the measured data can not be obtained. To overcome this matter, one mechanism that can deliberately excite the system is usually needed. This can be done by setting up certain set point or by injecting an appropriate signal.

However, the used of excitation test signal may strongly influence the quality or/and the performance of the process since the plant may deviate from more or less economical operation. In order to strike a balance between the need to quantify process dynamics for control purposes and the urge to operate

in the most economical manner, the test-signal excitation and duration should be minimized subject to the demand that a sufficiently accurate process model can be identified, aiming at optimal experiment design [160]. For this experiment, the random signal is used as an excitation signal. There are four data set taken from the experiment. In block diagram, the setup can be shown as in Figure (B.2).

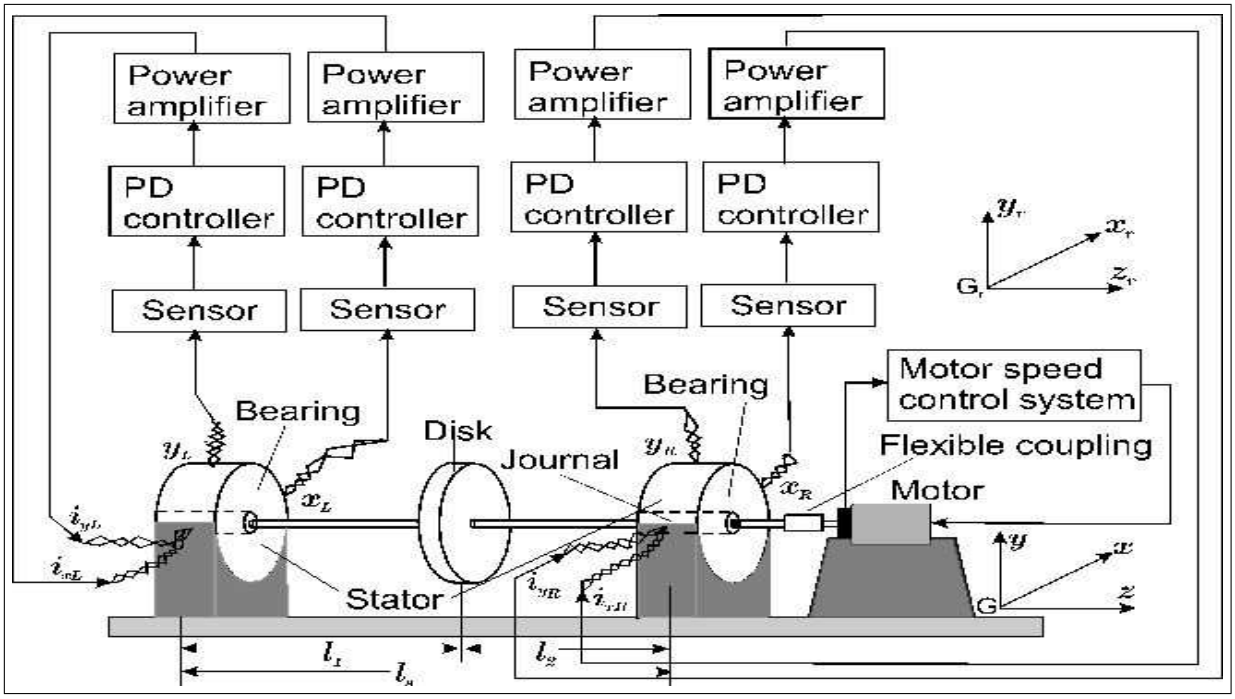

Figure B.1: Magnetic bearing system setup with PD controller

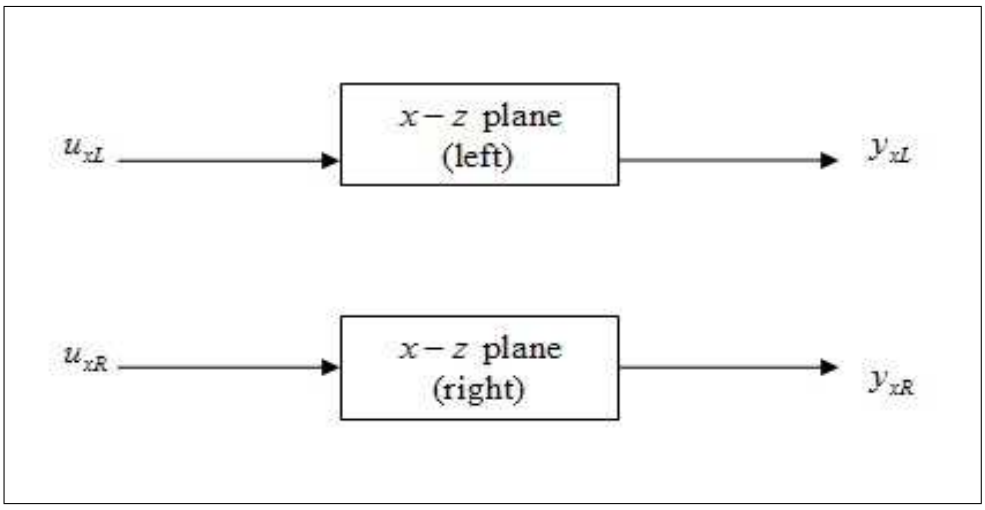

Figure B.2: Block diagram for data acquisition

Appendix C

Matlab Code - Time Domain (Chapter 3 & 4)

C.1 Generalized Random Binary Signal

```
function [u] = grbs(N,u1,u2,p);

% GRBS   Usage: U = GRBS(N,u1,u2,p)
%       Generates a Generalized Random Binary Signal [*] of length N,
%       with spectrum defined by probability p and signal levels
%       defined by u1, u2.
%
%       U=GRBS(n) returns a GRBS with u1=-1, u2=1 and p=0.5 of
%       length n. It should be noted that p=0.5 gives a GRBS of
%       uniform richness in frequency.
%
%       [*] H.J.A.F. Tulleken, Automatica, vol. 26, 37-49, 1990.
%       The implementation algorithm has been slightly modified.

rand('seed',0);
if nargin==1,
   u(1)=sign(rand-0.5);
   u1=-1;
```

```
   u2=1;
   p=0.5;
else
   if u2<u1
      temp=u1;
      u1=u2;
      u2=temp;
   end
   u(1)=0.5*(u2-u1)*sign(rand-0.5)+0.5*(u2+u1);
end
for k=2:N
   if rand>p
      u(k)=u(k-1)-(u2-u1)*sign(u(k-1)-0.5*(u2+u1));
   else
      u(k)=u(k-1);
   end
end
```

C.2 Generate Filtered Input & Output

```
function [uf,yf,Pf] = filter_io(u,y,dt,p,k)

% Generate the filtered input and output
% Generate the Laguerre filter network
%       u = measured input
%       y = measured output
%       N = number of sample data
%       dt = sampling interval
%       p = Laguerre parameter
%       k = 2*i, expanding row for past and future value

N = length(y); BB=sqrt(2*p)*ones(k,1); AA=-p*eye(k,k);

for a=1:k
    for b=1:k
        if b<a, AA(a,b)=-2*p;
        end
    end
end

[f1,f2]=size(BB);
x1=zeros(f1,1); x2=zeros(f1,1);
x3=BB;
for a=1:N
    x1 = x1 + AA*x1.*dt + dt.*BB.*u(1,a);
    x2 = x2 + AA*x2.*dt + dt.*BB.*y(1,a);
    x3 = x3 + AA*x3.*dt;

    % download the filtered input and output
    uf(:,a)=x1(:,1);
    yf(:,a)=x2(:,1);
    Pf(:,a)=x3(:,1);
end
```

C.3 Modified Gram-Schmidt

```
function [R,Q] = RQ_Gram(A);

% [R,Q] = RQ_Gram(A)
% The A matrix can be of any size, but there should be more columns than rows
% Q is the same size as A with orthonormal rows
% R is a lower triangular square matrix
%      A = RQ'

% make sure that A is correctly orientated
if size(A,1) > size(A,2)
    A = A';
end [m,n] = size(A);

% initialize Q and R
Q = zeros(n,m) R = zeros(m,m);

% begin loop
for j = 1:m
    % calculate the values of R and Q for jth entry
    R(j,j) = sqrt(A(j,:)*A(j,:)');
    Q(:,j) = 1/R(j,j)*A(j,:)';

    % calculate the rest of the R values in the jth row
    R(j+1:m,j) = A(j+1:m,:)*Q(:,j);

    % update the A matrix
    A(j+1:m,:) = A(j+1:m,:) - R(j+1:m,j)*Q(:,j)';
end
```

C.4 Estimating A & C

```
function [A,C] = estimate_AC(no_y,i,p,n,U_s);

% Estimate A & C matrices for continuous time state space model
%       no_y = number of output
%       i = number of Hankel matrix when expanding rows
%       p = Laguerre parameter
%       n = model order
%       U_s = n times of column of U matrix from SVD

% Create identity matrix
iden_mat2=eye(no_y,no_y);
iden_mat3=eye((i-1).*no_y,(i-1).*no_y);
iden_mat4=eye(n,n);

% Find Cw
J3 = [iden_mat2 zeros(no_y,(i-1).*no_y)];
Cw = J3*U_s;

% Find Aw
J1=[iden_mat3 zeros((i-1).*no_y,no_y)];
J2=[zeros((i-1).*no_y,no_y)iden_mat3];
N1=J1*U_s;
M1 = J2*U_s;
Aw=(pinv(N1'*N1))*N1'*M1;

% Compute A & C
A=p*(pinv(iden_mat4 - Aw))*(iden_mat4 + Aw);
C=sqrt(2*p)*Cw*(pinv(iden_mat4 - Aw));
```

C.5 Estimating B & D

```
function [B,D] = estimate_BD(u,y,N,dt,n,A,C)

% Calculation of B matrix using the estimated A and C matrices
% generating data matrix for C(sI-A)-1u(s)
%       u = measured input
%       y = measured output
%       N = number of sample data
%       dt = sampling interval
%       n = model order
%       A = estimated A matrices
%       C = estimated C matrices

xu=zeros(n,n);
for a=1:N
    xu = xu + A*xu*dt + dt*eye(n,n)*u(1,a);
    Phif(a,:)=C*xu;
end
y= y.';
theta = (pinv(Phif'*Phif))*Phif'*y;

%Reconstruct B & D
B = theta(1:n,1);
D=0;
```

C.6 System Identification - Open-loop

```
function [A,B,C,D]=sub_lag(no_u,no_y,u,y,i,n,dt,p)

% Function for estimating continuous time state space model
%       no_u = number of input
%       no_y = number of output
%       u = measured input
%       y = measured output
%       i = number of Hankel matrix when expanding rows
%       n = model order
%       dt = sampling interval
%       p = Laguerre parameter
%       k=2*i, expanding row for past and future value

N=length(y);

% Generate filtered data of input and output and Laguerre filter network
[uf,yf,Pf] = filter_io(u,y,dt,p,k);

Y_0iN = zeros(i,N); %Hankel matrix for past output
Y_ijN = zeros(i,N); %Hankel matrix for future output
U_0iN = zeros(i,N); %Hankel matrix for past input
U_ijN = zeros(i,N); %Hankel matrix for future input
W_0iN = zeros(i,N); %Hankel matrix for past Laguerre filter
W_ijN = zeros(i,N); %Hankel matrix for future Laguerre filter

Y_ijN = yf(i+1:k,1:N); %future output
U_ijN = uf(i+1:k,1:N); %future input
W_ijN = Pf(i+1:k,1:N); %future Laguerre filter
Y_0iN = yf(1:i,1:N);   %past output
U_0iN = uf(1:i,1:N);   %past input
W_0iN = Pf(1:i,1:N);   %past Laguerre filter

% Perform the QR - Orthogonal triangular decomposition
A2 = [W_0iN;U_0iN;U_ijN;Y_ijN;Y_0iN];
```

```
[R,Q] = RQ_Gram(A2);
R53=R(4*i+1:5*i,2*i+1:3*i);
R54=R(4*i+1:5*i,3*i+1:4*i);

% Perform the SVD - singular value decomposition
[U,S,V] = svd([R53 R54]);

U_s=U(:,1:n);

% Estimate A & C
[A,C] = estimate_AC(no_y,i,p,n,U_s);

% Estimate B & D
[B,D] = estimate_BD(u,y,N,dt,n,A,C);
```

C.7 System Identification - Closed-loop

```
function [A,B,C,D]=sub_lag(no_u,no_y,u,y,i,n,dt,p)

% Function for estimating continuous time closed-loop model
%       no_u = number of input
%       no_y = number of output
%       u = measured input
%       y = measured output
%       i = number of Hankel matrix when expanding rows
%       n = model order
%       dt = sampling interval
%       p = Laguerre parameter
%       k=2*i, expanding row for past and future value

N=length(y);

% Generate filtered data of input and output and Laguerre filter network
[uf,yf] = filter_io(u,y,dt,p,k);

Y_0iN = zeros(i,N); %Hankel matrix for past output
Y_ijN = zeros(i,N); %Hankel matrix for future output
U_0iN = zeros(i,N); %Hankel matrix for past input
U_ijN = zeros(i,N); %Hankel matrix for future input

Y_ijN = yf(i+1:i+i/2,1:N);    %future output
U_ijN = uf(i+1:i+i/2,1:N);    %future input
Y_0iN = yf(1:i,1:N);          %past output
U_0iN = uf(1:i,1:N);          %past input
Z1 = [U_0iN;U_ijN;Y_ijN;Y_0iN];

% Perform the QR - Orthogonal triangular decomposition
[R,Q] = RQ_Gram(Z1);
R32 = R(2*i+1:3*i,i+1:2*i);

% Perform the SVD - singular value decomposition
[U,S,V] = svd(R32);
```

```
U_s=U(:,1:n);

% Estimate A & C
[A,C] = estimate_AC(no_y,i,p,n,U_s);

% Estimate B, D
[B,D] = estimate_BD(u,y,N,dt,n,A,C);
```

Appendix D

Matlab Code - Data Compression (Chapter 5)

D.1 Frequency Sampling Filter Model

```
function [g,v,G]=fsfmodel(xRaw,yRaw,N,n,CutPoints)

%  xRaw - matrix of input variables
%  yRaw - matrix of output variable;
%  N - a row vector with numbers of step response coefficients
%  n - a row vector with maximum numbers of FSF parameters
%  CutPoints - a row vector containing sampling instants
               specifying the segments of data to be used;
%              if not specified all data  will be taken.
%
%  g - Estimated step response coefficients for each input-output pair
%  v - Standard deviations of the estimated step response coefficients
%  G - Estimated frequency response

P = []; y = [];

for (iSliceCounter = 1:2:length(CutPoints))
    xSlice = xRaw(CutPoints(iSliceCounter):CutPoints(iSliceCounter+1),:);
```

```
    ySlice = yRaw(CutPoints(iSliceCounter):CutPoints(iSliceCounter+1),:);
    [Prow,ySlAnAvg]=fsfreg(xSlice,ySlice,N,n);
    P = [P;Prow];
    y = [y;ySlAnAvg];
end

i_loop=1;
Pf=P;  % the regressor matrix
yf=y;  % process output data vector

numb_iter=4; %Default value = 4
theta_p=zeros(sum(n),1);
while (i_loop < numb_iter)
    %Model estimation based on PRESS
    [press1,thetaw,Covar] = mfpress(Pf,yf);

    %Obtain optimal orders for each input according to PRESS values
    [nNew,PressN] = minOrder(press1,n);
    nNew=n;

    %Re-estimate process models according to the optimal orders
    Pn=Pf(:,1:nNew(1));
    kk=n(1);
    for i=1:number_inputs-1
        Pn=[Pn Pf(:,kk+1:kk+nNew(i+1))];
        kk=kk+n(i+1);
    end
    [press2,theta,Covar] = mfpress(Pn,yf);

    %Loop-break
    %measurement for convergence of the estimates
    pa_err=(thetaw-theta_p)'*(thetaw-theta_p);
    pa_err=pa_err/(thetaw'*thetaw);
    if (pa_err<10e-4)
        break;
    end
```

```
    %calculate model prediction error
    P_pred=P(:,1:nNew(1));
    kk=n(1);
    for i=1:number_inputs-1
        P_pred=[P_pred P(:,kk+1:kk+nNew(i+1))];
        kk=kk+n(i+1);
    end
    y_pred=real(P_pred*theta); %model prediction
    e_resi=y(N(1):length(y))-y_pred(N(1):length(y));  %residual

    %Noise model estimation
    [E,n_op,noi_press]=aupress(e_resi); %maximum model order is at default value of 15

    %Pre-filtering process input and output data
    for i=1:sum(n)
        Pf(:,i)=filter(E,1,P(:,i));
    end
    yf=filter(E,1,y);

    i_loop=i_loop+1;
    theta_p=thetaw;
end

%Iterations using Generalized least squares completed
Para = theta; g  = []; v = [];

%Transform frequency estimates into step response estimates with confidence bounds

kk=nNew(1); KK=N(1);
[g(1:N(1)),v(1:N(1))]=tdf2se(Covar(1:kk,1:kk),Para(1:kk,1),N(1),nNew(1));
for i=1:number_inputs-1
    [g(KK+1:KK+N(i+1)),v(KK+1:KK+N(i+1))]=tdf2se(Covar(kk+1:kk+nNew(i+1),
    kk+1:kk+nNew(i+1)),Para(kk+1:kk+nNew(i+1),1),N(i+1),nNew(i+1));
    kk=kk+nNew(i+1);
    KK=KK+N(i+1);
end
```

```
%Frequency response bound
[G]=tfsb(Covar(1:nNew(1),1:nNew(1)),Para(1:nNew(1)),N(1),nNew(1));
```

D.2 FSF Regressor

```
function [Pn,y] = FSFreg(x,y,N1,n)

% Function: Construct FSF Regressive Matrix Pn
%   Pn - Parameter Regression Matrix
%   x - the time-domain input data matrix
%   y - the time-domain output data matrix
%   N1 - No. of frequencies in FSF filter
%   n - No. of parameters chosen in FSF model

[d1, ni]=size(x); [yc,yr]=size(y);
if yr>yc
    y=y';
end
j = sqrt(-1);

%construct the numerator of the FSF filter
for k=1:ni
    dx(:,k) = (x(:,k) - [zeros(N1(k),1);
    x(1:length(x)-N1(k),k)])/N1(k);
end
num = [1]; ci=1;
for k=1:ni
    P(:,ci) = filter(num,[1 -1],dx(:,k));
    for i=1:(n(k)-1)/2
        den = [1 -exp(j*2*i*pi/N1(k))];
        P(:,2*i+ci-1) = filter(num,den,dx(:,k));
        P(:,2*i+ci) = conj(P(:,2*i+ci-1));
    end
    ci=ci+n(k);
end
Pn=P;
```

D.3 FSF Identification

```
function [press,theta,cov] = mfpress(P,y)

% Function: Identification of FSF(truncated) of Linear Systems
            Using Orthogonal Decomposition
            Term selection included using PRESS criterion
%   press - PRESS corresponding to index n
%   theta - FSF model parameters
%   cov - Covariance of the parameter estimates(theta)
%   P - Process data matrix
%   y - Process output truncated by the FSF

[nr,nc]=size(P); W=P(:,1); T=eye(nc,nc);

% Wn is the vector containing the diagonal elements of W'*W;
one=ones(nr,1);
Wn(1)=W'*W;
g(1,1)=W'*y/Wn(1);
es(:,1)=y-g(1,1)*W;
h=abs(W.*W/Wn(1));
epress(:,1)=es(:,1)./(one-h);

%orthogonal decomposition, W is the orthogonal matrix
for i=1:nc-1
    alpha=W'*P(:,i+1);
    for j=1:i;
        alpha(j,1)=alpha(j,1)/(W(:,j)'*W(:,j));
    end
    W=[W P(:,i+1)-W*alpha];
    T(:,i+1)=[alpha; 1; zeros(nc-i-1,1)];

    %parameter estimation
    Wn(i+1)=W(:,i+1)'*W(:,i+1);
    g(i+1,1)=W(:,i+1)'*y/Wn(i+1);

    %calculate prediction error
```

```
    es(:,i+1)=es(:,i)-g(i+1,1)*W(:,i+1);
    h=h+abs(W(:,i+1).*W(:,i+1))/Wn(i+1); %h is the inflation matrix
    epress(:,i+1)=es(:,i+1)./(one-h); %epress is the press error
end

press=diag(epress'*epress);
theta=T\g;
yp=real(P(:,:)*theta);
e=y-yp;
sig=(e'*e)/(length(e)-nc);
PP=T'*diag(Wn)*T;
cov=inv(PP)*sig;
```

D.4 Min Numbers of FSF Parameters

```
function [nNew,PressN] = minOrder(Press,n)

% Function: Finds the minimum numbers of FSF parameters
            based on the Press Error criterion
%   Press - PRESS corresponding to index n
%   n - maximum numbers of FSF parameters
%   nNew - minimum numbers of FSF parameters
%   PressN - values of minimum PRESS corresponding to nNew

number_inputs=length(n);
global DEBUG
kk=n(1);
[a,b]=min(Press(1:kk)); nNew(1)=b; PressN(1)=a;

for i=1:number_inputs-1
    [a,b]=min(Press(kk+1:kk+n(i+1)));
    nNew(i+1)=b;
    PressN(i+1)=a;
    kk=kk+n(i+1);
end

for i=1:number_inputs
    if nNew(i)/2==ceil(nNew(i)/2),
        nNew(i) = nNew(i)+1;
    end
end
```

D.5 Noise Model Estimation

```
function [E,press,e_pred]=aupress(e)

% Function: Noise model estimation based on PRESS
%   e - the process variable
%   E - the autoregressive model
%   press - sum of squared prediction errors;
%   e_pred - prediction error

me=0;
e=e-me;
[n,m]=size(e);

if (m>n)
    e=e';
end
nmax=10; %default value for maximum model order

%form the auto-regressor
L=length(e); P=[0;-e(1:L-1)];
for i=2:nmax
   P=[P [zeros(i,1);-e(1:L-i,1)]];
end

%calculate sum of squared prediction errors for different model structure
[press,theta,covar]=mfpress(P,e);

%decide the best model order for the noise model
pd=diff(press);
for k=1:length(pd)
    if pd(k)>0
        n_best=k;
        break;
    elseif -pd(k)/press(k)<0.005
        n_best=k;
        break;
```

```
    end
end

%re-estimate the model using the structure determined
P=P(:,1:n_best);
[pre_noise,theta,covar]=mfpress(P,e);

press=[e'*e; press];
E=[1 theta'];
e_pred=P*theta+me;
```

D.6 Step Response Estimates

```
function [g,Vg]=tdf2se(Vart,fg,N,n)

% Function: Obtain step response estimates
%   g - Estimated step response coefficients for each input-output pair
%   Vg - Standard deviations of the estimated step response coefficients
%   Vart - Covariance of the parameter estimates
%   fg - FSF model parameters
%   N - a row vector with numbers of step response coefficients
%   n - minimum numbers of FSF parameters

j=sqrt(-1);
ep(1,1)=1;
for k=1:(n-1)/2
    wk=2*k*pi/N;
    ep(1,2*k)=exp(j*wk);
    ep(1,2*k+1)=exp(-j*wk);
end

wei=zeros(1,n);

for m=1:N;
    weight(m,:)=wei+ep.^(m-1);
    wei=weight(m,:);
    r(m)=weight(m,:)*fg/N;

    g(m)=real(r(m));

    %variance
    Vg(m)=wei*Vart*wei'/(N*N);
end

Vg=sqrt(real(Vg));
```

D.7 Frequency Response Estimates

```
function [G]=tfsb(covt,para,N,n)

% Function: Frequency response estimates
%   G - Estimated frequency response
%   covt - Covariance of the parameter estimates
%   para - FSF model parameters
%   N - a row vector with numbers of frequency response
%   n - minimum numbers of FSF parameters

j=sqrt(-1);
dw=0.005;
w=dw:dw:pi*n/N;
epk(1,1)=1;
for k=1:(n-1)/2
    wk=2*k*pi/N;
    epk(1,2*k)=exp(j*wk);
    epk(1,2*k+1)=exp(-j*wk);
end

w=w';
ep=exp(-j*w);
for k=1:n
    v1=ones(length(w),1);
    for i=1:N-1
        v1=v1+(ep*epk(1,k)).^i;
    end
    dep(:,k)=v1/N;
end

for k=1:length(w)
    G(k)=dep(k,:)*para;
end
```

Appendix E

Matlab Code - Frequency Domain (Chapter 6)

E.1 System Identification - Frequency Domain

```
function [A,B,C,D]=sub_lagf(no_u,no_y,G,i,n,w,p)

% Function for estimating continuous time state space model
%       no_u = number of input
%       no_y = number of output
%       G = measured frequency response data
%       i = number of Hankel matrix when expanding rows
%       n = model order
%       w = sampling frequency
%       p = Laguerre parameter

N=length(w);

% Generate W-operator
W = (j*w - p)./(j*w + p);

% Compute 1st order Laguerre filter
L = ((2*p)^0.5)./(j*w + p);
```

```
GW = zeros(i,N); phi = zeros(i,N); P = zeros(i,N);
for a=1:i
    GW(a,:) = L.*(W.^(a - 1)).*G;
    phi(a,:) = L.*(W.^(a - 1));
    P(a,:) = (W.^(a+i-1));
end

% Separate into real and imaginary part
GW2=[real(GW) imag(GW)];
phi2=[real(phi) imag(phi)];
P2=[real(P)imag(P)];

% Perform the QR - Orthogonal triangular decomposition
A1 = [phi2;GW2;P2];
[R,Q] = RQ_Gram(A1);
R22=R(i+1:2*i,i+1:2*i);
R32=R(2*i+1:3*i,i+1:2*i);
R_i=R22*R32';

% Perform the SVD - singular value decomposition
[U,S,V] = svd(R_i);

U_s=U(:,1:n);

% Create identity matrix
iden_mat2=eye(no_y,no_y);
iden_mat3=eye((i-1).*no_y,(i-1).*no_y);
iden_mat4=eye(n,n);

% Find Cw
J3 = [iden_mat2 zeros(no_y,(i-1).*no_y)];
Cw = J3*U_s;

% Find Aw
J1=[iden_mat3 zeros((i-1).*no_y,no_y)];
J2=[zeros((i-1).*no_y,no_y)iden_mat3];
```

```
N1 = J1*U_s;
M1 = J2*U_s;
Aw=(pinv(N1'*N1))*N1'*M1;

sai_temp = zeros(N,n+1);
for a = 1:N
    sai_temp(a,:) = [Cw*(pinv(((W(a)).*iden_mat4) - Aw)) 1];
end

sai=[real(sai_temp);imag(sai_temp)];
Gtemp = G.';
Gmeas=[real(Gtemp); imag(Gtemp)];

% Find Bw & Dw via least squares solution
theta = (pinv(sai'*sai))*sai'*Gmeas;
Bw = theta(1:n,1);
Dw=theta(n+1,1);

% Calculate A,B,C & D
A=p*(pinv(iden_mat4 - Aw))*(iden_mat4 + Aw);
B=sqrt(2*p)*(pinv(iden_mat4 - Aw))*Bw;
C=sqrt(2*p)*Cw*(pinv(iden_mat4 - Aw));
D=Dw+Cw*(pinv(iden_mat4-Aw))*Bw;
```

Bibliography

[1] Magnetic bearings. `http://www.skf.com`, 2005.

[2] Critical speed. `http://en.wikipedia.org/wiki/Critical_speed`, 2006.

[3] Control tutorials for Matlab. `http://www.engin.umich.edu/group/ctm/pid/pid.html`, 2007.

[4] Inertia. `http://en.wikipedia.org/wiki/Inertia`, 2007.

[5] H-J. Ahn, S-W. Lee, S-H. Lee, and D-C. Han. Frequency domain control-relevant identification of MIMO AMB rigid rotor. *Automatica*, 39(2):299–307, 2003.

[6] H. Akcay, S.M. Islam, and B. Ninnes. Subspace-based identification of power transformer models from frequency response data. *IEEE Trans. on Inst. and Measurement*, 48(3):700–704, 1999.

[7] N.G. Albritton and J.Y. Hung. Nonlinear control with digital signal processors: Room for improvement. In *Proc. of Industrial Electronics Conf.*, volume 1, pages 197–201, 1997.

[8] G.M. Allan, P. Schroder, and P.J. Fleming. Fuzzy controllers for active magnetic bearings. In *Proc. of 8th IFAC Symp. on Computer Aided Control Systems Design*, pages 27–32, 2001.

[9] M. Antila, E. Lantto, and A. Arkkio. Determination of forces and linearized parameter of radial active magnetic bearing by finite element method. *IEEE Trans. on Magnetics*, 34(3):684–694, 1998.

[10] M. Aoki. *State space modeling of time series*. Springer-Verlag, Berlin, 2nd. edition, 1990.

[11] K.J. Astrom. *Introduction to stochastic control theory*. Academic Press, New York, 1970.

[12] K.J. Astrom. Maximum likelihood and prediction error methods. *Automatica*, 16:551–574, 1980.

[13] K.J. Astrom and B. Wittenmark. *Computer-controlled systems: Theory and design.* Prentice Hall, New Jersey, 3rd edition, 1997.

[14] T. Barry. A data driven approach to constrained control. Master thesis, School of Electrical & Computer Eng., RMIT University, Australia, 2004.

[15] T. Bastogne, H. Garnier, and P. Sibille. A PMF-based subspace method for continuous time model identification. Application to a multivariable winding process. *Int. J. of Control*, 74(2):118–132, 2001.

[16] T. Bastogne, H. Garnier, P. Sibille, and M. Mensler. PMF-based subspace method for continuous time model identification deterministic study. In *Proc. of 35th Conf. on Decision & Control*, pages 1665–1670, Fukuoka, Japan, 1996.

[17] S. Beghelli, P. Castaldi, and U. Soverini. A frequential approach for errors-in-variables models. In *Proc. of European Control Conf.*, Brussel, Belgium, 1997.

[18] S. Beghelli, R.P. Guidorzi, and U. Soverini. The frisch scheme in dynamic system identification. *Automatica*, 26(1):171–176, 1990.

[19] F. Betschon and C.R. Knospe. Reducing magnetic bearing currents via gain scheduled adaptive control. *IEEE/ASME Trans. on Mechatronics*, 6(4):437–443, 2001.

[20] H. Bleuler, C. Gahler, R. Herzog, R. Larsonneur, T. Mizuno, R. Siegwart, and W. Shao-Ju. Application of digital signal processors for industrial magnetic bearings. *IEEE Trans. on Control System Technology*, 2(4):280–289, 1994.

[21] T. Bohlin. On the problem of ambiguities in maximum likelihood identification. *Automatica*, 7:199–210, 1971.

[22] J. Cao, Q. Chen, and L. Yu. Input-output linearizing control for levitated rotating motors. In *Proc. of Int. Conf. on Power System Technology*, volume 3, pages 1650–1654, 2002.

[23] S. Carlson-Skalak, E. Maslen, and Y. Teng. Magnetic bearing actuator design using genetic algorithms. *Journal of Engineering Design*, 10(2):143–164, 1999.

[24] P. Castaldi, R.P. Guidorzi, U. Soverini, and S. Beghelli. On the application of the frisch scheme identification. In *3rd. European Control Conf.*, pages 851–855, Rome, 1995.

[25] H. Chang and S-C. Chung. Integrated design of radial active magnetic bearing systems using genetic algorithms. *Mechatronics*, 12:19–36, 2002.

[26] S-C. Chang and P-C. Tung. Identification of a non-linear electromagnetic system: An experimental study. *Journal of Sound and Vibration*, 214(5):853–871, 1998.

[27] S-C. Chang and P-C. Tung. Nonlinear identification of a magnetic bearing system with closed loop control. *JSME Int. J., Series C*, 42(4):982–990, 1999.

[28] S-L. Chen, S-H. Chen, and S-T. Yan. Stabilization of a current-controlled three-pole magnetic rotor-bearing system by integral sliding mode control. In *Proc. of IEEE Int. Conf. on Networking, Sensing and Control*, volume 2, pages 949–954, 2004.

[29] A. Chiuso and G. Picci. Consistency analysis of some closed-loop subspace identification methods. *Automatica*, 41:377–391, 2005.

[30] C.T. Chou and M. Verhaegen. Subspace algorithms for the identification of multivariable dynamic errors-in-variables models. *Automatica*, 33(10):1857–1869, 1997.

[31] C.T. Chou, M. Verhaegen, and R. Johansson. Continuous time identification of SISO system using laguerre functions. *IEEE Trans. on Signal Processing*, 47(2):349–362, 1999.

[32] N.L.C. Chui and J.M. Maciejowski. Realization of stable models with subspace methods. *Automatica*, 32(11):1587–1595, 1996.

[33] F. Demourant and G. Ferreres. A frequency domain identification-control approach for a flexible aircraft. In *Proc. of IEEE Int. Conf. on Control Applications*, pages 126–137, 2002.

[34] P.P.J. Van den Bosch and A.C. Van der Klauw. *Modeling, identification and simulation of dynamical systems*. CRC Press, Florida, 1994.

[35] P.M.J. Van den Hof and R.J.P. Schrama. An indirect method for transfer function estimation from closed loop data. *Automatica*, 29(6):1523–1527, 1993.

[36] G. Ding, Z. Zhou, Y. Hu, and D. He. FEA-based optimal design of the radial magnetic bearings in magnetic suspended hard disk drive. In *Proc. of 2nd IEEE/ASME Int. Conf. on Mechatronic and Embedded Systems and Applications*, pages 1–6, 2006.

[37] V. Elnaz, S. Bahram, and B. Stuart. Estimation and rejection of unknown sinusoidal disturbances using a generalized adaptive forced balancing method. In *American Control Conf.*, pages 3529–3534, 2007.

[38] A. Escalante, V. Guzman, M. Parada, L. Medina, and S.E. Diaz. Neural network emulation of a magnetically suspended rotor. *American Society of Mechanical Engineers*, 4B:615–625, 2002.

[39] P. Eykhoff. Some fundamental aspects of process-parameter estimation. *IEEE Trans. on Automatic Control*, 8:347–357, 1963.

[40] W. Favoreel, B. De-Moor, and P. Van-Overschee. Subspace identification of bilinear systems subject to white inputs. *IEEE Trans. on Automatic Control*, 44(6):1157–1165, 1999.

[41] R.L. Fittro, C.R. Knospe, and L.S. Stephens. Rotor point compliance minimization via [mu]-synthesis. In *Proc. of the American Control Conf.*, volume 2, pages 1319–1323, 1997.

[42] R.L. Fittro, C.R. Knospe, and L.S. Stephens. [mu]-synthesis applied to the compliance minimization of an active magnetic bearing HSM spindle's thrust axis. *Machining Science and Technology*, 7(1):19–51, 2003.

[43] S. Font, G. Duc, and F. Carrere. H-infinity control of a magnetic bearing. In *Proc. of IEEE on Control Applications*, volume 1, pages 581–585, USA, 1994.

[44] U. Forsell. *Closed-loop Identification: Methods, Theory and Applications.* Linkoping University, Sweden, 1999.

[45] U. Forsell and L. Ljung. A projection method for closed-loop identification. *IEEE Trans. on Automatic Control*, 45(11):2101–2106, 2000.

[46] C. Gahler, M. Mohler, and R. Herzog. Multivariable identification of active magnetic bearing systems. *JSME Int. Journal*, 40(4C):584–592, 1997.

[47] H. Garnier and P. Sibille A. Richard. Continuous time canonical state space model identification via Poisson moment functions. In *Proc. of 34th. Conf. on Decision & Control*, pages 3004–3009, New Orleans, LA, 1995.

[48] P.J. Gawthrop and L. Wang. Estimation of physical parameters of stable and unstable systems via estimation of step response. In *Proc. of Control, Automation, Robotics & Vision Conf.*, volume 2, pages 889–893, 2004.

[49] P.J. Gawthrop and L. Wang. Data compression for estimation of the physical parameters of stable and unstable linear systems. *Automatica*, 41(8):1313–1321, 2005.

[50] N.S. Gibson, H. Choi, and G.D. Buckner. H-infinity control of active magnetic bearings using neural network identification of uncertainty. In *Proc. of IEEE Int. Conf. on Syst. Man & Cybernetics*, volume 2, pages 1449–1456, 2003.

[51] M. Gilson and P Van den Hof. On the relation between a bias eliminated least-squares (BELS) and an IV estimator in closed-loop identification. *Automatica*, 37:1593–1600, 2001.

[52] K.R. Godfrey. Correlation methods. *Automatica*, 16:527–534, 1980.

[53] G.H. Golub and C.F. Van-Loan. *Matrix computations*. John Hopkins University Press, Baltimore, Maryland, 3rd. edition, 1996.

[54] G.C. Goodwin, S.T. Graebe, and M.E. Salgado. *Control System Design*. Prentice Hall, New Jersey, 2001.

[55] T. Gustafsson, M. Lovera, and M.H. Verhaegen. A novel algorithm for recursive instrumental variable based subspace identification. In *Proc. of IEEE Conf. on Decision and Control*, pages 3920–3925, 1998.

[56] K. Hashimoto, F. Matsumura, and M. Fujita. Experimental comparison between H-infinity and H2 control for a magnetic suspension system with double flexible beam. In *Proc. of 32nd IEEE Conference on Decision and Control*, volume 3, pages 2949–2954, 1993.

[57] B.R.J. Haverkamp. *State Space Identification; Theory and Practice*. Phd. thesis, Faculty of Information Technology & Systems, Delft University, The Netherlands, 2001.

[58] B.R.J. Haverkamp, C.T. Chou, M. Verhaegen, and R. Johansson. Identification of continuous-time MIMO state space models from sampled data, in the presence of process and measurement noise. In *Proc. of the 35th Decision and Control Conf.*, pages 1539–1544, Kobe, Japan, December 1996.

[59] B.R.J. Haverkamp, M. Verhaegen, C.T. Chou, and R. Johansson. Continuous-time subspace model identification using Laguerre filtering. In *11th. IFAC/IFORS Symp. on Identification and System Parameter Estimation*, pages 1143–1148, 1997.

[60] R. Herzog, P. Buhler, C. Gahler, and R. Larsonneur. Unbalance compensation using generalized notch filters in the multivariable feedback of magnetic bearings. *IEEE Trans. on Control System Technology*, 4(5):580–586, 1996.

[61] M. Hisatani. Identification and control system design based on eigenvalues move method for a flexible rotor suspended by magnetic bearings. *JSME Int. Journal*, 63(606C):464–469, 1997.

[62] B.L. Ho and R.E. Kalman. Effective construction of linear, state-variable models from input/output functions. *Regelungstechnik*, 44:545–548, 1966.

[63] S-K. Hong and R. Langari. Fuzzy modeling and control of a nonlinear magnetic bearing system. *Journal of Intelligent & Fuzzy Systems*, 7(4):335–346, 1999.

[64] S-K. Hong and R. Langari. Robust fuzzy control of a magnetic bearing system subject to harmonic disturbances. *IEEE Trans. on Control System Technology*, 8(2):366–371, 2000.

[65] S.K. Hong, R. Langari, and J. Joh. Fuzzy modeling and control of a nonlinear magnetic bearing system. In *Proc. of IEEE Conf. on Control Applications*, pages 213–218, 1997.

[66] D. Huang and T. Katayama. A subspace-based method for continuous time identification by using delta operator model. *Trans. of ISCIE*, 14(1):1–9, 2001.

[67] J. Huang, L. Wang, and Y. Huang. Continuous time model predictive control for a magnetic bearing system. *PIERS online*, 3(2):202–208, 2007.

[68] S. Van Huffel. *Recent advances in total least squares techniques and errors-in-variables modelling*. SIAM, Philadelphia, USA, 1997.

[69] S. Van Huffel and P. Lemmerling. *Total least squares and errors-in-variables modelling. Analysis, algorithms and applications*. Kluwer Academics, Dordrecht, The Netherlands, 2002.

[70] S. Van Huffel and J. Vandewalle. Comparison of total least squares and instrumental variable methods for parameter estimation of transfer function models. *Int. J. Control*, 50(4):1039–1056, 1989.

[71] J.Y. Hung. Magnetic bearing control using fuzzy logic. *IEEE Trans. on Industry Applications*, 31(6):1462–1467, 1995.

[72] T. Ito and K. Nonami. [mu] synthesis of flexible rotor-magnetic bearing system. *Trans. of the Japan Society of Mechanical Engineers, Part C*, 61(584):1437–1442, 1995.

[73] M-J. Jang, C-L. Chen, and Y-M. Tsao. Sliding mode control for active magnetic bearing system with flexible rotor. *Journal of the Franklin Institute*, 342(4):401–419, 2005.

[74] I. Jaworska and B. Stanczyk. On robustness of PID control. In *Int. Conf. on Methods and Models in Automation and Robotics*, volume 1, pages 397–400, 2000.

[75] V. Jayanth, H. Choi, and G. Buckner. Identification and control of a flexible rotor supported on active magnetic bearing. In *Proc. of IEEE Southeastcon*, pages 273–278, 2002.

[76] J-T. Jeng and T-T. Lee. Control of magnetic bearings via the Chebyshev polynomial based unified model neural network. *Intelligent Autonomous Systems*, 5:213–218, 1998.

[77] Y. Jiang. *Application of Advanced Technologies for Magnetic Bearing System Control.* Ph.d thesis, Electrical & Computer Eng. RMIT University., Melbourne, Australia, 1999.

[78] J. Jin-Tsong and L. Tsu-Tian. Control of magnetic bearing systems via the Chebyshev polynomial-based unified model (CPBUM) neural network. *IEEE Trans. on Systems, Man and Cybernetics, Part B*, 30(1):85–92, 2000.

[79] R. Johansson. *System modeling and identification.* Prentice Hall, New Jersey, 1993.

[80] R. Johansson. Identification of continuos-time models. *IEEE Trans. on Signal Processing*, 42(4):887–897, 1994.

[81] R. Johansson and G. Lindstedt. An algorithm for continuous time state space identification. In *Proc. of 34th. Conf. on Desicion & Control*, pages 721–722, New Orleans, LA, 1995.

[82] R. Johansson, M. Verhaegen, and C.T. Chou. Stochastic theory of continuous time state space identification. *IEEE Trans. on Signal Processing*, 47(1):41–51, 1999.

[83] L. Jun-Ho, K. Hyun-Ki, L. Jung-Suk, and L. Keng-Seo. Experimental evaluation of Q-parameterization control for the imbalance compensation of magnetic bearing systems. *Trans. of Korean Inst. Of Electrical Engineers*, 48(3):278–287, 1999.

[84] T. Katayama. *Subspace methods for system identification.* Springer-Verlag, London, 2005.

[85] T. Katayama and T. Yamamoto. A state-space model identification of closed-loop system based on subspace method. In *Proc. of American Control Conference*, volume 5, pages 3564–3565, 1995.

[86] H. Kato, S. Wakui, T. Mayama, A. Toukairin, H. Takanashi, and S. Adashi. System identification of anti-vibration units in semiconductor exposure apparatus. In *Proc. of IEEE Int. Conf. on Control Applications*, pages 1312–1317, 1999.

[87] C-H. Kim and C-W. Lee. Fuzzy control algorithm for multi-objective problems by using orthogonal array and its application to an AMB system. In *Annual Conf. of the North American Fuzzy Information Processing Society*, volume 3, pages 1752–1757, 2001.

[88] C.S. Kim and C.W. Lee. In situ runout identification in active magnetic bearing system by extended influence coefficient method. *IEEE/ASME Trans. on Mechatronics*, 2(1):51–57, 1997.

[89] S.J. Kim and C.W. Lee. On-line identification of current and position stiffness by LMS algorithm in active magnetic bearing system equipped with force transducers. *Mechanical Systems and Signal Processing*, 13(5):681–690, 1999.

[90] M. Korenberg, S.A. Billings, Y.P. Liu, and P.J. McIlroy. Orthogonal parameter estimation algorithm for nonlinear stochastic systems. *Int. J. Control*, 48(1):193–210, 1988.

[91] S.K. Kung. A new low-order approximation algorithm via singular value decomposition. In *Proc. of 12th. Asilomar Conf. on Circuits, Systems and Computers*, pages 705–714, 1978.

[92] W.E. Larimore. System identification, reduced-order filtering and modeling via canonical variate analysis. In *American Control Conf.*, pages 445–451, San Francisco, 1983.

[93] W.E. Larimore. Canonical variate analysis in identification, filtering and adaptive control. In *29th IEEE Conf. on Decision & Control*, pages 596–604, Honolulu, Hawaii, 1990.

[94] J-H. Lee, A.M. Mohamed, and F. Matsumura. Experimental evaluation of Q-parameterization controllers to a magnetic bearing with imbalance. *Trans. of the Inst. of Electrical Engineers of Japan, Part D*, 117(10):1212–1220, 1997.

[95] H. Lev-Ari and A.J. Devaney. The time-reversal technique re-interpreted: Subspace-based signal processing for multi-static target location. In *Proc. of IEEE on Sensor Array and Multi-channel Signal Processing Workshop*, pages 509–513, 2000.

[96] W. Lin, S.J. Qin, and L. Ljung. On consistency of closed-loop subspace identification with innovation estimation. In *43th. IEEE Conf. on Decision & Control*, pages 2195–2200, 2004.

[97] K. Liu, R.N. Jacques, and D.W. Miller. Frequency domain structural system identification by observability range space extraction. In *Proc. of America Control Conf.*, volume 1, pages 107–111, 1994.

[98] Z-H. Liu and K. Nonami. Adaptive vibration control using frequency estimation for multiple periodic disturbances with noise. *JSME Int. J. Series C: Mechanical Systems, Machine Elements and Manufacturing*, 43(3):719–725, 2000.

[99] L. Ljung. *System Identification: Theory for the User*. Prentice Hall, New Jersey, 1999.

[100] L. Ljung and T. McKelvey. Subspace identification from closed loop data. *Signal Processing*, 52(2):209–215, 1996.

[101] F. Losch. *Identification and automated controller design for active magnetic bearing systems*. Ph.d thesis, Swiss Federal Inst. of Technoloy, Zurich, 2002.

[102] J.M. Maciejowski. Guaranteed stability with subspace methods. *Systems & Control Letters*, 26:153–156, 1995.

[103] J.M. Maciejowski. *Predictive Control with Constraints*. Prentice Hall, England, 2002.

[104] K. Mahata. An improved bias-compensation approach for errors-invariables model identification. *Automatica*, 43:1339–1354, 2007.

[105] F. Matsumura, T. Namerikawa, K. Hagiwara, and M. Fujita. Application of gain scheduled H infinity robust controllers to a magnetic bearing. *IEEE Trans. on Control Systems Technology*, 4(5):484–493, 1996.

[106] T. McKelvey. *Identification of state-space models from time and frequency data*. Phd thesis, Dept. of Electrical Eng., Linkoping University, Sweden, 1995.

[107] T. McKelvey and H. Akcay. An efficient frequency domain state-space identification algorithm. In *Proc. of the 33rd Conf. on Decision & Control*, volume 4, pages 3359–3364, Florida, USA, 1994.

[108] T. McKelvey, H. Akcay, and L. Ljung. Subspace-based identification of infinite-dimensional multivariable systems from frequency response data. *Automatica*, 32(6):885–902, 1996.

[109] T. McKelvey, H. Akcay, and L. Ljung. Subspace-based multivariable system identification from frequency response data. *IEEE Trans. on Automatic Control*, 41(7):960–979, 1996.

[110] S. Michael, G. Scheinert, and H. Uhlmann. Semianalytic modelling of a magnetic levitated disk with nonuniform polarization. In *Int. Conf. on Modeling and Simulation of Microsystems, Semiconductors, Sensors and Actuators*, pages 655–659.

[111] A.M. Mohamed and I. Busch-Vishniac. Imbalance compensation and automatic balancing in magnetic bearing systems using the Q-parameterization theory. In *Proc. of the American Control Conf.*, volume 3, pages 2952–2957, 1994.

[112] A.M. Mohamed and I. Busch-Vishniac. Imbalance compensation and automation balancing in magnetic bearing systems using the Q-parameterization theory. *IEEE Trans. on Control System Technology*, 3(2):202–211, 1995.

[113] A.M. Mohamed, F. Matsumura, T. Namerikawa, and J-H. Lee. Q-parameterization control of vibrations in a variable speed magnetic bearing. In *Proc. of the IEEE Int. Conf. on Control Applications*, pages 540–546, 1997.

[114] R. Mohd-Mokhtar and L. Wang. A review on identification and control methodologies for magnetic bearing systems. In *Int. Conf. on Robotics, Vision, Information and Signal Processing*, pages 232–236, Penang, Malaysia, July 2005.

[115] R. Mohd-Mokhtar and L. Wang. System identification of MIMO magnetic bearing via continuous time and frequency response data. In *Proc. of IEEE Int. Conf. on Mechatronics*, pages 191–196, Taipei, Taiwan, July 2005.

[116] R. Mohd-Mokhtar and L. Wang. Continuous time system identification using subspace methods. *ANZIAM J*, 47:712–732, 2007.

[117] R. Mohd-Mokhtar and L. Wang. 2-stage approach for continuous time identification using step response estimates. In *IEEE Int. Conf. on Systems, Man & Cybernetics*, Singapore, October 2008. Published.

[118] R. Mohd-Mokhtar and L. Wang. Continuous time state space model identification using closed-loop data. In *2nd Asia Int. Conf. on Modelling & Simulation*, pages 812–817, Kuala Lumpur, Malaysia, May 2008.

[119] R. Mohd-Mokhtar, L. Wang, L. Qin, and T. Barry. Continuous time system identification of magnetic bearing systems using frequency response data. In *5th. Asian Control Conf.*, pages 2066–2072, Melbourne, Australia, 2004.

[120] B. De Moor and J. Vandewalle. A geometrical strategy for the identification of state space models of linear multivariable systems. In *Proc. of the 3rd int. Symp. Appl. Multivariable System*, pages 59–69, 1987.

[121] R.H. Myers. *Classical and Modern Regression with Applications*. Duxbury Press, Boston, 2nd ed. edition, 1990.

[122] T. Namerikawa and M. Fujita. Uncertain model and [mu]-synthesis of a magnetic bearing. In *Proc. of IEEE Conf. on Control Applications*, volume 1, pages 558–563, Hawaii, USA, 1999.

[123] T. Namerikawa, M. Fujita, and F. Matsumura. Experimental verification on gain scheduled H-infinity robust control of a magnetic bearing. *JSME Int. Journal C*, 40(4):561–569, 1997.

[124] C. Nasr, J. Constantin, and A. Charara. Neural network control of magnetic levitation system. *Intelligent Engineering Systems through Artificial Neural Networks*, 12:521–526, 2002.

[125] K. Nonami and T. Ito. [mu]-synthesis of flexible rotor-magnetic bearing systems. *IEEE Trans. on Control System Technology*, 4(5):503–512, 1996.

[126] A. Ohsumi, K. Kameyama, and K-I. Yamaguchi. Subspace identification for continuous time stochastic systems via distribution-based approach. *Automatica*, 38:63–79, 2002.

[127] R. Pintelon, P. Guillaume, Y. Rolain, J. Schoukens, and H. Van Hamme. Parametric identification of transfer functions in the frequency domaina survey. *IEEE Transactions on Automatic Control*, 39(11):2245–2260, 1994.

[128] R. Pintelon and J. Schoukens. *System identification. A frequency domain approach*. IEEE Press, New York, USA, 2001.

[129] R. Pintelon and J. Schoukens. Frequency domain maximum likelihood estimation of linear dynamic errors-in-variables models. *Automatica*, 43(4):621–630, 2007.

[130] L. Qin. *Micro Magnetic Bearing: Investigation on New Design and Control Methodology*. Phd. thesis, Electrical & Computer Eng. RMIT University, Melbourne, Australia, 2000.

[131] L. Qin and R.B. Zmood. A simplified approach for accurate estimation of transverse magnetic forces in micro-actuators having inclined pole faces. *Journal of Micromechanics and Microengineering*, 10(1):28–33, 2000.

[132] S.J. Qin. An overview of subspace identification. *Computers & Chemical Eng.*, 30:1502–1513, 2006.

[133] S.J. Qin and L. Ljung. On the role of future horizon in closed-loop subspace identification. In *14th. IFAC Symp. on System Identification*, pages 1080–1084, New Castle, Australia, 2006.

[134] H. Rake. Step response and frequency response methods. *Automatica*, 16:519–526, 1980.

[135] H. Rodriguez, R. Ortega, and I. Mareels. A novel passivity-based controller for an active magnetic bearing benchmark experiment. In *Proc. of American Control Conf.*, volume 3, pages 2144–2148, Chicago, USA, 2000.

[136] T. Sato and Y. Tanno. Magnetic bearing having PID controller and discontinuous controller. In *Int. Conf. on Industrial Electronics, Ctrl and Inst.*, volume 3, pages 2121–2125, 1993.

[137] J. Schoukens and R. Pintelon. *Identification of linear systems: A practical guideline to accurate modeling.* Pergamon Press, New York, 1991.

[138] R.J.P. Schrama. An open-loop solution to the approximate closed-loop identification problem. In *9th IFAC/IFORS System Identification & System Parameter Estimation*, pages 1602–1607, Budapest, Hungary, 1991.

[139] G. Schweitzer. Active magnetic bearing - chances and limitations. Technical report, Int. Centre for Magnetic Bearing, ETH Zurich, 2002.

[140] G. Schweitzer, H. Bleuler, and A. Traxler. *Active Magnetic Bearing: Basics, Properties and Applications of Active Magnetic Bearings.* Hochschulverlag AG an der ETH Zurich, 1994.

[141] J. Shi and J. Revell. System identification and re-engineering controllers for a magnetic bearing system. In *Proc. of IEEE Region 10 Conf. on Computers, Communications, Control & Power Eng.*, volume 3, pages 1591–1594, Beijing, China, 2002.

[142] R. Shi. *Subspace identification methods for process dynamic modeling.* Phd thesis, McMaster University, Canada, 2002.

[143] L. Shuliang, A. Palazzolo, N. Uhnjoo, and A. Kascak. Non-linear fuzzy logic control for forced large motions of spinning shafts. *J. of Sound and Vibration*, 235(3):435–449, 2000.

[144] N.K. Sinha and B. Kuszta. *Modeling and identification of dynamic systems.* Van Nostrand Reinhold Comp., USA, 1983.

[145] N.K. Sinha and G.P. Rao. *Identification of continuous time systems.* Kluwer Academic Publishers, 1991.

[146] T. Soderstrom. Error-in-variables methods in system identification. *Automatica*, 43:939–958, 2007.

[147] T. Soderstrom, H. Fan, B. Carlsson, and M. Mossberg. Some approaches on how to use the delta operator when identifying continuous time process. In *IEEE Conf. on Decision & Control*, pages 890–895, San Diego, 1997.

[148] T. Soderstrom, U. Soverini, and K. Mahata. Perspectives on errors-invariables estimation for dynamic systems. *Signal Processing*, 8:1139–1154, 2002.

[149] T. Soderstrom and P. Stoica. *Instrumental variable methods for system identification.* Springer, Berlin, 1983.

[150] T. Soderstrom and P. Stoica. *System Identification.* Prentice Hall, London, 1989.

[151] S. Srinivasan and Y.M. Cho. Modeling and system identification of active magnetic bearing systems. In *Proc. of American Control Conf.*, pages 252–260, New York, USA, 1995.

[152] P. Stoica, M. Cedervall, and A. Eriksson. Combined instrumental variable and subspace fitting approach to parameter estimation of noisy input output systems. *IEEE Trans. on Signal Processing*, 43:2386–2397, 1995.

[153] T. Sugie, M. Fujita, and S. Hara. Multiobjective controller design with the guaranteed H-infinity control performance. In *Proc. of the 12th Triennial World Congress of the Int. Fed. of Automatic Control.*, volume 2, pages 149–152, 1994.

[154] L. Sun, H. Ohmori, and A. Sano. Frequency domain approach to closed-loop identification based on output inter-sampling scheme. In *Proc. of American Control Conf.*, volume 3, pages 1802–1806, Chicago, USA, 2000.

[155] H. Tian and K. Nonami. Robust control of flexible rotor-magnetic bearing systems using discrete time sliding mode control. *JSME Int. Journal C*, 37(3):504–512, 1994.

[156] M. Torres, H. Sira-Ramirez, and G. Escobar. Sliding mode nonlinear control of magnetic bearings. In *IEEE Conf. on Control Applications*, volume 1, pages 743–748, Hawaii,USA, 1999.

[157] N-V. Truong, L. Wang, and J. Huang. Nonlinear modeling of a magnetic bearing system using SDP model and linear wavelet parameterization. In *Proc. of American Control Conf.*, pages 2254–2259, New York, USA, 2007.

[158] N-C. Tsai, W.C. Chao, and H.K. Chien. Robust sliding mode control for axial AMB systems. In *5th Asian Control Conf.*, pages 64–69, 2004.

[159] J-G. Tsao, L-T. Shea, and L-F. Yang. Adaptive synchronization control of the magnetically suspended rotor system. *Dynamics and Control*, 10(3):239–253, 2000.

[160] H.J.A.F Tulleken. Generalized binary noise test-signal concept for improved identification-experiment design. *Automatica*, 26(1):37–49, 1990.

[161] E. Turker. *Investigation of digital control for magnetic bearing systems.* Phd thesis, School of Electrical & Computer Eng., RMIT University, Australia, 2005.

[162] H. Unbehauen and G.P. Rao. Continuous-time approach to system identification - A survey. *Automatica*, 26(1):23–35, 1990.

[163] H. Unbehauen and G.P. Rao. A review of identification in continuous-time systems. *Annual Reviews in Control*, 22:145–171, 1998.

[164] P. Van-Overschee and B. De-Moor. Continuous-time frequency domain subspace system identification. *Signal Processing*, 52(2):179–194, 1996.

[165] P. Van-Overschee and B. De-Moor. *Subspace identification for linear systems: Theory, implementation & applications.* Kluwer Academic Publishers, Boston, 1996.

[166] P. Van-Overschee and B. De-Moor. Closed loop subspace system identification. In *Proc. of IEEE Conf. on Decision & Control*, volume 2, pages 1848–1853, 1997.

[167] P. Van-Overschee and B. De Moor. N4SID: Numerical algorithms for state space subspace system identification. In *12th IFAC World Congress*, pages 361–364, Sydney, Australia, 1993.

[168] P. Van-Overschee and B. De Moor. N4SID: Subspace algorithm for the identification of combined deterministic-stochastic systems. *Automatica*, 30(1):75–93, 1994.

[169] J.M. Vance. *Rotordynamics of Turbomachinery*. John Wiley & Sons, New York, 1988.

[170] M. Verhaegen. Application of a subspace model identification technique to identify LTI systems operating in closed-loop. *Automatica*, 29(4):1027–1040, 1993.

[171] M. Verhaegen. Subspace model identification. part III: Analysis of the ordinary output-error state space model identification algorithm. *Int. J. Control*, 58:555–586, 1993.

[172] M. Verhaegen and P. Dewilde. Subspace model identification part 1: The output error state-space model identification class of algorithm. *Int. J. Control*, 56(5):1187–1210, 1992.

[173] M. Verhaegen and P. Dewilde. Subspace model identification part 2: Analysis of the elementary output error state-space model identification algorithm. *Int. J. Control*, 56(5):1211–1241, 1992.

[174] M.H. Verhaegen. Identification of the deterministic part of MIMO state space models given in innovations form from input-output data. *Automatica*, 30(1):61–74, 1994.

[175] M. Viberg. Subspace-based methods for the identification of linear time-invariant systems. *Automatica*, 31(12):1835–1851, 1995.

[176] L. Wang. A tutorial on model predictive control - using a linear velocity-form model. In *4th Asian Control Conf.*, pages 1394–1399, Singapore, 2002.

[177] L. Wang and W.R. Cluett. System identification based on closed-loop step response data. *IEE - Control Theory Applications*, 141(2):107–110, 1994.

[178] L. Wang and W.R. Cluett. Use of PRESS residuals in dynamic system identification. *Automatica*, 32:781–784, 1996.

[179] L. Wang and W.R. Cluett. Frequency-sampling filters: An improved model structure for step-response identification. *Automatica*, 33(5):939–944, 1997.

[180] L. Wang and W.R. Cluett. *From Plant Data to Process Control: Ideas for Process Identification and PID Design*. Francis & Taylor, London, 2000.

[181] L. Wang, M.L. Desarmo, and W.R. Cluett. Real-time estimation of process frequency response and step response from relay feedback experiments. *Automatica*, 35:1427–1436, 1999.

[182] L. Wang, P. Gawthrop, and C. Chessari. Indirect apppoach to continuous time system identification of food extruder. *J. of Process Control*, 14(6):603–615, 2004.

[183] L. Wang and P.J. Gawthrop. On the estimation of continuous time transfer functions. *Int. J. Control*, 74(9):889–904, 2001.

[184] J. Watkins, K. Lee, C. Hernandez, K. Blumenstock, and J. Schepis. Adaptive auto-balancing control of magnetic bearings for an optical chopper. In *Proc. of American Control Conf*, volume 2, pages 1298–1303, 2001.

[185] D. Watterson. FE modeling of magnetic devices. *J. of Engineering London*, 236(5):30–31, 1995.

[186] P.E. Wellstead. Non parametric methods of system identification. *Automatica*, 17:55–69, 1981.

[187] W. Xiao and B. Weidemann. Fuzzy modeling and its application to magnetic bearing systems. *Fuzzy Sets & Systems*, 73:201–217, 1995.

[188] Z. Yang. Frequency domain subspace model identification with the aid of $w-$operator. In *Proc. of the SICE Annual Conf.*, pages 1077–1080, 1998.

[189] T-J. Yeh and K. Youcef-Toumi. Adaptive control of nonlinear, uncertain systems using local function estimation. *Trans. of ASME Journal*, 120(4):429–438, 1998.

[190] C. Zhang and K.J. Tseng. Design and FEM analysis of a flywheel energy storage system assisted by integrated magnetic bearings. In *Proc. of 30th IEEE Annual Conf. on Industrial Electronics Society*, volume 2, pages 1634–1639, 2004.

[191] C. Zhang, P. Wu, and K.J. Tseng. FEM analyses for the design and modeling of a novel flywheel energy storage system assisted by integrated magnetic bearing. In *Proc. of IEEE Int. Conf. on Electric Machines and Drives*, pages 1157–1164, 2005.

[192] Y. Zhao and D. Westwick. A direct approach to closed-loop identification of Wiener models using subspace methods. In *Proc. of the American Control Conf.*, volume 4, pages 3585–3589, Colorado, June 2003.

[193] W.X. Zheng and C.B. Feng. Identification of a class of dynamic errors-in-variables models. *Int. J. Adaptive Control & Signal Processing*, 6:431–440, 1992.

[194] R.B. Zmood and Y. Jiang. Decentralised neural network control of magnetic bearings. In *Proc. of Canadian Conf. on Electrical and Computer Engineering*, volume 1, pages 257–260, 1996.